VNIVERSITAT DE VALÈNCIA

Departament de Física Teòrica
i Institut de Física Corpuscular (IFIC, UV-CSIC)

DOCTORAT EN FÍSICA

Discrete symmetries in entangled neutral meson systems

Ph. D. thesis dissertation by

Pablo Villanueva Pérez

Under the supervision of

José Bernabéu Alberola

and

Fernando Martínez Vidal

Valencia, Spain
May, 2013

"*-Minino de Cheshire -empezó Alicia tímidamente, pues no estaba del todo segura de si le gustaría este tratamiento: pero el Gato no hizo más que ensanchar su sonrisa, por lo que Alicia decidió que sí le gustaba -. Minino de Cheshire, ¿podrías decirme, por favor, qué camino debo seguir para salir de aquí?*

-Esto depende en gran parte del sitio al que quieras llegar - dijo el Gato.

-No me importa mucho el sitio... -dijo Alicia.

-Entonces tampoco importa mucho el camino que tomes - dijo el Gato.

- ... siempre que llegue a alguna parte - añadió Alicia como explicación.

- ¡Oh, siempre llegarás a alguna parte - aseguró el Gato -, si caminas lo suficiente! "

L. Carroll

Contents

AGRADECIMIENTOS

Mi agradecimiento más sincero al Dr. José Bernabéu y al Dr. Fernando Martínez que han hecho posible este trabajo y he tenido el placer de recorrer todo este camino junto a ellos. El Dr. José Bernabéu me ofreció la oportunidad de realizar una tesis híbrida entre teoría y experimento y su idea ha sido el germen de esta tesis. El Dr. Fernando Martínez ha sido capaz de hacer que un físico teórico pueda amar la física experimental e incluso me llegue a plantear una orientación experimental en mi futuro; agradezco su supervisión que me ha hecho aprender y esforzarme tanto en los fracasos como en los éxitos. También quisiera darles las gracias a ambos por su comprensión y amistad, pues una tesis con meros directores es una travesía por el desierto.

Gracias a mis padres, Rosalía y Adolfo, por haberme apoyado y educado, cuya mano invisible y otras veces no tanto ha dirigido mi vida. Ellos son las personas a las que les debo quien soy y seré, por lo que este trabajo es fruto de sus cuidados y desvelos. A mi hermanita, Elena, que siempre me ha dado ese pequeño empujoncito que todos necesitamos y no nos atrevemos a pedir. A mis familiares y seres queridos, que siempre se han acordado de mi dándome su apoyo, comprensión y motivación.

Gracias al Instituto de Física Corpuscular (IFIC) y a su director Francisco Botella, por ofrecer un ambiente donde la investigación se convierte en un agradable viaje rodeado de buenos compañeros. Al CSIC por las becas JAE que han financiado mi trabajo y me han permitido una formación de primer nivel, esperemos que las autoridades perciban la importancia de mantener ayudas como estas, pues son necesarias para garantizar la formación de las futuras generaciones de científicos. A la Universitat de València por ser mi alma máter y ofrecerme la oportunidad de conocer a grandes científicos, en especial aquellos que han guiado este trabajo.

Gracias a los miembros de BaBar tanto del IFIC, como toda la colaboración, por sus consejos y guía, que han hecho posible este trabajo. A todas las personas involucradas en el detector BaBar y el acelerador PEP-2, cuyo esfuerzo y trabajo bien hecho ha permitido obtener los datos, que permitieron el análisis presentado en esta tesis.

Gracias a los Drs. Nick Mavromatos y Antonio di Domenico y a sus

respectivas universidades el “King’s College” y la “Sapienza Università, di Roma” por acogerme como si fuese su doctorando y hacerme sentir como en casa mientras investigágamos y aprendía de ellos.

Gracias a los amigos que siempre están ahí para echarte una mano o “cubo” y darte ánimos cuando lo necesitas. Especialmente por enriquecer mi vida y ser una escapatoria del mundo de la Física. A Cristina, por toda su inspiración y sus consejos para construir los diagramas de “patatas”. Al Colegio Mayor San Juan de Ribera, a su director Don J.V. Puig y colegiales que hicieron la “chapancia” agradable y cuya amistad conservaré toda mi vida.

INTRODUCCIÓN

Simetría, del griego "con medida", es un rasgo característico de formas geométricas, sistemas, ecuaciones y otros objetos materiales, o entidades abstractas, relacionada con su invariancia bajo ciertas transformaciones, movimientos o intercambios. A nuestro alrededor percibimos las simetrías como un rasgo geométrico que aporta belleza y armonía en la naturaleza, puesta de manifiesto a la perfección en el hombre de Vitruvio de Leonardo. No obstante también es interesante su ruptura, que atrae igual o más la atención en un mundo que parece estar construido bajo el paradigma de la simetría y armonía.

Este concepto de simetría se traslada a la Física como la invariancia de las leyes físicas bajo una transformación y a dicha invariancia podemos asociar en ocasiones una cantidad conservada. A lo largo de la historia de la Física ha habido grandes hitos, momentos que han cambiado la concepción de la realidad y han significado un nuevo paradigma físico. Uno de estos momentos se produjo con el teorema de Emmy Noether, uno de los pilares fundamentales de la Física teórica moderna. El teorema enuncia así: "cualquier simetría diferenciable, proveniente de un sistema físico, tiene su correspondiente ley de conservación". Este teorema ha cambiado el paradigma para construir un sistema físico, pues si sabemos bajo qué transformaciones el sistema es invariante (simetrías o leyes de conservación) podemos determinar la forma de las interacciones, y a la inversa, sabida la forma de las interacciones podemos saber qué simetrías exhibe. Es más, si un sistema físico no exhibe una simetría es igual o incluso más relevante si cabe conocer el mecanismo que conduce a la ruptura de la simetría.

Para entender mejor el teorema de Noether supongamos una cantidad O que se puede observar experimentalmente, como puede ser posición, momento lineal, momento angular, tiempo, energía, etc. Dada una transformación U sobre el sistema en que hemos observado O obtenemos una nueva medida del observable O' ($O \xrightarrow{U} O'$). Entre las numerosas transformaciones U que podemos realizar a un sistema tenemos translaciones, rotaciones, inversión espacial o paridad, inversión temporal, etc. Si la ley física escrita en términos de los nuevos observables O', es igual a la ley escrita en términos de los originales O, decimos que tenemos una ley simétrica bajo la transformación

U, con lo que experimentalmente podemos comprobar la ley resultante de conservación. Por ejemplo, si un sistema es invariante bajo translaciones espaciales, el momento lineal se conserva; si un sistema es invariante bajo rotaciones, el momento angular se conserva.

En el caso del mundo de las partículas o mundo microscópico hay unas transformaciones de gran relevancia que son C, transformación que relaciona partículas y antipartículas, P, o la simetría de reflexión en un espejo, y T, de inversión temporal. En un principio se pensaba que eran buenas simetrías, pero en los años 50 Lee y Yang, a raíz de la paradoja sobre kaones neutros, barajaron la posibilidad de que P no se conservara, siendo observada su ruptura en las interacciones débiles un año después por Wu y col. en la desintegración β del Co polarizado. Se creyó entonces que el producto o composición de transformaciones CP sí que se conservaba en interacciones débiles. Esta idea perduró hasta el año 1964, cuando Cronin, Fitch, Christenson y Turlay pusieron de manifiesto que esta simetría también fallaba en las desintegraciones débiles de kaones neutros. Esto nos lleva a preguntarnos si la combinación de las tres transformaciones discretas CPT es una buena simetría. En nuestro conocimiento actual CPT es una buena simetría, tal y como ocurre en cualquier teoría con invariancia Lorentz local y hermiticidad [1]. Un ejemplo de teoría con invariancia Lorentz local es la teoría cuántica de campos en la que se basa nuestro modelo de interacciones, el Modelo Estándar. Esta simetría sigue siendo estudiada y todavía no se ha encontrado ninguna prueba experimental que apunte a su no conservación; si se encontrase algún resultado que indicase su ruptura estaríamos sin lugar a dudas ante una señal de nueva Física.

La invariancia bajo CPT nos dice algo más acerca de la simetría T, pues si CPT es exacta y hemos descubierto la ruptura de la simetría CP, tal y como sucede en un balancín, T se debe romper en sentido opuesto para dejar CPT invariante. Pese a que esto es conocido desde 1964, hasta hoy no ha habido ninguna prueba concluyente directa de ruptura de T, dado que su test no es trivial al tener que invertir los estados inicial y final exactamente, lo que representa un reto experimental. Obtener un test de T ha sido uno de los objetivos principales de esta tesis sin descuidar otras simetrías.

En el Capítulo 1 haremos un repaso teórico e histórico de las principales simetrías en la Física de partículas, así como motivaremos el estudio de las mismas en diferentes sistemas. Uno de estos sistemas es el de mesones neutros B, del que en el Capítulo 2 realizaremos un estudio de simetrías en las factorías de mesones B. Utilizando el entrelazamiento cuántico, discutiremos cómo realizar el primer test genuino de ruptura de T [2]. En el Capítulo 3 presentaremos el detector *BABAR* y la factoría de mesones B de SLAC, y describiremos la muestra de datos que utilizaremos para nuestro análisis. El

Capítulo 4 recoge el análisis experimental de los datos, así como los resultados obtenidos, dando lugar al primer test genuino de T [3]. El Capítulo 5 versa sobre el estudio de simetrías discretas en el sistema de mesones K neutros con un método similar al explicado en el Capítulo 2, basado en el uso del entrelazamiento cuántico en las Factorías de mesones ϕ [4]. Finalmente el Capítulo 6, dadas las diferencias sustanciales en la evolución temporal entre mesones B y K introduciremos un nuevo formalismo que soluciona problemas de interpretación probabilista, intrínsecos a la aproximación de Weisskopf-Wigner para el caso de los kaones [5].

INTRODUCTION

Symmetry, from Greek "measure together", is a characteristic feature of geometrical figures, systems, equations and other material objects, or abstract entities, related to the invariance under certain transformations, movements or interchanges. In our surroundings we perceive the symmetries as a geometrical characteristic which provides beauty and harmony in Nature, as shown perfectly in the Vitruvian Man by Leonardo da Vinci. Nevertheless it is also interesting the symmetry breaking, which catches the eye in a world which seems to be built under the symmetry and harmony paradigm.

The symmetry concept is transferred to Physics as the invariance of the physical laws under a transformation, this invariance can be associated to a conserved quantity. Throughout Physics history there have been milestones, big moments which have changed the conception of the reality and they have meant a new physical paradigm. One of these moments took place with Emmy Noether's theorem, one of the fundamental modern theoretical physics breakthroughs. The theorem states that any differentiable symmetry of the action of a physical system has a corresponding conservation law. This theorem has changed the way to understand a physical system, because if we know under which transformations the system is invariant (symmetries or conservation laws) we can determine the structure of the interactions, and inversely, if we know the structure of the interactions, we can derive the symmetries. Even more, if a physical system does not show a certain symmetry it is likewise interesting to know the mechanism which arises the symmetry breaking.

To get a better understanding of Noether's theorem let us suppose an experimental observable quantity O, like position, linear momentum, rotational momentum, time, energy, etc. Given a certain transformation U on the system where O was observed, we obtain a new measurement of the observable O' ($O \xrightarrow{U} O'$). We can make different transformations, among them translations, rotations, space or parity inversion, time reversal, etc. If the physical law in terms of the new observables O' is exactly the same as the law written in terms of the original O, we declare that we have a symmetric law under the transformation U, therefore we can test the conservation law experimentally. For example, if a system is invariant under translations the

linear momentum is conserved; if a system is invariant under rotations the angular momentum is conserved.

In the particle physics world or the microscopic world, there are certain relevant transformations like C, the transformation which relates particles and antiparticles, P, the mirror image transformation, and T, time inversion. It was thought that they were good symmetries, but in the 50s Lee and Yang thought about the possibility that P was not conserved, and in fact its violation was observed in the weak interactions by Wu *et al.* a year later. Then it was thought that CP the product of C and P transformations was conserved in the weak interactions. This idea prevailed until 1964, when Cronin, Fitch, Christenson and Turlay showed that this symmetry was also broken in weak interactions. This CP violation led us to postulate that a new composition CPT had to be invariant. With our current knowledge, CPT is a good symmetry as it occurs in any local Lorentz invariant theory and hermiticity [1]. An example of Lorentz invariant theory is the quantum field theory, which is the base for our Standard Model of interactions. Nowadays, this symmetry is being tested and evidence of symmetry breaking has not been found yet; if any violation result were found that would be a new physics signal.

CPT invariance tells us more about the T symmetry, because as long as CPT is invariant and we have found CP violation, as it happens in a seesaw, T has to be violated in the opposite sense to compensate CP to preserve the CPT product invariant. Despite this is known since 1964, until now there has been no concluding direct test of T, since it is a highly non-trivial test as requires to exactly inverse the initial and final states. One of the main goals of this thesis is to obtain the first test of T without any experimental or theoretical connection to CP, even though other symmetries are going to be studied as well.

In the first Chapter we do a theoretical and historical review of the main symmetries in particle physics, moreover we motivate the study of these symmetries in different systems. One of those is the B neutral meson system, which is discussed in Chapter 2, where a method to study discrete symmetries is delineated, exploiting the Einstein-Podolski-Rosen entanglement available at B factories [2]. This method has lead to the first genuine direct test of T. In Chapter 3 we give a general description of the B factory at SLAC and the *BABAR* detector, and we describe the data sample used for our analysis. Chapter 4 explains the data analysis and the results obtained, which constitute the first direct and genuine test of T violation [3]. Chapter 5 is about discrete symmetry studies in the K neutral meson system with a similar method as the one delineated in Chapter 2, exploiting the quantum entanglement at ϕ factories [4]. In the last Chapter, we introduce, due to the

differences between the time evolution of the B meson and K meson systems, a new formalism which solves the intrinsic probabilistic interpretation of the Weisskopf-Wigner approach for the K system [5].

1. DISCRETE SYMMETRIES IN PHYSICS

The study of symmetries is fundamental in Physics. A conservation law in Physics corresponds to the invariance of the system under a definite symmetry operation which is associated with an observable, whose knowledge determines the behavior of the system. Thus it is relevant to understand the nature of symmetry transformations and the way they act on physical systems. According to the way they act on physical systems, an operation may be space-time-like if it induces effects only on the space-time coordinates describing the system, or internal if the change affects only the internal charges. Attending to the nature of symmetry transformations, when they can be obtained by applying a succession of infinitesimal transformations are continuous, if not they are discrete.

An example of exact continuous symmetry is the space-time symmetry of Lorentz invariance. This means invariance under the group of Lorentz transformations which includes translations and rotations as well as pure Lorentz transformations, i.e., the orthochronous proper group. Associated with translational invariance in space and time we have a conserved four-momentum, and a conserved angular momentum vector which arises from rotational invariance. Restricting ourselves to orthochronous transformations, i.e., excluding inversions in either space or time, invariance under Lorentz transformations seems to be an exact symmetry within the present limits of experimental verification.

In this thesis we are going to focus on discrete symmetries like C, P, T, and their products. It has been shown that they are preserved by strong and electromagnetic interactions, but are broken in weak processes. Moreover it is also known that, while C and P are maximally violated in Nature by weak interactions, CP breaking happens under experimental additional conditions. Regarding T symmetry, although the CPT theorem [1] relates it with CP, a direct proof independent of CP was lacking before the work developed in this thesis context was done. As discrete symmetries have a special interest, in our work we will discuss them in some detail.

1.1 Parity or Space Inversion (P)

Parity symmetry (P), also called space inversion, consists of the invariance of the physical laws under a discrete transformation which changes the sign of the space coordinates x, y, and z, leaving invariant the time coordinate (t). This corresponds to the inversion of the handedness of the axis system, so a right-handed system becomes left-handed upon the parity transformation. In three dimensions, the inversion of the coordinate axes may be achieved in two steps, through a mirror reflection on a coordinate plane followed by a rotation of angle π around the axis perpendicular to that plane. The relevant point for us is whether the physical laws are invariant under P or not. Under P invariance, a process cannot be distinguished from its specular image and one cannot define absolutely the concepts of left and right.

It is obvious that if we apply two parity transformations in succession is equivalent to no transformation at all, i.e., the square of the parity transformation is the identity. There are two types of vectors respecting this property: those which change sign under P (polar vectors) and those which do not (axial vectors or pseudo-vectors). Analogously we can define quantities which are invariant under P transformations, the so-called scalars, as opposed to pseudo-scalars, which change sign under P.

As the parity transformation changes the sign of the position vector, $\vec{r} \to -\vec{r}$, the velocity

$$\vec{v} = \frac{d\vec{r}}{dt} \tag{1.1}$$

changes sign under P. The momentum is reversed too, $\vec{p} \to -\vec{p}$, since

$$\vec{p} = m\vec{v} \ , \tag{1.2}$$

and the orbital angular momentum,

$$\vec{L} = \vec{r} \times \vec{p} \ , \tag{1.3}$$

is invariant under P, because both $\vec{r}$ and $\vec{p}$ change sign. Therefore angular momenta, including spin, are P-even quantities.

According to Newton's law,

$$\vec{F} = \frac{d\vec{p}}{dt} \ , \tag{1.4}$$

the force $\vec{F}$ is a polar vector.

We can ask ourselves which are the kind of questions that P addresses and what does P invariance means [6]: imagine we are watching an event in a mirror, does the event that one sees there look real? Does the event seen in the mirror correspond to something allowed by the laws of Nature?

1.2 Time Reversal (T) and $\widehat{T}$

Time-reversal transformation, usually called T, consists formally of changing the sign of the time coordinate t. From Eq. (1.1) we see that, when $t \to -t$, then the velocity $\vec{v} \to -\vec{v}$, while $\vec{x}$ remains invariant. So both linear and angular momenta are reversed under T ($\vec{p} \to -\vec{p}$ and $\vec{J} \to -\vec{J}$). On the other hand, $\vec{F}$ does not change sign as can be deduced from Eq. (1.4).

The mathematical transformation described above, under which t, $\vec{p}$, and other entities change sign, may be called $\widehat{T}$. The genuine time-reversal transformation (T) goes beyond $\widehat{T}$ as it also implies the interchange of final states and initial states, i.e., T invariance means that the rate $in \to out$ has to be equal to the rate for $out \to in$ once the initial configurations, namely in in one case and out in the other have been precisely realized. However, the probability to realize in or out as initial states is generally different, i.e., the likelihood of the time reversed version of a complex reaction to happen is very low indeed. An extreme example of irreversibility is a decay process, which seems to prevent a T test in unstable systems. Thus, in case of T invariance, one process and its time-reversed would be equally physical and occur with the same probability. One would not be able to define a direction for the time arrow in an absolute way, independent of boundary conditions.

A daily experience can illustrate perfectly the difficulties to reverse initial and final states [7]: parking a car between two other cars standing along the kerbside is considered a harder maneuver than leaving the parking space. The reason is the following: to park the car you have to fit it into more or less a single cell of final configurations; for leaving, you can use any of many possible trajectories to final states outside the parking slot.

As we did with P, we can try to think which are the most basic questions about the fundamental laws of Nature that T is trying to answer [6]. We can imagine a physical event filmed and then watched backwards. Would the events watched on both films will they be realistic? Or will they be odd with the laws of Nature?

In Nature, there are even other asymmetries related to t inversion, the Universe and the t-asymmetries for complex systems [8], which we will try to clarify that they are not related to T.

The Universe t-asymmetry is connected to the fact that our Universe is expanding and the expansion rate is increasing with time. In spite of the symmetric structure of the general relativity equations under the exchange $t \leftrightarrow -t$, the Universe which fulfills the opposite time evolution ($-t$) would be completely disconnected from (and thus unobservable from) our Universe with different initial conditions. This difference between those t-conjugated

solutions is a matter of mathematical rather than a physical interest.

The macroscopic t-asymmetry, also called *arrow of time*, is the second law of Thermodynamics, which says that in an isolated system the entropy tends to increase with time. The *arrow of time* concept was developed by A. Eddington which implies that in the thermodynamic systems the time always seems to flow in the same direction, the direction governed by the increase of entropy. Let us imagine a vase which breaks into millions of small pieces. The second law of Thermodynamics forbids that the vase pieces fly back and reassemble again reforming the vase. This effect has nothing to do with T violation which as we have motivated is related to microscopic and fundamental processes, therefore it has nothing to do with entropy.

1.3 Charge Conjugation (C)

Contrary to P and T, charge-conjugation symmetry C does not have an analogue in classical physics. C is an internal operation, which changes the sign of all internal charges, such as electric charge or baryon number, and leaves the space-time properties unaltered. This is a prediction for relativistic quantum theory which has been brilliantly confirmed by experiment, in particular through the discovery of the positron (Anderson 1933) and of the antiproton (Chamberlain et al. 1955). If C was a good symmetry, all experiments performed in a world of antimatter would give the same results as they would give in ours. However, C is not a good symmetry in Nature, and it does not transform a physical particle in its antiparticle, because its definition is made on free fields, which do not necessarily correspond to the physical ones.

To define the antiparticle one has to make use of the combined transformation CPT. Given a physical state, its CPT-transformed has to exist, contrary to its C-transformed.

1.4 Violation of C, P and CP

Before 1956 it was assumed that P and C were separately conserved in elementary processes. The possibility of left-right asymmetry in physical laws was suggested that year by Lee and Yang [9] and discovered experimentally a few months later in a nuclear β decay processes by Wu et al [10]. It turns out that the whole body of weak interactions works differently for matter and antimatter. Weak interactions also are left-right asymmetric. On the other hand, under CP, made out of simultaneous C and P transformations, (most) weak interactions remain identical under, i.e., the partial decay rates

and cross sections remain unchanged. Namely, the conceptual problem of distinguishing matter from antimatter can only acquire a solution if we are able to eliminate the convention of what is "left" and what is "right" from the game. It is not enough that C be violated, CP must be violated too in order that matter may be distinguished from antimatter in this behavior.

The fact that CP symmetry is preserved even while C and P symmetries are violated was first pointed out by Landau (1957) [11]. A few years later CP was discovered to be violated too (Christenson et al. 1964) [12]. The first evidence for CP violation came from the decay $K_L \to \pi\pi$, which should be forbidden by CP conservation. Later the charge asymmetry in K_{l3} was observed. The K_L is a neutral particle with well-defined mass and decay width. Even more, there is no other particle with equal mass, therefore K_L must be its own antiparticle. It decays both to $\pi^+ e^- \bar{\nu}_e$ and to the CP-conjugate mode $\pi^- e^+ \nu_e$. However, it decays slightly less often to the first than to the second mode. This fact unequivocally establishes both C violation and CP violation. CP violation is explained in the Standard Model (SM) with the existence of three families in the (unitary) quark-mixing matrix, the so-called Cabibbo-Kobayashi-Maskawa matrix (CKM) [13]. Three families allow the presence of one irreducible physical phase in the CKM matrix, which is the responsible for all CP-violation effects in the quark sector of the SM. This mechanism was confirmed not only in the neutral K system but also in the neutral B mesons system, where the B factories have played a crucial role. One of the main channels to study CP violation in the B sector is the comparison between $B^0 \to J/\psi K_S$ and its CP conjugate ($\overline{B}^0 \to J/\psi K_S$), which give rise to the largest CP-violating asymmetry found in Nature. This result contribute to the Nobel Prize in Physics given in 2008 to Kobayashi and Maskawa.

At present there is direct or indirect evidence that in our Universe each of the three discrete symmetries C, P and T is violated. The same happens to any bilinear product, such as CP, TC, etc. However, the triple product CPT represents an exact symmetry in any local quantum field theory with Lorentz invariance and Hermiticity [1].

1.5 Violation of T and searches

As said in Sec. 1.4, in the context of local quantum field theories with Lorentz invariance and Hermiticity, the CPT theorem [1] ensures a theoretical constraint between the CP and T symmetries. Although all present tests of CPT invariance confirm the validity of this symmetry, particularly in the neutral kaon system where there are strong limits [14, 15], the theoretical connec-

tion between CP and T does not imply an experimental identity, except for processes which are identical under CPT transformation. Moreover, it is worthwhile to search for direct evidence of T non-invariance, with neither experimental nor theoretical connection to CP violation. There is at present no existing result that clearly shows T violation in this sense [16].

We discuss in this Section different types of experiments that by themselves are seen to violate T: T-odd observables in final states or non-degenerate stationary states, and T observables in transitions [16].

First of all we discuss non-zero expectation values of a T-odd operator for an elementary particle in a non-degenerate stationary state. The most accessible observable is the electric dipole moment (EDM). The interaction of an elementary particle or an atom with an electric field $\vec{E}$ contains in the multipolar expansion a term of the form $d\vec{S}\cdot\vec{E}$ where d is the EDM and $\vec{S}$ is the spin. This contribution violates T and P, as $\vec{S}$ is odd under T but $\vec{E}$ is not. Higher order multipolar contributions, like quadrupole moments, would violate T as well.

One can find in the literature lots of experimental searches to measure EDMs and the interpretation of the results in terms of theoretical models. In principle, the simplest procedure to measure an EDM is to observe the shift of energies ($d\vec{S}\cdot\vec{E}$) after applying an external electric field. In practice, this simple procedure only works for neutral particles since the charged particles would be accelerated by the electric field. Instead of doing so, one can try to detect the EDM of a charged particle inside an atom applying an external electric field. However, when a point-like charged particle is in equilibrium under electric forces, the electric field at the particle vanishes (including the dipole interaction energy). The atomic nucleus is not point-like, therefore the electric field seen by the electrons is not uniform over the nuclear volume. Thus there is no exact cancellation of the electric forces, it only reduces the EDM of the atom relative to the original one. This shielding effect reduces the EDM relatively to the original one, but doesvnot cancel it out. This reduction is proportional to a factor $Z^2(\text{nuclear size})^2/(\text{atomic size})^2$, where Z is the atomic number. All current experiments observe how affects an external electric field ($\vec{E}$) to the spin ($\vec{S}$) of the elementary particles or atoms having an EDM. Most of those experiments also apply a magnetic field ($\vec{B}$) parallel to $\vec{E}$. In the case of a spin 1/2 particle, with only two spin states (parallel or antiparallel to the fields), the energy difference between the two states is

$$\Delta E = h\nu = 2\vec{\mu}\cdot\vec{B} \pm 2d\vec{S}\cdot\vec{E}\ , \tag{1.5}$$

where h is the Planck's constant, ν is the spin resonance frequency, and $\vec{\mu}$ is the magnetic dipole moment. The usual EDM experiments measure ν and

extract the EDM effect by reversing $\vec{E}$ as opposed to $\vec{B}$. Following this idea, we give the most recent experimental limits on the EDMs of the electron (d_e) [17] and the neutron (d_n) [18]:

$$\begin{aligned} d_e &< 1. \times 10^{-27} e^- \text{ cm} , \\ d_n &< 3. \times 10^{-26} e^- \text{ cm} . \end{aligned} \tag{1.6}$$

In the SM d_n can be derived from second-order weak interactions and the calculations depend on long-distance effects giving an effect of the order 10^{-32} e^- cm. On the other hand, d_e is a third order effect and perhaps of order 10^{-38} e^- cm.

Other experiments are focused on a non-zero expectation value of a T-odd observable in the final states of a weak decay. These observables are based in decay amplitudes which may depend on the initial spin $\vec{S}_i$ and the momenta and spin of the final particles ($\vec{P}_f$ and $\vec{S}_f$ respectively). One can also determine the expectation value of scalars or pseudoscalars made from these vectors, e.g., polarization studies in certain decays, like μ polarization in $K \to \pi\mu\nu$.

Those observables violate T only in the Born approximation, i.e., avoiding Final State Interactions (FSI). The imaginary part arisen can be originated either because of T violation or higher order in perturbation theory as required by unitarity (with equal sign for the phase of particles and antiparticles). Let us assume H_W the weak interaction Hamiltonian, from T invariance one can derive [16]

$$\langle f|H_W|i\rangle = \langle fT|T^\dagger H_W T|T^\dagger i\rangle = \langle -i|H_W|-f\rangle^* . \tag{1.7}$$

If the Born approximation can be used, then $|-f\rangle$ just involves reversing momenta and spin,

$$\langle f|H_W|i\rangle = \langle -f|H_W|-i\rangle . \tag{1.8}$$

As a remark, to claim this kind of observables as a test of T we require to apply the Born approximation, i.e., to neglect FSI.

We can comment different observables but we will focus on the observable A in the decay $K_L \to \pi^+\pi^- e^+ e^-$. This observable can be written as [19]

$$A = \vec{n}_e \times \vec{n}_\pi \cdot \hat{z}(\vec{n}_e \cdot \vec{n}_\pi) , \tag{1.9}$$

where $\vec{n}_\pi$ and $\vec{n}_e$ are the normals to the planes of the pion pair and the lepton pair respectively, and $\hat{z}$ is a unit vector in the direction of the center-of-mass of the pion pair. The large value of this observable obtained by E799 at FNAL [20] is the result from the interference between two *CP*-conserving

decay amplitudes: a relatively large amplitude for K_+ and a small amplitude for K_-. The interference is given by [19]

$$A \approx 0.15 \sin(\varphi_\epsilon + \Delta) \ , \tag{1.10}$$

where φ_ϵ is the ϵ phase (ϵ is the well-known *CP* violating parameter) and Δ depends on the FSI phase shifts on the final $\pi\pi$ state. Δ already evidences the presence of pseudo-T violation. Even in the limit of $\Delta = 0$ you need $\Delta\Gamma = 0$ to interpret this effect as a genuine T-violation signal [16].

Oscillations are a good place to search for T non-invariance, i.e., if the probability of $in \to out$ and $out \to in$ at a given time are different we have T violation. One can think about neutrino oscillation comparing $\nu_e \to \nu_\mu$ and $\nu_\mu \to \nu_e$ as a function of time. The *CP*-violation test with the first process would be any difference between $\nu_e \to \nu_\mu$ and $\bar{\nu}_e \to \bar{\nu}_\mu$ not directly connected to the T test. The possibility to perform these kind of tests requires beams of both ν_μ and ν_e as proposed in the "neutrino factories" based on μ storage rings and long-base lines.

Finally we will discuss in a more detailed way transition processes and their T-transformed versions,

$$S_{f,i} \leftrightarrow S_{-i,-f} \ , \tag{1.11}$$

where S denotes the transition matrix.

In this case, due to the antiunitarity of the operator implementing the symmetry, T invariance requires that the likelihood for reaction $in \to out$ equals that of $out \to in$ once the initial configurations, *in* in one case and *out* in the other, have been precisely prepared. However, the likelihood of the time reversed version of the process to happen is very low or impractical in most cases, like for unstable systems. This explains why T is much more difficult to study directly than P, C, and *CP*.

Since the SM is *CPT* invariant, it predicts T-violating effects in parallel to each *CP*-violation effect that arises due to the interference of amplitudes with different weak phases. Consequently, this may appear in three different ways: T violation in decay; T violation in the mixing of neutral states; and T violation that arises from the interference between decay with and without mixing.

T violation matched to *CP* violation in decay has not been observed, because the difficulties of the preparation of the time-reversed decay process. Let us see the example [8] of the rare weak decay of neutral B mesons to $K^+\pi^-$, for which direct *CP* violation is well established [21] (different decay rates R_1 and R_2 for $B^0 \to K^+\pi^-$ and $\overline{B}^0 \to K^-\pi^+$, respectively) due to the ability of B factories to produce hundreds of millions of B mesons. T

violation as implied by this result, combined with CPT invariance, tells us that the rates for the inverse processes $K^+\pi^- \to B^0$ and $K^-\pi^+ \to \overline{B}^0$ should be R_2 and R_1, respectively. However, there is little chance to measure these inverse rates and check directly this prediction since the weak interaction production mechanism is highly suppressed ($B^0 \to K^+\pi^-$ branching ratio of order 10^{-5}) and the strong interaction would completely swamp the feeble weak process.

T violation associated to CP violation in the mixing [22] has been experimentally analyzed in K [23] and B mesons [24]. Here one looks whether the rate for a neutral K (B) meson tagged at its production as K^0 (B^0) and identified afterward as $\overline{K}^0$ ($\overline{B}^0$) is equal to the rate for the neutral particle tagged at its production as $\overline{K}^0$ ($\overline{B}^0$) and identified later as K^0 (B^0). Any difference in this case is both CP and T violating [22], because CP and T are experimentally identical for this process. The experimental results for kaons yielded a T-violating difference in these rates. Such a difference is proportional not only to the T-violating term of the $K^0\overline{K}^0$ matrix that defines the mass eigenstates in terms of the flavor eigenstates, but also to the width difference $\Delta\Gamma$ between the two mass eigenstates, thus T non-invariance would not be present in the limit $\Delta\Gamma \to 0$. Therefore, this asymmetry shows T violation proportional to $\Delta\Gamma$, time independent, experimentally identical to CP violation, thus it is not an independent T non-invariance test as one might like [16]. In the $B^0\overline{B}^0$ system no asymmetry has been yet found, as expected within the SM since in this case $\Delta\Gamma$ almost vanishes [25].

The largest CP-violating asymmetry in Nature has been found between the rate for $B^0 \to J/\psi K_S$ (and other similar CP-odd $c\overline{c}K_S$ final states, e.g., $\psi(2S)K_S$, $\chi_{c1}K_S$, or the CP-even $J/\psi K_L$ final state) and the CP-conjugate rate for $\overline{B}^0$ to decay to the same CP-eigenstate, which is originated in the interference between the time-dependent decay amplitudes with and without mixing [26, 27]. Here, CP violation arises because the mixing phase, i.e., the relative phase between the complex parameters defining the mass eigenstates in terms of the flavor eigenstates [28] minus the relative phase of the ratio of the amplitude for the decay and its CP conjugate, does not vanish. In the SM this phase difference is 2β, where β is the angle between the $V_{cd}V_{cb}^*$ and $V_{td}V_{tb}^*$ sides of the CKM unitarity triangle. At B factories the experimental studies are performed using the two B mesons produced in the antisymmetric coherent state from the $\Upsilon(4S)$ decay. One neutral B meson decays into a definite flavor state and the other is reconstructed in the CP-eigenstate final state of interest with a given decay time difference $\Delta t = t_{CP} - t_{\text{flavor}}$. The measured asymmetry is large, proportional to $\sin 2\beta \approx 0.7$, a time-odd dependent function that reverses sign between B^0 and $\overline{B}^0$ flavor identified events, and between $B^0 \to J/\psi K_S$ and $B^0 \to J/\psi K_L$ events with the same

flavor identified. This is a CP-violating effect. Since there is no reversal of *in* and *out* states, this time asymmetry cannot be interpreted as genuine T violation.

We have justified in this Section that there is no current T violating experiment, which clearly shows T non-invariance without any experimental nor theoretical connection to CP through the exchange of $initial$ and $final$ states. The main goal of this thesis is the study of discrete symmetries in entangled neutral systems. The Einstein-Podolsky-Rosen entanglement [29], as we will explain later, is the key ingredient which will allow us to perform the first direct observation of T Violation in the sense we have delineated above.

2. DISCRETE SYMMETRIES STUDIES IN THE NEUTRAL B MESON SYSTEM

In this Chapter, we describe a methodology that makes use of the Einstein-Podolsky-Rosen (EPR) entanglement [29] available at B factories to perform studies of CP, CPT and specially T, in the neutral B meson system[1]. The method relies precisely on the possibility for preparing the quantum mechanical individual state of the neutral B meson by the observation of particular decay channels of its orthogonal entangled partner, and studying the time evolution of the filtered state of the still living meson. This strategy allows the interchange of initial and final states for a given process, as needed for a genuine test of T non-invariance. The basic ideas of this methodology have been presented previously [30] and scrutinized later [8, 16, 31, 32], the discussion of the steps to implement these concepts into a B-factory experiment able to produce the desired result has been presented [2] and observed in the neutral B meson system [3] last year. Another aim of this Chapter is the presentation and discussion of the Weisskopf-Wigner approximation which will allow us to have an effective description of any neutral meson system which mixes and decays. Through this formalism we will obtain the probability density functions (PDF) for the different decay rates required to obtain the results presented in Ref. [3].

2.1 Symmetry studies in entangled neutral B meson system

In this Section we are going to focus on how to exploit the entanglement produced in a B factory operating at the $\Upsilon(4S)$ peak to perform CP, CPT and T studies.

In the decay of the $\Upsilon(4S)$, the two B mesons are in an entangled antisymmetric state, as required by angular momentum conservation for a P-wave particle system. This two-body state is usually written in terms of the flavor

[1] In the course of this thesis we will refer as the neutral B meson system to the neutral B_d meson system, furthermore whenever we talk about $B^0(\overline{B}^0)$ we mean B^0_d ($\bar{B}^0_d$), unless otherwise is specified.

eigenstates[2],

$$|i\rangle = \frac{1}{\sqrt{2}}[B^0(t_1)\overline{B}^0(t_2) - \overline{B}^0(t_1)B^0(t_2)] \ , \tag{2.1}$$

but can also be expressed in terms of any linear combination of $|B^0\rangle$ and $|\overline{B}^0\rangle$, such as $|B_+\rangle$ $|B_-\rangle$ projected by *CP* final states [36],

$$|i\rangle = \frac{1}{\sqrt{2}}[B_+(t_1)B_-(t_2) - B_-(t_1)B_+(t_2)] \ . \tag{2.2}$$

In these Eqs t_1 and t_2 are the labels to specify the states "1" and "2" of each neutral B meson by means of the time of its future decay, with $\Delta\tau = t_2 - t_1 > 0$. The antisymmetry remains invariant with the time evolution, including mixing, before the first decay at t_1. In Eq. (2.2), B_- is the neutral B state filtered by its decay to $J/\psi K_+$, K_+ being the neutral K state filtered by its decay to $\pi\pi$, and B_+ is orthogonal to B_-, not connected to $J/\psi K_+$. Analogously, B_+ is the state connected to J/ψ K_- experimentally filtered by the state $J/\psi K_L$. Similarly, in Eq. (2.1), $\overline{B}^0$ (B^0) is the neutral B state filtered by its decay to $\ell^- X$ ($\ell^+ X$) , for example a semileptonic decay with a negatively (positively) charged lepton or a hadronic final state containing a D^+ (D^-) or D^{*+} (D^{*-}) meson.

Therefore, in addition to the *flavor tagging* used in standard *CP* studies at B factory experiments [26, 37], we can apply a *CP tagging* [36] to one of the B mesons decaying into the *CP*-odd final state $J/\psi K_s$, preparing the orthogonal B meson as B_+ state at the initial time t_1. Afterward it decays at t_2 and is reconstructed in the flavor (B^0 or $\overline{B}^0$) final state of interest ($\ell^+ X$ or $\ell^- X$, respectively). These combinations of flavor and *CP* tags allow to filter initial and final states to compare, for example, the rate for a $\overline{B}^0$ evolving to B_- ($\ell^+ X$ decay product of the B partner first, $J/\psi K_S$ final state later) with the rate for a B_- evolving to $\overline{B}^0$ ($J/\psi K_L$ decay product of the B partner first, $\ell^- X$ final state later). The relation between these T-conjugated transitions and the reconstructed final states in the experimental B factory scheme is illustrated in Fig. 2.1. The comparison between the time evolution of the neutral B meson from its preparation as $\overline{B}^0$ until its decay as B_-, $\overline{B}^0(t_1) \to B_-(t_2)$, and its T transformed $B_-(t_1) \to \overline{B}^0(t_2)$ is a test of T symmetry.

There are other three independent comparisons between T-conjugated processes, as summarized in Table 2.1. A non-vanishing asymmetry in the

[2] Implicitly we have assumed *CPT* at a microscopic level here. According to Wald's theorem [33], if *CPT* is not a well-defined operator, due to quantum gravity, extra contamination from terms involving B^0B^0 or $\overline{B}^0\overline{B}^0$ pairs will appear in Eq. (2.1) proportional to ω [34]. We do not include this effect, or any further correction to EPR, as the data collected by the B-factories is not sensitive [35].

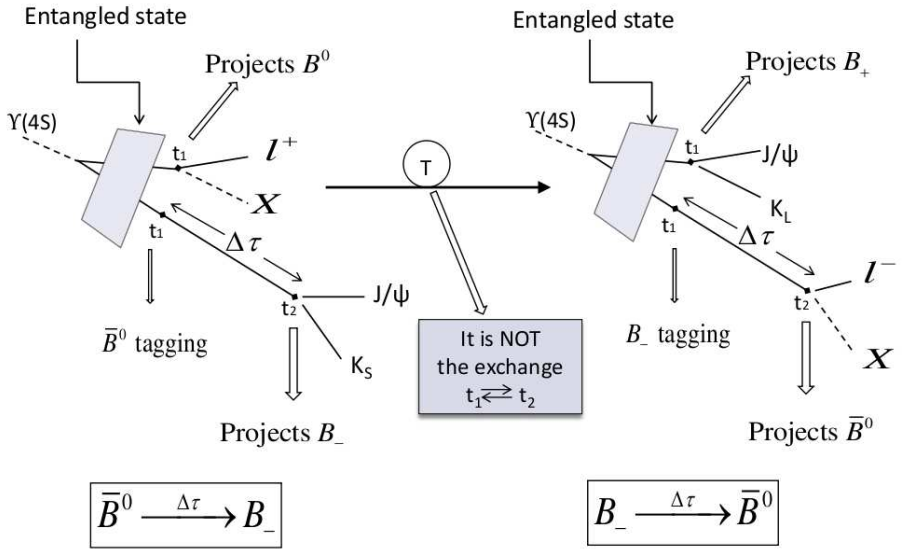

Fig. 2.1: Sketch of two T-conjugate transitions in an experimental B factory scheme. The observation of the final states associated to the T-transformed transitions is divided into three well defined steps. We first observe the decay of one of the entangled B particles, produced in the $\Upsilon(4S)$ decay, into a definite flavor (or a definite CP) decay products at t_1, preparing the state of the other entangled B particle, which has not yet decayed at t_1, into its orthogonal state. This tagged B meson state evolves in time to finally decay at $t_2 > t_1$ into a CP (or a flavor) final state. It should be noted that T asymmetry is clearly different from the Δt ($t_1 \leftrightarrow t_2$) exchange and CP asymmetries. In fact, in the former we require to compare the reference transition $\overline{B}^0 \to B_-$, flavor-tagged by ℓ^+X and decayed to $J/\psi K_S$ (ℓ^+X,$J/\psi K_S$), to the transition $B_- \to \overline{B}^0$, CP-tagged by $J/\psi K_L$ and decayed to ℓ^-X ($J/\psi K_L$,ℓ^-X), whereas for Δt exchange and CP asymmetries the reference decay products must be compared to ($J/\psi K_S$,ℓ^+X) and (ℓ^-X,$J/\psi K_S$), respectively.

rates for any pair of T-conjugated transitions thus constitutes a direct and independent observation of T violation, in the sense discussed previously.

We can also apply this methodology for similar tests of CP violation and CPT invariance, providing a proof that T non-invariance is compensated by CP violation. Tables (2.2) and (2.3) summarize all the possible comparisons

Reference		T conjugate	
Transition	Final state	Transition	Final state
$\overline{B}^0 \to B_-$	$(\ell^+X, J/\psi K_S)$	$B_- \to \overline{B}^0$	$(J/\psi K_L, \ell^-X)$
$B_+ \to B^0$	$(J/\psi K_S, \ell^+X)$	$B^0 \to B_+$	$(\ell^-X, J/\psi K_L)$
$\overline{B}^0 \to B_+$	$(\ell^+X, J/\psi K_L)$	$B_+ \to \overline{B}^0$	$(J/\psi K_S, \ell^-X)$
$B_- \to B^0$	$(J/\psi K_L, \ell^+X)$	$B^0 \to B_-$	$(\ell^-X, J/\psi K_S)$

Tab. 2.1: Possible comparisons between T-conjugated transitions and the associated time-ordered decay products in the experimental B factory scheme.

of *CP*- and *CPT*-conjugated transitions, together with the corresponding final states. As anticipated, the transitions involved in the experimental tests of *CP* and T symmetries are different. For example, a test of *CP* symmetry can be done with the $J/\psi K_S$ final state only. On the contrary, a test of T invariance necessarily involves both $J/\psi K_S$ and $J/\psi K_L$ final states. Furthermore, one may check that none of all comparisons between T-, *CP*-, or *CPT*-conjugated transitions in Tables 2.1, 2.2, and 2.3, respectively, corresponds to exchange of the decay products at t_1 and t_2.

Reference		*CP* conjugate	
Transition	Final state	Transition	Final state
$\overline{B}^0 \to B_-$	$(\ell^+X, J/\psi K_S)$	$B^0 \to B_-$	$(\ell^-X, J/\psi K_S)$
$B_+ \to B^0$	$(J/\psi K_S, \ell^+X)$	$B_+ \to \overline{B}^0$	$(J/\psi K_S, \ell^-X)$
$\overline{B}^0 \to B_+$	$(\ell^+X, J/\psi K_L)$	$B^0 \to B_+$	$(\ell^-X, J/\psi K_L)$
$B_- \to B^0$	$(J/\psi K_L, \ell^+X)$	$B_- \to \overline{B}^0$	$(J/\psi K_L, \ell^-X)$

Tab. 2.2: Possible comparisons between *CP*-conjugated transitions and the associated time-ordered decay products in the experimental B factory scheme.

2.2 The $|B_-\rangle$ and $|B_+\rangle$ states

The $|B_-\rangle$, $|B_+\rangle$ states are experimentally identified as those filtered by the observation of the decay to definite *CP* eigenstates. The only requirement needed for the analysis is their existence, independent of the underlying the-

Reference		*CPT* conjugate	
Transition	Final state	Transition	Final state
$\overline{B}^0 \to B_-$	$(\ell^+X, J/\psi K_S)$	$B_- \to B^0$	$(J/\psi K_L, \ell^+X)$
$B_+ \to B^0$	$(J/\psi K_S, \ell^+X)$	$\overline{B}^0 \to B_+$	$(\ell^+X, J/\psi K_L)$
$B^0 \to B_-$	$(\ell^-X, J/\psi K_S)$	$B_- \to \overline{B}^0$	$(J/\psi K_L, \ell^-X)$
$B_+ \to \overline{B}^0$	$(J/\psi K_S, \ell^-X)$	$B^0 \to B_+$	$(\ell^-X, J/\psi K_L)$

Tab. 2.3: Possible comparisons between *CPT*-conjugated transitions and the associated time-ordered decay products in the experimental B factory scheme.

ory (*CPT* invariant or not), with the orthogonality property $\langle B_-|B_+\rangle = 0$. In this Section we construct these states explicitly.

Neutral kaons decaying inside the geometrical acceptance of detectors surrounding their production point are usually reconstructed through their decay into two pions. Thus we can first define $|B_-\rangle$ as the state filtered by the decay into $J/\psi K_+$, K_+ being the neutral K state decaying to $\pi\pi$, a pure *CP*-odd state. The state $|\tilde{B}_+\rangle$ is then defined as the state orthogonal to $|B_-\rangle$, $\langle\tilde{B}_+|B_-\rangle = 0$, which cannot decay into the $J/\psi\pi\pi$ final state, $\langle J/\psi\pi\pi|T|\tilde{B}_+\rangle = 0$, where T is the transition operator. The state $|\tilde{B}_+\rangle$ can be written in terms of flavor eigenstates as

$$|\tilde{B}_+\rangle \equiv \widetilde{\mathrm{N}}_+ \left[|B^0\rangle - \alpha|\overline{B}^0\rangle\right], \tag{2.3}$$

where $\alpha = \dfrac{\langle J/\psi\pi\pi|T|B^0\rangle}{\langle J/\psi\pi\pi|T|\overline{B}^0\rangle}$ and $\widetilde{\mathrm{N}}_+$ is a normalization constant. Since $|B_-\rangle$ is orthogonal to $|\tilde{B}_+\rangle$ it then follows

$$|B_-\rangle = \mathrm{N}_- \left[|\overline{B}^0\rangle + \alpha^*|B^0\rangle\right]. \tag{2.4}$$

Analogously, we define $|B_+\rangle$ as the state filtered by the decay into $J/\psi K_L$, a *CP*-even state up to $\mathcal{O}(10^{-3})$ due to *CP* violation in the neutral kaon system. We note that we could have defined $|B_+\rangle$ through its decay to $J/\psi K_-$, $K_- \to \pi^0\pi^0\pi^0$, in this case a pure *CP*-even state, but this final state cannot be reconstructed since long-lived neutral kaons tend to interact hadronically inside the detectors before they can undergo decay. Of course, both definitions become operationally identical when *CP* violation in neutral kaons is neglected. The state $|\tilde{B}_-\rangle$, defined as its orthogonal state, $\langle\tilde{B}_-|B_+\rangle = 0$ and $\langle J/\psi K_L|T|\tilde{B}_-\rangle = 0$, is

$$|\tilde{B}_-\rangle \equiv \widetilde{\mathrm{N}}_- \left[|B^0\rangle - \beta|\overline{B}^0\rangle\right], \tag{2.5}$$

where $\beta = \dfrac{\langle J/\psi K_L|T|B^0\rangle}{\langle J/\psi K_L|T|\overline{B}^0\rangle}$. Therefore the state $|B_+\rangle$ can be explicitly written as

$$|B_+\rangle = \mathrm{N}_+ \left[|\overline{B}^0\rangle + \beta^*|B^0\rangle\right] . \tag{2.6}$$

Let us note that here we keep separate the definitions of the states $|B_-\rangle$ and $|B_+\rangle$, which are observed through their decays to the $J/\psi\pi\pi$ and $J/\psi K_L$ final states, from the states $|\tilde{B}_-\rangle$ and $|\tilde{B}_+\rangle$, produced exploiting the EPR correlations in the entangled $B\overline{B}$ system. The two bases are the same when the orthogonality condition $\langle B_-|B_+\rangle = 0$ is fulfilled. As α and β correspond to opposite CP final states, we have $\alpha\beta^* = -1$ when only one weak amplitude is responsible of the decay ($|\alpha| = |\beta| = 1$). Consequently as all these considerations apply to our experimental framework,

$$\langle B_-|B_+\rangle = 1 + \alpha\beta^* = 0 , \tag{2.7}$$

which was to be demonstrated.

2.3 Neutral meson system formulation

In this Section, we are going to discuss a formalism to study the mixing and decays of neutral meson systems focusing on the B^0 and $\overline{B}^0$ neutral mesons. In general, the formalism described here can be used to delineate any neutral meson system denoted as P^0 and $\bar{P}^0$, where P^0 and $\bar{P}^0$ are in general distinguished by an internal quantum number F conserved by strong and electromagnetic interactions but not conserved by weak interactions, e.g., flavor.

In principle we consider the time evolution of the B^0 and $\overline{B}^0$ system including its decays of a state in the most general form

$$|\Psi(t)\rangle = a(t)|B^0\rangle + b(t)|\overline{B}^0\rangle + c(t)|f_1\rangle + d(t)|f_2\rangle + ... , \tag{2.8}$$

where f_1, f_2, and so on, are the states to which either B^0 or $\overline{B}^0$ may decay, and t is the time measured in the B^0 $-\overline{B}^0$ rest frame. This time evolution in general is beyond our capabilities, but we can achieve a great simplification if we reduce our demands to the following scenario [38, 39, 40]:

- The initial state $|\Psi(0)\rangle$ is a combination of B^0 and $\overline{B}^0$, thus only $a(0)$ and $b(0)$ are different from 0.
- We want only to compute the values of $a(t)$ and $b(t)$ and not the values of any other coefficients.

- We restrict ourselves to times that are much larger than a typical strong interaction scale. This is called the Weisskopf-Wigner approximation (WWA) [41].

With these simplifications we can write[3]

$$\frac{d}{dt}|\psi(t)\rangle = -i\mathcal{H}|\psi(t)\rangle \ , \tag{2.9}$$

where $|\psi(t)\rangle$ is a two component wave function

$$|\psi(t)\rangle = a(t)|B^0\rangle + b(t)|\overline{B}^0\rangle \ , \tag{2.10}$$

and the 2×2 Hamiltonian matrix $\mathcal{H}$ is given by

$$\mathcal{H} = M - \frac{i}{2}\Gamma = \begin{pmatrix} M_{11} - \frac{i}{2}\Gamma_{11} & M_{12} - \frac{i}{2}\Gamma_{12} \\ M_{21} - \frac{i}{2}\Gamma_{21} & M_{22} - \frac{i}{2}\Gamma_{22} \end{pmatrix} \ . \tag{2.11}$$

$\mathcal{H}$ is not Hermitian, but M and Γ are 2×2 Hermitian matrices, describing respectively the mass and the decay-rate components defined by

$$M = \frac{1}{2}\big(\mathcal{H} + \mathcal{H}^\dagger\big) \ , \tag{2.12}$$

$$\Gamma = i\big(\mathcal{H} - \mathcal{H}^\dagger\big) \ . \tag{2.13}$$

Up to second order in perturbation theory the elements of the matrices M and Γ are given by

$$M_{ij} = m_0\delta_{ij} + \langle i|\mathcal{H}_W|j\rangle + \sum_n P\frac{\langle i|\mathcal{H}_W|n\rangle\langle n|\mathcal{H}_W|j\rangle}{m_0 - E_n} \ , \tag{2.14}$$

$$\Gamma_{ij} = 2\pi\sum_n \delta(m_0 - E_n)\langle i|\mathcal{H}_W|n\rangle\langle n|\mathcal{H}_W|j\rangle \ , \tag{2.15}$$

where P projects out the principal part and $\mathcal{H}_W$ is the weak component which induces a transition between B^0 and $\overline{B}^0$ as one step process, i.e., an iteration of two reactions $\Delta F = 1$ through an intermediate state.

[3] We use natural units all along the thesis $\hbar = c = 1$

2.3.1 Constrains on $\mathcal{H}$ elements from CPT, CP, and T

The CP transformation interchanges B^0 and $\overline{B}^0$. Choosing $CP^2 = 1$,

$$\begin{aligned} CP|B^0\rangle &= e^{i\epsilon}|\overline{B}^0\rangle \ , \\ CP|\overline{B}^0\rangle &= e^{-i\epsilon}|B^0\rangle \ . \end{aligned} \tag{2.16}$$

Analogously,

$$\begin{aligned} CPT|B^0\rangle &= e^{i\nu}|\overline{B}^0\rangle \ , \\ CPT|\overline{B}^0\rangle &= e^{i\nu}|B^0\rangle \ . \end{aligned} \tag{2.17}$$

From Eqs (2.16) and (2.17) we get

$$\begin{aligned} T|B^0\rangle &= e^{i(\nu-\epsilon)}|B^0\rangle \ , \\ T|\overline{B}^0\rangle &= e^{i(\nu+\epsilon)}|\overline{B}^0\rangle \ . \end{aligned} \tag{2.18}$$

To simplify the expressions of CPT and T conjugations, Eqs (2.17) and (2.18), we have assumed that the "in" and "out" states form equivalent complete bases (n), where the antiunitary character of CPT and T has been taken into account. This assumption is not needed for CP as it does not relate 'in" and "out" states. With the previous ingredients we can easily derive the constrain on Table 2.4 on the matrix elements of $\mathcal{H}$ due to the conservation of discrete symmetries.

Symmetry	Matrix elements condition
CPT	$M_{11} = M_{22}$ and $\Gamma_{11} = \Gamma_{22}$
CP	$M_{11} = M_{22}$, $\Gamma_{11} = \Gamma_{22}$, $M_{21} = e^{i2\epsilon}M_{12}$, and $\Gamma_{21} = e^{i2\epsilon}\Gamma_{12}$
T	$M_{21} = e^{i2\epsilon}M_{12}$, and $\Gamma_{21} = e^{i2\epsilon}\Gamma_{12}$

Tab. 2.4: Effects of the discrete symmetries on the matrix elements of $\mathcal{H}$.

2.3.2 The "mass" eigenstates

Equation (2.9) is best solved diagonalizing the matrix $\mathcal{H}$. In principle this diagonalization is not trivial, because in general M and Γ are not compatible ($[M, \Gamma] \neq 0$), therefore $\mathcal{H}$ cannot be diagonalized by an unitary transformation as there are different unitary transformations for M and Γ. The simultaneous presence of CP violation in the mass matrix M and a difference of lifetimes in the antihermitian matrix Γ leads to a quantum incompatibility

between M and Γ. In this situation the eigenvectors obtained are not orthogonal, lacking physical meaning and preventing a consistent probabilistic interpretation. Fortunately in the case of neutral B mesons $\Delta\Gamma \approx 0$, circumventing the problem. Conversely, as the neutral K mesons are described by a non normal Hamiltonian, we shall discuss a method to avoid using the eigenvectors obtained diagonalizing $\mathcal{H}$ recovering a consistent probabilistic interpretation for this system, this method will be delineated in Chapter 6.

The mass eigenvalues $m_{H,L}$ and decay rates $\Gamma_{H,L}$ of the two eigenstates of $\mathcal{H}$ form the complex eigenvalues $\omega_{H,L}$,

$$\begin{aligned} \omega_{H,L} &\equiv m_{H,L} - \frac{i}{2}\Gamma_{H,L} \\ &= m - \frac{i}{2}\Gamma \pm \sqrt{\left(M_{12} - \frac{i}{2}\Gamma_{12}\right)\left(M_{12}^* - \frac{i}{2}\Gamma_{12}^*\right) + \frac{1}{4}\left(\delta m - \frac{i}{2}\delta\Gamma\right)^2} , \end{aligned} \tag{2.19}$$

where the real part of the square root is taken to be positive and we have defined

$$\begin{aligned} m &\equiv \frac{1}{2}(M_{11} + M_{22}) , & \Gamma &\equiv \frac{1}{2}(\Gamma_{11} + \Gamma_{22}) , \\ \delta m &\equiv M_{11} - M_{22} , & \delta\Gamma &\equiv \Gamma_{11} - \Gamma_{22} , \\ \Delta\Gamma &\equiv \Gamma_H - \Gamma_L , & \Delta m &\equiv m_H - m_L . \end{aligned}$$

With these definitions, Δm is the mass of the heavier eigenstate minus the mass of the lighter one. Thus, $\Delta\Gamma$ is the decay rates of the heavier state minus the decay rate of the lighter one and its sign is not known a priory.

The eigenvectors of $\mathcal{H}$ may be written as

$$\begin{aligned} |B_H\rangle &= p_H|B^0\rangle + q_H|\overline{B}^0\rangle , \\ |B_L\rangle &= p_L|B^0\rangle - q_L|\overline{B}^0\rangle . \end{aligned} \tag{2.20}$$

We have required the normalization condition on the definition of the coefficients p_H, q_H, p_L, and q_L. The diagonalization of $\mathcal{H}$ fixes the ratios

$$\begin{aligned} \frac{q_H}{p_H} &= \frac{\Delta\omega(1+\delta)}{2\mathcal{H}_{12}} = \frac{2\mathcal{H}_{21}}{\Delta\omega(1-\delta)} , \\ \frac{q_L}{p_L} &= \frac{\Delta\omega(1-\delta)}{2\mathcal{H}_{12}} = \frac{2\mathcal{H}_{21}}{\Delta\omega(1+\delta)} , \end{aligned} \tag{2.21}$$

where $\Delta\omega = \omega_H - \omega_L$ and $\delta = (\mathcal{H}_{22} - \mathcal{H}_{11})/\Delta\omega$. δ is a CPT and CP violating parameter as discussed in Table (2.4).

The time evolution of the mass eigenstates is given by

$$\begin{aligned} |B_H(t)\rangle &= e^{-i\omega_H t}|B_H\rangle = e^{-im_H t}e^{-\Gamma_H t/2}|B_H\rangle \ , \\ |B_L(t)\rangle &= e^{-i\omega_L t}|B_L\rangle = e^{-im_L t}e^{-\Gamma_L t/2}|B_L\rangle \ . \end{aligned} \tag{2.22}$$

The time t is measured in the rest frame of the decaying particle.

In general the bracket $\langle B_H|B_L\rangle$ is different from 0 as $\mathcal{H}$ is not Hermitian. Only if M and Γ commute the bracket is equal to zero. Despite this situation is not relevant for the B meson system, it is interesting to discuss it in the most general way.

$$\begin{aligned} |\langle B_H|B_L\rangle|^2 &= \frac{1+|q_H/p_H|^2|q_L/p_L|^2 - 2Re[(q_H/p_H)(q_L/p_L)^*]}{(1+|q_H/p_H|^2)(1+|q_L/p_L|^2)} \\ &= \frac{2|\mathcal{H}_{12}|^2 + 2|\mathcal{H}_{21}|^2 - |\Delta\omega|^2(1-|\delta|^2)}{2|\mathcal{H}_{12}|^2 + 2|\mathcal{H}_{21}|^2 + |\Delta\omega|^2(1+|\delta|^2)} \ . \end{aligned} \tag{2.23}$$

Therefore, $\langle B_H|B_L\rangle$ will vanish if $Im\delta = 0$ and $|\mathcal{H}_{21}| - |\mathcal{H}_{12}| = 0$, e.g., requiring *CP* invariance in the mixing we imply $\langle B_H|B_L\rangle = 0$, although the converse is not true.

2.3.3 *CPT* invariant case

As all present tests of *CPT* invariance confirm the validity of this symmetry, particularly in the neutral kaon system where there are strong limits [14, 15], we will dedicate this Section to the study of this particular scenario. Any signal of *CPT* violation in the mixing will be manifested through $\delta \neq 0$, where the phase convention independent parameter δ is defined as

$$\begin{aligned} \delta \equiv \frac{\mathcal{H}_{22}-\mathcal{H}_{11}}{\Delta\omega} &= \frac{\delta m - \frac{i}{2}\delta\Gamma}{2\sqrt{\left(M_{12}-\frac{i}{2}\Gamma_{12}\right)\left(M_{12}^*-\frac{i}{2}\Gamma_{12}^*\right)+\frac{1}{4}\left(\delta m-\frac{i}{2}\delta\Gamma\right)^2}} \\ &= \frac{\delta m - \frac{i}{2}\delta\Gamma}{\Delta m - \frac{i}{2}\Delta\Gamma} \ . \end{aligned} \tag{2.24}$$

From Eq. (2.21) we can deduce that when *CPT* is conserved ($\delta = 0$),

$$\frac{q_H}{p_H} = \frac{q_L}{p_L} \equiv \frac{q}{p} \ , \tag{2.25}$$

Note that this expressions fixes the relative phase of p_L and p_H to zero. Therefore,

$$\begin{aligned} |B_H\rangle &= p|B^0\rangle + q|\overline{B}^0\rangle \ , \\ |B_L\rangle &= p|B^0\rangle - q|\overline{B}^0\rangle \ . \end{aligned} \tag{2.26}$$

It is important to remark that, if we interchange $|B_H\rangle$ and $|B_L\rangle$ in Eq. (2.26), we have $q/p \to -q/p$, $\Delta m \to -\Delta m$, and $\Delta\Gamma \to -\Delta\Gamma$. Thus we need to choose a convention, i.e., $\Delta m > 0$. With this convention the eigenvalues are

$$\omega_{H,L} = m - \frac{i}{2}\Gamma \pm \sqrt{\left(M_{12} - \frac{i}{2}\Gamma_{12}\right)\left(M_{12}^* - \frac{i}{2}\Gamma_{12}^*\right)} \ , \tag{2.27}$$

and

$$\Delta\omega = 2\sqrt{\left(M_{12} - \frac{i}{2}\Gamma_{12}\right)\left(M_{12}^* - \frac{i}{2}\Gamma_{12}^*\right)} \ . \tag{2.28}$$

From Eq. (2.21) we derive

$$\frac{q}{p} = \frac{\Delta\omega}{2\mathcal{H}_{12}} = \frac{2\mathcal{H}_{21}}{\Delta\omega} = \sqrt{\frac{\mathcal{H}_{21}}{\mathcal{H}_{12}}} \ . \tag{2.29}$$

For the B meson system this magnitude is nearly the unity:

$$\left|\frac{q}{p}\right|^2 \approx 1 - Im\frac{\Gamma_{12}}{M_{12}} \ . \tag{2.30}$$

In the Standard Model (SM), the CP and T-violating quantity $|q/p|^2 - 1$ for the B mesons is small not just because $|\Gamma_{12}|$ is small, but additionally because the CP-violating quantity $Im(\Gamma_{12}/M_{12})$ is suppressed by an additional factor $(m_c^2 - m_u^2)/m_b^2 \approx 0.1$ relative to $|\Gamma_{12}/M_{12}|$.

Once we have assumed the phase convention between $|B_H\rangle$ and $|B_L\rangle$, the bracket $\langle B_L|B_H\rangle$ becomes real.

2.3.4 Decays

Until now we have just discussed the mixing. In this Section we are going to study the time evolution of the B^0 and $\overline{B}^0$ states to certain final states. For simplicity we will assume the CPT invariant case. Nevertheless, we will give some hints on how to treat the decays in the non-CPT invariant case and solve it in a coherent formalism context in Sec. 2.3.5.

The time evolution of B^0 and $\overline{B}^0$ states is described by

$$\begin{aligned} |B^0(t)> &= g_+(t)|B^0> + \frac{q}{p} g_-(t)|\overline{B}^0> , \\ |\overline{B}^0(t)> &= g_+(t)|\overline{B}^0> + \frac{p}{q} g_-(t)|B^0> , \end{aligned} \tag{2.31}$$

where we have introduced

$$g_\pm(t) \equiv \frac{1}{2}\Big(e^{-i\omega_H t} \pm e^{-i\omega_L t}\Big) . \tag{2.32}$$

Let us now define the amplitude decay of a B^0 and $\overline{B}^0$ to a certain final states A_f and $\bar{A}_f$ respectively, i.e.,

$$\begin{aligned} A_f &\equiv \langle f|T|B^0\rangle , \\ \bar{A}_f &\equiv \langle f|T|\overline{B}^0\rangle . \end{aligned} \tag{2.33}$$

Using these ingredients we can derive

$$\begin{aligned} \Gamma[B^0(t) \to f] \quad &\propto e^{-\Gamma_H t}|A_f|^2\Big\{1 + e^{\Delta\Gamma t} + 2e^{\frac{1}{2}\Delta\Gamma t}\cos(\Delta m t) \\ &\quad + |\lambda_f|^2\big[1 + e^{\Delta\Gamma t} - 2e^{\frac{1}{2}\Delta\Gamma t}\cos(\Delta m t)\big] \\ &\quad + 2\mathcal{R}e\Big(\lambda_f\big[1 - e^{\Delta\Gamma t} - 2ie^{\frac{1}{2}\Delta\Gamma t}\sin(\Delta m t)\big]\Big)\Big\} , \end{aligned} \tag{2.34}$$

$$\begin{aligned} \Gamma[\overline{B}^0(t) \to f] \quad &\propto e^{-\Gamma_H t}|\bar{A}_f|^2\Big\{1 + e^{\Delta\Gamma t} + 2e^{\frac{1}{2}\Delta\Gamma t}\cos(\Delta m t) \\ &\quad + |\lambda_f|^{-2}\big[1 + e^{\Delta\Gamma t} - 2e^{\frac{1}{2}\Delta\Gamma t}\cos(\Delta m t)\big] \\ &\quad + 2\mathcal{R}e\Big(\lambda_f^{-1}\big[1 - e^{\Delta\Gamma t} - 2ie^{\frac{1}{2}\Delta\Gamma t}\sin(\Delta m t)\big]\Big)\Big\} , \end{aligned} \tag{2.35}$$

where we have defined

$$\lambda_f \equiv \frac{q}{p}\frac{\bar{A}_f}{A_f} . \tag{2.36}$$

The generalizations of the eigenstates in Eq. (2.31) when we account for CPT violation can be written as

$$\begin{aligned} |B_H> &= p\sqrt{1-\delta}|B^0> + q\sqrt{1+\delta}|\overline{B}^0> , \\ |B_L> &= p\sqrt{1+\delta}|B^0> - q\sqrt{1-\delta}|\overline{B}^0> , \end{aligned} \tag{2.37}$$

where we maintain the definition of q/p given in Eq. (2.25) but using a new normalization. The result, when time evolution is included, is that states that begin as purely B^0 or $\overline{B}^0$ after a time t will be mixtures

$$\begin{aligned} |B^0_{phys}(t)> &= [g_+(t) + \delta g_-(t)]|B^0> - \sqrt{1-\delta^2}\frac{q}{p} g_-(t)|\overline{B}^0> , \\ |\overline{B}^0_{phys}(t)> &= [g_+(t) - \delta g_-(t)]|\overline{B}^0> - \sqrt{1-\delta^2}\frac{p}{q} g_-(t)|B^0> \ . \end{aligned} \tag{2.38}$$

It can be studied that the physical observables, the rephasing-invariant quantities, in a neutral meson system which mixes and decays are

$$\left|\frac{q}{p}\right|,\ |A_f|,\ |\bar{A}_f|, \lambda_f,\ \text{and}\ \delta. \tag{2.39}$$

Attending to the values of these observables we can qualify the sources of *CP* violation as follows [6]:

- *CP* violation in the mixing (indirect *CP* violation). This occurs whenever $\left|\frac{q}{p}\right| \neq 1$, i.e., when we have absorptive parts ($\Gamma_{12} \neq 0$).
- *CP* violation in the decay (direct *CP* violation). This kind of *CP* violation requires $|A_f| \neq |\bar{A}_{\bar{f}}|$, which is equivalent to $|A_{\bar{f}}| \neq |\bar{A}_f|$, this requirement can only achieved if there are at least two interfering amplitudes with different weak phases and different strong phases.
- *CP* violation in the interference between the mixing and the decay amplitudes (interference *CP* violation), as shown in Fig. 2.2. It occurs whenever $arg\lambda_f + arg\lambda_{\bar{f}} \neq 0$. If f is a *CP* eigenstate, this is equivalent to $\mathcal{I}m\lambda_f \neq 0$.

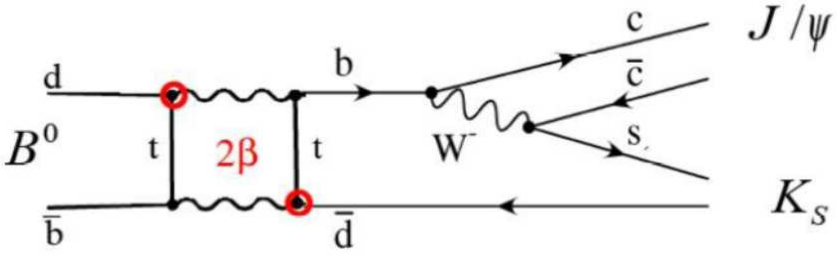

Fig. 2.2: Diagram describing *CP* violation in the interference between the time dependent amplitudes with or without mixing. This diagram illustrates the process $B^0 \to J/\psi K_S$ through the mixing $B^0 \to \overline{B}^0$, this process interferes with the same one without the mixing to $\overline{B}^0$. The phase difference in the SM is 2β, where β is the angle between the $V_{td}V_{tb}^*$ and $V_{cd}V_{cb}^*$ sides of the CKM unitary triangle.

As we did in the Sec. 1.5, in the *CPT* invariant case ($\delta = 0$) and only through the interpretation of the formalism, these manifestations of the *CP* violation sources can be understood as manifestations of T violation. We

have to keep in mind that measuring, e.g., $Im\lambda_f \neq 0$ is not an evidence of T violation by itself, only through the interpretation of the formalism assuming CPT invariance, because as it has been done until now $Im\lambda_f$ has been measured through a CP observable [37].

2.3.5 Time-dependent decay rates for coherent neutral mesons

At the $\Upsilon(4S)$ resonance, neutral B mesons are produced in coherent P-wave pairs, Eqs (2.1) and (2.2). We subsequently observe one B meson decay to the state f_1 at time t_1 and the other decay to the state f_2 at some later time t_2 ($\Delta\tau = t_2 - t_1 > 0$). We cannot in general know whether f_1 came from the decay of a B^0 or a $\overline{B}^0$, and similarly for the state f_2. If $A_{1,2}$ and $\bar{A}_{1,2}$ are the amplitudes for the decay of B^0 and $\overline{B}^0$ to the states f_1 and f_2, respectively, then the overall amplitude is given by

$$\mathcal{A} = a_+ g_+(\Delta\tau) + a_- g_-(\Delta\tau), \tag{2.40}$$

where

$$\begin{aligned} a_+ &= -A_1\bar{A}_2 + \bar{A}_1 A_2 \ , \\ a_- &= \sqrt{1-\delta^2}\left[\frac{p}{q}A_1 A_2 - \frac{q}{p}\bar{A}_1\bar{A}_2\right] + \delta[A_1\bar{A}_2 + \bar{A}_1 A_2] \ . \end{aligned} \tag{2.41}$$

Using the relations

$$|g_\pm(\Delta\tau)|^2 = \frac{1}{2}e^{\Gamma\Delta\tau}[\cosh(\Delta\Gamma\Delta\tau/2) \pm \cos(\Delta m\Delta\tau)] \tag{2.42}$$

and

$$g_+^*(\Delta\tau)g_-(\Delta\tau) = -\frac{1}{2}e^{-\Gamma\Delta\tau}[\sinh(\Delta\Gamma\Delta\tau/2) + i\sin(\Delta m\Delta\tau)] \ , \tag{2.43}$$

we find the expression for the decay rate analogous to Eqs (2.34) and (2.35)

$$\begin{aligned} \frac{dN}{d\Delta\tau} \ \propto e^{-\Gamma|\Delta\tau|} \ \Big\{ & \frac{1}{2}c_+\cosh(\Delta\Gamma\Delta\tau/2) + \frac{1}{2}c_-\cos(\Delta m\Delta\tau) \\ & -Re(s)\sinh(\Delta\Gamma\Delta\tau/2) + Im(s)\sin(\Delta m\Delta\tau)\Big\} \ , \end{aligned} \tag{2.44}$$

where

$$c_\pm = |a_+|^2 \pm |a_-|^2 \qquad , \qquad s = a_+^* a_- \ . \tag{2.45}$$

Now let us take $f_1 \equiv f_{\text{flav}}$ to be the state that is flavor identified (B^0 or $\overline{B}^0$), and $f_2 \equiv f_{CP}$ to be the final state with definite CP content projecting

to B_+ or B_-. Generally we can reconstruct other states, e.g., flavor states, but we will focus on the final states projection onto B_+ and B_- as we are interested in the study of the amplitudes involving flavor and definite *CP* final states. A reconstructed flavor state cannot always be unambiguously associated with either B^0 or $\overline{B}^0$. Double-Cabibbo-Suppressed (DCS) decays, such as the hadronic decay $B^0 \to D^+\pi^-$ shown in Fig. 2.3, occur at a rate suppressed by roughly $|V_{ub}^* V_{cd}/V_{cb}^* V_{ud}| \approx (0.02)^2$. These DCS decays induce an interference with the dominant decay. Note that when we identify the flavor of our B through semileptonic decays they are not affected by this DCS. Corrections to the decay amplitudes to describe the experimental data due to the DCS effect will be explained in Sec. 4.2.2.

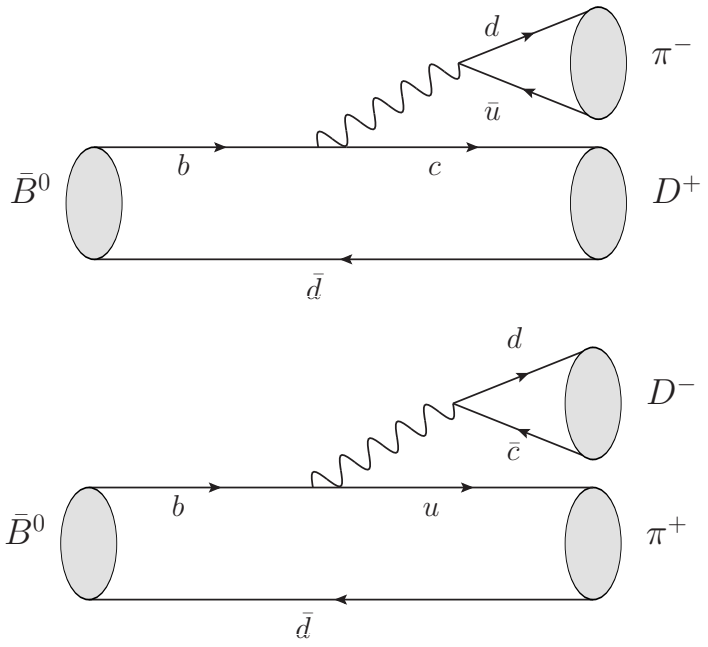

Fig. 2.3: The CKM-allowed ($\approx \lambda^2$) and CKM-suppressed ($\approx \lambda^4$) diagrams for $B \to D^{*\pm}\pi^{\mp}/\rho^{\mp}/a_1^{\mp}$ decays, where λ is the usual Wolfenstein parameter.

As not always the flavor decay occurs first ($f_1 \equiv f_{\text{flav}}$), we define $\Delta t_{\text{true}} \equiv t_{CP} - t_{\text{flav}}$ the proper time difference between the two B decays, which is a signed time quantity, i.e., Δt is positive or negative depending on whether the B which decayed first was into a flavor state or a *CP* state respectively. If the flavor decay does not occur first, i.e., it decays after the reconstructed

decay, the Eq. (2.44) is still valid changing $\Delta\tau \to -\Delta\tau$.

Using the new notation Eq. (2.41) becomes

$$\begin{aligned} a_+ &= -A_{\rm flav}\bar{A}_{CP} + \bar{A}_{\rm flav}A_{CP} \ , \\ a_- &= \sqrt{1-\delta^2}\left[\frac{p}{q}A_{\rm flav}A_{CP} - \frac{q}{p}\bar{A}_{\rm flav}\bar{A}_{CP}\right] + \delta[A_{\rm flav}\bar{A}_{CP} + \bar{A}_{\rm flav}A_{CP}] \ . \end{aligned} \tag{2.46}$$

The complete expressions for the real coefficients $c_\pm$ and the complex coefficient s, are

$$\begin{aligned} c_\pm = \Bigg\{ & |\bar{A}_{CP}A_{\rm flav} - A_{CP}\bar{A}_{\rm flav}|^2 \pm |\delta|^2|\bar{A}_{CP}A_{\rm flav} + A_{CP}\bar{A}_{\rm flav}|^2 \\ & \pm |1-\delta^2|\left|\frac{p}{q}A_{CP}A_{\rm flav} - \frac{q}{p}\bar{A}_{CP}\bar{A}_{\rm flav}\right|^2 \\ & \pm 2Re\left[\delta^*\sqrt{1-\delta^2}\left(\frac{p}{q}A_{CP}A_{\rm flav} - \frac{q}{p}\bar{A}_{CP}\bar{A}_{\rm flav}\right)(\bar{A}_{CP}A_{\rm flav} + A_{CP}\bar{A}_{\rm flav})^*\right]\Bigg\} \ , \end{aligned} \tag{2.47}$$

$$\begin{aligned} s = \Bigg\{ & (A_{CP}\bar{A}_{\rm flav} - \bar{A}_{CP}A_{\rm flav})^* \times \\ & \left[\sqrt{1-\delta^2}\left(\frac{p}{q}A_{CP}A_{\rm flav} - \frac{q}{p}\bar{A}_{CP}\bar{A}_{\rm flav}\right) + \delta(\bar{A}_{CP}A_{\rm flav} + A_{CP}\bar{A}_{\rm flav})\right]\Bigg\} \ . \end{aligned} \tag{2.48}$$

Terms proportional to $A_{CP}\bar{A}_{\rm flav}$ and $\bar{A}_{CP}A_{\rm flav}$ are associated with decays with no net oscillation between the two neutral B decays, while terms proportional to $(q/p)\bar{A}_{CP}\bar{A}_{\rm flav}$ and $(p/q)A_{CP}A_{\rm flav}$ represent a net oscillation. We characterize each final state f through the parameter λ_f defined in Eq. (2.36), where f can be "*CP*" or "flav". In the absence of DCS decays, would be either zero or infinite. If the final flavor state $f_{\rm flav}$ is ostensibly a B^0 then $|\lambda_{\rm flav}| \equiv |\lambda_{B^0}| \ll 1$. Conversely, if the reconstructed state appears to come from a $\overline{B}^0$, then $|\lambda_{\overline{B}^0}| \gg 1$, and it is convenient to introduce $\bar{\lambda}_{\bar{B}f} \equiv 1/\lambda_{\bar{B}f}$. For the case of definite *CP* final states, the $|\lambda_{CP}|$ is of order unity.

In practice, terms quadratic in δ or in a small λ_f are not important. The expressions for $c_\pm$ and s when only linear terms in small quantities are retained are shown in Tables 2.5, 2.6 and 2.7. From Eq. (2.44) and Tables 2.5, 2.6 and 2.7, it can be seen that while $Im\lambda_{CP}$, $Im\delta$, and $|q/p|$ are unambiguously determined, $Re\delta$ appears only in the product $Re\lambda_{CP}Re\delta$ or else is suppressed by the small factor $\Delta\Gamma/\Gamma$. Similarly, the sign of $\Delta\Gamma$ cannot be determined separately from the sign of $Re\lambda_{CP}$ since $\Delta\Gamma$ always appears multiplied by $Re\lambda_{CP}$ in its dominant contribution. Its value is known only

$B_{\rm flav}$	c_+
B^0	$\|A_{B^0}\|^2\|A_{CP}\|^2\|p/q\|^2[1+\|\lambda_{CP}\|^2-4Re(\lambda_{CP})Re(\lambda_{B^0})+ 2Re(\delta)Re(\lambda_{CP})-2Im(\delta)Im(\lambda_{CP})]$
$\overline{B}^0$	$\|\bar{A}_{\overline{B}^0}\|^2\|A_{CP}\|^2[1+\|\lambda_{CP}\|^2-4Re(\lambda_{CP})Re(\bar{\lambda}_{\overline{B}^0})- 2Re(\delta)Re(\lambda_{CP})-2Im(\delta)Im(\lambda_{CP})]$

Tab. 2.5: The coefficient c_+ from Eq. (2.47), evaluated to leading order in the small quantities δ, λ_{B^0}, and $\bar{\lambda}_{\overline{B}^0}$. The flavor identified B^0 ($\overline{B}^0$) observed state is ℓ^+X (ℓ^-X), for the *CP* final state we denote it generically by f_{CP}. The decay amplitudes are $A_{B^0}=\langle\ell^+X|H|B^0\rangle$, $\bar{A}_{B^0}=\langle\ell^+X|H|\overline{B}^0\rangle$, $A_{\overline{B}^0}=\langle\ell^-X|H|B^0\rangle$, $\bar{A}_{\overline{B}^0}=\langle\ell^-X|H|\overline{B}^0\rangle$, analogously for *CP* final states.

$B_{\rm flav}$	c_-
B^0	$\|A_{B^0}\|^2\|A_{CP}\|^2\|p/q\|^2[-1+\|\lambda_{CP}\|^2- 4Im(\lambda_{CP})Im(\lambda_{B^0})-2Re(\delta)Re(\lambda_{CP})+ 2Im(\delta)Im(\lambda_{CP})]$
$\overline{B}^0$	$\|A_{\overline{B}^0}\|^2\|A_{CP}\|^2[1-\|\lambda_{CP}\|^2+4Im(\lambda_{CP})Im(\bar{\lambda}_{\overline{B}^0})+ 2Re(\delta)Re(\lambda_{CP})+2Im(\delta)Im(\lambda_{CP})]$

Tab. 2.6: The coefficient c_- from Eq. (2.47), evaluated to leading order in the small quantities δ, λ_{B^0}, and $\bar{\lambda}_{\overline{B}^0}$. See the caption of Table 2.5 for the definition of the quantities.

through $Re\lambda_{CP}=\pm\sqrt{|\lambda_{CP}|^2-(Im\lambda_{CP})^2}$, where the choice of sign could be made by a separate measurement that directly determines the sign of $Re\lambda_{CP}$.

Once we know which are the decay rates expected in the WWA for the physical processes needed in the *CP*, *CPT*, and *T* comparisons, introduced in Tables 2.2, 2.3, and 2.1 respectively, we can extract the values of the different coefficients from the B-factories data. Any difference in the decay rate parameters between two *T* conjugate samples will be an evidence of *T* violation. Analogously for *CP* and *CPT*.

B_{flav}	s
B^0	$\lvert A_{B^0}\rvert^2 \lvert A_{CP}\rvert^2 \lvert p/q\rvert^2 [\lvert\lambda_{CP}\rvert^2 \lambda_{B^0} - \lambda^*_{CP} + \lambda^*_{B^0} - \lvert\lambda_{CP}\rvert^2]\delta$
$\overline{B}^0$	$\lvert \bar{A}_{\overline{B}^0}\rvert^2 \lvert A_{CP}\rvert^2 [\bar{\lambda}_{\overline{B}^0} - \lambda_{CP} + \lvert\lambda_{CP}\rvert^2 \bar{\lambda}^*_{\overline{B}^0} + \delta$

Tab. 2.7: The coefficient s from Eq. (2.48), evaluated to leading order in the small quantities δ, λ_{B^0}, and $\bar{\lambda}_{\overline{B}^0}$. See the caption of Table 2.5 for the definition of the quantities.

3. EXPERIMENTAL SETUP AND EVENT SELECTION

The following Chapter gives a brief overview of the purpose, design and performance of the *BABAR* detector, and how it has been used to reconstruct and select the events where a B meson appears in a B_+, B_-, B^0, or $\overline{B}^0$ quantum state. It is by no means complete. For a detailed description of *BABAR* detector one can refer to Ref. [42]. The data used for this analysis $\Upsilon(4S)$ sample recorded by the *BABAR* detector and is identical to that used for the last time-dependent *CP* analysis using the $c\bar{c}K^0$ final states [37].

3.1 General description of the BABAR experiment

The main goal of *BABAR* experiment was the measurement of *CP* violating asymmetries in the B^0 meson system. The PEP-II B factory consists of asymmetric e^+e^- beams running on the $\Upsilon(4S)$ resonance (Fig. 3.1). This asymmetry allows for the measurement of the separation (and subsequently the decay time difference) between the B meson decaying to a *CP* final state (B_{CP}) and the flavor identified B^0 or $\overline{B}^0$ ($B_{\rm flav}$).

There are three main features of clean *CP* violating measurements which guided the design of the detector:

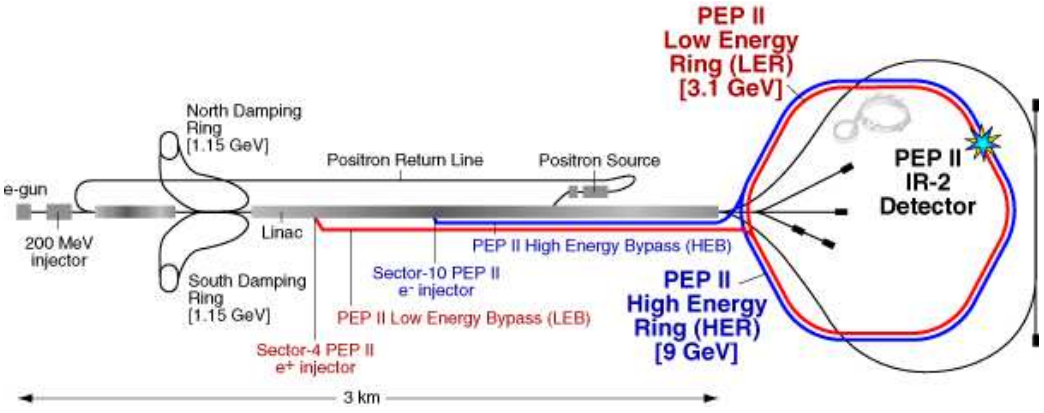

Fig. 3.1: Schematic view of PEP-II facility.

- Small branching fractions ($\backsim 10^{-4}$) of B^0 mesons to *CP* final states required the detector to be able to operate at high luminosities.
- The B^0 meson which does not decay to a *CP* final state (B_{flav}) must be identified to determine the flavor content of the other B^0 meson (B_{CP}) at production time, and therefore requires optimal particle identification of leptons and hadrons, since inclusive $\ell^{\pm}$ and $K^{\pm}$ from B decays account for almost 90% of B decays.
- The measurement of the time decay difference between the B_{CP} and the B_{flav} requires the final state of the B_{CP} to be fully reconstructed and contain at least two charged tracks.

The detector is comprised of five subsystems, as shown in Fig. 3.2. From smallest to largest radius:

- SVT - Silicon Vertex Tracker.
- DCH - Drift CHamber.
- DIRC - Detection of Internally Reflected Cherenkov light.
- EMC - ElectroMagnetic Calorimeter.
- IFR - Instrumented Flux Return.

A 1.5 T magnetic field is generated by a superconducting coil, which is just inside the instrumented flux return. The SVT and the DCH are responsible mostly for the tracking, where the SVT measures the vertex of tracks and the DCH measures their momentum. The DIRC's main role is the measurement of a particle's mass (and hence its identity) and was optimized to separate charged kaons from pions. The EMC detects electromagnetic showers which allow for the reconstruction of low energy $\pi^0 \to \gamma\gamma$ and $\eta \to \gamma\gamma$. The IFR was designed to identify muons and neutral hadrons. The five subsystems will be discussed in more detail in subsequent sections.

3.1.1 The PEP-II facility

The PEP-II facility consists of a LINAC, where the electrons and positrons are accelerated to their respective energies and two overlapping storage rings, where the electrons and positrons are crossed (called the interaction point) allowing them to collide. The $\Upsilon(4S)$ ($m_{\Upsilon(4S)} = 10.58$ GeV) lies just above the $B\bar{B}$ ($m_B = 5.279$ GeV) threshold and decays nearly 100% of the time to a $B\bar{B}$ pair, providing an ideal environment for the study of B mesons.

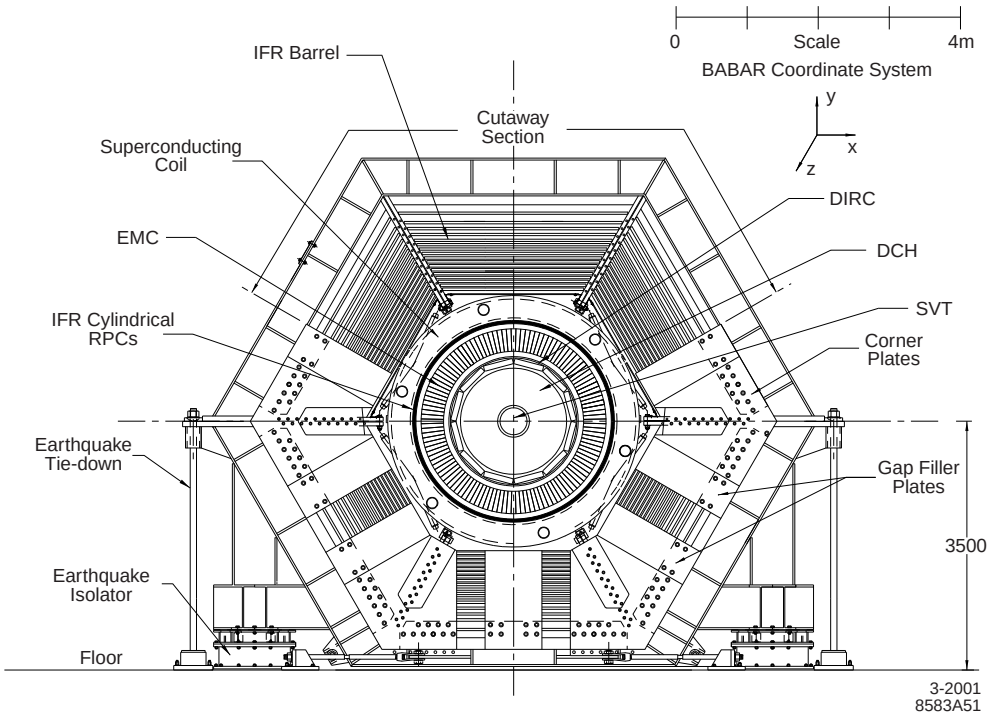

(a) End view

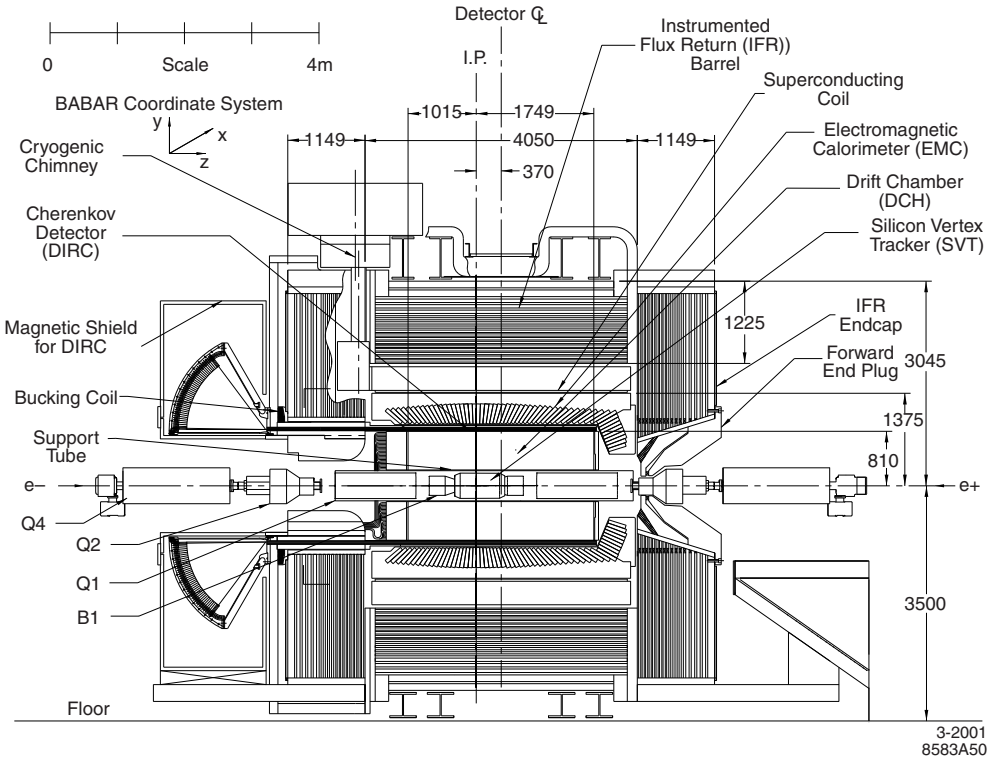

(b) Longitudinal section

Fig. 3.2: Schematic view of the *BABAR* detector.

The energies of the electron and positron beams are 9.0 GeV and 3.1 GeV, respectively, which provide a center-of-mass energy equal to the mass of the $\Upsilon(4S)$. The reaction rate for the process $e^+e^- \to \Upsilon(4S)$ is given by

$$\Gamma_{e^+e^-\to\Upsilon(4S)} = \sigma_{e^+e^-\to\Upsilon(4S)}\mathcal{L} \ , \tag{3.1}$$

where $\mathcal{L}$ is the instantaneous luminosity. The total number of $B\bar{B}$ pairs can be estimated by time integrating Eq. (3.1) and expressing the luminosity in units of inverse femtobarn (fb^{-1}).

3.1.2 The BABAR magnet and flux return

The magnet, which provides the 1.5 T magnetic field used by the tracking system to measure the momentum of charged particles, consists of a superconducting solenoid, a segmented flux return, and a field compensating coil. The superconducting solenoid is responsible for generating the 1.5 T magnetic field which causes charged particles to travel in helices through the silicon vertex tracker and the drift chamber allowing for the accurate measurement of their momenta. The superconducting coils consist of niobium-titanium filaments each less than 40 μm in diameter. The coils are cooled to 4.5 K operating with the current of 4596 A. The segmented flux return consists of many layers of segmented iron plates which provide the return medium for the 1.5 T magnetic field. The segmented flux return also serves as a muon filter and hadron absorber, aiding in the identification of muons. The field compensating coil, or bucking coil, consists of ten layers of water-cooled copper coils. It is main function is to cancel the leakage field into PEP-II and the DIRC's photomultiplier array. Typically it operates at currents of 200 A.

3.1.3 The Silicon Vertex Tracker (SVT)

The Silicon Vertex Tracker serves several purposes and is integral in *BABAR* 's ability to fulfill its primary goal which is the measurement of *CP* violation. A high vertex resolution is necessary to measure the decay time difference between a B meson which decays to a *CP* eigenstate and the flavor-identified B. The requirement on the vertex resolution in the z direction (along the longitudinal axis of the detector) was determined to be 80 μm. The SVT also serves as a standalone tracking system for low-p_t (transverse momenta) charged particles, since many of the tracks from B decays have low p_t. It was designed to provide a reconstruction efficiency of $\geq 70\%$ for charged tracks with $p_t \in$ (50,120) MeV.

The Drift Chamber's main goal is the detection of charged tracks and the measurement of their three-momenta. It is also able to complement the

DIRC by differentiating particle types by measuring their ionization energy loss while traversing the Drift Chamber.

3.1.4 The BABAR tracking system (SVT and DCH)

Charged tracks are characterized by five parameters (d_0, z_0, ω, ϕ_0, and $\tan\lambda$) measured at the point of closest approach to the z-axis. d_0 and z_0 are the distances from the point of closest approach to the origin in the $x-y$ plane and z axis respectively. The curvature $\omega \propto 1/p_t$, where the constant of proportionality depends on the track's charge and the strength of the B-field. ϕ_0 is the azimuthal angle of the track and λ is the dip angle relative to the transverse plane. The resolutions of these parameters are measured using cosmic ray muons. Since the muons passing through the entire detector are guaranteed to be a single track, fitting the two halves as separate tracks and comparing the differences gives a reliable estimate of the tracking resolutions.

3.1.5 The Detection of Internally Reflected Cherenkov light (DIRC)

The main purpose of the DIRC is the identification of charged tracks produced in B decays. Time dependent CP violation measurements in neutral B decays require flavor identification of one of the B mesons in an event. This is done by identifying the kaon or lepton in the inclusive decays $B^0 \to XK^+$ or $B^0 \to X\nu_l l^+$, respectively. Many of these tracks have momenta below 1 GeV and can have values as large as 2 GeV. Rare two-body B decays can produce kaon and pion tracks with momenta as large as 4 GeV. The DIRC provides four σ separations between kaons and pions for momenta between the pion Cherenkov threshold and 4 GeV.

3.1.6 The Electromagnetic Calorimeter (EMC)

The main purpose of the Electromagnetic Calorimeter is the detection of photons over a large range of energies, as low as 20 MeV and as high as 9 GeV. This allows for the reconstruction of $\pi^0 \to \gamma\gamma$ and $\eta \to \gamma\gamma$ as well as many other radiative decays. Another purpose is to aid in the identification of electrons, by comparing the energy collected in the calorimeter to the momentum reconstructed from the tracking system. Since electrons shower most of their energy in the calorimeter, the ratio E/p should be close to unity for highly relativistic electrons and less than one for heavier leptons and hadrons.

3.1.7 The Instrumented Flux Return (IFR)

The main purpose of the Instrumented Flux Return (IFR) is the detection of muons and neutral hadrons. The golden modes $B^0 \to J/\psi K^0$ and $B^0 \to \psi(2S)K^0$ contains both muons, in the $J/\psi, \psi(2S) \to \mu^+\mu^-$ final state, and neutral hadrons as K^0 decaying as K^0_L. Since the K^0_L is long lived, the first interaction with the detector is in the calorimeter which provides poor momentum and energy resolution as compared to the tracking system for charged particles.

3.2 Data sample and reconstruction

The experimental analysis exploits the same B meson sample, with the exception of $\eta_C K_S$ and $J/\psi K^{*0}$ ($\to K_S\pi^0$) final states, and identical reconstruction algorithms, selection criteria, and calibration techniques as the most recent *BABAR* time-dependent *CP* asymmetry measurement in $B \to c\bar{c}K^{(*)0}$ decays [37].

We select two samples of events in order to measure the time-dependent T, *CP* and *CPT* parameters: a sample of events in which one B candidate is reconstructed in a B_+ or B_- state, where B_+ and B_- are the states introduced in Sec. 2.2, and the flavor of the other B is identified (B_{CP} sample), and a sample of fully reconstructed B meson decays to flavor eigenstates ($B_{\rm flav}$ sample[1]). The $B_{\rm flav}$ samples is used to obtain experimental parameters, e.g., resolution and flavor mis-identification (misID), probability of assigning the incorrect flavor to the partially reconstructed B mesons, parameters. We also select a $B^{\pm}_{\rm flav}$ sample of fully reconstructed charged B meson decays to $J/\psi K^+$, $\psi(2S)K^+$, $\chi_{c1}K^+$, and $J/\psi K^{*+}(K^+\pi^0, K_S\pi^+)$, and $\overline{D}^{(*)0}\pi^+$, which is used as control sample.

The B_{CP} sample consists of B^0 decays to $J/\psi K_S$, $\psi(2S)K_S$, $\chi_{c1}K_S$, and $J/\psi K_L$. The $B_{\rm flav}$ sample consists of B^0 decays to $D^{(*)-}(\pi^+, \rho^+, a_1^+)$ and $J/\psi K^{*0}(K^+\pi^-)$ final states. Based on previous studies, we assume that the flavor misID and the resolution parameters are the same for the $B_{\rm flav}$ and B_{CP} samples, anyway this effect will be studied as a systematic effect.

J/ψ and $\psi(2S)$ mesons are reconstructed via their decays to e^+e^- or $\mu^+\mu^-$ final states. At least one of the leptons is required to pass a likelihood particle identification algorithm based on the information provided by the EMC, the IFR and from ionization energy-loss measured in the tracking

[1] The $B_{\rm flav}$ sample comprises events in which one of the B mesons is partially reconstructed in a flavor mode and the B totally reconstructed is reconstructed to a genuine flavor decay instead to a *CP* mode as it is done in the B_{CP} sample.

system. We require the invariant mass of the muon pair $m(\mu^+\mu^-)$ to be in the range 3.06–3.14 GeV for J/ψ or 3.636–3.736 GeV for $\psi(2S)$ candidates. For $J/\psi \to e^+e^-$ and $\psi(2S) \to e^+e^-$ decays, where the electron may have radiated bremsstrahlung photons, part of the missing energy is recovered by identifying neutral clusters with more than 30 MeV lying within 35 mrad in polar angle and 50 mrad in azimuth of the electron direction projected onto the EMC. The invariant mass of e^+e^- pairs is required to be within 2.95–3.14 GeV for J/ψ candidates, or 3.436–3.736 GeV for $\psi(2S)$ candidates.

We also construct $\psi(2S)$ mesons in the $J/\psi\pi^+\pi^-$ final state, where the J/ψ candidate is combined with a pair of oppositely-charged tracks assumed as pions with no particle identification applied, and the invariant mass of the pair between 400 MeV and 600 MeV. Candidates with 3.671 GeV$< m(J/\psi\pi^+\pi^-) <$ 3.701 GeV are retained.

The χ_{c1} candidates are reconstructed in the $J/\psi\gamma$ final state. The photon candidates are required to have an energy greater than 100 MeV but less than 2 GeV, and, when combined with other photons, not to form a π^0 candidate with invariant mass 120 MeV $< m(\gamma\gamma) <$ 150 MeV. The invariant mass of the χ_{c1} candidate is required to be between 3.477 GeV and 3.577 GeV. Mass constraints are applied afterward in the fits to improve the determinations of the energies and momenta of the J/ψ, $\psi(2S)$, and χ_{c1} candidates.

The decay channels $K^+\pi^-$, $K^+\pi^-\pi^0$, $K^+\pi^+\pi^-\pi^-$, and $K_S\pi^+\pi^-$ are used to reconstruct $\overline{D}^0$, while D^- candidates are selected in the $K^+\pi^-\pi^-$ and $K_S\pi^-$ modes. We require the $\overline{D}^0$ and D^- candidate invariant mass to be within $\pm 3\sigma$ of their respective nominal mass, where σ is the uncertainty calculated for each candidate. A mass-constrained fit is then applied to the $\overline{D}^0$ and D^- candidates satisfying these requirements. We form D^{*-} candidates from the decay $D^{*-} \to \overline{D}^0\pi^-$ by combining a $\overline{D}^0$ with a pion that has momentum greater than 70 MeV. The D^{*-} candidates are required to have $m(\overline{D}^0\pi^-)$ within ± 1.1 MeV of the nominal D^{*-} mass for the $\overline{D}^0 \to K^+\pi^-\pi^0$ mode and ± 0.8 MeV for all other modes.

We use both $K_S \to \pi^+\pi^-$ and $K_S \to \pi^0\pi^0$ decays; for other B decay modes we only use $K_S \to \pi^+\pi^-$. Candidates in the $K_S \to \pi^+\pi^-$ mode are selected by requiring an invariant $\pi^+\pi^-$ mass, computed at the vertex of the two oppositely-charged tracks, between 472.67 MeV and 522.67 MeV. We further apply a mass constraint fit to the K_S candidates before combining them with charmonium candidates to form B^0 candidates. Neutral pion candidates, in the mass range 100–155 MeV, are formed using two γ candidates from the EMC. Pairs of π^0 are combined to construct $K_S \to \pi^0\pi^0$ candidates. The minimum energy is required to be 30 MeV for γ, 200 MeV for π^0, and 800 MeV for K_S candidates. To select K_S candidates, the $\pi^0\pi^0$ invariant mass is restricted to the region between 470 MeV and 550 MeV.

Candidates for K_L are identified in the EMC and IFR detectors as reconstructed clusters that cannot be associated with any charged track in the event. As the energy of K_L cannot be measured well, the laboratory momentum of the K_L is determined by its flight direction and the constraint that the invariant mass of the $J/\psi K_L$ system has the known B^0 mass. For events with multiple $J/\psi K_L$ candidates, a hierarchy is imposed where the highest energy EMC cluster for multiple EMC combinations, or the IFR cluster with the largest number of layers for multiple IFR combinations, is selected. In case both EMC and IFR combinations are found, the EMC combination is chosen because of its better angular resolution.

The $\rho^+(770)$ candidates are reconstructed in the $\pi^+\pi^0$ final state, where the $\pi^+\pi^0$ mass is required to lie within ± 150 MeV of the nominal ρ^+ mass. Candidates in the decay mode $a_1^+ \to \pi^+\pi^-\pi^+$, where a_1^+ refers to the $a_1^+(1260)$ resonance, are reconstructed by combining three charged tracks with pion mass assumption, and restricting the three-pion invariant mass to lie between 1.0 and 1.6 GeV.

3.2.1 Data sample

We use the Run 1 to Run 6 *BABAR* data sample, recorded between 1999 and 2008. Table 3.1 gives the integrated luminosity values for the individual run blocks. These numbers were used to normalize the signal yield per fb^{-1}. The integrated luminosity (Int lumi) is determined using the `BbkLumi` [43] bookkeeping utility.

Sample	First run	Start date	Last run	End date	Int lumi (fb^{-1})
Run 1	9,931	22-10-1999	17,106	29-10-2000	20.4
Run 2	18,190	12-02-2001	29,435	30-06-2002	61.1
Run 3	32,915	06-12-2002	39,320	27-06-2003	32.3
Run 4	40,055	12-09-2003	50,635	31-07-2004	100.3
Run 5	53,736	17-04-2005	67,707	17-08-2006	133.3
Run 6	67,708	17-01-2007	76,494	04-09-2007	78.4
All	9,931	22-10-1999	76,494	04-09-2007	425.7

Tab. 3.1: Run ranges and integrated luminosity.

3.2.2 B meson flavor identification

A key ingredient in the measurement of time-dependent discrete symmetries studies is the determination of whether the non-fully reconstructed B was a

B^0 or a $\overline{B}^0$ at decay time.This flavor identification (flavor ID) is achieved with the analysis of the decay products of the recoiling B meson (B_{flav}). The overwhelming majority of B mesons decay to a final state that is flavor-specific, i.e., only accessible from either a B^0 or a $\overline{B}^0$. The purpose of the flavor ID algorithm is to determine the flavor of B_{flav} with the highest efficiency ϵ and lowest probability w of assigning the wrong flavor. It is not necessary to fully reconstruct B_{flav} in order to determine its flavor.

The figure of merit for the performance of the flavor algorithm is the effective flavor ID efficiency

$$Q = \epsilon(1 - 2w)^2, \tag{3.2}$$

which is related to the statistical uncertainty σ_S and σ_C in the coefficients S_f and C_f through

$$\sigma_{S,C} \propto \frac{1}{\sqrt{Q}}. \tag{3.3}$$

The flavor ID algorithm we employ, documented in [44, 45, 46], analyzes tracks not assigned to the fully reconstructed to assign a flavor and associated probability to B_{flav}. The flavor of B_{flav} is determined from a combination of nine different signatures, such as isolated primary leptons, kaons and pions from B decays to final states containing D^* mesons, and high momentum charged particles from B decays. The properties of those signatures are used as inputs to a single neural network (NN) that is trained to assign the correct flavor to B_{flav}. The output of this neural network then is divided into seven mutually-exclusive categories. These are (in order of decreasing signal purity) *Lepton*, *Kaon I*, *Kaon II*, *KaonPion*, *Pions*, *Other* and *Notag*. The events with the neural network output $|NN| > 0.8$ are defined as *Lepton* category, if they are also accompanied by an isolated primary lepton; otherwise they are categorized as *Kaon I*. For the other five categories (*Kaon II, KaonPion, Pion, Other* and *Notag*) the outputs of the neutral network are required to satisfy: $0.6 < |NN| < 0.8$, $0.4 < |NN| < 0.6$, $0.2 < |NN| < 0.4$, $0.1 < |NN| < 0.2$, and $|NN| < 0.1$, respectively. The events in the *Notag* category contain no flavor information, so carry no weight in the time-dependent analysis. They are excluded from further analysis.

The performance of this algorithm is evaluated using the B_{flav} sample. The final state of the B_{flav} sample can be classified as mixed or unmixed depending on whether the reconstructed flavor-eigenstate B_{flav} has the same or opposite flavor as the flavor ID B.

Table 3.2 lists the efficiency ϵ, B^0-$\overline{B}^0$ efficiency difference $\Delta\epsilon$, miss identified flavor fraction (misID) w, B^0-$\overline{B}^0$ flavor misID fraction difference Δw, and Q value, for all flavor ID categories. The efficiency ϵ is obtained by

performing $m_{\rm ES}$ fits on the $B_{\rm flav}$ sample. The other parameters are obtained from the time dependent fit Δt on the $B_{\rm flav}$ sample.

	$\epsilon(\%)$	$\Delta\epsilon(\%)$	$w(\%)$	$\Delta w(\%)$	$Q(\%)$
Lepton	8.96 ± 0.07	-0.1 ± 0.2	2.8 ± 0.3	0.3 ± 0.5	7.98 ± 0.11
Kaon I	10.82 ± 0.07	0.0 ± 0.2	5.3 ± 0.3	-0.1 ± 0.6	8.65 ± 0.14
Kaon II	17.19 ± 0.09	-0.2 ± 0.3	14.5 ± 0.3	0.4 ± 0.6	8.68 ± 0.17
KaonPion	13.67 ± 0.08	0.0 ± 0.2	23.3 ± 0.4	-0.7 ± 0.7	3.91 ± 0.12
Pions	14.18 ± 0.08	-0.7 ± 0.3	32.5 ± 0.4	5.1 ± 0.7	1.73 ± 0.09
Other	9.54 ± 0.07	0.3 ± 0.2	41.5 ± 0.5	3.8 ± 0.8	0.27 ± 0.04
Total	74.37 ± 0.10	-0.2 ± 0.6			31.2 ± 0.3

Tab. 3.2: Flavor ID performance evaluated using the $B_{\rm flav}$ sample. The efficiency ϵ, B^0-$\overline{B}^0$ efficiency difference $\Delta\epsilon$, flavor misID fraction w, B^0-$\overline{B}^0$ flavor misID fraction difference Δw, and Q value. The table is taken from Refs [44, 45, 46], which uses identical data samples and similar procedure, not identical, as our analysis. In our analysis, as we explain later, we perform a fit to the $B_{\rm flav}$ sample with the background allowed to have an effective mixing parameter, while such parameter was fixed to be equal to the signal Δm_{B^0}. Our signal $m_{\rm ES}$ purities or signal fractions are split by all the flavor ID categories

3.2.3 Measurement of the decay time difference

We explain briefly in this section the technique used at B factories, particularly in *BABAR* , to determine the difference of proper time Δt between the two decaying B mesons, as well as the flavor identification and the reconstruction algorithm. These techniques are described in detail in Ref. [47]. At the asymmetric-energy B factories the $\Upsilon(4S)$ decay products are Lorentz boosted along the beam longitudinal axis and fly enough for their decay paths to be comparable or larger than the experimental resolution. Since no charged stable particles emerge from the $\Upsilon(4S)$ decay point, the decay length of the individual B mesons from the $\Upsilon(4S)$ decay is unknown and we are left to determine the difference Δz between them, from which Δt can be calculated since the boost of the center-of-mass is well known. One of the two B mesons is fully reconstructed into a CP eigenstate (B_{CP}), while the other B is partially reconstructed through their decay products (e.g. semileptonic decays, dominant hadronic decays producing charged kaons, etc.) and used to identify as B^0 or $\overline{B}^0$ and for vertexing. In Fig. 3.3 we sketch the event topology and how the reconstruction of the $\Upsilon(4S)$ decay is performed.

We calculate the proper time difference Δt between the two B decays from the measured separation Δz between the decay vertices of and along the z (collision) axis [47]. The z position of the B_{CP} vertex is determined from the charged daughter tracks. The $B_{\rm flav}$ decay vertex is determined by fitting tracks not belonging to the B_{CP} candidate to a common vertex, including constraints from the beam spot location and the B_{CP} momentum [47].

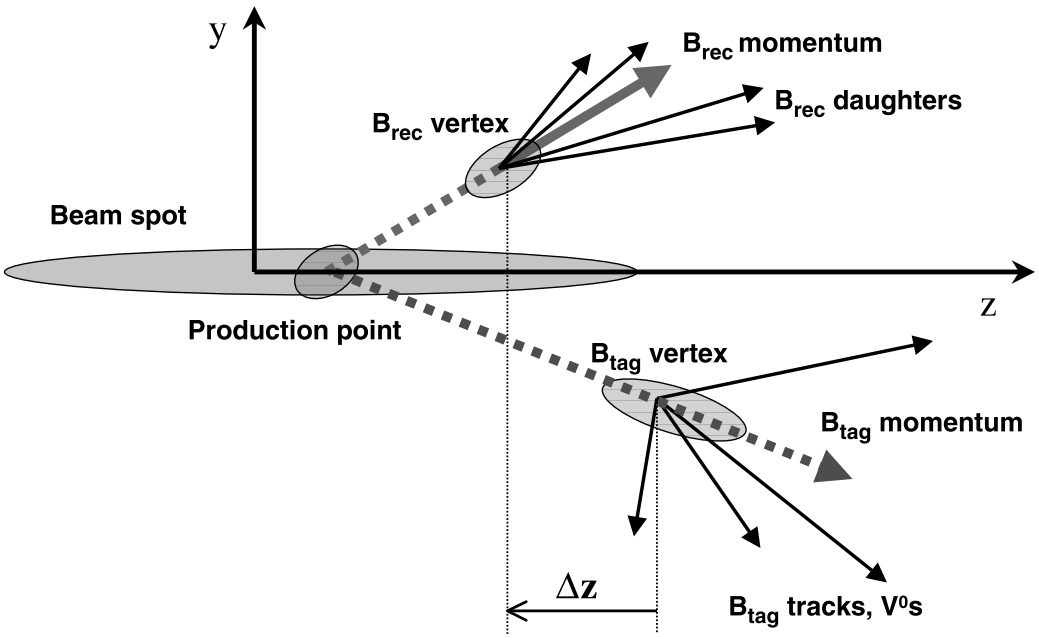

Fig. 3.3: $\Upsilon(4S)$ decay topology and reconstruction, where B_{rec} (B_{tag}) denotes the B which is fully (partially) reconstructed to a *CP* (flavor) state. In our notation $B_{rec} \equiv B_{CP}$ and $B_{tag} \equiv B_{\rm flav}$. The figure is not drawn to scale.

3.2.4 Event selection and kinematical variables

Events that pass the selection requirements are refined using kinematic variables. For the $J/\psi K_L$ mode, the difference ΔE between the candidate center-of-mass (c.m.) energy and the beam energy in the c.m. frame, $E^*_{\rm beam}$, is required to satisfy $|\Delta E| < 80$ MeV. For all other categories of events, we require $|\Delta E| < 20$ MeV and the beam-energy substituted mass $m_{\rm ES} = \sqrt{(E^*_{\rm beam})^2 - (p^*_B)^2}$ to be greater than 5.2 GeV, where p^*_B is the B momentum in the c.m. frame. When multiple B candidates (with $m_{\rm ES} > 5.2$ GeV) are found in the same event, the candidate with the smallest value of $|\Delta E|$ is selected.

Events are accepted if the calculated Δt uncertainty is less than 2.5 ps and $|\Delta t|$ is less than 20 ps. The fraction of signal Monte Carlo events satisfying such a requirement is 95 %.

We study the purities, $m_{\rm ES}$ shape parameters, and yields of each of the $c\overline{c}K_S$, $B_{\rm flav}$, $c\overline{c}K^{\pm}$ and $B^{\pm}_{\rm flav}$ data samples by decay mode split by run block and by flavor ID category. We define purity as the fitted signal yield divided by the total yield for $m_{\rm ES}$ greater than 5.27 GeV.

The $m_{\rm ES}$ of each event is used to estimate the probability that the event is signal or background. The $m_{\rm ES}$ fits are done before the reference time-dependent fit as to fix the signal probability for each event. The signal $m_{\rm ES}$ distribution for the full B_{CP} and $B_{\rm flav}$ samples, except for the $J/\psi K_L$ sample is described by a Gaussian function. The background $m_{\rm ES}$ distribution is modeled by an ARGUS threshold function [48], where a shape parameter is allowed to vary in the fit. The configuration of the $m_{\rm ES}$ fits is:

- The $m_{\rm ES}$ shape parameters ($\mu_{m_{\rm ES}}$, $\sigma_{m_{\rm ES}}$ and the Argus parameter) for the $B_{\rm flav}$ sample are split by B and D decay mode [$3\times4+3\times2+1\times2=$ 20 groups].

- The $m_{\rm ES}$ shape parameters ($\mu_{m_{\rm ES}}$, $\sigma_{m_{\rm ES}}$ and the Argus parameter) for the gold $c\overline{c}K$ sample are split by B and K_S decay mode [four groups: $J/\psi K_S(\pi^+\pi^-)$, $J/\psi K_S(\pi^0\pi^0)$, $\psi(2S)K_S$, $\chi_{c1}K_S$]. The fraction of the signal component is further split by lepton type, i.e. e^+e^- or $\mu^+\mu^-$ [$2\times2+4\times1+4\times1=12$ groups].

- The Argus parameter for the $B_{\rm flav}$ sample is further split by *Lepton* vs *non-Lepton* categories.

- The purity or signal fraction in the $c\overline{c}K_S$ decay modes, further split by flavor ID category.

- The purity or signal fraction in the $B_{\rm flav}$ decay modes, further split by flavor ID category. In the most recent analysis by *BABAR* [37] this splitting was done only by *Lepton* and *non-Lepton* categories, but it has been verified in this study that this splitting cannot account for differences in the background fractions among the different *non-Lepton* categories.

For $c\overline{c}K^{\pm}$ and $B^{\pm}_{\rm flav}$ control samples the $m_{\rm ES}$ of each event used to estimate the probability that the event is signal or background follows a similar procedure.

As in the most recent *CP* violation by *BABAR* [37], the time dependence in the mean fitted $m_{\rm ES}$ shown in Fig. 20 of [49] (for the R22d data processing

used for the analysis) has been corrected in the conditions database for Run 1 to Run 4. However to avoid having a run-dependent mean $m_{\rm ES}$ for Run 5 and 6, it has been applied the same procedure as documented in Ref. [49] using the $B_{\rm flav}$ data to derive a $m_{\rm ES}$ correction in blocks of runs that cover little more than one fb^{-1}. This $m_{\rm ES}$ correction is then applied to the Run 5 and Run 6 data. See Sec. 4.7 of Ref. [50] for additional details.

The $J/\psi\ K_L$ channel is handled differently, using the variable ΔE with the fit configuration explained in Sec. 3.2.8.

3.2.5 $c\bar{c}K_S$ data sample

Table 3.3 reports the signal yields of the $c\bar{c}K_S$ sample split by lepton type and flavor ID categories. Figure 3.4 shows the purity and the resolution $\sigma_{m_{\rm ES}}$ of the $m_{\rm ES}$ fits for all the gold $c\bar{c}K_S$ subsamples as a function of the flavor ID category. Figure 3.5 illustrates the $m_{\rm ES}$ distributions for $c\bar{c}K_S$ events which satisfy the flavor ID and vertexing requirements, overlaid with the best fit projections for signal and background components.

3.2.6 $B_{\rm flav}$ data sample

Table 3.4 reports the signal yields and purities of the $B_{\rm flav}$ sample, split by flavor ID categories. Figure 3.6 shows the purity and $\sigma_{m_{\rm ES}}$ of the $m_{\rm ES}$ fits for all the $B_{\rm flav}$ subsamples as a function of the flavor ID category. Figure 3.7 displays the $m_{\rm ES}$ distributions for $B_{\rm flav}$ events which satisfy the flavor ID and vertexing requirements, overlaid with the best fit projections for signal and background components.

3.2.7 Control data sample

Table 3.5 reports the signal yields and purities of the $c\bar{c}K^{\pm}$ and $B^{\pm}_{\rm flav}$ samples.

3.2.8 $J/\psi K_L$ data sample

The K_L data is divided by K_L reconstruction type (EMC or IFR) because the two samples have different detector-related backgrounds and thus different purity (signal fraction). The variable ΔE is used on an event-by-event basis to help distinguish between signal and background in the Δt maximum likelihood fit. As the form of the $J/\psi \to \ell\ell$ ($\ell = e,\ \mu$) decay is not expected to influence the ΔE shape, the PDFs were generated without regard to lepton type. For the $J/\psi K_L$ decay mode, the signal ΔE distribution is determined from Monte Carlo simulated events. The sample composition and ΔE distribution of the individual background sources are determined either from

Sample	*Lepton*	*Kaon I*	*Kaon II*	*KaonPion*	*Pions*	*Other*	*Notag*
$J/\Psi K_S(ee)$	300 ± 12	345 ± 13	565 ± 17	447 ± 15	458 ± 15	300 ± 13	877 ± 22
$J/\Psi K_S(\mu\mu)$	275 ± 13	302 ± 15	517 ± 20	403 ± 17	444 ± 19	283 ± 15	765 ± 24
$J/\Psi K_S$	666 ± 8	757 ± 12	1268 ± 17	994 ± 15	1044 ± 17	672 ± 14	1862 ± 26
$J/\Psi K_S(\pi^0\pi^0)(ee)$	64 ± 5	76 ± 9	116 ± 11	113 ± 11	122 ± 11	72 ± 9	190 ± 15
$J/\Psi K_S(\pi^0\pi^0)(\mu\mu)$	71 ± 4	74 ± 6	139 ± 9	123 ± 8	121 ± 8	86 ± 6	207 ± 12
$J/\Psi K_S(\pi^0\pi^0)$	141 ± 6	154 ± 10	261 ± 15	232 ± 14	244 ± 14	154 ± 12	381 ± 20
$\Psi(2S)K_S(ee)$	19 ± 3	28 ± 4	47 ± 6	32 ± 5	45 ± 6	38 ± 5	81 ± 8
$\Psi(2S)K_S(\mu\mu)$	15 ± 2	18 ± 1	34 ± 4	22 ± 2	31 ± 4	21 ± 2	47 ± 4
$\Psi(2S)K_S$	36 ± 4	45 ± 5	83 ± 7	55 ± 6	81 ± 7	60 ± 6	127 ± 10
$\Psi(2S)K_S(\Psi\pi\pi)(ee)$	28 ± 4	30 ± 3	59 ± 6	53 ± 6	45 ± 6	35 ± 4	103 ± 9
$\Psi(2S)K_S(\Psi\pi\pi)(\mu\mu)$	23 ± 3	28 ± 3	33 ± 4	26 ± 4	30 ± 5	31 ± 4	74 ± 6
$\Psi(2S)K_S(\Psi\pi\pi)$	46 ± 4	67 ± 5	71 ± 7	49 ± 6	76 ± 8	60 ± 6	138 ± 9
$\chi_{c1}K_S(ee)$	22 ± 4	35 ± 4	38 ± 5	24 ± 4	48 ± 6	30 ± 5	64 ± 7
$\chi_{c1}K_S(\mu\mu)$	11 ± 2	26 ± 4	39 ± 4	29 ± 3	20 ± 3	23 ± 3	55 ± 5
$\chi_{c1}K_S$	38 ± 3	68 ± 5	77 ± 6	52 ± 6	68 ± 6	52 ± 5	120 ± 8
$(c\bar{c})K_S(ee)$	487 ± 9	556 ± 15	873 ± 22	700 ± 20	745 ± 21	482 ± 18	1319 ± 31
$(c\bar{c})K_S(\mu\mu)$	448 ± 8	527 ± 11	904 ± 15	711 ± 13	765 ± 15	515 ± 11	1324 ± 21
$(c\bar{c})K_S$	937 ± 12	1083 ± 18	1779 ± 26	1410 ± 24	1508 ± 25	999 ± 21	2644 ± 37

Tab. 3.3: Signal yields of the $c\bar{c}K_S$ sample split by flavor ID categories. Taken from [50]

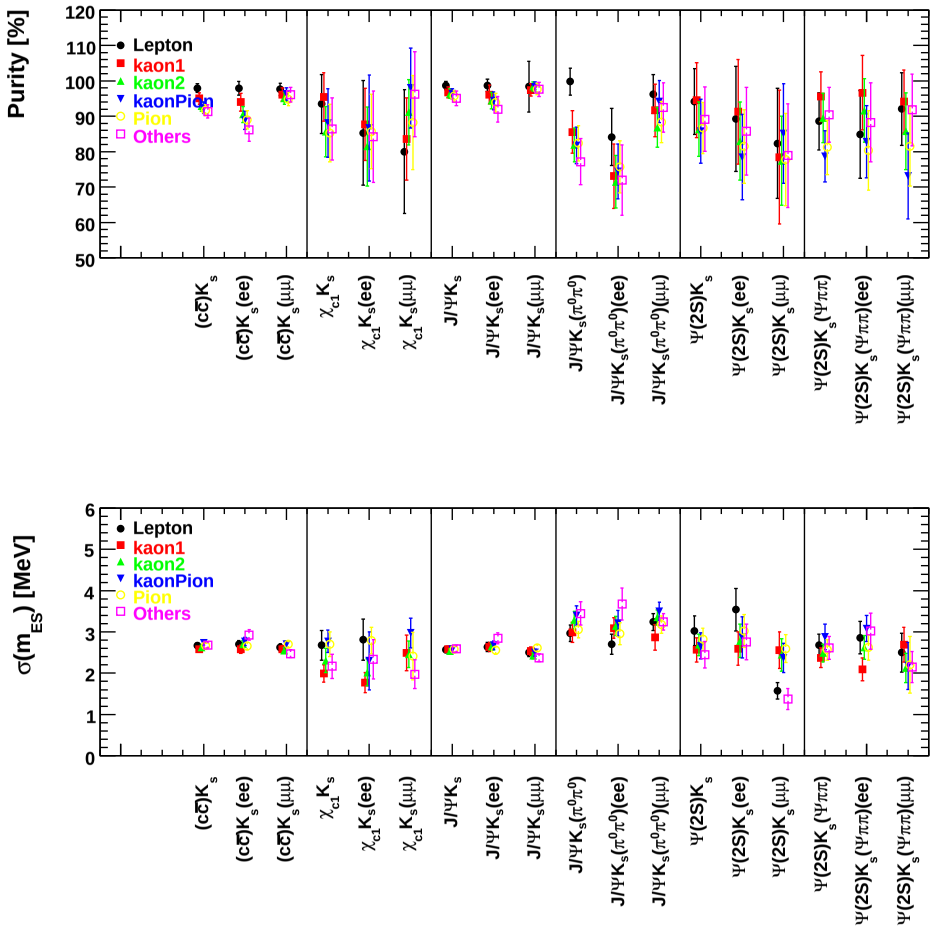

Fig. 3.4: Purity (top) and $\sigma_{m_{\rm ES}}$ (bottom) of the $c\bar{c}K_S$ subsamples as a function of the flavor ID category, after the vertexing requirements $|\Delta t| < 20$ ps and $\sigma_{\Delta t} < 2.5$ ps. Taken from [50].

Flavor ID	$D^{\mp(*)}h^{\pm}$		$J/\psi K^{*\pm}$ $(K^+\pi^-)$	
Category	Yield	Purity	Yield	Purity
Lepton	16251.6 ± 57.7	96.2 ± 0.3	607.0 ± 11.3	76.2 ± 7.9
Kaon I	19545.4 ± 101.8	88.4 ± 0.5	1923.4 ± 20.4	75.9 ± 4.8
Kaon II	31162.9 ± 146.8	83.6 ± 0.4	1007.2 ± 14.9	76.7 ± 6.5
KaonPion	25140.9 ± 131.8	83.3 ± 0.4	3133.0 ± 26.6	73.1 ± 3.8
Pions	26399.3 ± 137.2	81.7 ± 0.4	4017.9 ± 30.8	72.0 ± 3.7
Other	18154.2 ± 114.8	80.2 ± 0.5	2261.0 ± 22.8	74.1 ± 4.3
Notag	49153.1 ± 209.7	76.9 ± 0.3	12949.4 ± 54.2	73.8 ± 1.9

Tab. 3.4: Signal yields and purities of the B_{flav} sample split by flavor ID categories. Taken from [50].

Sample	Yield	Purity
$J/\psi K^+$	29550 ± 100	97.7 ± 0.3
$\psi(2S)K^+$	4459 ± 46	98.2 ± 1.3
$\chi_{c1}K^+$	2401 ± 29	92.9 ± 1.6
$c\bar{c}K^+$	36416 ± 115	94.3 ± 1.5
$J/\psi K^{*+}, (K^+\pi^0)$	6053 ± 69	96.5 ± 0.6
$J/\psi K^{*+}, (K_S\pi^+)$	3813 ± 42	96.1 ± 0.4

Tab. 3.5: Signal yields of the $c\bar{c}K^{\pm}$ and $B^{\pm}_{\text{flav}}$ samples. Taken from [50].

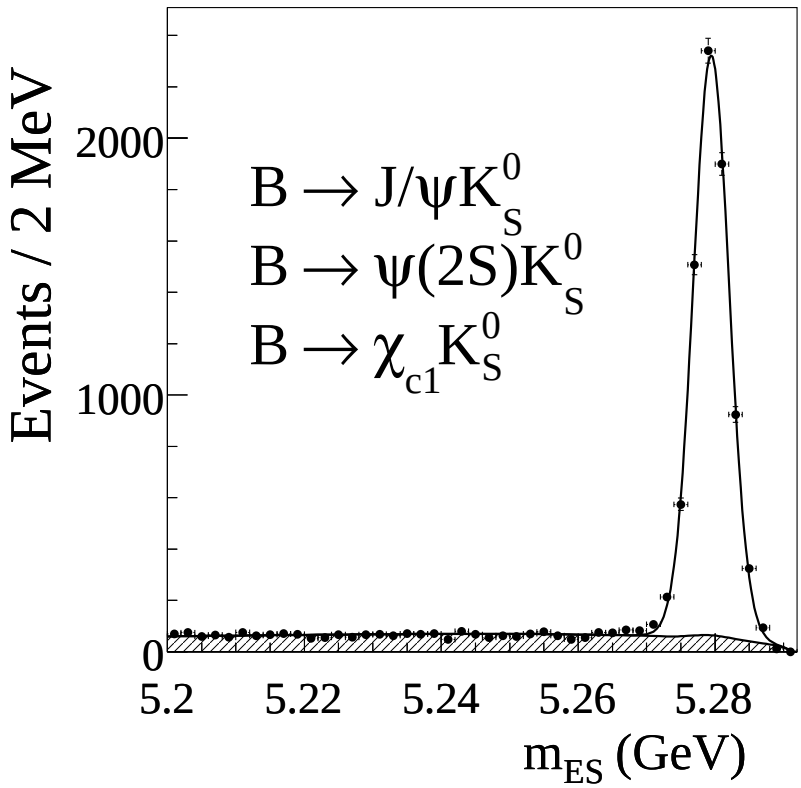

Fig. 3.5: Distributions of $m_{\rm ES}$ for the neutral B decays reconstructed in the $c\bar{c}K_S$ final states, after flavor ID and vertexing requirements. The shaded region is the estimated background contribution. The sample of events is identical to those used in the most recent *BABAR CP*-violation study [37], but excluding $\eta_c K_S$ and $J/\psi K^{*0}(\to K_S\pi^0)$ final states.

simulation (for $B \to J/\psi X$) or from the sidebands of the $J/\psi \to \ell\ell$ in data (for non-J/ψ background). We use eight separate ΔE PDFs, four for the EMC K_L and four for the IFR K_L. These are:

- $J/\psi K_L$ (signal),
- $J/\psi K_S$ background,
- J/ψX background, excluding $J/\psi K_S$,
- non-J/ψ background.

More than 90% of the events that pass the selection contain a real J/ψ. Events from the J/ψ di-lepton invariant mass sideband are used to determine

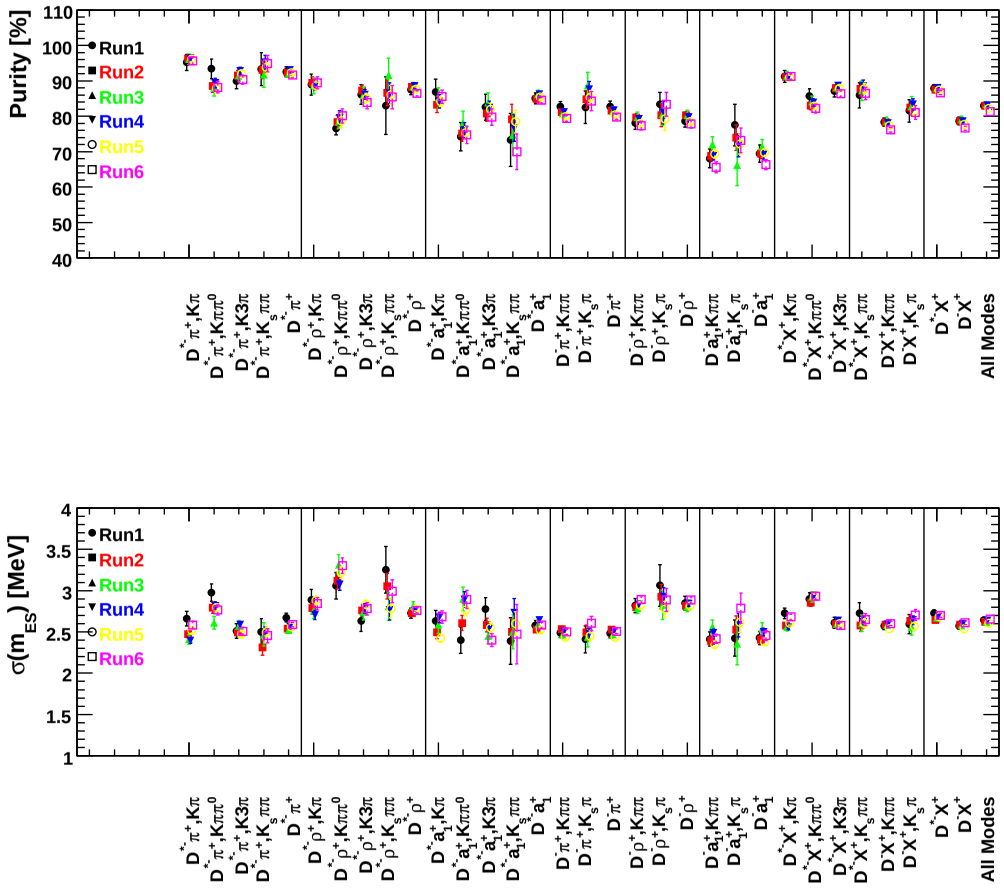

Fig. 3.6: Purity (top) and $\sigma_{m_{\rm ES}}$ (bottom) of the $B_{\rm flav}$ subsamples as a function of the Run number, after the vertexing requirements $|\Delta t| < 20$ ps and $\sigma_{\Delta t} < 2.5$ ps. Taken from [50].

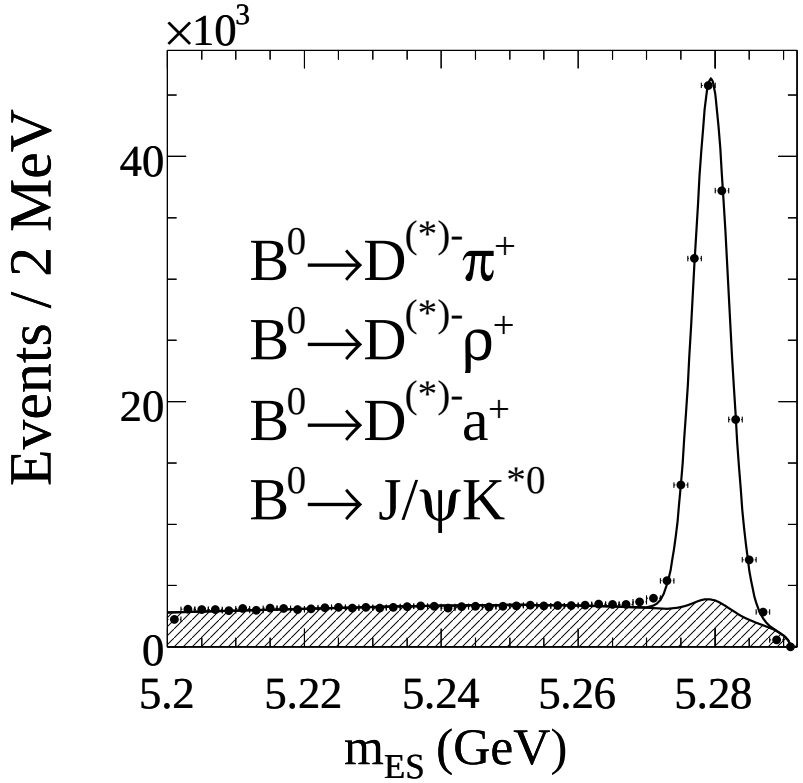

Fig. 3.7: Distributions of $m_{\rm ES}$ for the $B_{\rm flav}$ events, after flavor ID and vertexing requirements. The shaded region is the estimated background contribution. The sample of events is identical to that used in the most recent *BABAR CP*-violation study [37].

the properties of the remaining non-J/ψ background. The sideband is defined as

- $J/\psi \to \mu^+\mu^-$; $2.90 < m(\mu\mu) < 3.00$ GeV and $3.175 < m(\mu\mu) < 3.50$ GeV,
- $J/\psi \to e^+e^-$; $3.175 < m(ee) < 3.50$ GeV.

The sideband events are required to pass all other event selection criteria. It has been observed that the background resolution function for the $B_{\rm flav}$ sample describes well the non-$J/\psi K_L$ sideband data in each flavor ID category. Therefore, the resolution function and lifetime for the non-J/ψ background events are taken from the $B_{\rm flav}$ background, and the fractions of the prompt component are determined from Δt fits in each flavor ID category.

A binned maximum likelihood fit of the ΔE spectrum in the data is performed to determine the relative amounts of signal, inclusive-J/ψ background, and non-J/ψ background. The signal, inclusive-J/ψ and $J/\psi K_S$ ΔE distributions are obtained from Monte Carlo and fit with a two Gaussian plus Argus function [48], while the non-ψ background is determined from an Argus fit to the J/ψ mass sideband region. The fit to the Argus function is performed because of the lower statistics in the sideband sample. The fit was executed separately for the EMC and the IFR event sample, due to differences in purity and background composition which are dependent on K_L reconstruction type. Further, we split the ΔE fit according to J/ψ lepton type in the decay to account for a more significant muon component on the non-ψ background with respect to the electron contribution. Figure 3.8 shows the results of fitting the ΔE distributions for EMC versus IFR K_L candidates and e^+e^- versus $\mu^+\mu^-$ candidates. The fitted yields are given in Table 3.6 for all events, and in Tables 3.7 and 3.8 for the EMC and IFR as split by flavor ID category. Figure 3.9 illustrates the ΔE distributions for $J/\psi K_L$ events which satisfy the flavor ID and vertexing requirements, overlaid with the best fit projections for signal and background components. We consider the range $|\Delta E| < 80$ MeV as used in the most recent *CP* violation measurement by *BABAR* [37].

EMC K_L				
	ΔE Fit $\psi \to ee$		ΔE Fit $\psi \to \mu\mu$	
	Events	Fraction	Events	Fraction
Signal	996 ± 42	29.6 ± 1.1	1113 ± 43	24.9 ± 0.9
Psi-X	1762 ± 59	52.3 ± 1.4	1988 ± 72	44.4 ± 1.3
non-Psi	609 ± 30	18.1 ± 0.9	1376 ± 38	30.7 ± 0.9

IFR K_L				
	ΔE Fit $\psi \to ee$		ΔE Fit $\psi \to \mu\mu$	
	Events	Fraction	Events	Fraction
Signal	735 ± 37	47.8 ± 2.0	826 ± 37	44.0 ± 1.8
Psi-X	638 ± 37	41.5 ± 2.2	724 ± 46	38.6 ± 2.1
non-Psi	165 ± 15	10.7 ± 1.0	325 ± 19	17.4 ± 1.1

Tab. 3.6: Results of binned ΔE fit for all flavor-identified events. The fractions and yields are for the range $|\Delta E| < 80$ MeV, as used in the nominal fit. Taken from [50] and [51].

EMC K_L- $J/\psi \to ee$						
	Lepton Frac(%)	*Kaon I* Frac(%)	*Kaon II* Frac(%)	*KaonPion* Frac(%)	*Pions* Frac(%)	*Other* Frac(%)
Signal	30.2 ± 3.1	33.8 ± 2.9	31.8 ± 2.3	25.2 ± 2.5	29.7 ± 2.5	26.7 ± 3.1
Psi-X	54.4 ± 3.7	54.6 ± 3.4	49.9 ± 2.9	54.0 ± 3.2	49.5 ± 3.2	56.0 ± 3.8
non-Psi	15.4 ± 2.6	11.7 ± 2.1	18.3 ± 1.9	20.8 ± 2.2	20.7 ± 2.3	17.4 ± 2.5
EMC K_L- $J/\psi \to \mu\mu$						
	Lepton Frac(%)	*Kaon I* Frac(%)	*Kaon II* Frac(%)	*KaonPion* Frac(%)	*Pions* Frac(%)	*Other* Frac(%)
Signal	31.8 ± 3.2	28.6 ± 2.4	26.3 ± 1.8	20.0 ± 1.9	24.4 ± 2.0	20.8 ± 2.3
Psi-X	57.9 ± 3.7	46.7 ± 3.2	41.8 ± 2.7	43.5 ± 3.1	41.1 ± 3.0	44.1 ± 3.6
non-Psi	10.3 ± 1.8	24.7 ± 2.2	31.8 ± 2.0	36.5 ± 2.4	34.4 ± 2.2	35.1 ± 2.8

Tab. 3.7: Results of ΔE fit as split by flavor ID category for events in the range $|\Delta E| < 80$ MeV. Taken from [50] and [51].

IFR K_L- $J/\psi \to ee$						
	Lepton Frac(%)	*Kaon I* Frac(%)	*Kaon II* Frac(%)	*KaonPion* Frac(%)	*Pions* Frac(%)	*Other* Frac(%)
Signal	56.3 ± 5.5	51.1 ± 5.2	40.2 ± 4.1	50.8 ± 4.7	48.0 ± 4.8	44.8 ± 5.4
Psi-X	36.8 ± 5.7	44.2 ± 5.4	48.5 ± 4.5	38.4 ± 5.1	38.5 ± 5.1	40.3 ± 6.0
non-Psi	6.8 ± 2.3	4.6 ± 1.8	11.2 ± 2.2	10.8 ± 2.4	13.5 ± 2.5	14.9 ± 3.4
IFR K_L- $J/\psi \to \mu\mu$						
	Lepton Frac(%)	*Kaon I* Frac(%)	*Kaon II* Frac(%)	*KaonPion* Frac(%)	*Pions* Frac(%)	*Other* Frac(%)
Signal	56.9 ± 5.4	46.0 ± 4.5	36.6 ± 3.6	45.9 ± 4.1	43.8 ± 4.1	42.1 ± 4.8
Psi-X	37.6 ± 5.8	40.2 ± 5.2	44.7 ± 4.4	35.1 ± 4.9	35.6 ± 5.0	38.3 ± 5.8
non-Psi	5.4 ± 1.9	13.9 ± 2.5	18.7 ± 2.4	19.0 ± 2.6	20.6 ± 2.8	19.6 ± 3.0

Tab. 3.8: Results of ΔE fit as split by flavor ID category for events in the range $|\Delta E| < 80$ MeV. Taken from [50] and [51].

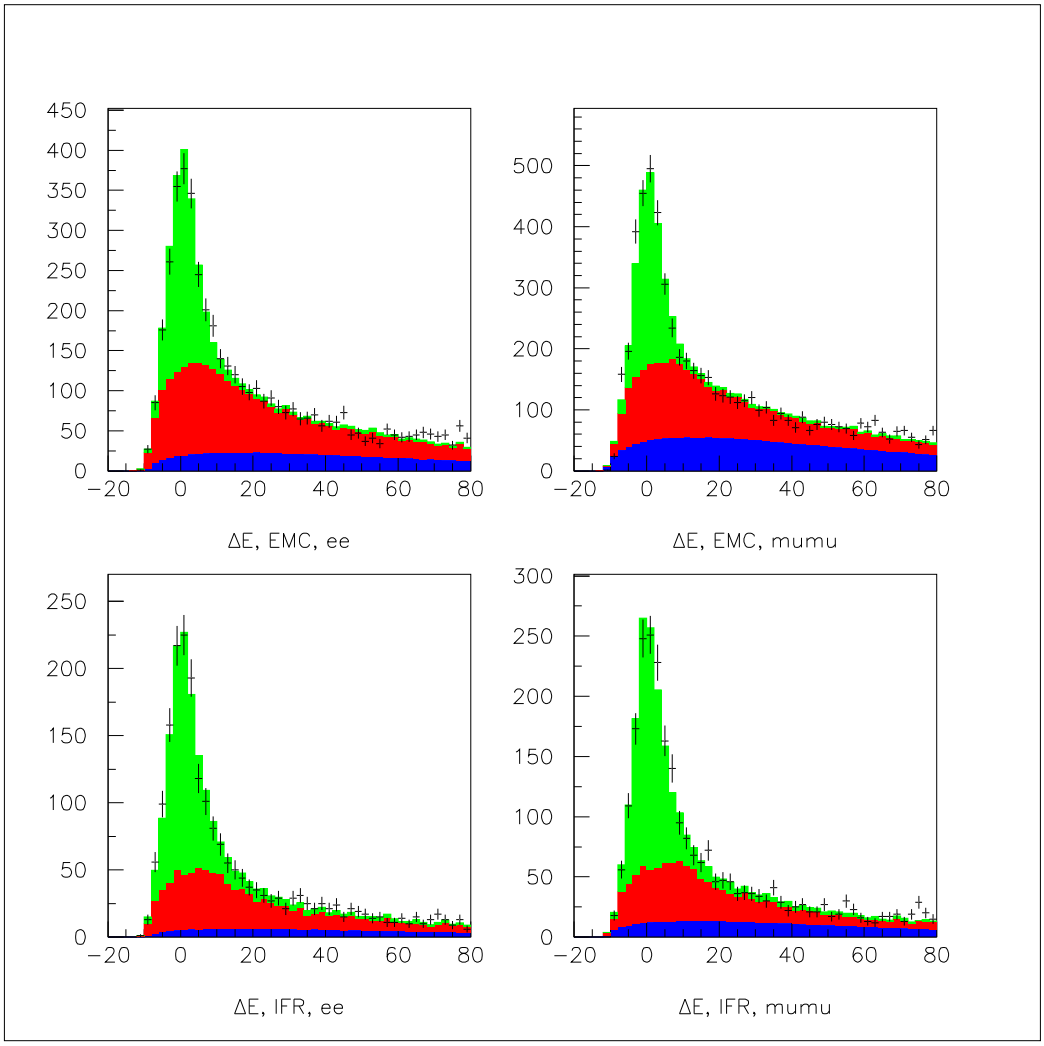

Fig. 3.8: Fitted ΔE distributions for EMC (top) and IFR (bottom), split by (left) $J/\psi \to e^+e^-$ and (right) $J/\psi \to \mu^+\mu^-$. Taken from [50] and [51]. The green area represent the signal component, the red one the inclusive-J/ψ background component, and the blue one the non-J/ψ background component.

3.2.9 Data reduction

In the typical *BABAR* analysis the selection of signal candidates is performed in several stages. Since it is not efficient to process all available data for each analysis, a pre-selection, or *skim*, is performed at the first stage. The *skim* is usually designed to have a high signal selection efficiency at the same time

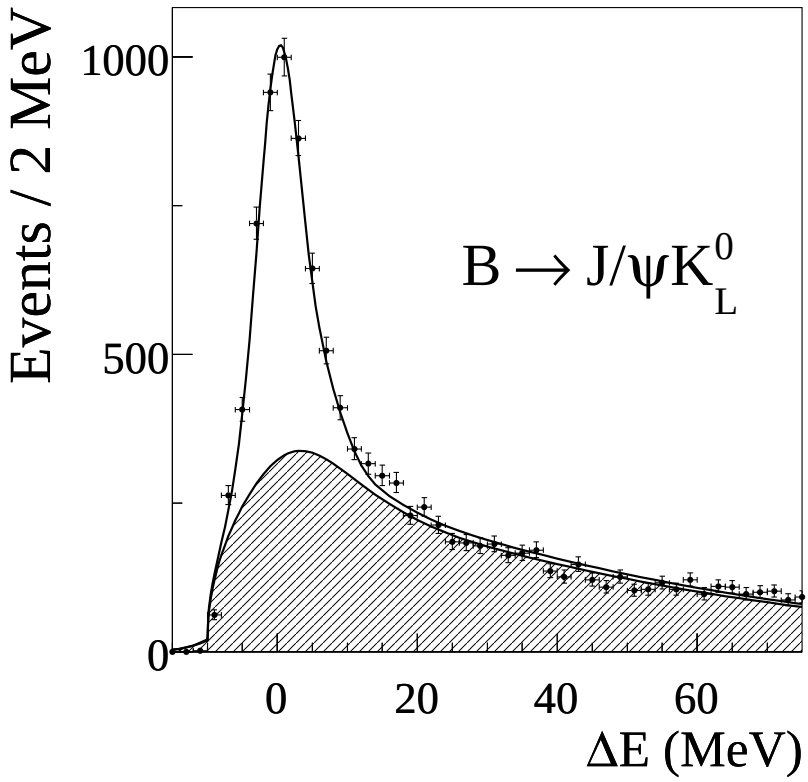

Fig. 3.9: Distributions of ΔE for the neutral B decays reconstructed in the $J/\psi K_L$ final states, after flavor ID and vertexing requirements. The shaded region is the estimated background contribution. The sample of events is identical to that used in the most recent *BABAR CP*-violation study [37].

a high background rejection is aimed at this stage. Usually a single *skim* is used as a starting sample for multiple analysis.

The second selection stage is under control of the analyst. The optimization of this stage is performed on the "skimmed" dataset and depends on the physics goal of the analysis. To obtain the data samples needed in our analysis we use the `B0ToccKFinal`, `JPsitoll`, and `BFlav_Final` skims to define our primary data samples which were derived from the `CharmUser` and `BRecoUser` codes, used in previous iterations of this analysis. In addition, we use `BchToccKFinal`, `BchToccKstarFinal`, and `BchFlav_Final` skims for some of the cross check studies. Briefly these skims are as follows:

- `B0ToccKFinal`: this skim contains the main charmonium K_S modes.
- `Jpsitoll`: this skim contains the $J/\psi\ell^-\ell^+$ or $\psi\ell^-\ell^+$ events (for the

$J/\psi K_L$ sample).

- `BFlav_Final`: this skim contains the full reconstructed $B^0/\overline{B}^0$ decays, as known as B_{flav} sample.
- `BchToccKFinal`: this skim contains a control sample of $B^{\pm} \to c\bar{c}K^{\pm}$.
- `BchToccKstarFinal`: this skim contains a control sample of $B^{\pm} \to c\bar{c}K^{*\pm}$.

These skims are all defined in the standard FilterTools/SkimMiniApp framework.

Usually at the user level, two additional selections are performed. The first is a pre-selection defined to have a high signal selection efficiency with the goal of reducing the sample size so that the optimizations process is faster. The second is the final selection from which the observables are obtained and used as input to perform the final an unbinned maximum likelihood fit.

4. EXPERIMENTAL ANALYSIS

This Chapter describes the physics motivation, experimental strategy and the results to perform a direct observation of Time Reversal Violation or equivalently T violation (TV) or T non-invariance. By this we mean to experimentally demonstrate TV experimentally independent of any CP violation (CPV) and CPT invariance. The data used for this study are the same as used in the 2008 (last published) CP analysis [37]. Since the Physics behind is different, the experimental analysis has been completely redone in a coherent way in order to study the different decay channels appropriately to be in a position to claim for the first direct observation of TV [8, 16, 30].

4.1 Methodology and definition of the parameters

Genuine tests of an asymmetry under T and/or CPT transformations in the fundamental laws of Physics imply the interchange between initial (in) states and final (out) states for a given process, a request particularly difficult to be accomplished for particles that decay during their time evolution. The obvious question then is whether Time Reversal Violation can be searched for in unstable systems. In this Section a methodology to perform model-independent, separate measurements of the three discrete symmetry violations (CP, T and CPT) for transitions involving the decay of neutral meson systems is described. It makes use of the EPR entanglement existing in B (and ϕ) factories and quantum mechanics, with no other theoretical ingredient [8]. There, the preparation of a quantum mechanical individual state of the neutral meson is not made by measurements performed on it, but by the observation of the decay of its orthogonal correlated partner. This strategy allows the quantum preparation of a given individual state of the (still living) neutral meson by selecting a particular decay channel of the other neutral meson. The strategy and fundamental parameters for the measurements of these three asymmetries as a function of the time interval $\Delta t > 0$ between the first and second decay was discussed in Sec. 2.1.

Violation of the CP invariance has been observed in the K^0-$\overline{K}^0$ and B^0-$\overline{B}^0$ systems. Up to now, the experimental results are in agreement with

the standard Cabibbo-Kobayashi-Maskawa (CKM) mechanism of the electroweak theory [27]. Although all present tests of CPT invariance confirm the validity of this symmetry, as imposed by any local quantum field theory with Lorentz invariance and hermiticity [1], it would be of great interest to observe TV directly, independently of assumptions on CPT invariance, this would also provide a test of Lorentz invariance, quantum coherence, etc. A direct evidence for TV would mean an experiment that, considered by itself, clearly demonstrates T violation independent of, and unconnected to, the results for CP violation. There was no existing result prior to the work developed during this thesis that clearly showed TV in this sense [16].

We are interested in microscopic T-symmetry violations. In particle physics odd effects under the change of the sign of time $t \leftrightarrow -t$ are not necessarily T-violating. These observables can occur in theories with exact T-symmetry and are called T-odd effects, like those induced by absorptive components of the amplitude. Well known time asymmetries are the Universe t-asymmetry and the macroscopic t-asymmetry called the "arrow of time". But none of these t-asymmetries is a test of TV since there is no interchange between *in* and *out* states. In the fundamental laws of Physics, T violation exists in the Standard Model or any field theory extension of it. The observed CP violation in the neutral meson systems tells us that T should be violated as well. However, as emphasized above, TV has not been observed directly up to now. On the other hand, there are intriguing subtleties introduced by the antiunitary character of the symmetry operator.

There is no doubt that the Universe is expanding, even accelerating at present cosmological era. This natural t-asymmetry $t \leftrightarrow -t$ is perfectly compatible with fundamental laws of Physics that are T symmetric. It is due to the initial condition for our Universe, like inflation. This asymmetry is similar to the fact that in our Universe we have a privileged reference frame, the one associated with the Cosmic Microwave Background (CMB) radiation at a definite temperature with fluctuations. This asymmetry is in the nature of thermodynamics. According to Eddington [52], the time's arrow is a property of entropy alone: time is asymmetric with respect to the amount of order in an isolated system.

In particle physics, particle decays are an example of a time-asymmetric phenomenon. If we start with an initial collection of identical unstable particles we arrive after decay at a large collection of final states. There is little, if any, chance of any collection of such final states evolving to become a set of identical unstable particles as in the initial state. This phenomenon has nothing to do with T violation. In fact, it looks like it prevents a direct test of T-symmetry in unstable systems [8, 16], since it requires an exchange between *in* and *out* states.

Direct evidence for TV can be obtained from two types of experiments:

1. A non-zero expectation value of a T-odd operator for a non-degenerate stationary state, such as a permanent Electric Dipole Moment (EDM) for a particle with spin, which is a P-odd, C-even, T-odd operator. A review of the present experimental status can be found in [53]. The EDM can be generated by either strong T violation, like the θ-term $\epsilon_{\mu\nu\zeta\sigma}F^{\mu\nu}F^{\zeta\sigma}$ in the QCD Lagrangian, or weak T violation. The experimental small value of the θ-term needs a mechanism that protects it, the Peccei-Quinn symmetry [54]. The Standard Model theory of electroweak interactions or any local field theory with CP violation predicts T-violating effects in parallel.

2. For a transition $i \to f$, under the exchange $in \leftrightarrow out$ and $\Delta t \leftrightarrow -\Delta t$, T symmetry implies the connection $S_{f,i} \to S_{-i,-f}$, where $-i(-f)$ means the T-transformed state of the $i(f)$ state and S is the transition matrix.

The mixing asymmetry K^0-$\overline{K}^0$ vs. $\overline{K}^0$-K^0 (also known as Kabir asymmetry) has been measured in CPLEAR [23] with non-vanishing value. However, since it is a CPT-even transition, CP and T are experimentally identical, and requires $\Delta\Gamma \neq 0$. The observed effect is time-independent. In the $B^0\overline{B}^0$ system no asymmetry has been yet found [24], as expected within the SM since in this case $\Delta\Gamma$ almost vanishes [25].

The question now is whether it is possible to search for TV in the interference between decay amplitudes with and without mixing, where the associated CP-violating effect is large [26, 27]. The opportunity arises [30] in B (and ϕ) factories as a consequence of the quantum mechanical entanglement imposed by the Einstein-Podolsky-Rosen (EPR) correlation [29]. This correlation allows the quantum preparation of a physical state of a living particle by observing the decay of its partner particle: the individual state of each particle in the system is not defined before this observation. Depending on the selection of the decay channel, one may have separate tests of CP, T and CPT-symmetries.

At B factories the coherence between orthogonal B^0, $\overline{B}^0$ states has been used to identify the flavor,

$$|i\rangle = \frac{1}{\sqrt{2}}[B^0(t_1)\overline{B}^0(t_2) - \overline{B}^0(t_1)B^0(t_2)], \tag{4.1}$$

where the states "1" and "2" are defined by the time of their decay with $t_1 < t_2$. The observation of $B^0 \to \ell^+ X$, for example, at time t_1, tells us that the complementary (still living) state is $\overline{B}^0$ at t_1. This is the preparation

of the initial state for single state time evolution. As said, the individual state of each neutral meson is, however, not defined before its collapse as a filter imposed by the observation of the decay of its companion. One can rewrite the same state Eq. (4.1) of the system $|i\rangle$ in terms of any other pair of orthogonal states of the individual neutral B mesons, like the B_+ and the B_- states described in Sec. 2.2. The entangled state of the two-body system can be rewritten as

$$|i\rangle = \frac{1}{\sqrt{2}}[B_+(t_1)B_-(t_2) - B_-(t_1)B_+(t_2)]. \tag{4.2}$$

We can now proceed to a partition of the complete set of final states with definite flavor and *CP* content into eight pairs, defined by the first decaying B at t_1 and preparing the state of the still living meson, i.e., B^0, $\overline{B}^0$, B_-, B_+, as a function of $\Delta\tau = t_2 - t_1 > 0$. Each of these eight processes has a time-dependent decay rate $g^{\pm}_{\alpha,\beta}(\Delta\tau)$, where indexes $\alpha \in \{\ell^+, \ell^-\}$ and $\beta \in \{K_S, K_L\}$ run over the final states with definite flavor (ℓ^+X, ℓ^-X) and *CP* eigenstates ($c\overline{c}K_S$, $J/\psi K_L$), respectively, and the upper index + or − indicates if the decay to the flavor final state α occurred before or after to the *CP*-eigenstate final state β. Thus a $+ \to\ -$ replacement corresponds to Δt exchange, which means experimentally the exchange of the two decay products at t_1 and t_2.

From only quantum mechanics each decay rate can be written as function of $\Delta\tau$

$$\begin{aligned} g^{\pm}_{\alpha,\beta}(\Delta\tau) \quad \propto e^{-\Gamma\Delta\tau}\big\{ \quad & C^{\pm}_{\alpha,\beta}\cos(\Delta m\Delta\tau) + S^{\pm}_{\alpha,\beta}\sin(\Delta m\Delta\tau) + \\ & D^{\pm}_{\alpha,\beta}\cosh(\Delta\Gamma\Delta\tau/2) + E^{\pm}_{\alpha,\beta}\sinh(\Delta\Gamma\Delta\tau/2)\ \big\}, \end{aligned} \tag{4.3}$$

where Γ is the average decay width, Δm and $\Delta\Gamma$ are the mass and width differences between the mass eigenstates, and $C^{\pm}_{\alpha,\beta}$, $S^{\pm}_{\alpha,\beta}$, $D^{\pm}_{\alpha,\beta}$ and $E^{\pm}_{\alpha,\beta}$ are generic coefficients. This construction makes no assumptions about neither *CPT* invariance nor *CP* or T violation. Assuming $\Delta\Gamma = 0$ in the time dependence and normalizing to the coefficient of the $\cosh(\Delta\Gamma\Delta\tau)$ term, Eq. (5.40) simplifies to

$$g^{\pm}_{\alpha,\beta}(\Delta\tau) \quad \propto \quad e^{-\Gamma\Delta\tau}\big\{1 + C^{\pm}_{\alpha,\beta}\cos(\Delta m\Delta\tau) + S^{\pm}_{\alpha,\beta}\sin(\Delta m\Delta\tau)\big\}. \tag{4.4}$$

The sine term in Eq. (4.4) results from the interference between amplitudes with and without mixing, whereas the cosine term arises from the interference between decay amplitudes with different weak and strong phases. Effects due to any small lifetime difference in the time dependence, and the renormalization of all coefficients to the $\cosh(\Delta\Gamma\Delta\tau)$ term for each subsample separately, introduce small corrections.

It then follows that asymmetries in decay rates for any pair of T-conjugated transitions (Table 2.1) would be apparent through differences between their respective best-fit $S^{\pm}_{\alpha,\beta}$ and $C^{\pm}_{\alpha,\beta}$ coefficients. For example, a significant difference between the $S^{+}_{\ell^+,K_S}$ and $S^{-}_{\ell^-,K_L}$ coefficients would imply observation of T violation. In general, a net difference of $S^{\pm}_{\alpha,\beta}$ or $C^{\pm}_{\alpha,\beta}$ parameters between two T-, CP-, or CPT-transformed processes (Tables 2.1, 2.2, or 2.3) would be a proof of T, CP, or CPT violation, respectively.

The standard CP violation studies performed by the B factory experiments [37] extract a single set of best-fit S and C coefficients, reversing the sign of S under $\Delta t \leftrightarrow -\Delta t$, or $B_+ \leftrightarrow B_-$, or $B^0 \leftrightarrow \overline{B}^0$ exchanges, and reversing the sign of C only under $B^0 \leftrightarrow \overline{B}^0$ exchange,

$$\begin{aligned} S &= \frac{2Im(\lambda)}{1+|\lambda|^2} = S^{+}_{\ell^+,K_S} = -S^{+}_{\ell^-,K_S} = -S^{-}_{\ell^+,K_S} = S^{-}_{\ell^-,K_S} = \\ &\quad -S^{+}_{\ell^+,K_L} = S^{+}_{\ell^-,K_L} = S^{-}_{\ell^+,K_L} = -S^{-}_{\ell^-,K_L}, \end{aligned} \tag{4.5}$$

$$\begin{aligned} C &= \frac{1-|\lambda|^2}{1+|\lambda|^2} = C^{+}_{\ell^+,K_S} = -C^{+}_{\ell^-,K_S} = C^{-}_{\ell^+,K_S} = -C^{-}_{\ell^-,K_S} = \\ &\quad C^{+}_{\ell^+,K_L} = -C^{+}_{\ell^-,K_L} = C^{-}_{\ell^+,K_L} = -C^{-}_{\ell^-,K_L}. \end{aligned} \tag{4.6}$$

This construction is valid under the assumptions of CPT invariance and $\Delta\Gamma = 0$ [30]. If $\Delta\Gamma = 0$, automatically there is no CP violation in the mixing. Under these assumptions the $\Delta t \leftrightarrow -\Delta t$ (or equivalently $t_1 \leftrightarrow t_2$) exchange, which is not a T-symmetry operation, becomes related to T (exchange of the *in* and *out* neutral B states), and to CP (exchange of B^0 and $\overline{B}^0$ states), $CP \leftrightarrow T \leftrightarrow \Delta t$ [55]. In other words, the resulting statement that particle $\leftrightarrow$ antiparticle invariance test is related to the exchange $\Delta t \leftrightarrow -\Delta t$. In the SM, $\lambda \approx e^{i2\beta}$, therefore

$$\begin{aligned} S &\approx \sin 2\beta\ , \\ C &\approx 0. \end{aligned} \tag{4.7}$$

As most of the currently available data on neutral B mesons are well described by the SM, whether our proposed T-violating observables are also well accounted for in the SM or not, the direct observation of T violation would provide a proof of principle.

It is now convenient to introduce the asymmetry parameters $\Delta S^{\pm}_{T}$, $\Delta C^{\pm}_{T}$ (and similarly $\Delta S^{\pm}_{CP}$, $\Delta C^{\pm}_{CP}$, and $\Delta S^{\pm}_{CPT}$, and $\Delta C^{\pm}_{CPT}$), defined in Table 4.1, as the difference of $S^{\pm}_{t,r}$, $C^{\pm}_{t,r}$ coefficients between the corresponding symmetry-transformed processes for two reference Δt-exchanged transitions, for example $S^{+}_{\ell^+,K_S}$ and $S^{-}_{\ell^+,K_S}$. Using these parameters rather than the $S^{\pm}_{\alpha,\beta}$, $C^{\pm}_{\alpha,\beta}$ coefficients has the main advantage that the symmetry violation will be apparent

through a non-vanishing value of any of the associated four parameters. In other words, if $\Delta S_T^+ \neq 0$ or $\Delta S_T^- \neq 0$ or $\Delta C_T^+ \neq 0$ or $\Delta C_T^- \neq 0$, then there is T violation, and similarly for CP and CPT symmetries. Table 4.2 summarizes the values and relations among the asymmetry parameters in the case of invariance under the three space-time discrete symmetry transformations. We would like to emphasize that the definition of these parameters requires to choose as reference two Δt-exchanged samples, in our case $S^{\pm}_{\ell^+,K_S}$ since $J/\psi K_S$ events are cleaner and more efficiently reconstructed than $J/\psi K_L$ [37].

Coefficient	Approximate expected SM values
$\Delta S_T^+ = S^-_{\ell^-,K_L}$- $S^+_{\ell^+,K_S}$	-1.4
$\Delta S_T^- = S^+_{\ell^-,K_L}$- $S^-_{\ell^+,K_S}$	1.4
$\Delta C_T^+ = C^-_{\ell^-,K_L}$- $C^+_{\ell^+,K_S}$	0.0
$\Delta C_T^- = C^+_{\ell^-,K_L}$- $C^-_{\ell^+,K_S}$	0.0
$\Delta S_{CP}^+ = S^+_{\ell^-,K_S}$- $S^+_{\ell^+,K_S}$	-1.4
$\Delta S_{CP}^- = S^-_{\ell^-,K_S}$- $S^-_{\ell^+,K_S}$	1.4
$\Delta C_{CP}^+ = C^+_{\ell^-,K_S}$- $C^+_{\ell^+,K_S}$	0.0
$\Delta C_{CP}^- = C^-_{\ell^-,K_S}$- $C^-_{\ell^+,K_S}$	0.0
$\Delta S_{CPT}^+ = S^-_{\ell^+,K_L}$- $S^+_{\ell^+,K_S}$	0.0
$\Delta S_{CPT}^- = S^+_{\ell^+,K_L}$- $S^-_{\ell^+,K_S}$	0.0
$\Delta C_{CPT}^+ = C^-_{\ell^+,K_L}$- $C^+_{\ell^+,K_S}$	0.0
$\Delta C_{CPT}^- = C^+_{\ell^+,K_L}$- $C^-_{\ell^+,K_S}$	0.0
$S^+_{\ell^+,K_S}$	0.7
$S^-_{\ell^+,K_S}$	-0.7
$C^+_{\ell^+,K_S}$	0.0
$C^-_{\ell^+,K_S}$	0.0

Tab. 4.1: Definition of the T-, CP-, and CPT-asymmetry parameters. These parameters are defined as the differences between the $S^{\pm}_{\alpha,\beta}$, $C^{\pm}_{\alpha,\beta}$ coefficients for two reference Δt-exchanged processes and those of the corresponding symmetry-transformed transitions. We show the approximate expected values based on the SM CP violation studies at B factory experiments, as given in Eqs (4.5) and (4.6).

T invariance	CP invariance	CPT invariance
$\Delta S_T^+ = 0$	$\Delta S_{CP}^+ = 0$	$\Delta S_{CPT}^+ = 0$
$\Delta S_T^- = 0$	$\Delta S_{CP}^- = 0$	$\Delta S_{CPT}^- = 0$
$\Delta S_{CP}^+ = \Delta S_{CPT}^+$	$\Delta S_T^+ = \Delta S_{CPT}^+$	$\Delta S_T^+ = \Delta S_{CP}^+$
$\Delta S_{CP}^- = \Delta S_{CPT}^-$	$\Delta S_T^- = \Delta S_{CPT}^-$	$\Delta S_T^- = \Delta S_{CP}^-$
$\Delta C_T^+ = 0$	$\Delta C_{CP}^+ = 0$	$\Delta C_{CPT}^+ = 0$
$\Delta C_T^- = 0$	$\Delta C_{CP}^- = 0$	$\Delta C_{CPT}^- = 0$
$\Delta C_{CP}^+ = \Delta C_{CPT}^+$	$\Delta C_T^+ = \Delta C_{CPT}^+$	$\Delta C_T^+ = \Delta C_{CP}^+$
$\Delta C_{CP}^- = \Delta C_{CPT}^-$	$\Delta C_T^- = \Delta C_{CPT}^-$	$\Delta C_T^- = \Delta C_{CP}^-$

Tab. 4.2: Expected values and relations among the asymmetry parameters under invariance of one of the three discrete space-time symmetry transformations.

It is interesting to derive from Tables 2.5, 2.6, and 2.7 the values of all the coefficients of Table 4.1 in terms of the Weisskopf-Wigner parameters, up to the linear terms in the CPT parameter δ.

$$\begin{aligned}
\Delta S_T^{\pm} &\simeq \pm 2\Big[Im(\lambda_{CP}) + Im(\lambda_{CP})Re(\lambda_{CP})Re(\delta)\Big] \,, \\
\Delta C_T^{\pm} &\simeq 2Im(\delta)Im(\lambda_{CP}) \,, \\
\Delta S_{CP}^{\pm} &\simeq \pm 2\Big[Im(\lambda_{CP}) + Im(\delta) + Im(\lambda_{CP})Re(\lambda_{CP})Re(\delta)\Big] \,, \\
\Delta C_{CP}^{\pm} &\simeq -2Re(\delta)Re(\lambda_{CP}) \,, \\
\Delta S_{CPT}^{\pm} &\simeq \pm 2Im(\delta) \,, \\
\Delta C_{CPT}^{\pm} &\simeq -2Re(\delta\lambda_{CP}) \,, \\
S_{\ell^+,K_S}^{\pm} &\simeq \mp\Big[Im(\delta) + Im(\lambda_{CP}) + Im(\lambda_{CP})Re(\delta\lambda_{CP})\Big] \,, \\
C_{\ell^+,K_S}^{\pm} &\simeq Re(\delta\lambda_{CP}) \,,
\end{aligned} \tag{4.8}$$

where δ is the CPT parameter defined in Eq. (2.24) and λ_{CP} is equivalent to λ_f, introduced in Eq. (2.36), when the final state (f) is a CP eigenstate. To obtain the parameters in Eq. (4.8) we make certain assumptions that are consistent with our analysis described in this Chapter. First we have assumed $\Delta\Gamma = 0$, therefore $|q/p| = 1$. We also neglect direct CP violation, this implies that $|A_{CP}| = |\bar{A}_{CP}|$, and CP violation in the kaon sector to force $\langle B_+|B_-\rangle = 0$, therefore $c\bar{c}K_S$ is a CP-odd eigenstate and $J/\psi K_L$ is a CP-even eigenstate. With these approximations, we constrain $\lambda_{K_S} = \eta_{K_S}\lambda_{CP} =$

$-\eta_{K_L}\lambda_{CP} = -\lambda_{K_L}$, where $\eta_{K_L} = -\eta_{K_S} = 1$. The reader should note that the coefficients shown in Eq. 4.8 have been calculated normalizing to the cosh coefficient.

4.2 Fit description

This Section describes the details of the likelihood fit and its configuration used to determine the T-, CP- and CPT-violating parameters $\Delta S_T^{\pm}$, $\Delta C_T^{\pm}$, $\Delta S_{CP}^{\pm}$, $\Delta C_{CP}^{\pm}$, $\Delta S_{CPT}^{\pm}$, $\Delta C_{CPT}^{\pm}$, and the reference parameters $S_{\ell^+,K_S}^{\pm}$ and $C_{\ell^+,K_S}^{\pm}$. The configuration used for this analysis is almost identical to that used in the most recent CP analysis [37, 50, 51], except for the signal model, treatment of the outliers component of the Δt resolution function, and the splitting per B and D decay modes and flavor identification (flavor ID) category of the signal fraction of the $B_{\rm flav}$ sample $m_{\rm ES}$ distributions, as described in Sec. 3.2.

4.2.1 Fitting program

We use an enhanced version of the *BABAR* standard fitter program developed for the most recent CP violation analysis, adapted to the new signal model, including the features, and some technical modifications to facilitate running, plotting, bookkeeping, etc. The fitter uses a RooFit-based package [56] for the construction and configuration of the probability density functions (PDFs). The PDF prototypes are defined in the class RooBCPTFit and the configuration is steered with the class RooBCPTFitMaster [57]. Both these classes are part of the RooFitBabar library.

4.2.2 Signal description

Physics model and parameters

The primary physics parameters under study were summarized in Table 4.1 in Sec. 4.1. We fix the B^0 lifetime and mass difference Δm to the values summarized in Table 4.3. Systematic uncertainties in our measurement include variations of these values within the quoted errors. This is discussed in Sec. 4.5. We do not make any assumption about the T, CP and CPT symmetries in the signal.

The complete expression of the signal PDF for a flavor-identified and fully CP-reconstructed sample in terms of the $(S_{\alpha,\beta}^{\pm}, C_{\alpha,\beta}^{\pm})$ base and notation

Parameter	Value
Δm	0.507 ± 0.005 ps^{-1}
τ_{B^0}	1.530 ± 0.009 ps
τ_{B^+}	1.638 ± 0.011 ps
$\Delta\Gamma$	0

Tab. 4.3: Inputs for fixed physics parameters in our fit, taken from [15].

introduced at the end of Sec. 4.1 is

$$\begin{aligned} G_{\alpha,\beta}(\Delta t_{\text{true}}) &\propto g^{+}_{\alpha,\beta}(\Delta t_{\text{true}}) \times H(\Delta t_{\text{true}}) \\ &+ g^{-}_{\alpha,\beta}(-\Delta t_{\text{true}}) \times H(-\Delta t_{\text{true}}) \ , \end{aligned} \tag{4.9}$$

where Δt_{true} is the signed difference of proper times between the two B decays, H is the Heaviside step function, the $g^{\pm}_{\alpha,\beta}$ is given by Eq. (5.40), the index $\alpha \in \{\ell^+, \ell^-\}$ runs over the flavor-identified states, and the index $\beta \in \{K_S, K_L\}$ runs over reconstructed *CP* final states. In total there are four independent samples, regardless the sign of the reconstructed proper time difference

$$\begin{aligned} \alpha, \beta \ \in \ \{ & \ \ell^+, K_S \ [\text{or } K_S, \ell^+] \ , \ \text{ i.e., } c\overline{c}K_S, \ \ell^+ X \ , \\ & \ \ell^-, K_S \ [\text{or } K_S, \ell^-] \ , \ \text{ i.e., } c\overline{c}K_S, \ \ell^- X \ , \\ & \ \ell^+, K_L \ [\text{or } K_L, \ell^+] \ , \ \text{ i.e., } J/\psi K_L, \ \ell^+ X \ , \\ & \ \ell^-, K_L \ [\text{or } K_L, \ell^-] \ , \ \text{ i.e., } J/\psi K_L, \ \ell^- X \ \} \ . \end{aligned} \tag{4.10}$$

The first term of the sum is related to $\Delta t_{\text{true}} > 0$ (i.e., the flavor-identified B, identified as B^0 or $\overline{B}^0$, decayed before the opposite B, reconstructed as $c\overline{c}K_S$ or $J/\psi K_L$ state) and the second one is related to $\Delta t_{\text{true}} < 0$ (the flavor-identified B decayed after). We should stress here that the variable Δt_{true} is the variable strictly related to the positive or negative part of the time-dependent decay rate, in other words, the variable required to identify which B meson decayed first and used to further split the $c\overline{c}K_S$ and $J/\psi K_L$ samples, B^0 or $\overline{B}^0$ identified, into the final eight physics subsamples. Due to proper time resolution, $\Delta t > 0$ ($\Delta t < 0$) has a dominant contribution of $\Delta t_{\text{true}} > 0$ ($\Delta t_{\text{true}} < 0$) but also contains a large contribution of $\Delta t_{\text{true}} < 0$ ($\Delta t_{\text{true}} > 0$). Distinguishing between $\Delta t_{\text{true}} < 0$ and $\Delta t_{\text{true}} > 0$ in the presence of a Δt limited resolution is one of the main challenges of this analysis with respect to the most recent *CP* violation analysis, as it can be better understood from Fig. 4.1. This is exactly the reason of the Heaviside step function in Eq. (4.9), and the $\pm$ index in the upper part of the C and S parameters.

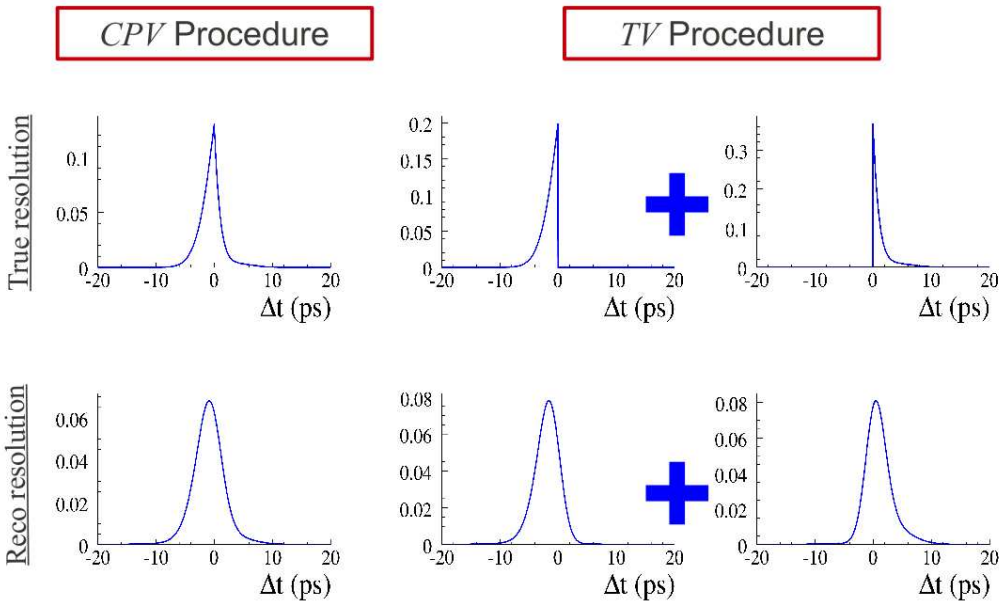

Fig. 4.1: Δt distributions for the most recent *CP* violation analysis on the left side (red), and our *TV* analysis procedure on the right side (blue). The top row graphs are produced without Δt resolution effects, while the bottom row graphs are produced with Δt resolution effects. In the latter it is explicitly shown that the $\Delta t > 0$ ($\Delta t < 0$) part has a contribution of $\Delta t_{\rm true} \equiv \Delta t_{true} > 0$ ($\Delta t_{\rm true} < 0$) and $\Delta t_{\rm true} < 0$ ($\Delta t_{\rm true} > 0$) due to the convolution of the signal model with the resolution function. Since we cannot separate directly $\Delta t_{\rm true} > 0$ or $\Delta t_{\rm true} < 0$ we have to disentangle those regions through our maximum likelihood fit to combined $\Delta t > 0$ and $\Delta t < 0$ data.

We can rewrite the decay rates in terms of the $(\Delta C^{\pm}, \Delta S^{\pm})$ base, taking as reference intensity parameters $(S^{+}_{\ell^+,K_S}, C^{+}_{\ell^+,K_S})$ and $(S^{-}_{\ell^+,K_S}, C^{-}_{\ell^+,K_S})$. The explicit relations between the $(C^{\pm}, S^{\pm})$ and $(\Delta C^{\pm}, \Delta S^{\pm})$ basis are as follows (also given in Table 4.1 of Sec. 4.1),

$$\begin{aligned}
S^{+}_{\ell^-,K_S} &= \Delta S^{+}_{CP} + S^{+}_{\ell^+,K_S} \ , \\
S^{-}_{\ell^-,K_L} &= \Delta S^{+}_{T} + S^{+}_{\ell^+,K_S} \ , \\
S^{-}_{\ell^+,K_L} &= \Delta S^{+}_{CPT} + S^{+}_{\ell^+,K_S} \ , \\
S^{-}_{\ell^-,K_S} &= \Delta S^{-}_{CP} + S^{-}_{\ell^+,K_S} \ , \\
S^{+}_{\ell^-,K_L} &= \Delta S^{-}_{T} + S^{-}_{\ell^+,K_S} \ , \\
S^{+}_{\ell^+,K_L} &= \Delta S^{-}_{CPT} + S^{-}_{\ell^+,K_S} \ ,
\end{aligned} \tag{4.11}$$

$$\begin{aligned}
C^{+}_{\ell^-,K_S} &= \Delta C^{+}_{CP} + C^{+}_{\ell^+,K_S} \ , \\
C^{-}_{\ell^-,K_L} &= \Delta C^{+}_{T} + C^{+}_{\ell^+,K_S} \ , \\
C^{-}_{\ell^+,K_L} &= \Delta C^{+}_{CPT} + C^{+}_{\ell^+,K_S} \ , \\
C^{-}_{\ell^-,K_S} &= \Delta C^{-}_{CP} + C^{-}_{\ell^+,K_S} \ , \\
C^{+}_{\ell^-,K_L} &= \Delta C^{-}_{T} + C^{-}_{\ell^+,K_S} \ , \\
C^{+}_{\ell^+,K_L} &= \Delta C^{-}_{CPT} + C^{-}_{\ell^+,K_S} \ .
\end{aligned} \tag{4.12}$$

Treating $c\overline{c}K_S$ and $J/\psi K_L$ states as if there were CP eigenstates of opposite CP parity introduces effects that are completely negligible on the scale of statistical and systematic uncertainties of this analysis as discussed in Sec. 2.2.

We perform four different types of unbinned likelihood fits to extract the physics parameters for the eight intensities given in Eqs (4.9) and (4.10) from the four independent samples, $c\overline{c}K_S$ and $J/\psi K_L$, B^0 or $\overline{B}^0$ identified. In the first fit, thereafter referred to as *reference*, *nominal* or *nominal TV fit*, we extract the four reference parameters $(S^{\pm}_{\ell^+,K_S}, C^{\pm}_{\ell^+,K_S})$ together with the remaining 12 T-, CP-, and CPT-violating parameters $(\Delta S^{\pm}_{T}, \Delta C^{\pm}_{T})$, $(\Delta S^{\pm}_{CP}, \Delta C^{\pm}_{CP})$, and $(\Delta S^{\pm}_{CPT}, \Delta C^{\pm}_{CPT})$. Three other fits are also performed in order to assess the significance of T-, CP- and CPT-symmetry violations, by imposing T (and equivalently CP and CPT) conjugated parameters to be identical. We refer to these fits as *No TV*, *No CPV*, and *No CPTV fits*, respectively. The explicit restrictions for each of these fits are given in Table 4.2. These no symmetry breaking constrains are written down with the $(\Delta C^{\pm}, \Delta S^{\pm})$ base formalism. They can be easily expressed in the $(C^{\pm}, S^{\pm})$ base formalism using Eqs (4.11) and (4.12).

Since the data sample used here is identical to that used in the most recent *CP* analysis, which was extensively validated, our *TV* fits on data are done unblind. We performed a number of validation studies on simulation (full signal Monte Carlo and signal plus background parametrized Monte Carlo) and control sample data to check the consistency of our *TV* signal model. In addition, we also performed fits like in the last *CP* violation analysis to reproduce the previous results. For this check, we do use our *TV* signal model with the appropriate constraints on our physics parameters (i.e., assume *CPT* invariance, no *CPV* in mixing, in addition to $\Delta\Gamma = 0$), thus we can apply the constrains in Eqs (4.5) and (4.6) where we already considered the opposite *CP* eigenvalue for $c\overline{c}K_S$ and $J/\psi K_L$ states, $\eta_f = -1$ and $+1$, respectively, thus the only free parameters are ($f = K_S$)

$$S^+_{\ell^+,K_S} \equiv S_f = \frac{2Im\lambda_f}{1+|\lambda_f|^2}, \qquad C^+_{\ell^+,K_S} \equiv C_f = \frac{1-|\lambda_f|^2}{1+|\lambda_f|^2}. \tag{4.13}$$

Within the Standard Model with $\Delta\Gamma = 0$, we expect $\lambda_f = \eta_f e^{-2i\beta}$, therefore

$$C^+_{\ell^+,K_S} = 0, \qquad S^+_{\ell^+,K_S} \simeq \sin 2\beta. \tag{4.14}$$

Finally, the signal model used for the $B_{\rm flav}$ samples is identical to that in the most recent *CP* analysis,

$$h_\pm(\Delta t_{\rm true}) \;\propto\; e^{-\Gamma|\Delta t_{\rm true}|}\left[1 \pm \cos(\Delta m \Delta t_{\rm true})\right] \;, \tag{4.15}$$

where the $\pm$ sign refers to mixed ($-$) and unmixed ($+$) events. The assumptions in this $B_{\rm flav}$ signal model (no symmetry violations) have a completely negligible effect on the scale of statistical uncertainties of this analysis, although a systematic uncertainty will be assigned (see Sec. 4.5).

Resolution function

We assume, based on Monte Carlo studies, the same resolution for signal $B_{\rm flav}$ and $c\overline{c}K^0$ events and assign a systematic error due to this assumption. The splitting of the parameters and the value of the fixed parameters were checked in the *CP* violation analysis and we repeated and confirmed this validation, except for the treatment of the width of the outliers component (see below). The signal resolution function ($\mathcal{R}(\delta_t;\sigma_{\Delta t})$), where $\delta_t = \Delta t - \Delta t_{\rm true}$ and $\sigma_{\Delta t}$ is the estimate of the $\Delta t_{\rm rec}$ uncertainty obtained by the reconstruction algorithms, is a triple (core, tail, outliers) Gaussian function, where the mean and width of the core, tail and outliers Gaussians scale with $\sigma_{\Delta t}$. We fix the tail scale factor to be 3.5 and the outliers scale factor to be 12, values which were derived from studies performed on signal only Monte Carlo

studies and B_{flav} samples. We fix these scale factors due to the large correlations with other resolution function parameters. To motivate this change in the resolution function we have compared the likelihoods obtained with and without scaling the outliers, observing a gain of 50 in log-likelihood. Another evidence to support this choice [58] is shown in Fig. 4.2, where the root mean square (RMS) residual clearly scales with the per-event error up to 2.5 ps. The effect of fixing them will be considered in the systematic error determination. As in the case of the most recent *CP* violation analysis, only events satisfying the vertexing requirements $|\Delta t| < 20$ ps and $\sigma_{\Delta t} < 2.5$ ps are considered for further analysis.

In summary, there are seven floating parameters of the signal resolution function. These are (with the number of floating parameters indicated in parenthesis):

- *Core scale factor*, split between *Lepton* and *non-Lepton* flavor ID events (2): $Scale_{(\text{core,signal})-Lepton}$, $Scale_{(\text{core,signal})-non-Lepton}$.
- *Core bias*, split between *Lepton* and *non-Lepton* flavor ID events (2): $\delta_{(\text{core,signal})-Lepton}(\Delta t)$, $\delta_{(\text{core,signal})-non-Lepton}(\Delta t)$.
- *Core fraction*, common for all flavor ID categories (1): $f_{\text{core,signal}}$.
- *Tail bias*, common for all flavor ID categories (1): $\delta_{\text{tail}}(\Delta t)$.
- *Outliers fraction*, common for all flavor ID categories (1): $f_{outlier}$.

The following three resolution parameters are fixed:

- Tail scale factor to 3.5.
- Outliers scale factor to 12.
- Outliers mean to 0.

Taking into account the resolution function, we describe the observed decay rate as a function of Δt, as

$$\begin{aligned} G_{\alpha,\beta}(\Delta t) \;\propto\; & G^{+}_{\alpha,\beta}(\Delta t_{\text{true}})H(\Delta t_{\text{true}}) \otimes \mathcal{R}(\Delta t;\sigma_{\Delta t}) + \\ & G^{-}_{\alpha,\beta}(-\Delta t_{\text{true}})H(-\Delta t_{\text{true}}) \otimes \mathcal{R}(\Delta t;\sigma_{\Delta t}), \end{aligned} \tag{4.16}$$

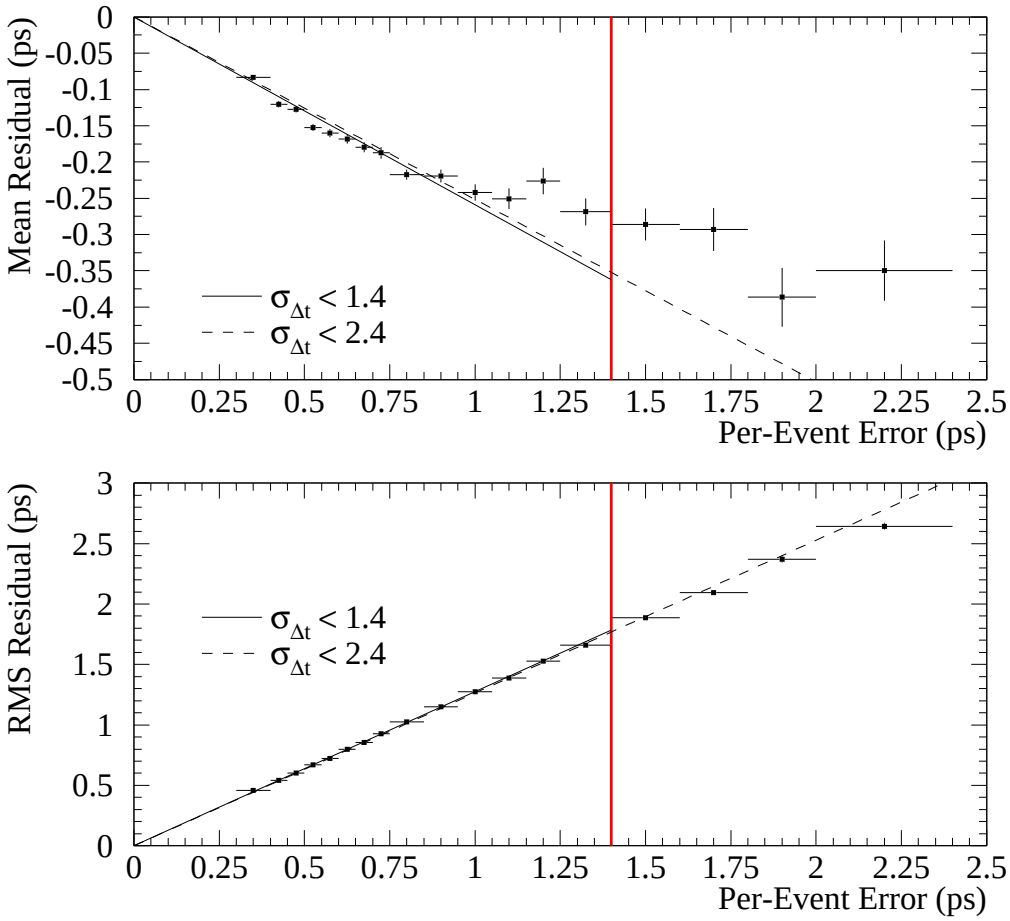

Fig. 4.2: Mean and width of the Monte Carlo Δt residual in bins of the per-event error $\sigma_{\Delta t}$. Fits are shown to aline constrained to pass through the origin for $\sigma_{\Delta t} < 1.4$ ps and $\sigma_{\Delta t} < 2.4$ ps.

Flavor misID, flavor ID and reconstruction efficiency differences

The complete expression of the signal PDF given in Eq. (4.9) must be modified to account for mistakes in the flavor ID (misID fractions w), differences in mistakes between B^0 and $\overline{B}^0$ events (misID fraction differences Δw), and efficiency difference ratios between B^0 and $\overline{B}^0$ for reconstruction (ρ_β) and flavor ID states (τ_α),

$$\mathcal{G}_{\alpha,\beta}(\Delta t_{\rm true}) \;\propto \rho_\beta \left\{\tau_\alpha(1-w_\alpha)G_{\alpha,\beta}(\Delta t_{\rm true}) + \tau_{\bar\alpha} w_{\bar\alpha} G_{\bar\alpha,\beta}(\Delta t_{\rm true})\right\} \;, \quad (4.17)$$

with $\alpha \in \{\ell^+, \ell^-\}$ and $\beta \in \{K_S, J/\psi K_L\}$. The index $\bar\alpha$ denotes the opposite flavor ID to that given by α. For the $B_{\rm flav}$ signal model we have a similar expression,

$$\mathcal{H}_{\alpha,\beta}(\Delta t_{\rm true}) \;\propto \rho_\beta \left\{\tau_\alpha(1-w_\alpha)h_{\alpha,\beta}(\Delta t_{\rm true}) + \tau_{\bar\alpha} w_{\bar\alpha} h_{\bar\alpha,\beta}(\Delta t_{\rm true})\right\} \;, \quad (4.18)$$

where here $\beta = B^0, \overline{B}^0$, and $h_{\alpha,\beta}(\Delta t_{\rm true}) \equiv h_-(\Delta t_{\rm true})$ when α and β refer both to the same flavor state (B^0 or $\overline{B}^0$), conversely $h_{\alpha,\beta}(\Delta t_{\rm true}) \equiv h_+(\Delta t_{\rm true})$ when α and β refer to different flavor states (B^0 and $\overline{B}^0$). The parameters ρ_β and τ_α represent the reconstruction and flavor ID efficiencies for the given state, $\beta = B^0, \overline{B}^0, K_S, K_L$ and $\alpha = \ell^+, \ell^-$, respectively, regardless of whether the assigned flavor is correct or not. Since the average reconstruction and flavor ID efficiencies, $\rho = (\rho_{B^0} + \rho_{\overline{B}^0})/2$ and $\tau = (\tau_{\ell^+} + \tau_{\ell^-})/2$, are reabsorbed in the normalization (see Sec. 4.2.2 below), only the efficiency difference ratio between B^0 and $\overline{B}^0$ reconstruction (for $B_{\rm flav}$ sample states) and flavor ID (for both $B_{\rm flav}$ and B_{CP} samples) are relevant,

$$\begin{aligned} \nu &= \frac{\rho_{B^0} - \rho_{\overline{B}^0}}{\rho_{B^0} + \rho_{\overline{B}^0}} \;, \\ \mu &= \frac{\tau_{\ell^+} - \tau_{\ell^-}}{\tau_{\ell^+} + \tau_{\ell^-}} \;. \end{aligned} \quad (4.19)$$

The average misID fractions $w = (w_{\ell^+} + w_{\ell^-})/2$ and misID fraction differences $\Delta w = w_{\ell^+} - w_{\ell^-}$ (therefore $w_{\ell^+} = w + \Delta w/2$ and $w_{\ell^-} = w - \Delta w/2$) are split by flavor ID category, so in total there are 12 misID parameters (w^{signal}-*Lepton*, w^{signal}-*Kaon I*, w^{signal}-*Kaon II*, w^{signal}-*KaonPion*, w^{signal}-*Pions*, w^{signal}-*Other*, Δw^{signal}-*Lepton*, Δw^{signal}-*Kaon I*, Δw^{signal}-*Kaon II*, Δw^{signal}-*KaonPion*, Δw^{signal}-*Pions*, and Δw^{signal}-*Other*). The reconstruction (flavor) efficiency difference ratio between B^0 and $\overline{B}^0$ is floated (μ, one parameter) as well as the flavor ID efficiency difference ratio, split by flavor ID category, in total there are six free parameters ($\epsilon^{signal}_{ratio}$-*Lepton*, $\epsilon^{signal}_{ratio}$-*Kaon I*, $\epsilon^{signal}_{ratio}$-*Kaon II*, $\epsilon^{signal}_{ratio}$-*KaonPion*, $\epsilon^{signal}_{ratio}$-*Pions*, and $\epsilon^{signal}_{ratio}$-*Other*). All these parameters, together with the resolution function parameters, are first extracted from the $B_{\rm flav}$ sample and then fixed in the nominal fit to the $c\overline{c}K^0$ samples ($c\overline{c}K_S$ and $J/\psi K_L$).

Normalization

The final signal PDF will therefore be obtained from the convolution of Eq. (4.17) with the signal resolution function $\mathcal{R}(\delta_t;\sigma_{\Delta t})$ discussed in Sec. 4.2.2. The normalization of this PDF is done simultaneously for both terms of the decay rate (positive and negative Δt) in Eq. (4.9), and for B^0 and $\overline{B}^0$ flavor ID together, while $c\overline{c}K_S$ and $J/\psi K_L$ samples are normalized separately,

$$\sum_{\alpha=\ell^+,\ell^-}\int_{t_0}^{t_1}\mathcal{G}_{\alpha,\beta}(\Delta t_{\rm true})\otimes\mathcal{R}(\delta_t;\sigma_{\Delta t})d\Delta t = 1 \quad \forall\sigma_{\Delta t},\forall\ \beta = K_S,K_L\ , \tag{4.20}$$

where $\delta_t = \Delta t - \Delta t_{true}$, and $t_0 = -\infty$ (-20) ps, $t_1 = +\infty$ $(+20)$ ps, for asymptotic (finite) normalization. The reference fit uses asymptotic normalization, but finite normalization using the experimental $[-20,20]$ ps interval is also performed to study systematic uncertainties. The normalization is applied separately for each flavor ID category. The normalization of the $B_{\rm flav}$ sample is performed similarly, but in this case mixed and unmixed states are normalized simultaneously.

4.2.3 Combinatorial background description

The combinatorial background model is identical to that used in the most recent *CP* violation analysis [37]. We summarize below some of the main features.

Background Δt structure

The background in both the $B_{\rm flav}$ and the $c\overline{c}K^0$ sample has contributions from continuum events $(u\bar{u},d\bar{d},s\bar{s},c\bar{c})$, B^+B^- decays and $B^0\overline{B}^0$ decays. The continuum is parametrized as a prompt time-dependent component while the $B\bar{B}$ backgrounds are treated as having a single "effective" lifetime, which is left floating in the fit. The lifetime is assumed to be the same for $c\overline{c}K^0$ and $B_{\rm flav}$ events while the fraction of the prompt background component is split by *Lepton* and *non-Lepton* flavor ID categories and floated in the fit separately for $c\overline{c}K^0$ and $B_{\rm flav}$ events.

The prompt (labeled with 1) and non-prompt (labeled with 2) PDF for the $B_{\rm flav}$ sample are

$$\begin{aligned}
\mathcal{B}^{\rm flav}_{\pm,i,1} &= (1/2)(1\pm\mathcal{D}^{\rm flav}_{i,1})\ \delta(\Delta t)\otimes\mathcal{R}_{\rm bg}(\delta_{\rm t};\sigma_{\Delta t})\ , \\
\mathcal{B}^{\rm flav}_{\pm,i,2} &= (\Gamma_{\rm bg,eff}/4)[1\pm\mathcal{D}^{\rm flav}_{i,2}\cos(\Delta m_{\rm bg,eff}\Delta t)]{\rm e}^{-\Gamma_{\rm bg,eff}|\Delta t|}\otimes\mathcal{R}(\delta_{\rm t};\sigma_{\Delta t})\ ,
\end{aligned} \tag{4.21}$$

where $\pm$ refers to mixed (unmixed) events and i is the flavor ID category; $\mathcal{D}^{\rm flav}_{i,1} = 1-2w^{\rm flav}_{i,1}$ is the dilution of each category measured in the $B_{\rm flav}$ sample,

where $w_{i,1}^{\rm flav}$ is the corresponding misID rate. The mixing component of the lifetime background $\Delta m_{\rm bg,eff}$ is allowed to be a free parameter in the nominal fit. For the $c\overline{c}K^0$ samples, the prompt and non-prompt PDFs are

$$\begin{aligned}\mathcal{B}^{CP}_{\pm,i,1} &= (1/2)\delta(\Delta t)\otimes\mathcal{R}(\delta_{\rm t};\sigma_{\Delta t}), \qquad (4.22)\\ \mathcal{B}^{CP}_{\pm,i,2} &= (\Gamma_{\rm bg,eff}/4)\left\{1\pm[S^{\rm bg,eff}_{i,2}\sin(\Delta m\Delta t)-C^{\rm bg,eff}_{i,2}\cos(\Delta m\Delta t)]\right\}\times \\ &\quad {\rm e}^{-\Gamma_{\rm eff}|\Delta t|}\otimes\mathcal{R}(\delta_{\rm t};\sigma_{\Delta t}),\end{aligned}$$

where $\pm$ refers here to B^0 ($\overline{B}^0$) flavor-identified events, i.e., ℓ^+ (ℓ^-), and i is the flavor ID category. The parameters $S^{\rm bg,eff}_{i,2} = \frac{2\mathcal{I}m\lambda_{\rm bg,eff}}{1+|\lambda_{\rm bg,eff}|^2}$ and $C^{\rm bg,eff}_{i,2} = \frac{1-|\lambda_{\rm bg,eff}|^2}{1+|\lambda_{bg,eff}|^2}$ are effective *CP*- and *T*-violating parameters (*CPT* is assumed in our background model to be a good symmetry). Note that these parameters absorb the effective misID in the non-prompt combinatorial background component. In the nominal *TV* fit we assume $|\lambda_{\rm bg,eff}|^2 = 1$ and fit $\mathcal{I}m\lambda_{\rm bg,eff}$ separately for each flavor ID category taking $\eta_{\rm bg,eff} = +1$ (see below).

Background resolution function

We describe the background resolution function using a double (core plus outliers) Gaussian functions. The core Gaussian has a floating bias and width, both of which scale with the per-event Δt error $\sigma_{\Delta t}$. The outliers Gaussian has a fixed mean (0) and width (12). In contrast to the signal resolution function discussed in Sec. 4.2.2, we assume the background resolution function to be the same for all flavor ID categories, i.e., we do not split the scale factor and the bias between *Lepton* and *non-Lepton*. The resolution function of the background is assumed to be the same for the $B_{\rm flav}$ and $c\overline{c}K^0$ modes.

In summary, we float a total of 39 background parameters. These are (where the number of floating parameters is indicated in parenthesis):

- *Effective lifetime* $\Gamma_{\rm bg,eff}$, common to $B_{\rm flav}$ and $c\overline{c}K^0$ samples and all flavor ID categories (1).
- *Effective mixing frequency*, common to all $B_{\rm flav}$ flavor ID categories (1). The non-prompt combinatorial background mixing frequency for $c\overline{c}K^0$ has been fixed to 0.507 ps^{-1}.
- *Fraction of prompt vs lifetime events*, split into $B_{\rm flav}$ and $c\overline{c}K^0$ modes, and then split into *Lepton* and *non-Lepton* events (4).
- *MisID fractions and* B^0-$\overline{B}^0$ *differences in misID-fractions of the* $B_{\rm flav}$ *sample*, floated separately for each of the six flavor ID categories, and then separately for each prompt and exponential component (24).

- *Effective CP parameters for non-prompt background of the $c\bar{c}K^0$ samples, $\mathcal{I}m\lambda_{\rm bg,eff}$* with $\eta_{\rm bg,eff} = +1$, which are floated separately for each of the six flavor ID categories (6). Direct *CP* conservation is assumed, i.e., $|\lambda_{\rm bg,eff}|^2 = 1$.

- *Core scale factor*, common to both $B_{\rm flav}$ and $c\bar{c}K^0$ modes and all six flavor ID categories (1).

- *Core bias*, common to both $B_{\rm flav}$ and $c\bar{c}K^0$ modes and all six flavor ID categories (1).

- *Outliers fraction*, common to both $B_{\rm flav}$ and $c\bar{c}K^0$ modes and all six flavor ID categories (1).

In practice, all background parameters common to $B_{\rm flav}$ and $c\bar{c}K^0$ samples are first extracted from the fit to the $B_{\rm flav}$ sample, and then fixed in the reference fit to the $c\bar{c}K^0$ samples.

4.2.4 Peaking backgrounds for $c\bar{c}K_s$ and $B_{\rm flav}$ modes

The small fraction of events that peak in the $m_{\rm ES}$ spectrum is due to background events from incorrectly reconstructed charged or neutral B decays. The treatment of these peaking backgrounds is different for the $B_{\rm flav}$ and the B_{CP} sample modes, and is identical to the most recent *CP* violation analysis [37, 50, 51]. This is summarized in the following.

$c\bar{c}K_s$ modes

The peaking backgrounds in the $c\bar{c}K_s$ modes include both B^+B^- and $B^0\overline{B}^0$ decays. In general these peaking fractions are kept fixed in the fit and are treated as pure B^0 decays (similar to the true signal) but are assumed to have no *CP* content in the reference fit.

As described in Ref. [50], the evaluation of the peaking background contribution for the $c\bar{c}K_s$ modes has been performed using a large sample (from simulation production 9, SP9) of inclusive $B \to J/\psi$ Monte Carlo simulation. We assume (as previously validated) that the small amount of events where the charmonium meson is incorrectly reconstructed do not peak in $m_{\rm ES}$. We evaluate the peaking background separately for each mode, but combined for all flavor ID categories. We consider only flavor ID events that satisfy the vertexing requirements. The procedure is the following:

1. Fit the $m_{\rm ES}$ distribution of the full signal plus background inclusive J/ψ Monte Carlo sample for each decay mode, $J/\psi K_s(\pi^+\pi^-)$, $J/\psi K_s(\pi^0\pi^0)$,

$\psi(2S)K_S$, and $\chi_{c1}K_S$. This fit determines the full Gaussian yield, signal width, signal mean and background Argus shape parameter.

2. Repeat the fit on the events in the inclusive J/ψ Monte Carlo sample where the reconstructed channel does not match the generated one. For this fit, all parameters except the number of events in the Gaussian peak and the number of events in the Argus distribution are fixed to the values obtained in step 1.

3. The input for the peaking background to the reference fit is the ratio between the number of events in the Gaussian peak from the two fits.

The results of this procedure are reported in Table 4.4. Detailed figures of this procedure can be found in [50].

Mode	f_{peak}
$J/\psi K_S(\pi^+\pi^-)$	0.0026 ± 0.0005
$J/\psi K_S(\pi^0\pi^0)$	0.0088 ± 0.0022
$\psi(2S)K_S$	0.018 ± 0.004
$\chi_{c1}K_S$	0.021 ± 0.004

Tab. 4.4: Peaking background fractions for the $c\bar{c}K_S$ channels. Errors are statistical only. Taken from [50].

For each $c\bar{c}K_S$ mode, the events in the signal region $m_{\text{ES}} > 5.27$ GeV are studied to analyze which decay modes contribute with a known *CP* content in order to reduce the systematic error because in the reference fit we assume the peaking background in the *CP* sample to have no *CP* content (so we are assigning a PDF similar to that of the signal but without the sinus term). The peaking background composition is summarized in Table 4.5,taken from [50]:

B_{flav} modes

The peaking background for the B_{flav} sample modes includes contributions only from B^+B^- decays. The peaking background from $B^0\overline{B}^0$ is treated as part of the signal. Its fraction is estimated separately for each reconstructed mode (see Table 4.6) using generic Monte Carlo B^+B^- decays. The peaking background fractions are then fixed in the reference fit and varied in the systematic error evaluation. These events are treated as B^+B^- decays, with a fixed lifetime of $\tau_{B^\pm} = 1.638$ ps [15] with no mixing and fixed flavor ID parameters extracted from a previous fit to the $B^\pm \to D^{(*)0}\pi^\pm$ control sample [59]. The same procedure as for the $c\bar{c}K_S$ modes, described previously, has

Background component	η_f	Decay Mode fractions $J/\psi K_S(\pi^+\pi^-)$	$J/\psi K_S(\pi^0\pi^0)$	$\psi(2S)K_S$	$\chi_{c1}K_S$
B^+B^-	0	0.51	0.49	0.44	0.52
$J/\psi K^{*0}(K_S\pi^0)$	0.504	0.0196	0.12	0.012	0.166
$J/\psi K^{*0}$ $K\pi$	0	0.28	0.011	0.025	0.050
$J/\psi K_L$	1	0.011	0.067	–	–
$J/\psi K^{*0}$ $K_L\pi^0$	-0.504	–	0.067	–	–
$J/\psi\pi^0$	1	–	0.063	–	–
Other $B^0\overline{B}^0$	unknown	0.193	0.182	0.52	0.272

Tab. 4.5: Peaking background composition for the $c\overline{c}K_S$, where η_f is the *CP* eigenvalue of the background assumin $S = \sin 2\beta$.

been adopted but the fraction of peaking background is computed separately for B^+ and B^0 decays (from generic $B^0\overline{B}^0$ and B^+B^- Monte Carlo). The peaking background from B^0 is treated as part of the signal in the baseline fit, but it is explicitly considered in the evaluation of systematic uncertainties, since in principle these mis-reconstructed events might have different flavor ID parameters. Table 4.6 shows the $B^0\overline{B}^0$ and B^+B^- peaking background fractions. Details of the $m_{\rm ES}$ distributions for the various modes can be found in [50].

4.2.5 $J/\psi K_L$ mode

Several parameters are unique to describe the $J/\psi K_L$ decay:

- The relative fractions for signal and background modes: $J/\psi K^{*0}$, $J/\psi K^{*+}$, $J/\psi K_S$, $J/\psi K_L\pi^0$, $J/\psi K_L\pi^+$, $\chi_c(1)K_L$, the rest of J/ψ inclusive background, non-ψ prompt and non-prompt backgrounds. They are split by reconstruction type (EMC or IFR), J/ψ lepton decay type (e^+e^-, $\mu^+\mu^-$) and flavor ID category.

- The parameters of the ΔE PDFs to the ΔE shapes for signal, inclusive J/ψ, $J/\psi K_S$, and the non-ψ distributions derived from ΔE fits (see Sec. 3.2) are split by reconstruction type (EMC or IFR) and J/ψ lepton decay type.

The sample composition fractions from the ΔE fit described in Sec. 3.2 ($F_{\rm sig}$, $F_{\psi X}$ and $F_{\rm non-\psi}$) are evaluated simultaneously for $J/\psi \to e^+e^-$ and $J/\psi \to \mu^+\mu^-$ and separately for EMC and IFR, and are fixed inputs to the nominal *TV* fit split by flavor ID categories. The fractions given in Tables 3.7 and 3.8 are used to calculate the input parameters. The fractions

$B_{\rm flav}$ sample decay mode	$f_{\rm peak}$ (% $B^0\overline{B}^0$)	$f_{\rm peak}$ (% B^+B^-)
$D^{*-}\pi^+, K\pi$	0.44 ± 0.04	0.94 ± 0.09
$D^{*-}\pi^+, K\pi\pi^0$	1.20 ± 0.14	1.08 ± 0.12
$D^{*-}\pi^+, K3\pi$	0.80 ± 0.08	0.90 ± 0.09
$D^{*-}\pi^+, K_S\pi\pi$	1.05 ± 0.20	0.80 ± 0.15
$D^{*-}\rho^+, K\pi$	1.71 ± 0.22	0.84 ± 0.11
$D^{*-}\rho^+, K\pi\pi^0$	2.06 ± 0.34	0.87 ± 0.14
$D^{*-}\rho^+, K3\pi$	1.87 ± 0.26	0.57 ± 0.06
$D^{*-}\rho^+, K_S\pi\pi$	3.06 ± 0.57	0.57 ± 0.08
$D^{*-}a_1^+, K\pi$	0.98 ± 0.16	0.90 ± 0.15
$D^{*-}a_1^+, K\pi\pi^0$	1.49 ± 0.30	0.86 ± 0.17
$D^{*-}a_1^+, K3\pi$	1.36 ± 0.23	0.69 ± 0.12
$D^{*-}a_1^+, K_S\pi\pi$	0.73 ± 0.36	0.96 ± 0.47
$D^-\pi^+, K\pi\pi$	0.82 ± 0.05	1.40 ± 0.08
$D^-\pi^+, K_S\pi$	3.27 ± 0.29	0.49 ± 0.04
$D^-\rho^+, K\pi\pi$	1.05 ± 0.10	1.21 ± 0.11
$D^-\rho^+, K_S\pi$	1.78 ± 0.42	0.45 ± 0.11
$D^-a_1^+, K\pi\pi$	7.13 ± 0.26	0.42 ± 0.02
$D^-a_1^+, K_S\pi$	7.62 ± 0.79	0.06 ± 0.01
$J/\psi K^{*0}, K^+\pi^-, e^+e^-$	2.47 ± 0.15	0.90 ± 0.13
$J/\psi K^{*0}, K^+\pi^-, \mu^+\mu^-$	2.55 ± 0.16	0.79 ± 0.13

Tab. 4.6: Peaking background fractions for the $B_{\rm flav}$ sample. For some of the $B_{\rm flav}$ decay modes there is a peaking contribution from modes that have the same flavor ID side that the mode under consideration, for example $B^0 \to D^-K^+$ for $B^0 \to D^-\pi^+$. These are excluded from the peaking background fractions. Taken from [50].

of signal events ($J/\psi K_L$) given in Tables 3.7 and 3.8 are also included in Tables 4.7 and 4.8. The fraction for the $J/\psi X$ component is adjusted accordingly to the various contents of the itemized background composition. For each background mode, the number of events is taken from Table 1 in Ref. [51] and normalized with respect to the other background modes. This number is then multiplied by the fractions in Tables 3.7 or 3.8 to obtain the corresponding fractions in Tables 4.7 and 4.8 for the EMC and IFR, respectively. For the non-ψ component, the prompt fractions obtained from the Δt fits to the non-$J/\psi K_L$ sideband data (see Sec. 3.2) for each flavor ID category are used as input for the calculation of the final fractions. Together with the fractions in Tables 3.7 and 3.8, they give us the non-J/ψ prompt and lifetime fractions shown in Tables 4.7 and 4.8. We note that the $J/\psi K_L$, $J/\psi K^{*0}$, $J/\psi K^{*+}$, $J/\psi K_S$, $J/\psi K_L\pi^+$, $\chi_c(1)K_L$, other J/ψ X, non$-J/\psi$, life-

time, and non$-J/\psi$, prompt component fractions sum to 1.0 as expected. The $J/\psi K_L\pi^0$ component shown falls into the other J/ψ X category, which is also shown.

As in the last *CP* violation analysis, the $J/\psi K_L$ part of the *TV* fit is described using different background components: $\chi_{c1}K_L$ with $\eta_f = +1$, $J/\psi K^{*0}$ with $\eta_f = -0.504 \pm 0.033$ [60], $J/\psi K_S$ with $\eta_f = -1$, a mixture of exclusive J/ψ decays with no *CP* content (which contains the charged B decays $J/\psi K^{*+}$ and $J/\psi K_L\pi^+$), other $J/\psi X$ decays (which includes the $J/\psi K_L\pi^0$ component) with η_f varying in the range $(-0.003, 0.07)$ depending on the K_L (EMC or IFR) and lepton type ($J/\psi \to e^+e^-$ or $\mu^+\mu^-$), and a non$-J/\psi$ component with prompt and lifetime contributions for which we assume no *CP* content ($\eta_f = 0$).

Direct *CP* asymmetries are assumed zero for all components, except for the lifetime term of the non$-J/\psi$ component where a small asymmetry is included with $|\lambda_{\text{non}-\text{J}/\psi,\text{non}-\text{prompt}}| = 0.964$ kept fixed, and for $J/\psi K^{*0}$ and $J/\psi K_S$ where the parameters $|\lambda_{J/\psi K^{*0}}|$ and $|\lambda_{J/\psi K_S}|$ are floated on data applying constraints coming from the Δt fit to the corresponding samples. The constraints are applied as two extra Gaussian terms summed to the log likelihood. The $S = \frac{2\mathcal{I}m\lambda}{1+|\lambda|^2}$ parameters for all background components containing a real J/ψ is fixed with $\mathcal{I}m\lambda = 0.703$ (i.e., large *CP* asymmetry). For the non-J/ψ lifetime component the *CP* asymmetries are left floated and kept common to the non-prompt combinatorial background component of the $c\bar{c}K_S$ sample, i.e., $\mathcal{I}m\lambda_{\text{bg,eff}}$ (the sensitivity comes from the ΔE sidebands), although in the nominal *TV* fit it has no effect since for this component the reference *CP* content is zero as indicated above. A number of different variations to these assumptions will be done in the evaluation of the systematic uncertainties.

4.3 Construction of *T*, *CP*, and *CPT* asymmetries

The difference in the rates for any pair of symmetry-transformed transitions normalized to their sum is usually used as observable to probe the symmetry violation. In practice, we construct raw asymmetries using the number of events for each pair of transitions in bins of Δt, normalized to the total number of events of the given subsample. This normalization is particularly relevant for T (and *CPT*) asymmetries since it involves comparison of $c\bar{c}K_S$ and $J/\psi K_L$ states, which overall have different reconstruction efficiencies. Since for a given discrete symmetry there are four possible comparisons between conjugated processes, we have four independent asymmetries or comparisons. For example, for the $\overline{B}^0 \to B_-$ reference transition the raw T

EMC K_L- $J/\psi \to ee$						
Decay mode	Flavor ID category					
	Lepton	*Kaon I*	*Kaon II*	*KaonPion*	*Pions*	*Other*
$J/\psi K_L$	0.3020	0.3380	0.3180	0.2520	0.2970	0.2670
$J/\psi K^{*0}$	0.0794	0.0797	0.0729	0.0789	0.0723	0.0818
$J/\psi K^{*+}$	0.1177	0.1181	0.1080	0.1168	0.1071	0.1212
$J/\psi K_S$	0.0385	0.0386	0.0353	0.0382	0.0350	0.0396
$J/\psi K_L\pi^0$	0.0044	0.0044	0.0041	0.0044	0.0040	0.0046
$J/\psi K_L\pi^+$	0.0059	0.0059	0.0054	0.0058	0.0053	0.0060
$\chi_{c1}K_L$	0.0129	0.0130	0.0119	0.0128	0.0118	0.0133
Other $J/\psi X$	0.2896	0.2906	0.2656	0.2874	0.2635	0.2981
non$-J/\psi$, lifetime	0.0885	0.0626	0.0937	0.1202	0.1002	0.0710
non$-J/\psi$, prompt	0.0654	0.0544	0.0893	0.0878	0.1068	0.1030
EMC K_L- $J/\psi \to \mu\mu$						
Decay mode	Flavor ID category					
	Lepton	*Kaon I*	*Kaon II*	*KaonPion*	*Pions*	*Other*
$J/\psi K_L$	0.3180	0.2860	0.2630	0.2000	0.2440	0.2080
$J/\psi K^{*0}$	0.0846	0.0682	0.0610	0.0635	0.0600	0.0644
$J/\psi K^{*+}$	0.1253	0.1011	0.0904	0.0941	0.0889	0.0954
$J/\psi K_S$	0.0410	0.0330	0.0296	0.0308	0.0291	0.0312
$J/\psi K_L\pi^0$	0.0047	0.0038	0.0034	0.0035	0.0033	0.0036
$J/\psi K_L\pi^+$	0.0062	0.0050	0.0045	0.0047	0.0044	0.0048
$\chi_{c1}K_L$	0.0138	0.0111	0.0099	0.0103	0.0098	0.0105
Other $J/\psi X$	0.3082	0.2486	0.2225	0.2316	0.2188	0.2347
non$-J/\psi$, lifetime	0.0592	0.1321	0.1628	0.2110	0.1665	0.1432
non$-J/\psi$, prompt	0.0438	0.1149	0.1552	0.1540	0.1775	0.2078

Tab. 4.7: Sample composition fractions for $J/\psi K_L$ with K_L EMC and background modes split for each flavor ID category and J/ψ decay mode for $|\Delta E| < 0.08$ GeV.

IFR K_L- $J/\psi \to ee$						
Decay mode	Flavor ID category					
	Lepton	*Kaon I*	*Kaon II*	*KaonPion*	*Pions*	*Other*
$J/\psi K_L$	0.5630	0.5110	0.4020	0.5080	0.4800	0.4480
$J/\psi K^{*0}$	0.0760	0.0913	0.1002	0.0793	0.0795	0.0833
$J/\psi K^{*+}$	0.1452	0.1743	0.1913	0.1515	0.1519	0.1590
$J/\psi K_S$	0.0066	0.0079	0.0086	0.0068	0.0069	0.0072
$J/\psi K_L\pi^0$	0.0048	0.0057	0.0063	0.0050	0.0050	0.0052
$J/\psi K_L\pi^+$	0.0073	0.0088	0.0096	0.0076	0.0076	0.0080
$\chi_{c1}K_L$	0.0155	0.0186	0.0204	0.0162	0.0162	0.0170
Other $J/\psi X$	0.1175	0.1411	0.1548	0.1226	0.1229	0.1234
non$-J/\psi$, lifetime	0.0391	0.0246	0.0573	0.0624	0.0653	0.0608
non$-J/\psi$, prompt	0.0289	0.0214	0.0547	0.0456	0.0697	0.0882
IFR K_L- $J/\psi \to \mu\mu$						
Decay mode	Flavor ID category					
	Lepton	*Kaon I*	*Kaon II*	*KaonPion*	*Pions*	*Other*
$J/\psi K_L$	0.5690	0.4600	0.3660	0.4590	0.4380	0.4210
$J/\psi K^{*0}$	0.0777	0.0831	0.0924	0.0725	0.0736	0.0791
$J/\psi K^{*+}$	0.1483	0.1586	0.1763	0.1385	0.1404	0.1511
$J/\psi K_S$	0.0067	0.0072	0.0080	0.0063	0.0063	0.0068
$J/\psi K_L\pi^0$	0.0049	0.0052	0.0058	0.0045	0.0046	0.0050
$J/\psi K_L\pi^+$	0.0075	0.0080	0.0089	0.0070	0.0071	0.0076
$\chi_{c1}K_L$	0.0158	0.0169	0.0188	0.0148	0.0150	0.0161
Other $J/\psi X$	0.1200	0.1283	0.1427	0.1120	0.1136	0.1222
non$-J/\psi$, lifetime	0.0310	0.0744	0.0957	0.1098	0.0997	0.0800
non$-J/\psi$, prompt	0.0229	0.0646	0.0913	0.0802	0.1063	0.1160

Tab. 4.8: Sample composition fractions for $J/\psi K_L$ with K_L IFR and background modes split for each flavor ID category and J/ψ decay mode for $|\Delta E| < 0.08$ GeV.

asymmetry would explicitly be defined as

$$A_T(\Delta t) \equiv \frac{\mathcal{G}^-_{\ell^-,K_L}(\Delta t) - \mathcal{G}^+_{\ell^+,K_S}(\Delta t)}{\mathcal{G}^-_{\ell^-,K_L}(\Delta t) + \mathcal{G}^+_{\ell^+,K_S}(\Delta t)} \ , \tag{4.23}$$

where $\mathcal{G}^{\pm}_{\alpha,\beta}(\Delta t) = \mathcal{G}_{\alpha,\beta}(\pm\Delta t)H(\Delta t)$. With this construction, $A_T(\Delta t)$ is defined only for positive Δt values. Neglecting flavor misID and proper-time resolution effects, and assuming Eqs (4.5) and (4.6) in the denominator for simplicity, the raw T-asymmetry becomes proportional to $(\Delta C^+_T, \Delta S^+_T)$, reconstruction effects,

$$A_T(\Delta t) \approx \frac{\Delta S^+_T}{2}\sin(\Delta m\Delta t) + \frac{\Delta C^+_T}{2}\cos(\Delta m\Delta t) \ . \tag{4.24}$$

The other three T asymmetries are constructed similarly using the association between transitions and time-ordered decay products for reference and T-conjugate processes given in Table 2.1, and are proportional to $(\Delta C^-_T, \Delta S^-_T)$, $(\Delta C^-_{CP} - \Delta C^-_{CPT}, \Delta S^-_{CP} - \Delta S^-_{CPT})$, and $(\Delta C^+_{CP} - \Delta C^+_{CPT}, \Delta S^+_{CP} - \Delta S^+_{CPT})$, respectively. The raw CP and CPT asymmetries are constructed following a similar procedure using the conjugated processes shown in Tables 2.2, and 2.3 respectively.

It should be noted, that with the methodology proposed, these asymmetries are only used with the purpose of illustrating the symmetry violation effect, through direct comparisons of the time-dependent raw asymmetries from data and the projections of the best-fit results to the decay rates when we allow for both non-invariance and invariance under the symmetry transformation.

4.4 Fit results

4.4.1 Monte Carlo results

B_{flav} Monte Carlo sample results

We use the high statistics (SP9) B_{flav} Monte Carlo sample to determine the resolution and flavor ID parameters to be used in the CP signal Monte Carlo fits. These events are selected from the Monte Carlto Breco cocktail (SP mode 2222), which includes a large sample of $B^0 \to D^{(*)-}[\pi^+, \rho(770)^+, a_1(1260)^+]$, and from the signal $B^0 \to J/\psi K^{*0}(K^+\pi^-)$ Monte Carlo (SP mode 5127). The sample contains 5949k (3619k from SP mode 2222 and 2330k from SP mode 5127) flavor ID events that satisfy the vertexing requirements. Only Monte-Carlo-matched B decays are used in the fit and the

fraction of peaking backgrounds are fixed to zero. The mixing frequency and B lifetime are fixed to the values used in generation, $\Delta m = 0.489$ ps^{-1} and $\tau_{B^0} = 1.541$ ps. Table 4.9 shows the results of these fits. We will compare the flavor ID parameters from these fits to those found using the Monte Carlo truth as part of the systematic error.

	B_{flav} Monte Carlo sample
w^{signal}-*Lepton*	0.0291 ± 0.0004
w^{signal}-*Kaon I*	0.0611 ± 0.0005
w^{signal}-*Kaon II*	0.1600 ± 0.0005
w^{signal}-*KaonPion*	0.2556 ± 0.0006
w^{signal}-*Pions*	0.3490 ± 0.0006
w^{signal}-*Other*	0.4217 ± 0.0008
Δw^{signal}-*Lepton*	-0.0004 ± 0.0008
Δw^{signal}-*Kaon I*	-0.0010 ± 0.0009
Δw^{signal}-*Kaon II*	-0.0036 ± 0.0008
Δw^{signal}-*KaonPion*	-0.0179 ± 0.0010
Δw^{signal}-*Pions*	0.0627 ± 0.0010
Δw^{signal}-*Other*	0.0460 ± 0.0012
$\delta_{(\text{core,signal})-Lepton}(\Delta t)$	-0.0688 ± 0.0042
$\delta_{(\text{core,signal})-non-Lepton}(\Delta t)$	-0.2643 ± 0.0018
$Scale_{(\text{core,signal})-Lepton}$	1.0518 ± 0.0067
$Scale_{(\text{core,signal})-non-Lepton}$	1.1436 ± 0.0030
$f_{\text{core,signal}}$	0.9223 ± 0.0010
f_{outlier}	0.0039 ± 0.0001
$\delta_{\text{tail}}(\Delta t)$	-1.4427 ± 0.0254
$\epsilon^{\text{signal}}_{\text{ratio}}-Lepton$	-0.0128 ± 0.0014
$\epsilon^{\text{signal}}_{\text{ratio}}-Kaon\ I$	-0.0136 ± 0.0014
$\epsilon^{\text{signal}}_{\text{ratio}}-Kaon\ II$	-0.0022 ± 0.0012
$\epsilon^{\text{signal}}_{\text{ratio}}-KaonPion$	0.0029 ± 0.0013
$\epsilon^{\text{signal}}_{\text{ratio}}-Pions$	-0.0267 ± 0.0013
$\epsilon^{\text{signal}}_{\text{ratio}}-Other$	-0.0031 ± 0.0016
$\epsilon^{\text{flav}}_{\text{ratio}}$	0.0071 ± 0.0010

Tab. 4.9: B_{flav} Monte Carlo results for signal flavor ID and resolution function parameters.

Signal Monte Carlo results

To check that our fitting procedure is unbiased, we fit SP9 signal *CP* Monte Carlo samples. In each case the resolution and flavor-identification parameters are fixed to the values obtained from the fit to the Monte Carlo $B_{\rm flav}$ sample (Table 4.9). The free parameters are $\Delta S^{\pm}_{T}$, $\Delta C^{\pm}_{T}$, $\Delta S^{\pm}_{CP}$, $\Delta C^{\pm}_{CP}$, $\Delta S^{\pm}_{CPT}$, and $\Delta C^{\pm}_{CPT}$, and the references $S^{+}_{\ell^+,K_S}$, $S^{-}_{\ell^+,K_S}$, $C^{+}_{\ell^+,K_S}$, and $C^{-}_{\ell^+,K_S}$. Since Monte Carlo matching is required, the fractions of peaking background are fixed at zero. Also, for $J/\psi K_L$ all the background fractions are set to zero. The mixing frequency and B lifetime are fixed to the values used in generation, $\Delta m = 0.489$ ps^{-1} and $\tau = 1.541$ ps. The generated value in the Monte Carlo is $S = 0.703$ and $C = 0$. Note that with these generated values, our model independent T-, *CP*- and CPT-violating parameters are as given in Table 4.10.

($\Delta S^{\pm}$,$\Delta C^{\pm}$) base			
Parameter	Value	Parameter	Value
$S^{+}_{\ell^+,K_S}$	0.703	$C^{+}_{\ell^+,K_S}$	0.0
ΔS^{+}_{T}	-1.406	ΔC^{+}_{T}	0.0
ΔS^{+}_{CP}	-1.406	ΔC^{+}_{CP}	0.0
ΔS^{+}_{CPT}	0.0	ΔC^{+}_{CPT}	0.0
$S^{-}_{\ell^+,K_S}$	-0.703	$C^{-}_{\ell^+,K_S}$	0.0
ΔS^{-}_{T}	1.406	ΔC^{-}_{T}	0.0
ΔS^{-}_{CP}	1.406	ΔC^{-}_{CP}	0.0
ΔS^{-}_{CPT}	0.0	ΔC^{-}_{CPT}	0.0

Tab. 4.10: Generated values for the T-, *CP*- and CPT-violating parameters in the signal Monte Carlo.

We divide the available signal Monte Carlo sample into 345 data-size samples, and then these are grouped into 3 samples containing 115 data-sized samples (i.e. virtually infinite statistics). Firstly, we fit the 115 times data-sized signal Monte Carlo samples; second we fit one by one the 345 data-sized samples and then examine the distribution of the results. The numerical results for the 115 times the data-sized sample fits minus the generated values are summarized in Table 4.11. Table 4.12 summarizes the mean and RMS values of the residual distributions for the 345 data-sized experiments, together with the estimated coverage, i.e., the fraction of experiments where the generated value of the corresponding physics parameter falls into the 1σ interval reported by the fit (with parabolic errors).

A close inspection to Tables 4.11 and 4.12 reveals biases in some parameters which are statistically significant given the large sample of simulated signal Monte Carlo, but still well below the statistical uncertainties from the current data sample (estimated here through the RMS of the residual distributions from the 345 data-sized signal Monte Carlo experiments). The observed pattern is the same for very high statistics and data-sized fits, proving that these effects are not related to the size of the data sample but rather to other systematic effects, very likely the small differences in Δt resolution function and flavor ID performance between the *CP* and $B_{\rm flav}$ samples, and the approximations implicit in the empirical models used to describe the resolution function and flavor ID details. Nevertheless, the absolute bias is actually quite small. We will take the biases or the statistical uncertainties, whichever is larger, as the systematic uncertainty.

Parameter	1-115	116-230	231-345
$C^-_{\ell^+,K_S}$	0.022 ± 0.005	0.012 ± 0.005	0.007 ± 0.005
$C^+_{\ell^+,K_S}$	0.002 ± 0.006	0.015 ± 0.006	-0.001 ± 0.006
ΔC^-_{CP}	-0.015 ± 0.009	-0.006 ± 0.009	-0.018 ± 0.009
ΔC^-_{CPT}	-0.028 ± 0.010	-0.019 ± 0.010	-0.017 ± 0.010
ΔC^-_{T}	0.008 ± 0.011	-0.014 ± 0.011	-0.023 ± 0.011
ΔC^+_{CP}	0.002 ± 0.009	-0.015 ± 0.009	-0.013 ± 0.009
ΔC^+_{CPT}	0.013 ± 0.011	-0.004 ± 0.012	-0.000 ± 0.011
ΔC^+_{T}	-0.002 ± 0.010	-0.006 ± 0.010	-0.033 ± 0.010
ΔS^-_{CP}	0.015 ± 0.012	0.002 ± 0.012	-0.018 ± 0.012
ΔS^-_{CPT}	-0.013 ± 0.009	-0.021 ± 0.010	-0.039 ± 0.009
ΔS^-_{T}	-0.064 ± 0.015	0.079 ± 0.015	-0.092 ± 0.015
ΔS^+_{CP}	-0.017 ± 0.010	-0.006 ± 0.010	0.008 ± 0.010
ΔS^+_{CPT}	0.045 ± 0.017	0.016 ± 0.017	-0.010 ± 0.016
ΔS^+_{T}	-0.075 ± 0.012	0.005 ± 0.012	0.045 ± 0.012
$S^-_{\ell^+,K_S}$	0.005 ± 0.006	0.020 ± 0.006	0.022 ± 0.006
$S^+_{\ell^+,K_S}$	0.003 ± 0.008	0.002 ± 0.009	-0.011 ± 0.008

Tab. 4.11: Fitted minus generated values for all the *T*-, *CP*- and *CPT*-violating parameters for the 115 times data-sized signal Monte Carlo samples.

Figures 4.3, 4.4 and 4.5 show the raw *T*-, *CP*- and *CPT*-asymmetries respectively, for the first 115 times data-sized signal Monte Carlo experiment, for flavor ID categories containing leptons and kaons combined. Note that these asymmetries correspond to a virtually infinite statistics, but with misID and Δt resolution incorporated.

Parameter	Mean residual	RMS residual	Coverage
$C^-_{\ell^+,K_S}$	0.015 ± 0.004	0.062 ± 0.003	0.63 ± 0.04
$C^+_{\ell^+,K_S}$	0.006 ± 0.004	0.070 ± 0.003	0.69 ± 0.04
ΔC^-_{CP}	-0.013 ± 0.005	0.099 ± 0.004	0.68 ± 0.05
ΔC^-_{CPT}	-0.022 ± 0.006	0.108 ± 0.004	0.68 ± 0.05
ΔC^-_{T}	-0.011 ± 0.006	0.114 ± 0.005	0.68 ± 0.04
ΔC^+_{CP}	-0.008 ± 0.006	0.102 ± 0.004	0.63 ± 0.04
ΔC^+_{CPT}	0.005 ± 0.008	0.137 ± 0.006	0.64 ± 0.04
ΔC^+_{T}	-0.014 ± 0.006	0.110 ± 0.004	0.67 ± 0.04
ΔS^-_{CP}	0.003 ± 0.007	0.128 ± 0.005	0.68 ± 0.04
ΔS^-_{CPT}	-0.026 ± 0.006	0.106 ± 0.004	0.62 ± 0.04
ΔS^-_{T}	-0.075 ± 0.009	0.166 ± 0.007	0.63 ± 0.04
ΔS^+_{CP}	-0.009 ± 0.007	0.123 ± 0.005	0.66 ± 0.04
ΔS^+_{CPT}	0.016 ± 0.009	0.174 ± 0.007	0.66 ± 0.04
ΔS^+_{T}	0.012 ± 0.007	0.136 ± 0.005	0.68 ± 0.05
$S^-_{\ell^+,K_S}$	0.017 ± 0.004	0.063 ± 0.003	0.67 ± 0.04
$S^+_{\ell^+,K_S}$	0.003 ± 0.005	0.099 ± 0.004	0.64 ± 0.04

Tab. 4.12: Mean and RMS values of the residual (fitted−generated) distributions for all the T-, CP- and CPT-violating parameters for 345 data-sized signal Monte Carlo samples. The one-dimensional coverages, i.e., the fraction of experiments where the generated value of the corresponding physics parameter falls into the 1σ interval reported by the fit (with parabolic errors), are also reported.

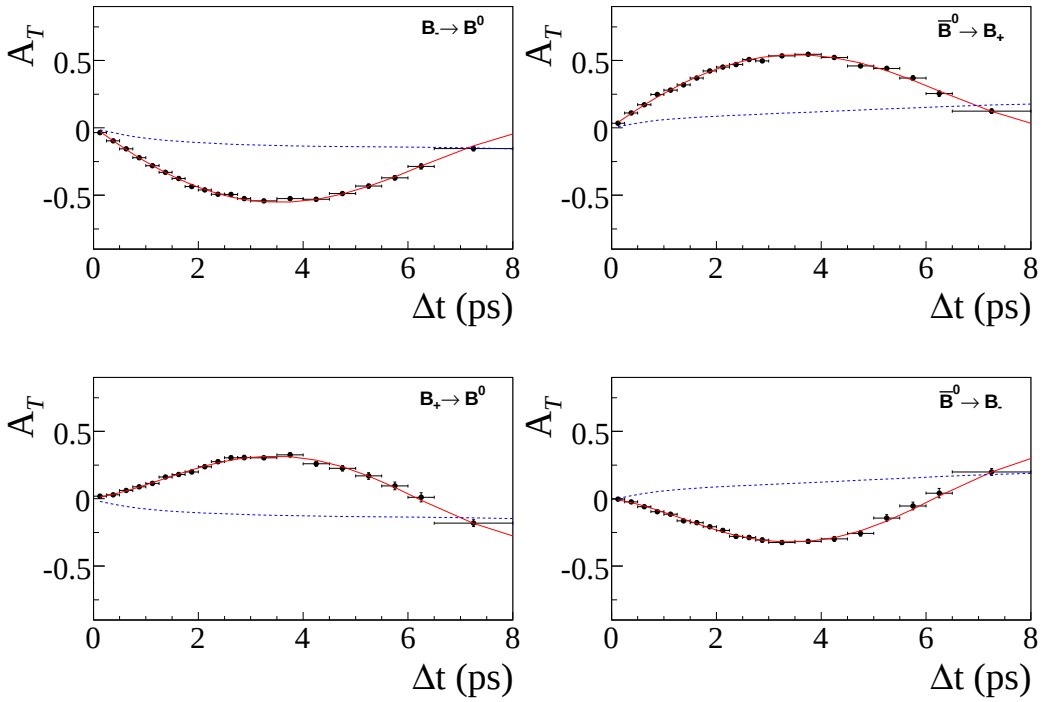

Fig. 4.3: The four independent raw T-asymmetries of the first 115 times data-sized signal Monte Carlo sample for flavor ID categories containing leptons and kaons combined. The points with error bars represent the signal Monte Carlo data, the solid (red) curves represent the projection of the reference fit, while the dashed (blue) curves represent the projection of the fit assuming no TV. The slope clearly observed in the blue curves is due to the bias in the resolution function, as we compare Δt exchanged processes to build the T or CPT asymmetries. On the contrary this slope is not present in the CP asymmetries as they are built without exchanging Δt. The legend on top of each asymmetry represents the reference physical process, e.g., "$\overline{B}^0 \to B_-$" denotes the raw asymmetry $A_T(\Delta t)$, which involves the comparison between the reference decay rate ($\ell^+ X$, $c\bar{c}K_S$) with positive Δt and the decay rate ($J/\psi K_L$, $\ell^- X$) with negative Δt. These illustrate the shape of the raw T-asymmetries in the limit of virtually infinite statistics with no background but with resolution and misID effects accounted for.

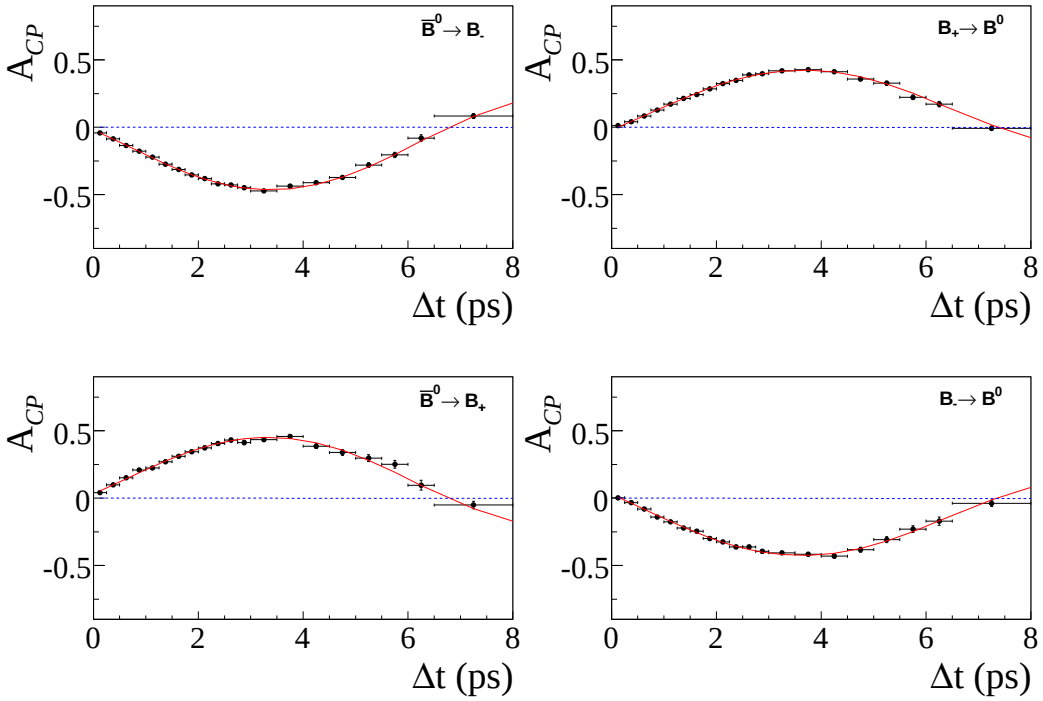

Fig. 4.4: The four independent raw *CP*-asymmetries of the first 115 times data-sized signal Monte Carlo sample for flavor ID categories containing leptons and kaons combined. The points with error bars represent the signal Monte Carlo data, the solid (red) curves represent the projection of the reference fit, while the dashed (blue) curves represent the projection of the fit assuming no *CP*. The legend is equivalent to the one used in Fig. 4.3. These illustrate the shape of the raw *CP*-asymmetries in the limit of virtually infinite statistics with no background but with resolution and misID effects accounted for.

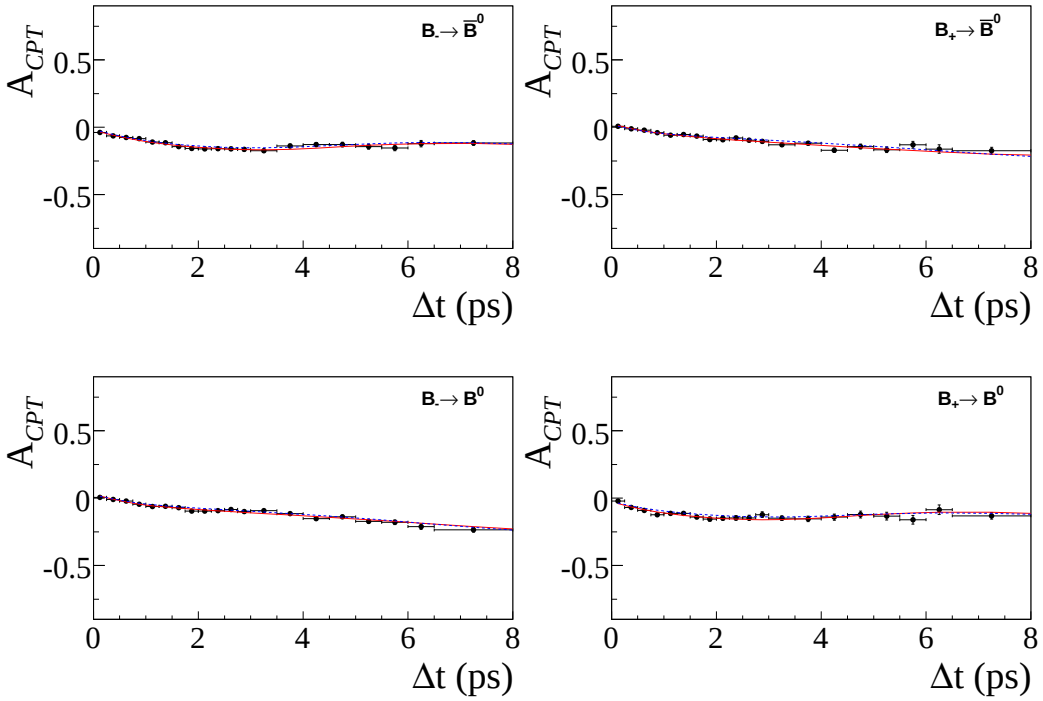

Fig. 4.5: The four independent raw *CPT*-asymmetries of the first 115 times data-sized signal Monte Carlo sample for flavor ID categories containing leptons and kaons combined. The points with error bars represent the signal Monte Carlo data, the solid (red) curves represent the projection of the reference fit, while the dashed (blue) curves represent the projection of the fit assuming no *CPT* violation. The legend is equivalent to the one used in Fig. 4.3. These illustrate the shape of the raw *CPT*-asymmetries in the limit of virtually infinite statistics with no background but with resolution and misID effects accounted for.

Signal parametrized Monte Carlo results

We also validated our fitting procedure using signal parametrized Monte Carlo experiments generated using identical PDF shapes as used to fit the signal Monte Carlo and data samples. For the T-, CP-, and CPT-violating parameters we used in the generation the same values as in the signal Monte Carlo, as given in Table 4.10. MisID fractions, efficiency ratios and resolution function are taken very similar to those from the signal Monte Carlo. We generated a total of 345 data-sized experiments, as previously. Table 4.13 summarizes the mean and RMS values of the residual distributions for the 345 data-sized experiments, together with the estimated coverage. Looking closely to the results in the Table 4.13, we observe that the relative small biases in some parameters observed in the case of the signal Monte Carlo (Table 4.12) have now disappeared. This seems to confirm that the effects observed in the signal Monte Carlo are related to differences in flavor ID performance and Δt resolution between the CP and $B_{\rm flav}$ samples, and the limitations of our empirical Δt resolution and misID models reproducing the Monte Carlo data. These effects will be accounted for in the systematic uncertainties.

4.4.2 $B_{\rm flav}$ data sample results

Table 4.14 summarizes the fit results with the $B_{\rm flav}$ sample. The mixing frequency and B lifetime are fixed to the values $\Delta m = 0.507$ ps $^{-1}$ and $\tau_{B^0} = 1.530$ ps [61]. We observe a scale factor for the core Gaussian which is consistent with one for *Lepton* flavor ID category events while it is not consistent with one for *non-Lepton* flavor ID category events. The flavor ID efficiency ratios agree with zero within 2.7σ. We observe large misID fraction differences in the *Pions* and *Other* categories. All these values are very similar, but not identical, to those obtained in the most recent CP violation analysis [37] due to the differences in the treatment of the outliers component of the Δt resolution function, and the splitting per B and D decay modes and flavor ID category of the signal fraction of the $B_{\rm flav}$ $m_{\rm ES}$ distributions, as described in Sec. 3.2.

It has been verified that the projections of the $B_{\rm flav}$ fit for mixed and unmixed events in the $m_{\rm ES}$ signal and sideband regions for all flavor ID categories are consistent to those reported previously in Refs [37, 50]. We allow to mix the lifetime background component, obtaining $\Delta m_{B_{\rm flav},\rm background} = -0.331 \pm 0.013$ ps^{-1}, with an effective lifetime $\tau_{B_{\rm flav},\rm background} = 1.331 \pm 0.018$ ps. Figures 4.6 and 4.7 show the Δt distributions of the $B_{\rm flav}$ data overlaid to the fit projections in the signal region ($m_{\rm ES} > 5.27$ GeV).

Parameter	Mean Residual	RMS Residual	Coverage
$C^-_{\ell^+,K_S}$	0.007 ± 0.003	0.060 ± 0.003	0.68 ± 0.05
$C^+_{\ell^+,K_S}$	0.001 ± 0.004	0.069 ± 0.003	0.67 ± 0.05
ΔC^-_{CP}	-0.003 ± 0.006	0.104 ± 0.004	0.68 ± 0.05
ΔC^-_{CPT}	-0.001 ± 0.007	0.129 ± 0.005	0.70 ± 0.05
ΔC^-_{T}	-0.005 ± 0.010	0.163 ± 0.009	0.64 ± 0.05
ΔC^+_{CP}	0.002 ± 0.006	0.104 ± 0.004	0.64 ± 0.05
ΔC^+_{CPT}	0.016 ± 0.008	0.145 ± 0.006	0.70 ± 0.05
ΔC^+_{T}	-0.002 ± 0.008	0.142 ± 0.006	0.65 ± 0.05
ΔS^-_{CP}	0.017 ± 0.007	0.124 ± 0.005	0.70 ± 0.05
ΔS^-_{CPT}	0.013 ± 0.008	0.138 ± 0.006	0.66 ± 0.05
ΔS^-_{T}	0.030 ± 0.011	0.203 ± 0.008	0.65 ± 0.05
ΔS^+_{CP}	-0.008 ± 0.007	0.128 ± 0.005	0.60 ± 0.05
ΔS^+_{CPT}	0.009 ± 0.012	0.214 ± 0.009	0.67 ± 0.05
ΔS^+_{T}	0.001 ± 0.008	0.149 ± 0.006	0.71 ± 0.05
$S^-_{\ell^+,K_S}$	-0.007 ± 0.003	0.060 ± 0.002	0.66 ± 0.05
$S^+_{\ell^+,K_S}$	0.010 ± 0.006	0.102 ± 0.004	0.63 ± 0.04

Tab. 4.13: Mean and RMS values of the residual (fitted−generated) distributions for all the T-, CP- and CPT-violating parameters for 345 data-sized signal parametrized Monte Carlo samples. The one-dimensional coverages, i.e., the fraction of experiments where the generated value of the corresponding physics parameter falls into the 1σ interval reported by the fit (with parabolic errors), are also reported.

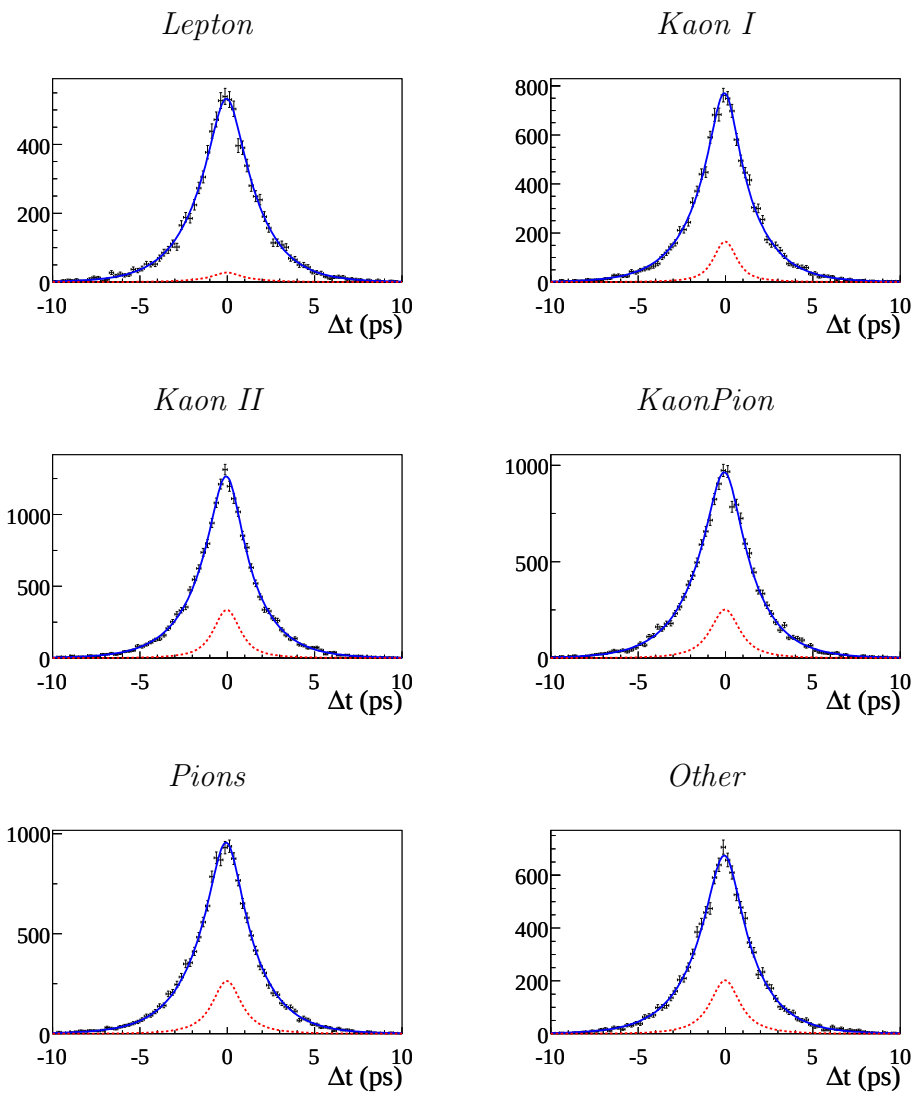

Fig. 4.6: $B_{\rm flav}$ Δt data distributions and fit projections in the signal region ($m_{\rm ES} > 5.27$ GeV) for B^0-identified events, for each of the six flavor ID categories. The points with error bars represent the data, the solid (blue) curves represent the projection of the reference fit, while the dashed (red) curves represent the background projection of the fit.

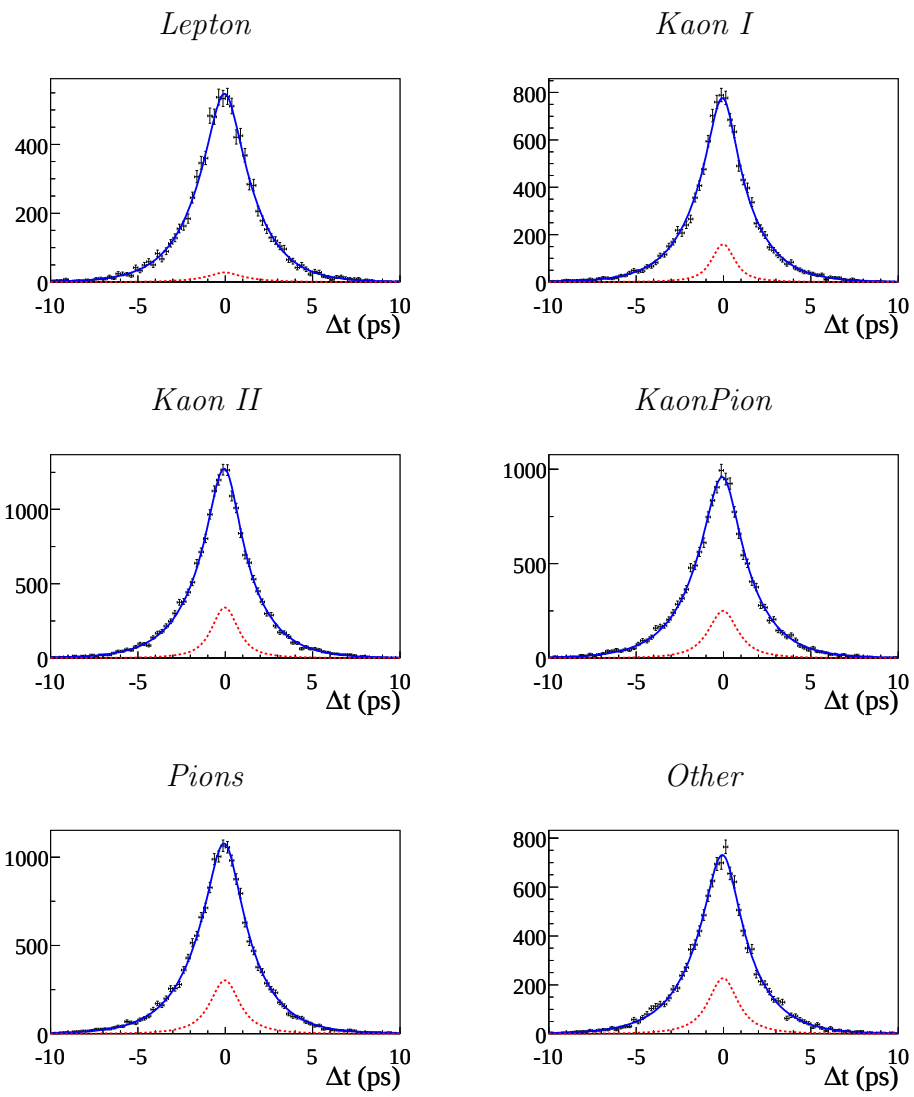

Fig. 4.7: B_{flav} Δt data distributions and fit projections in the signal region ($m_{\text{ES}} > 5.27$ GeV) for $\overline{B}^0$-identified events, for each of the six flavor ID categories. The points with error bars represent the data, the solid (blue) curves represent the projection of the reference fit, while the dashed (red) curves represent the background projection of the fit.

	B_{flav} Monte Carlo sample
w^{signal}-*Lepton*	0.0299 ± 0.0027
w^{signal}-*Kaon I*	0.0586 ± 0.0031
w^{signal}-*Kaon II*	0.1489 ± 0.0032
w^{signal}-*KaonPion*	0.2340 ± 0.0040
w^{signal}-*Pions*	0.3277 ± 0.0043
w^{signal}-*Other*	0.4153 ± 0.0054
Δw^{signal}-*Lepton*	-0.0001 ± 0.0051
Δw^{signal}-*Kaon I*	-0.0003 ± 0.0057
Δw^{signal}-*Kaon II*	0.0017 ± 0.0055
Δw^{signal}-*KaonPion*	-0.0024 ± 0.0065
Δw^{signal}-*Pions*	0.0499 ± 0.0065
Δw^{signal}-*Other*	0.0360 ± 0.0081
$\delta_{(\text{core,signal})-Lepton}(\Delta t)$	-0.0873 ± 0.0251
$\delta_{(\text{core,signal})-non-Lepton}(\Delta t)$	-0.2113 ± 0.00110
$Scale_{(\text{core,signal})-Lepton}$	1.0703 ± 0.0388
$Scale_{(\text{core,signal})-non-Lepton}$	1.1539 ± 0.0182
$f_{\text{core,signal}}$	0.9178 ± 0.0056
f_{outlier}	0.0029 ± 0.0005
$\delta_{\text{tail}}(\Delta t)$	-1.1731 ± 0.1301
$\epsilon^{\text{signal}}_{\text{ratio}}-Lepton$	-0.0023 ± 0.0092
$\epsilon^{\text{signal}}_{\text{ratio}}-Kaon\ I$	-0.0001 ± 0.0089
$\epsilon^{\text{signal}}_{\text{ratio}}-Kaon\ II$	-0.0069 ± 0.0079
$\epsilon^{\text{signal}}_{\text{ratio}}-KaonPion$	0.0064 ± 0.0089
$\epsilon^{\text{signal}}_{\text{ratio}}-Pions$	-0.0243 ± 0.0089
$\epsilon^{\text{signal}}_{\text{ratio}}-Other$	-0.0325 ± 0.0103
$\epsilon^{\text{flav}}_{\text{ratio}}$	0.0080 ± 0.0043

Tab. 4.14: Signal parameters determined from the B_{flav} data sample.

4.4.3 CP data sample results

Table 4.15 reports the results obtained from the reference fit to the $c\overline{c}K^0$ data samples. The results are stable within statistical uncertainties against flavor ID category and running period, as it is shown in Tables 4.16 and 4.17, respectively. The floated *CP* background parameters for the $c\overline{c}K_S$ sample, i.e. the fraction of prompt component for *Lepton* and *non-Lepton* categories, and the combined $c\overline{c}K_S$ and $J/\psi K_L$ *CP* asymmetries for the components that have an effective B lifetime (the lifetime background fraction is one minus the prompt background fraction), are reported in Table 4.18.

Parameter	All $c\bar{c}K^0$ modes
ΔC^-_{CP}	0.08 ± 0.10
ΔC^-_{CPT}	0.03 ± 0.12
ΔC^-_{T}	0.04 ± 0.14
ΔC^+_{CP}	0.07 ± 0.09
ΔC^+_{CPT}	0.14 ± 0.15
ΔC^+_{T}	0.10 ± 0.14
ΔS^-_{CP}	1.33 ± 0.12
ΔS^-_{CPT}	-0.03 ± 0.13
ΔS^-_{T}	1.17 ± 0.18
ΔS^+_{CP}	-1.30 ± 0.11
ΔS^+_{CPT}	0.16 ± 0.21
ΔS^+_{T}	-1.37 ± 0.14
$C^-_{\ell^+,K_S}$	-0.05 ± 0.06
$C^+_{\ell^+,K_S}$	0.01 ± 0.07
$S^-_{\ell^+,K_S}$	-0.67 ± 0.06
$S^+_{\ell^+,K_S}$	0.55 ± 0.09

Tab. 4.15: T-, CP- and CPT-violating parameters as obtained with the reference fit to the $c\bar{c}K^0$ data samples.

Parameter	*Lepton*	*Kaon I*	*Kaon II*	*KaonPion*	*Pions+Other*
ΔC^-_{CP}	0.01 ± 0.17	0.01 ± 0.17	0.50 ± 0.19	-0.05 ± 0.31	-0.35 ± 0.39
ΔC^-_{CPT}	-0.23 ± 0.24	-0.23 ± 0.24	0.24 ± 0.26	-0.02 ± 0.35	-0.46 ± 0.45
ΔC^-_{T}	-0.03 ± 0.32	-0.03 ± 0.32	0.49 ± 0.32	-0.44 ± 0.39	0.46 ± 0.47
ΔC^+_{CP}	0.35 ± 0.16	0.35 ± 0.16	-0.12 ± 0.17	0.07 ± 0.29	-0.00 ± 0.36
ΔC^+_{CPT}	0.48 ± 0.34	0.48 ± 0.34	0.19 ± 0.32	-0.23 ± 0.39	0.22 ± 0.47
ΔC^+_{T}	0.26 ± 0.28	0.26 ± 0.28	-0.16 ± 0.30	0.43 ± 0.42	-0.26 ± 0.45
ΔS^-_{CP}	1.39 ± 0.24	1.39 ± 0.24	1.02 ± 0.21	1.25 ± 0.36	1.68 ± 0.44
ΔS^-_{CPT}	0.37 ± 0.28	0.37 ± 0.28	0.01 ± 0.28	-0.45 ± 0.35	-0.17 ± 0.48
ΔS^-_{T}	1.33 ± 0.40	1.33 ± 0.40	1.48 ± 0.43	1.21 ± 0.51	1.20 ± 0.52
ΔS^+_{CP}	-1.34 ± 0.18	-1.34 ± 0.18	-1.01 ± 0.20	-1.71 ± 0.32	-1.14 ± 0.39
ΔS^+_{CPT}	0.19 ± 0.50	0.19 ± 0.50	0.38 ± 0.45	0.54 ± 0.67	0.35 ± 0.57
ΔS^+_{T}	-1.28 ± 0.29	-1.28 ± 0.29	-1.08 ± 0.30	-1.91 ± 0.42	-1.46 ± 0.48
$C^-_{\ell^+,K_S}$	-0.08 ± 0.10	0.01 ± 0.13	-0.19 ± 0.10	0.03 ± 0.18	0.17 ± 0.20
$C^+_{\ell^+,K_S}$	-0.13 ± 0.15	0.22 ± 0.15	0.07 ± 0.12	-0.05 ± 0.18	0.02 ± 0.20
$S^-_{\ell^+,K_S}$	-0.84 ± 0.090	-0.55 ± 0.13	-0.70 ± 0.11	-0.55 ± 0.18	-0.65 ± 0.22
$S^+_{\ell^+,K_S}$	0.48 ± 0.18	0.57 ± 0.22	0.32 ± 0.16	0.86 ± 0.25	0.53 ± 0.23

Tab. 4.16: T-, CP- and CPT-violating parameters as obtained with the reference fit to the $c\bar{c}K^0$ data samples, split by flavor ID category.

Parameter	Run 1+2	Run 3+4	Run 5	Run 5+6
ΔC^-_{CP}	0.07 ± 0.22	0.11 ± 0.17	0.14 ± 0.19	0.08 ± 0.15
ΔC^-_{CPT}	-0.03 ± 0.28	0.12 ± 0.23	0.11 ± 0.23	0.02 ± 0.17
ΔC^-_{T}	0.29 ± 0.38	0.16 ± 0.26	0.03 ± 0.26	-0.15 ± 0.19
ΔC^+_{CP}	-0.08 ± 0.19	0.14 ± 0.15	-0.05 ± 0.19	0.08 ± 0.14
ΔC^+_{CPT}	-0.19 ± 0.36	0.33 ± 0.28	0.03 ± 0.28	0.12 ± 0.20
ΔC^+_{T}	0.34 ± 0.38	0.33 ± 0.25	0.00 ± 0.27	-0.03 ± 0.19
ΔS^-_{CP}	1.34 ± 0.27	1.41 ± 0.20	1.43 ± 0.25	1.27 ± 0.18
ΔS^-_{CPT}	0.03 ± 0.31	0.37 ± 0.26	-0.20 ± 0.24	-0.29 ± 0.17
ΔS^-_{T}	1.54 ± 0.50	1.15 ± 0.34	1.04 ± 0.33	1.05 ± 0.24
ΔS^+_{CP}	-1.18 ± 0.21	-1.38 ± 0.16	-1.18 ± 0.21	-1.29 ± 0.15
ΔS^+_{CPT}	1.28 ± 0.63	0.23 ± 0.38	0.15 ± 0.40	-0.18 ± 0.26
ΔS^+_{T}	-2.03 ± 0.38	-1.37 ± 0.25	-1.45 ± 0.28	-1.30 ± 0.20
$C^-_{\ell^+,K_S}$	-0.07 ± 0.13	-0.09 ± 0.09	-0.02 ± 0.11	-0.01 ± 0.09
$C^+_{\ell^+,K_S}$	0.06 ± 0.14	-0.08 ± 0.11	0.11 ± 0.13	0.06 ± 0.10
$S^-_{\ell^+,K_S}$	-0.67 ± 0.13	-0.77 ± 0.09	-0.58 ± 0.12	-0.57 ± 0.09
$S^+_{\ell^+,K_S}$	0.44 ± 0.17	0.53 ± 0.14	0.68 ± 0.18	0.60 ± 0.13

Tab. 4.17: T-, CP- and CPT-violating parameters as obtained with the reference fit to the $c\bar{c}K^0$ data samples, split by running period.

$c\bar{c}K_S + J/\psi K_L$ *CP* background parameter	
$f_{\text{bg,prompt, } Lepton}(c\bar{c}K_S)$	0.07 ± 0.13
$f_{\text{bg,prompt, } non-Lepton}(c\bar{c}K_S)$	0.40 ± 0.03
$\mathcal{I}m\lambda_{\text{bg,eff, } Lepton}$	-0.12 ± 0.26
$\mathcal{I}m\lambda_{\text{bg,eff, } Kaon\ I}$	-0.36 ± 0.17
$\mathcal{I}m\lambda_{\text{bg,eff, } Kaon\ II}$	0.01 ± 0.12
$\mathcal{I}m\lambda_{\text{bg,eff, } KaonPion}$	0.07 ± 0.14
$\mathcal{I}m\lambda_{\text{bg,eff, } Pions}$	0.03 ± 0.15
$\mathcal{I}m\lambda_{\text{bg,eff, } Other}$	0.05 ± 0.13

Tab. 4.18: CP background parameters determined by fitting the $c\bar{c}K^0$ data with the reference fit configuration.

The Δt distributions and projections of the reference fit on the $c\bar{c}K^0$ data sample are shown in Figs 4.8 to 4.11. In particular, Figs 4.8 and 4.9 show the Δt distributions for signal enriched $c\bar{c}K_S$ events ($m_{\text{ES}} > 5.27$ GeV) with a B^0 or $\overline{B}^0$ flavor ID, respectively, for each of the six flavor ID categories.

Similarly, Figs 4.10 and 4.11 show the corresponding distributions for signal enriched $J/\Psi K_L$ events ($|\Delta E| < 10$ MeV).

Figure 4.12 shows the four independent raw T asymmetries for flavor ID categories containing leptons and kaons combined, overlaid with the projection of the best-fit results together with the projection of the fit under the assumption of T symmetry. The same T asymmetries split by flavor ID category are shown in Fig. 4.13. The corresponding raw *CP*- and *CPT*-asymmetries for categories containing leptons and kaons combined are shown in Figs 4.14 and 4.15, respectively.

A way to estimate the significance of the results (i.e., significance of T violation) is to build two-dimensional confidence-level (C.L.) contours in the $(\Delta S_T^{\pm}, \Delta C_T^{\pm})$ planes, since this asymmetry shows up if $\Delta S_T^{\pm} \neq 0$ or $\Delta C_T^{\pm} \neq 0$. These 2-dimensional contours for the $c\overline{c}K^0$ data sample are illustrated in Fig. 4.16. It can be observed that looking at the two-dimensional projections on $(\Delta S_T^{+}, \Delta C_T^{+})$ and $(\Delta S_T^{-}, \Delta C_T^{-})$ our best-fit results are inconsistent with the T symmetry hypothesis at eight standard deviations, including only statistical uncertainties. How the conditions $\Delta S_T^{+} \neq 0$ or $\Delta S_T^{-} \neq 0$ or $\Delta C_T^{+} \neq 0$ or $\Delta C_T^{-} \neq 0$ are combined to determine the global significance of T violation in the presence of systematic uncertainties is discussed in detail in Sec. 4.6. Similar C.L. contours can be made for the *CP*- and *CPT*-violating parameters, in the planes $(\Delta S_{CP}^{\pm}, \Delta C_{CP}^{\pm})$ and $(\Delta S_{CPT}^{\pm}, \Delta C_{CPT}^{\pm})$, respectively, as show in Fig. 4.17, for the same $c\overline{c}K^0$ data sample. As expected, the significance of *CP* violation is larger (exceeds 10 σ for each pair of variables) than for T violation since the former involves only comparison between flavor-identified ℓ^+X and ℓ^-X samples, while the latter requires in addition comparisons of $c\overline{c}K_S$ and $J/\psi K_L$ samples with opposite Δt sign. *CPT* symmetry is verified within 1 σ (statistical only).

4.4.4 *CP violation results from the CP data sample*

As a cross-check of our signal model implementation, we have also fit the data using only one pair of S and C parameters for all the samples, reversing the sign of S under $\Delta t \leftrightarrow -\Delta t$, or $c\overline{c}K_S \leftrightarrow J/\psi K_L$, or $B^0 \leftrightarrow \overline{B}^0$ exchanges, and reversing the sign of C under $B^0 \leftrightarrow \overline{B}^0$ exchange, as described in Sec. 4.2.2 applying the constraints from Eqs (4.5) and (4.6). This is equivalent to the signal model used in the last *CPV* analysis [37, 50, 51]. We obtain $S = 0.6856 \pm 0.0290$ and $C = 0.0216 \pm 0.0207$ (statistical only), which are essentially identical to our previous results, even taking into account the small differences in the $c\overline{c}K_S$ sample (no $\eta_c K_S$ nor $J/\psi K^{*0}$) and the analysis procedure.

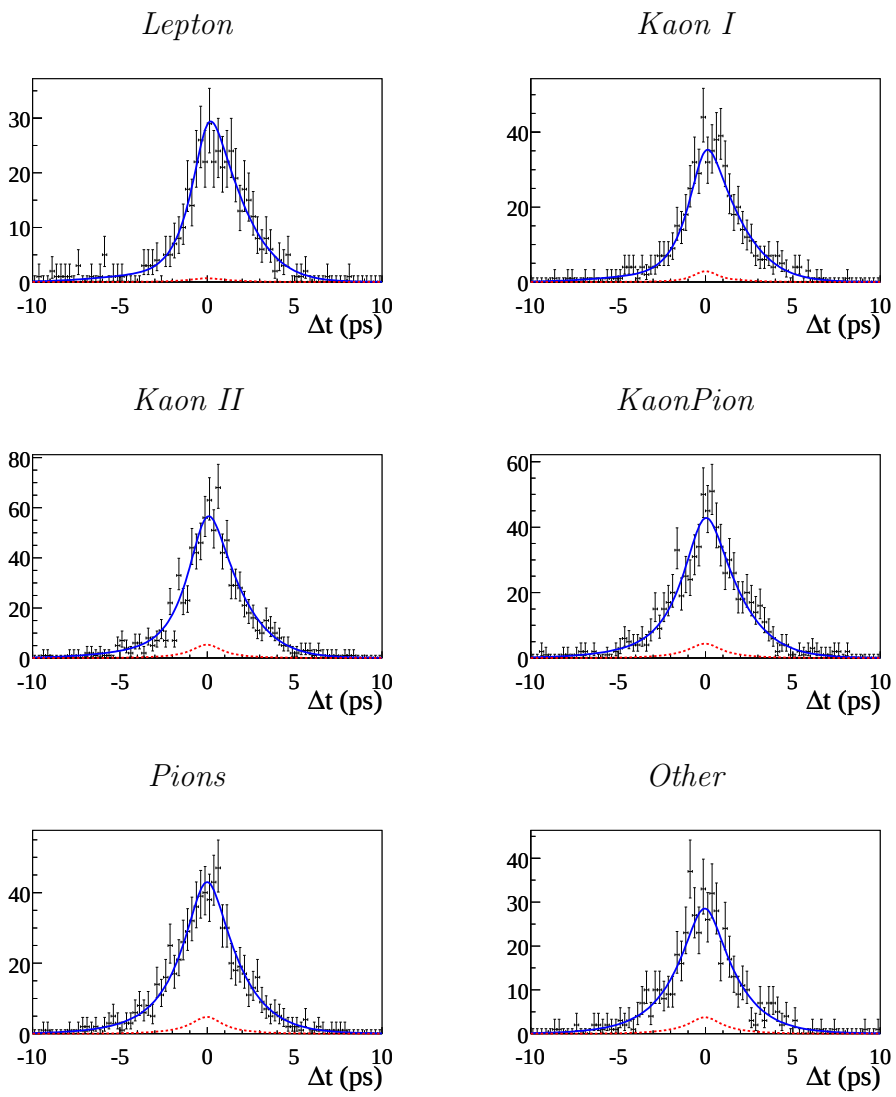

Fig. 4.8: $c\bar{c}K_s$ Δt data distributions and reference fit projections in the signal region ($m_{\rm ES} > 5.27$ GeV) for flavor-identified B^0 events, for each of the six flavor ID categories. The points with error bars represent the data, the solid (blue) curves represent the projection of the fit, while the dashed (red) curves represent the background projection of the fit.

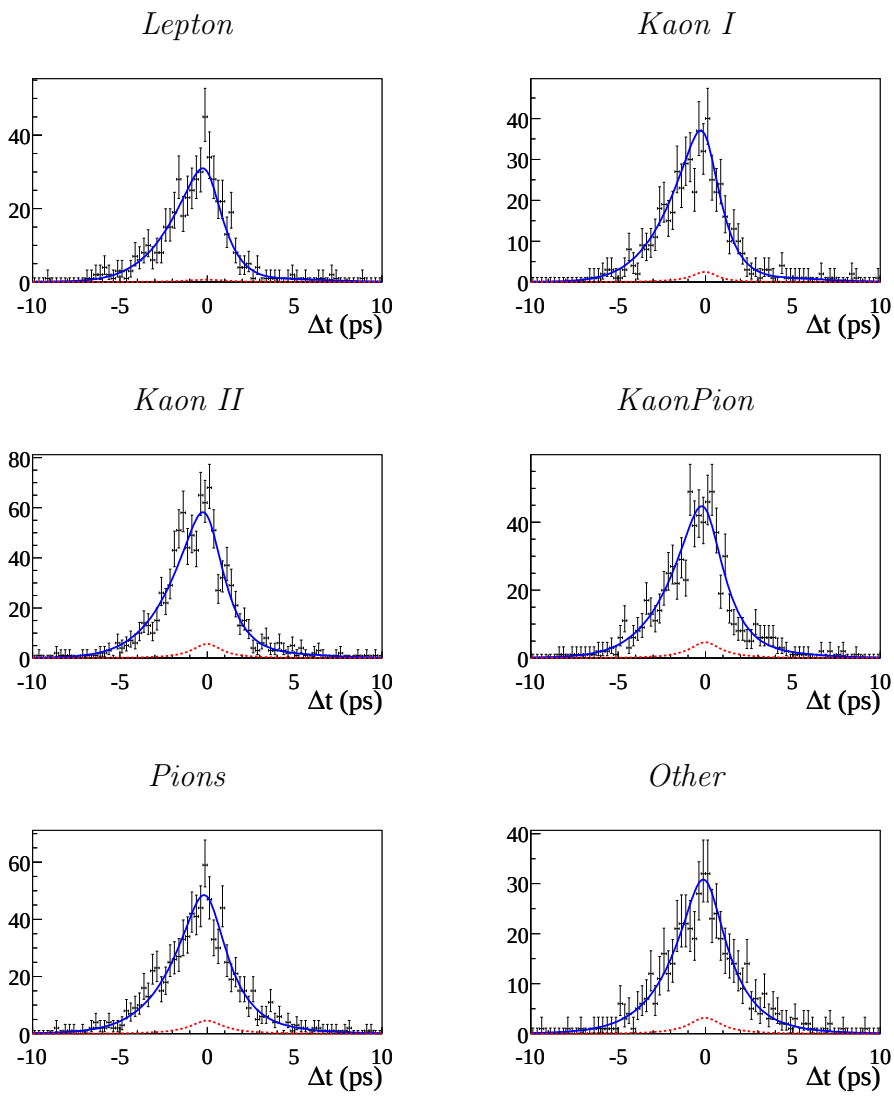

Fig. 4.9: $c\bar{c}K_s$ Δt data distributions and reference fit projections in the signal region ($m_{\rm ES} > 5.27$ GeV) for flavor-identified $\overline{B}^0$ events, for each of the six flavor ID categories. The points with error bars represent the data, the solid (blue) curves represent the projection of the fit, while the dashed (red) curves represent the background projection of the fit.

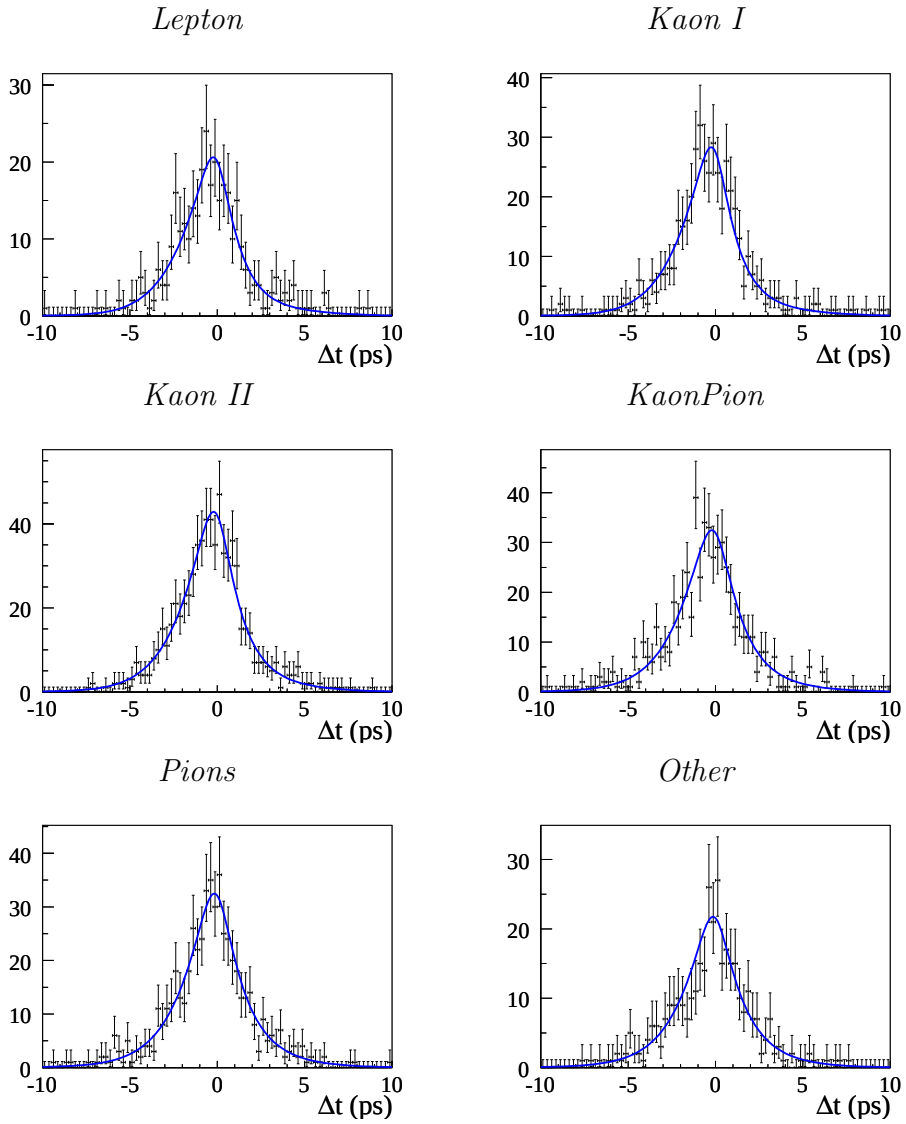

Fig. 4.10: $J/\Psi K_L$ Δt data distributions and reference fit projections in the signal region ($|\Delta E| < 10$ MeV) for flavor-identified B^0 events, for each of the six flavor ID categories. The points with error bars represent the data, the solid (blue) curves represent the projection of the fit. The background contribution is not shown.

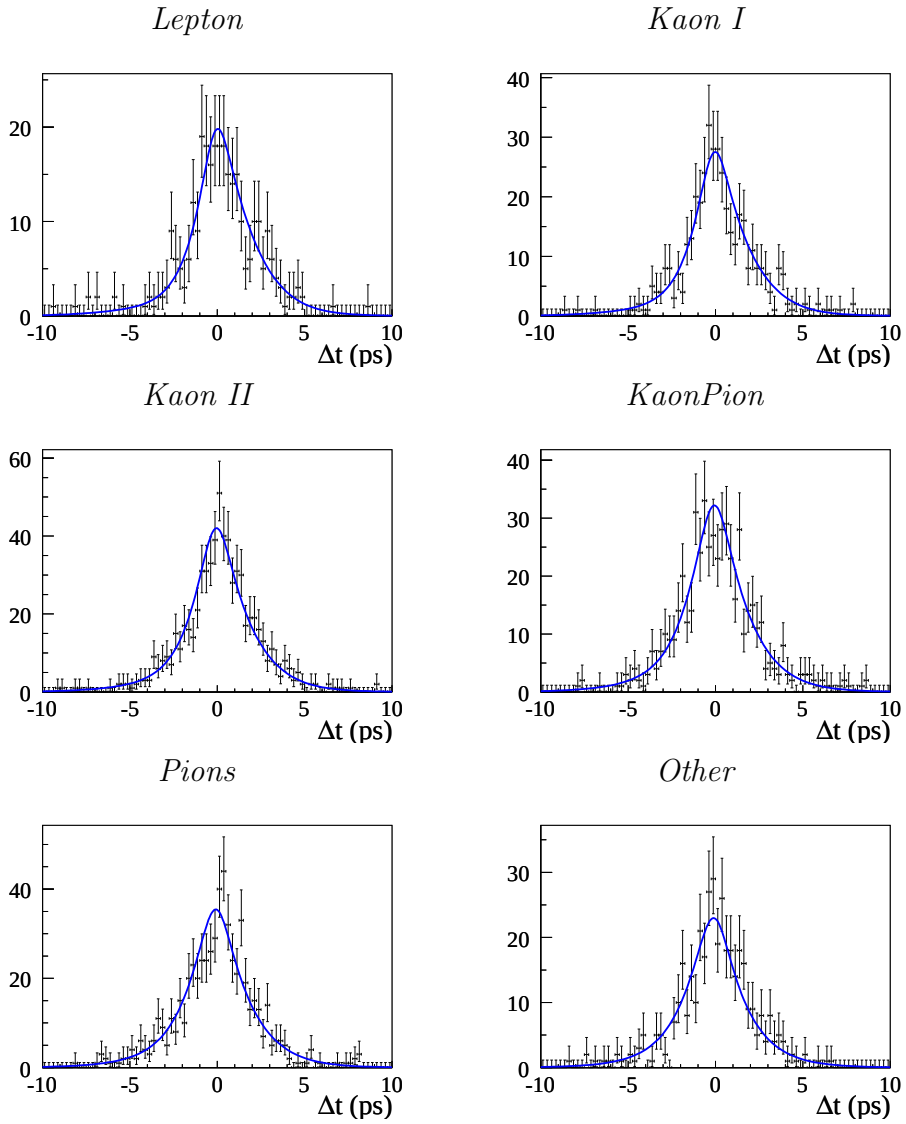

Fig. 4.11: $J/\Psi K_L$ Δt data distributions and reference fit projections in the signal region ($|\Delta E| < 10$ MeV) for flavor-identified $\overline{B}^0$ events, for each of the six flavor ID categories. The points with error bars represent the data, the solid (blue) curves represent the projection of the fit. The background contribution is not shown.

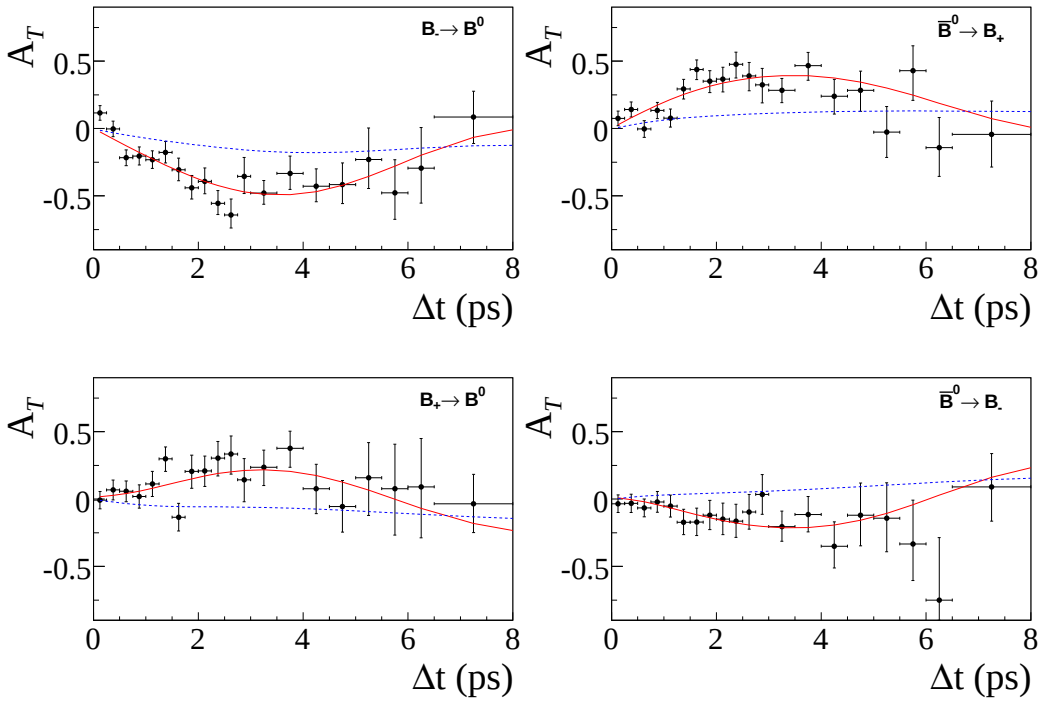

Fig. 4.12: The four independent raw T asymmetries for the $c\bar{c}K^0$ data sample for flavor ID categories containing leptons and kaons combined, for the signal enriched region ($m_{\rm ES} > 5.27$ GeV for $c\bar{c}K_S$ modes and $|\Delta E| < 10$ MeV for the $J/\psi K_L$ mode). The points with error bars represent the data, the solid (red) curves represent the projection of the reference fit, while the dashed (blue) curves represent the projection of the fit assuming T invariance. The legend on top of each asymmetry is analogous to that used in Fig. 4.3.

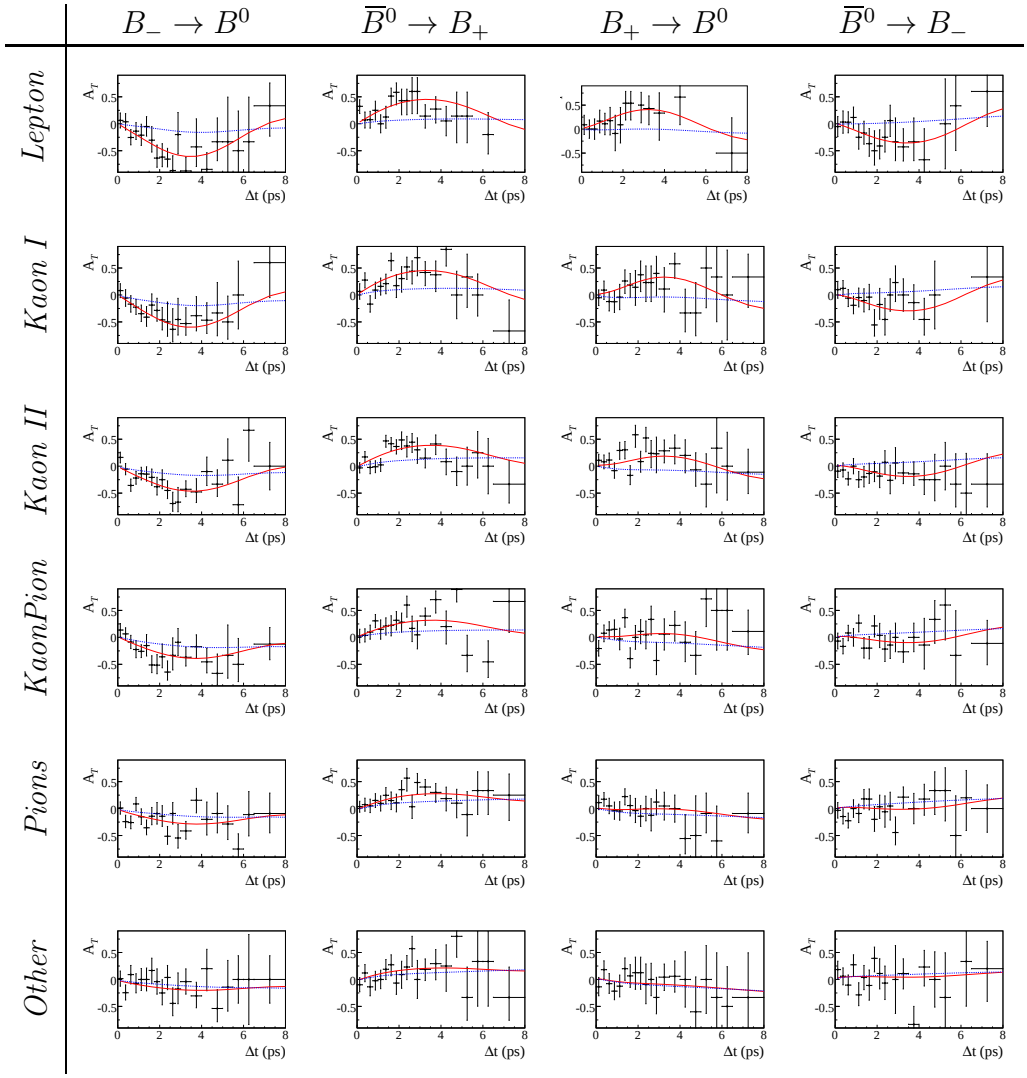

Fig. 4.13: The four independent raw T-asymmetries for the $c\overline{c}K^0$ (from left to right) data sample split by flavor ID category (from top to bottom), for the signal enriched region ($m_{\rm ES} > 5.27$ GeV for $c\overline{c}K_S$ modes and $|\Delta E| < 10$ MeV for the $J/\psi K_L$ mode). The notation $B_- \to B^0$ denotes the raw $A_T(\Delta t)$ asymmetry which involves the comparison of the decay rate for B_- events tagged as B^0 ($\ell^- X$, $c\overline{c}K_S$) to the decay rate of B^0 events tagged as B_- ($J/\psi K_L$, $\ell^+ X$).

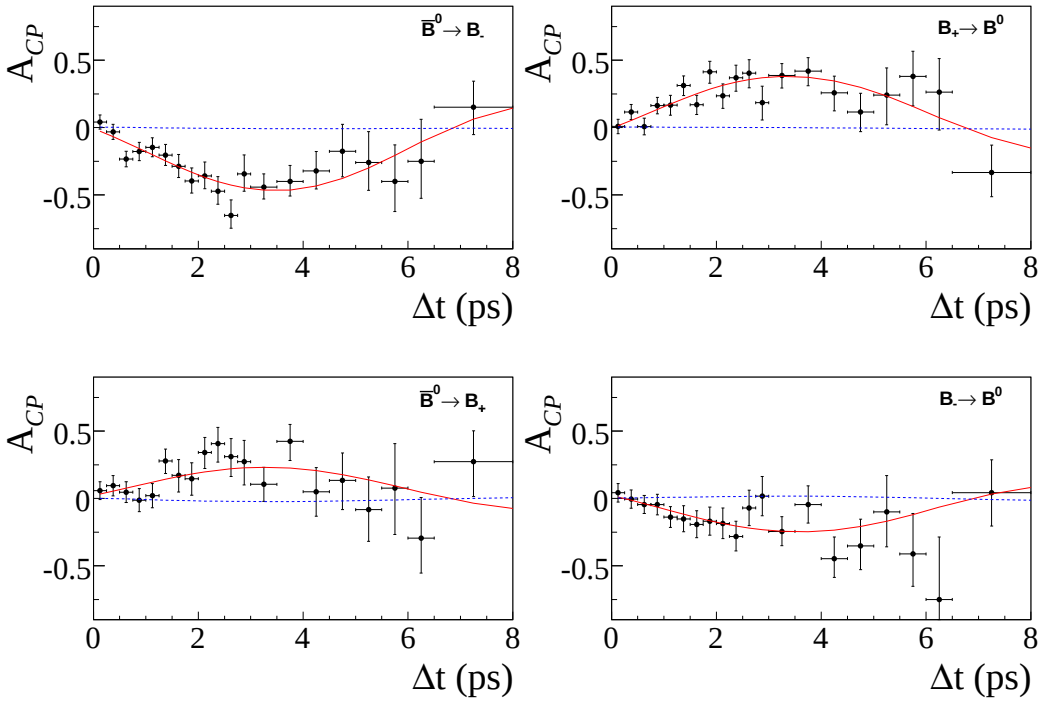

Fig. 4.14: The four independent raw *CP*-asymmetries for the $c\bar{c}K^0$ data sample for flavor ID categories containing leptons and kaons combined, for the signal enriched region ($m_{\rm ES} > 5.27$ GeV for $c\bar{c}K_S$ modes and $|\Delta E| < 10$ MeV for the $J/\psi K_L$ mode). The legend is equivalent to the one used in Fig. 4.3.

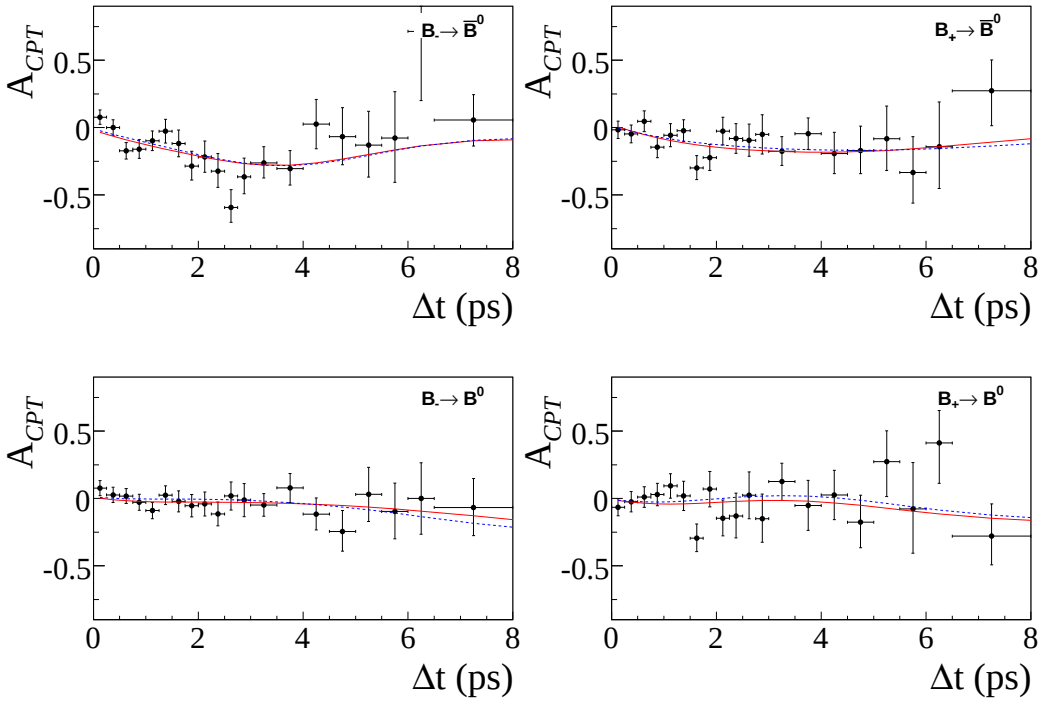

Fig. 4.15: The four independent raw *CPT*-asymmetries for the $c\bar{c}K^0$ data sample for flavor ID categories containing leptons and kaons combined, for the signal enriched region ($m_{\rm ES} > 5.27$ GeV for $c\bar{c}K_S$ modes and $|\Delta E| < 10$ MeV for the $J/\psi K_L$ mode). The legend is equivalent to the one used in Fig. 4.3.

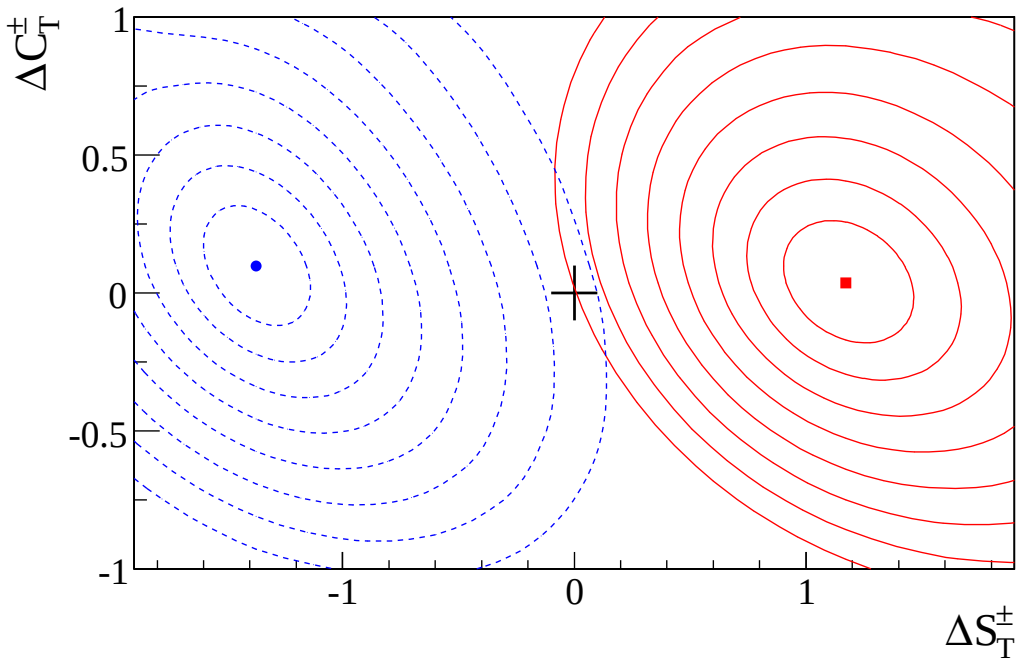

Fig. 4.16: Two-dimensional C.L. contours (up to eight standard deviations) in the $(\Delta S_T^{\pm}, \Delta C_T^{\pm})$ planes, for the $c\bar{c}K^0$ data sample, including statistical errors only. The solid (red) and dashed (blue) contours are for the pairs of T-violating variables $(\Delta S_T^-, \Delta C_T^-)$ and $(\Delta S_T^+, \Delta C_T^+)$, respectively. These contours have been obtained using the standard likelihood ratio method, $-2\Delta ln\mathcal{L}_{\rm exp} = s^2$, with s^2 =2.30, 6.18, 11. 83, 19.33, 28.74, 40.09, 53.38, 68.70, for 1-, 2-, 3-, 4-, 5-, 6-, 7-, 8-standard deviations, respectively. Thus, the C.L. in 2 dimensions for each pair of variables is $1-$C.L. $= 0.317, 4.6\times10^{-2}, 2.7\times10^{-3}, 6.3\times10^{-5}, 5.7\times10^{-7}$ for 1-, 2-, 3-, 4-, 5-σ. The marker at (0,0) represents the no T violation point, while the other markers represent the best-fit results.

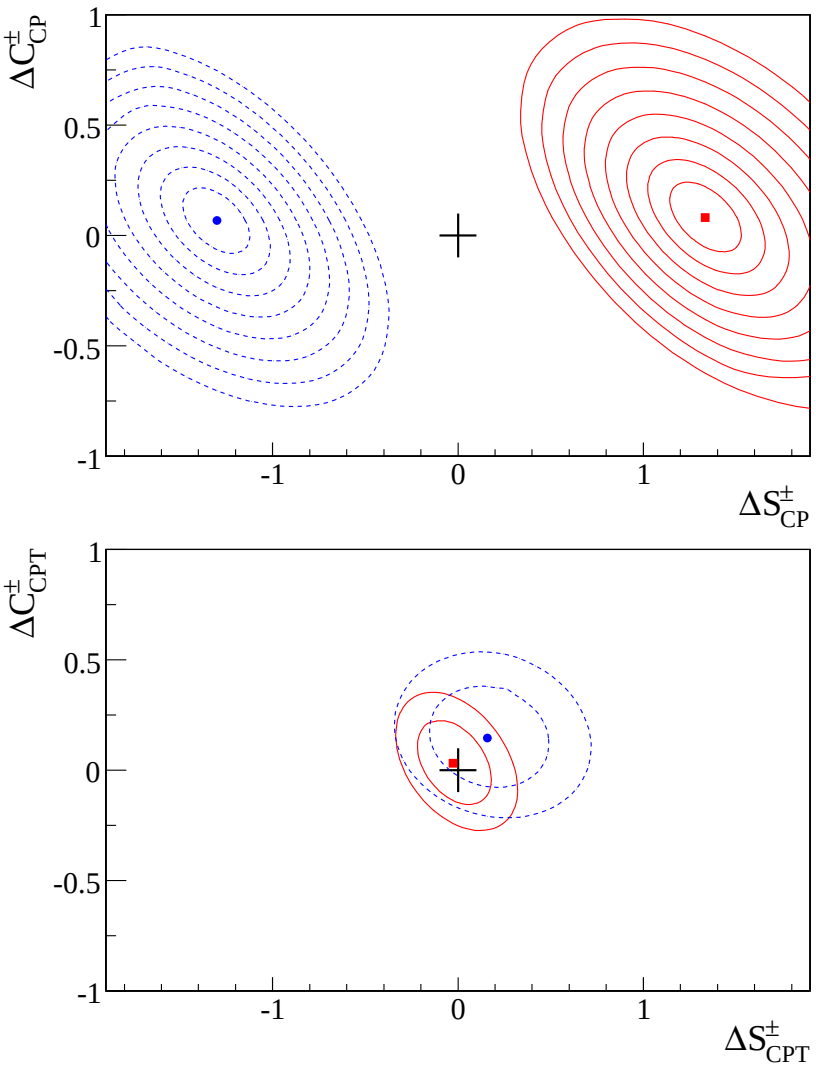

Fig. 4.17: Same as in Fig. 4.16, but for the *CP*-violating variables $(\Delta S^{\pm}_{T}, \Delta C^{\pm}_{T})$ (top) and the *CPT*-violating variables $(\Delta S^{\pm}_{CPT}, \Delta C^{\pm}_{CPT})$ (bottom). For the *CPT* case we only show the 1- and 2-σ regions. The markers at (0,0) represent the no *CP*- and no *CPT*-violating points, while the other markers represent the best-fit results.

4.4.5 Control data sample results

We applied the standard TV fit to high statistics B decay modes similar to the signal modes where we expect to find asymmetry parameters that are small or zero. For this test we do use the $c\bar{c}K^{\pm}$ and $J/\psi K^{*\pm}$ events. The former is used as the K_S sample, and the latter as the K_L sample. As noticed in previous analyses, the $B^{\pm} \to J/\psi K^{*\pm}(K^{\pm}\pi^0)$ data sample has a peaking background fraction that is more than 14%, although for the purpose of this check we have assumed it to be zero.

We first perform a $B_{\rm flav}$ style fit to the $c\bar{c}K^{\pm}$ and $J/\psi K^{*\pm}$ samples to derive the efficiency ratios, resolution and misID parameters. The mixing frequency has been fixed to zero while the $B^{\pm}$ lifetime has been used in place of the B^0 lifetime. The fractions of peaking background have all been fixed to zero. We observe in general consistent resolution parameters with respect to the $B_{\rm flav}$ sample, while the misID fractions are lower due to the different right-to-wrong sign kaon fraction in $B^{\pm}$ events. The flavor ID efficiency ratios are significantly higher [50]. Second, we take these efficiency, resolution and misID parameters to perform a T-, CP- and CPT-style fit to the same $c\bar{c}K^{\pm}$ and $J/\psi K^{*\pm}$ samples. The results for the T-, CP-, and CPT-violating parameters from this fit are reported in Table 4.19. No statistically significant deviation from zero is observed for any of the physical parameters. Another way to evaluate the absence of T-, CP- and CPT-violating effects in the control samples is through the construction of the two-dimensional C.L. contours. These are shown in Fig. 4.18 (up to two standard deviations) in the $(\Delta S_T^{\pm}, \Delta C_T^{\pm})$, $(\Delta S_{CP}^{\pm}, \Delta C_{CP}^{\pm})$ and $(\Delta S_{CPT}^{\pm}, \Delta C_{CPT}^{\pm})$ planes. In all cases we observe a good agreement with our expectation of no symmetry violations. Finally, the same conclusion is obtained from the observation of the raw asymmetries, as it can be seen in Fig. 4.19 for the case of the raw T-asymmetry (similar conclusions are obtained looking at the CP- and CPT-asymmetries, not shown here). We have also floated the B^+ lifetime obtaining 1.673 ± 0.028 ps, which is compatible with the current world average.

4.4.6 Nominal parametrized Monte Carlo results

The parametrized Monte Carlo validation with signal-only events described in Sec. 4.4.1 has been redone including the amount and type of backgrounds observed in the data, and with misID fractions, efficiency ratios and resolution function parameters as obtained from the reference TV fit to the $c\bar{c}K^0$ data sample. As previously, a total of 345 data-sized experiments have been generated and fitted. Table 4.20 summarizes the mean and RMS values of

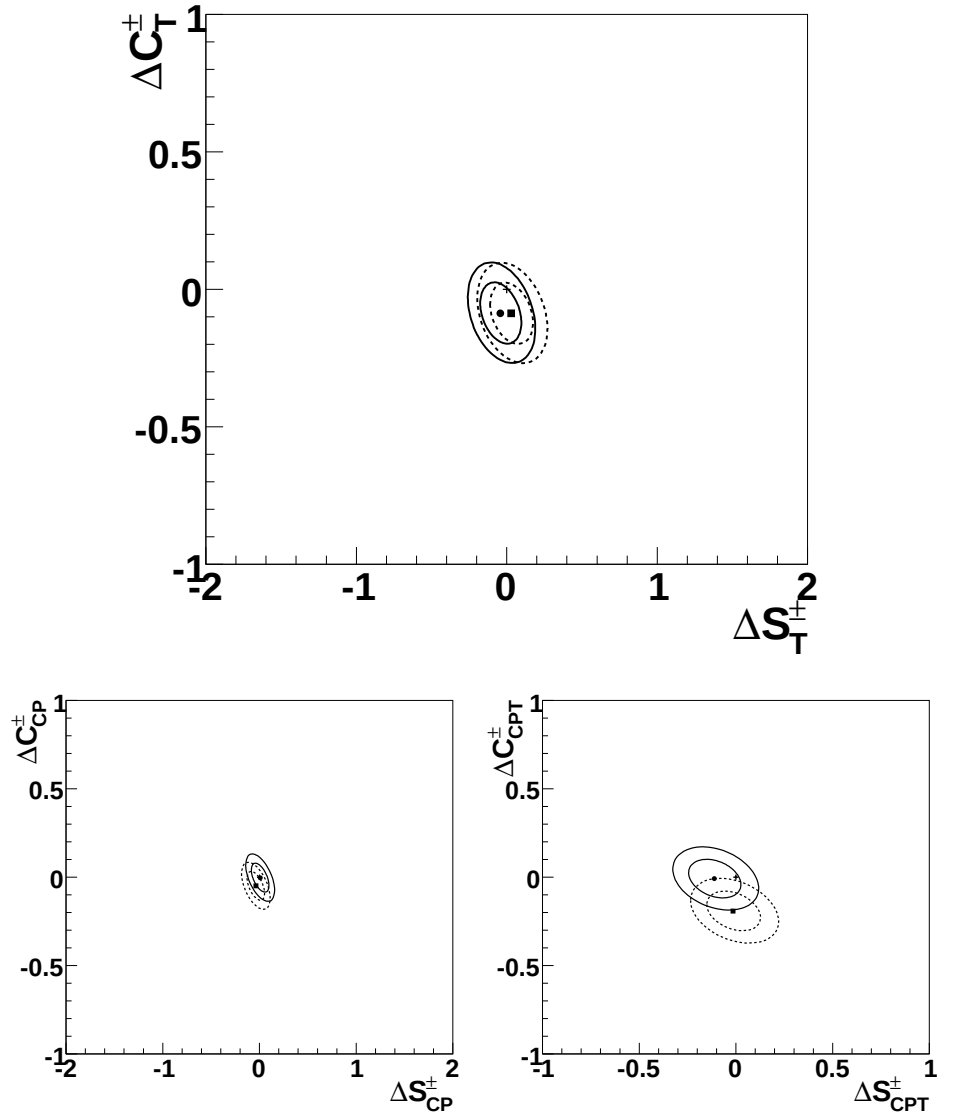

Fig. 4.18: Two-dimensional C.L. contours (up to two standard deviations) in the (top) $(\Delta S_T^{\pm}, \Delta C_T^{\pm})$, (bottom-left) $(\Delta S_{CP}^{\pm}, \Delta C_{CP}^{\pm})$, and (bottom-right) $(\Delta S_{CPT}^{\pm}, \Delta C_{CPT}^{\pm})$ planes, data control samples, including statistical errors only. The solid and dashed contours are for the pairs of T-violating variables $(\Delta S_T^-, \Delta C_T^-)$ and $(\Delta S_T^+, \Delta C_T^+)$, respectively, and similarly for the CP- and CPT-violating variables $(\Delta S_{CP}^-, \Delta C_{CP}^-)$, $(\Delta S_{CP}^+, \Delta C_{CP}^+)$ and $(\Delta S_{CPT}^-, \Delta C_{CPT}^-)$, $(\Delta S_{CPT}^+, \Delta C_{CPT}^+)$ These contours have been obtained using the standard likelihood ratio method, $-2\Delta ln\mathcal{L}_{\rm exp} = s^2$, with $s^2 = 2.30, 6.18$, for 1-, 2-standard deviations, respectively. Thus, the C.L. in two dimensions for each pair of variables is $1 - \text{C.L.} = 0.317, 4.6 \times 10^{-2}$ for 1, 2-σ. The marker at (0,0) represents the T-, CP-, and CPT-invariance points, while the other markers represent the best-fit results.

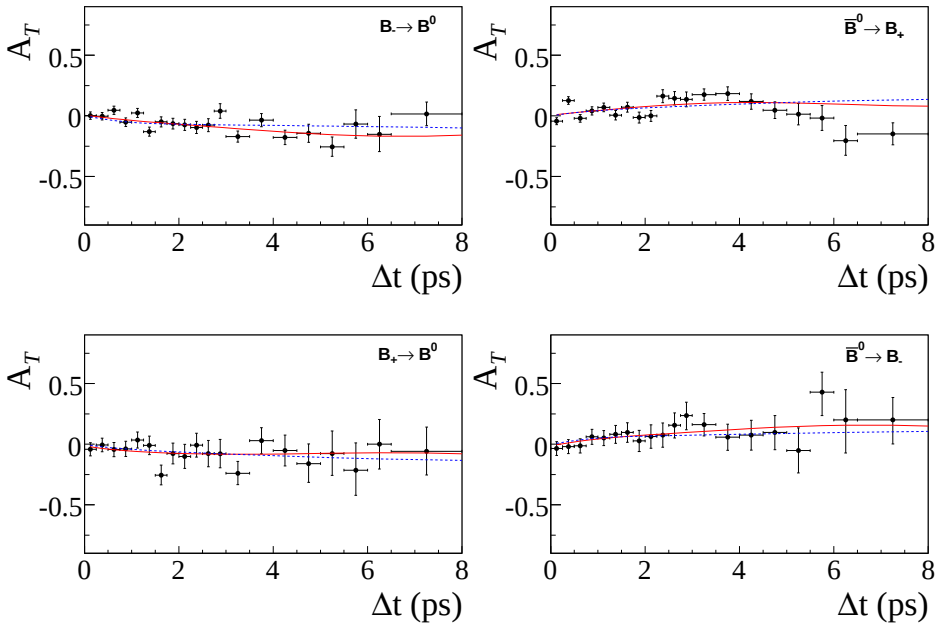

Fig. 4.19: The four independent raw T-asymmetries for the $c\bar{c}K^{\pm}$ and $c\bar{c}K^{*\pm}$ control samples (used instead for the signal $c\bar{c}K_S$ and the $J/\psi K_L$ samples, respectively) for flavor ID categories containing leptons and kaons combined, for the signal enriched region ($m_{\rm ES} > 5.27$ GeV). The points with error bars represent the data, the solid (red) curves represent the projection of the reference fit, while the dashed (blue) curves represent the projection of the fit assuming no T invariance. The legend on top of each asymmetry is equivalent to that used in Fig. 4.3.

Parameter	Value
ΔC^-_{CP}	0.04 ± 0.05
ΔC^-_{CPT}	-0.00 ± 0.07
ΔC^-_{T}	-0.04 ± 0.07
ΔC^+_{CP}	-0.00 ± 0.05
ΔC^+_{CPT}	-0.16 ± 0.07
ΔC^+_{T}	-0.02 ± 0.07
ΔS^-_{CP}	0.09 ± 0.05
ΔS^-_{CPT}	-0.10 ± 0.08
ΔS^-_{T}	0.04 ± 0.09
ΔS^+_{CP}	0.04 ± 0.05
ΔS^+_{CPT}	0.03 ± 0.09
ΔS^+_{T}	0.16 ± 0.09
$C^-_{\ell^+,K_S}$	0.03 ± 0.03
$C^+_{\ell^+,K_S}$	0.04 ± 0.03
$S^-_{\ell^+,K_S}$	-0.01 ± 0.04
$S^+_{\ell^+,K_S}$	-0.00 ± 0.04

Tab. 4.19: T-, CP- and CPT-violating parameters from the $c\bar{c}K^\pm$ and $J/\psi K^{*\pm}$ control sample fit with efficiency ratio, resolution and misID parameters as determined from the same control data sample.

the residual distributions for the 345 data-sized experiments, together with the estimated coverage. As in the case of the signal only parametrized Monte Carlo experiments, there are no statistically significant biases.

It is illustrative to compare the raw asymmetries and two-dimensional C.L. contours for one of the parametrized Monte Carlo experiments to those obtained from the actual $c\bar{c}K^0$ data sample. Figure 4.20 shows the four independent raw T-asymmetries for flavor ID categories containing leptons and kaons combined, overlaid with the projection of the best-fit results together with the projection of the fit under the assumption of T symmetry, for one of the same parametrized Monte Carlo experiments. These asymmetries can be compared to those in data, Fig. 4.12. Similarly, the raw CP- and CPT-asymmetries for the same experiment are shown in Figs 4.21 and 4.22, which can be compared to the same asymmetries as obtained in data, Figs 4.14 and 4.15. Finally, Fig. 4.23 shows the two-dimensional C.L. contours (up to eight standard deviations) in the $(\Delta S^\pm_T, \Delta C^\pm_T)$ planes. It can be observed that looking at the 2-dimensional projections $(\Delta S^+_T, \Delta C^+_T)$ and $(\Delta S^-_T, \Delta C^-_T)$ our best-fit results are inconsistent with the T-symmetry hy-

	Mean Residual	RMS Residual	Coverage
$C^-_{\ell^+,K_S}$	0.009 ± 0.003	0.061 ± 0.002	0.63 ± 0.04
$C^+_{\ell^+,K_S}$	0.003 ± 0.004	0.070 ± 0.003	0.68 ± 0.04
ΔC^-_{CP}	-0.008 ± 0.006	0.112 ± 0.005	0.61 ± 0.04
ΔC^-_{CPT}	-0.006 ± 0.006	0.103 ± 0.004	0.69 ± 0.05
ΔC^-_{T}	-0.007 ± 0.006	0.117 ± 0.005	0.65 ± 0.04
ΔC^+_{CP}	-0.003 ± 0.006	0.107 ± 0.004	0.66 ± 0.04
ΔC^+_{CPT}	0.003 ± 0.007	0.130 ± 0.006	0.66 ± 0.04
ΔC^+_{T}	0.001 ± 0.006	0.119 ± 0.005	0.64 ± 0.04
ΔS^-_{CP}	0.011 ± 0.007	0.128 ± 0.005	0.69 ± 0.05
ΔS^-_{CPT}	0.001 ± 0.006	0.113 ± 0.006	0.65 ± 0.04
ΔS^-_{T}	0.022 ± 0.009	0.163 ± 0.006	0.68 ± 0.04
ΔS^+_{CP}	0.002 ± 0.007	0.125 ± 0.005	0.62 ± 0.04
ΔS^+_{CPT}	0.002 ± 0.010	0.183 ± 0.007	0.67 ± 0.04
ΔS^+_{T}	0.004 ± 0.008	0.144 ± 0.006	0.64 ± 0.04
$S^-_{\ell^+,K_S}$	-0.002 ± 0.003	0.062 ± 0.002	0.63 ± 0.04
$S^+_{\ell^+,K_S}$	0.002 ± 0.006	0.107 ± 0.004	0.62 ± 0.04

Tab. 4.20: Mean and RMS values of the residual (fitted-generated) distributions for all the T-, CP- and CPT-violating parameters for 345 data-sized nominal parametrized Monte Carlo samples (signal plus background tuned to the data sample). The one-dimensional coverages, i.e. the fraction of experiments where the generated value of the corresponding physics parameter falls into the 1σ interval reported by the fit (with parabolic errors), are also reported.

pothesis at 8 standard deviations. Similar C.L. contours can be made for the *CP*- and *CPT*-violating parameters, in the planes $(\Delta S^{\pm}_{CP}, \Delta C^{\pm}_{CP})$ and $(\Delta S^{\pm}_{CPT}, \Delta C^{\pm}_{CPT})$, respectively, as shown in Fig. 4.24 for the same $c\overline{c}K^0$ data sample. These C.L. contours should be compared to those in data, Figs 4.16 and 4.17. It should be noted that in all cases the nominal parametrized Monte Carlo experiment shows very similar features to those observed in the data.

4.5 Systematic uncertainties

Tables 4.21, 4.22, and 4.23 summarize the detailed and main experimental systematic uncertainties. Details on how each contribution has been estimated are given below. We also report an estimate of the systematic correlations between the asymmetry parameters. To obtain this correlation, we assume each systematic source to be either uncorrelated, fully correlated (correlation coefficient $+1$), or fully anti-correlated (-1). The first case applies to systematic sources evaluated either as a RMS or a quadratic difference of fit error. All the other cases fall into the other two categories, for which the correlation coefficient (± 1) is calculated as

$$\rho_{ij,1} = \frac{\sigma_{i,1}\sigma_{j,1}}{|\sigma_{i,1}\sigma_{j,1}|} \ , \tag{4.25}$$

for source 1, and similarly for all other contributions $2, ..., N$. Here, $\sigma_{i,1}$ and $\sigma_{j,1}$ represent the (signed) systematic error 1 for parameters i and j (with the convention alternative $-$ nominal). The total experimental systematic covariance matrix can then be calculated as

$$\mathcal{V}_{\rm syst} \ = \ \sum_{\alpha=1}^{N} \begin{pmatrix} \sigma^2_{1,\alpha} & ... & \sigma_{1,\alpha}\sigma_{16,\alpha} \\ ... & ... & ... \\ \sigma_{16,\alpha}\sigma_{1,\alpha} & ... & \sigma^2_{16,\alpha} \end{pmatrix} \ , \tag{4.26}$$

where 16 is the total number of signal parameters. It is reported in Sec. 4.6.

4.5.1 Choice of the signal $m_{\rm ES}$ PDF

The per-event signal probabilities are determined assuming a single Gaussian for the signal distribution. The neglect of tails in the $m_{\rm ES}$ distribution is a source of systematic uncertainty. We have fitted our signal parameters space using a Crystal Ball shape, a PDF which consists in the combination of a Gaussian core portion and a power-law low-end tail below a certain

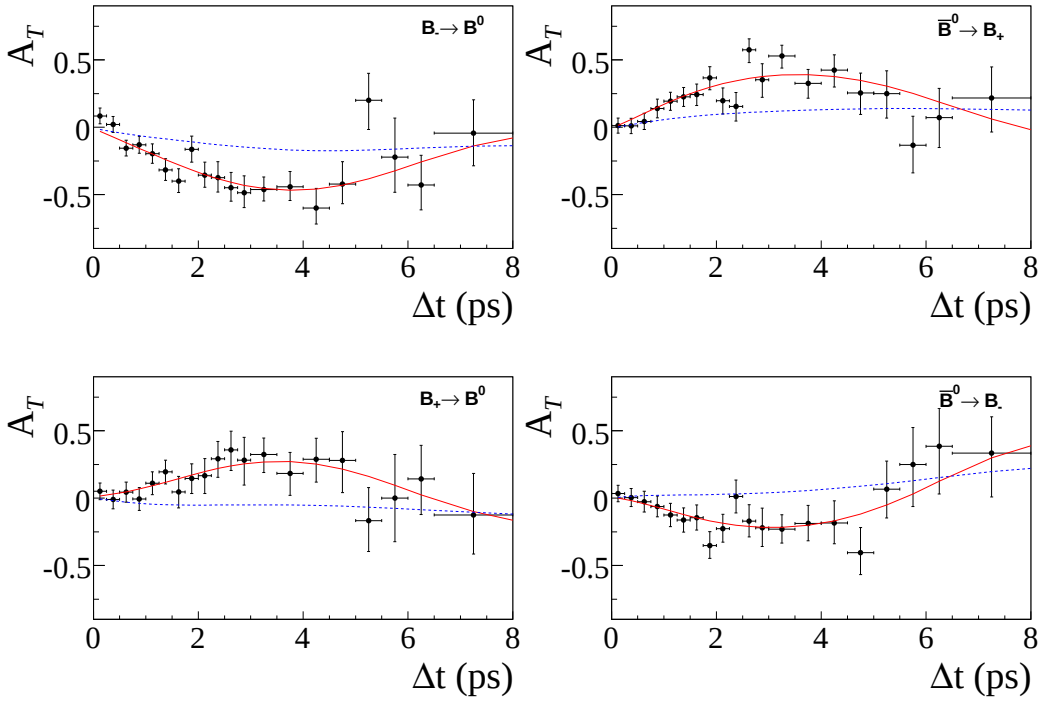

Fig. 4.20: The four independent raw T-asymmetries for one nominal data-sized parametrized Monte Carlo experiment (tuned to the $c\bar{c}K^0$ data) for flavor ID categories containing leptons and kaons combined, for the signal enriched region ($m_{\rm ES} > 5.27$ GeV for $c\bar{c}K_S$ modes and $|\Delta E| < 10$ MeV for the $J/\psi K_L$ mode). The points with error bars represent the Monte Carlo data, the solid (red) curves represent the projection of the reference fit, while the dashed (blue) curves represent the projection of the fit assuming no T invariance. The legend on top of each asymmetry is equivalent to that used in Fig. 4.3.

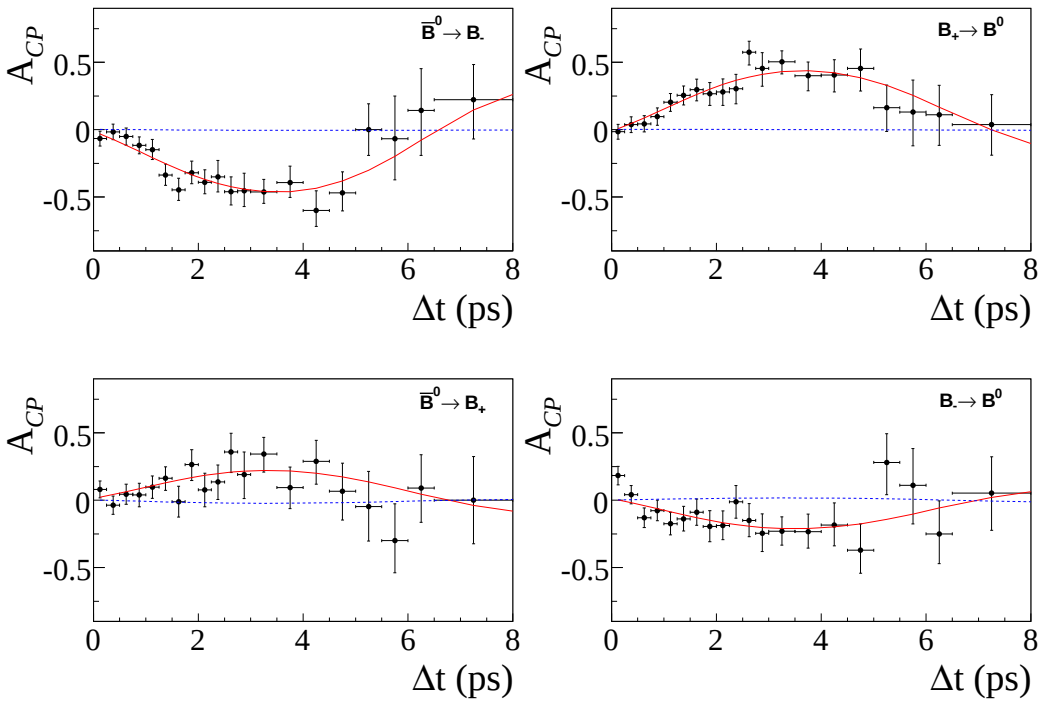

Fig. 4.21: The four independent raw *CP*-asymmetries (upper panel) for one nominal data-sized parametrized Monte Carlo experiment (tuned to the $c\overline{c}K^0$ data) for flavor ID categories containing leptons and kaons combined, for the signal enriched region ($m_{\rm ES} > 5.27$ GeV for $c\overline{c}K_S$ modes and $|\Delta E| < 10$ MeV for the $J/\psi K_L$ mode). The legend is equivalent to the one used in Fig. 4.3.

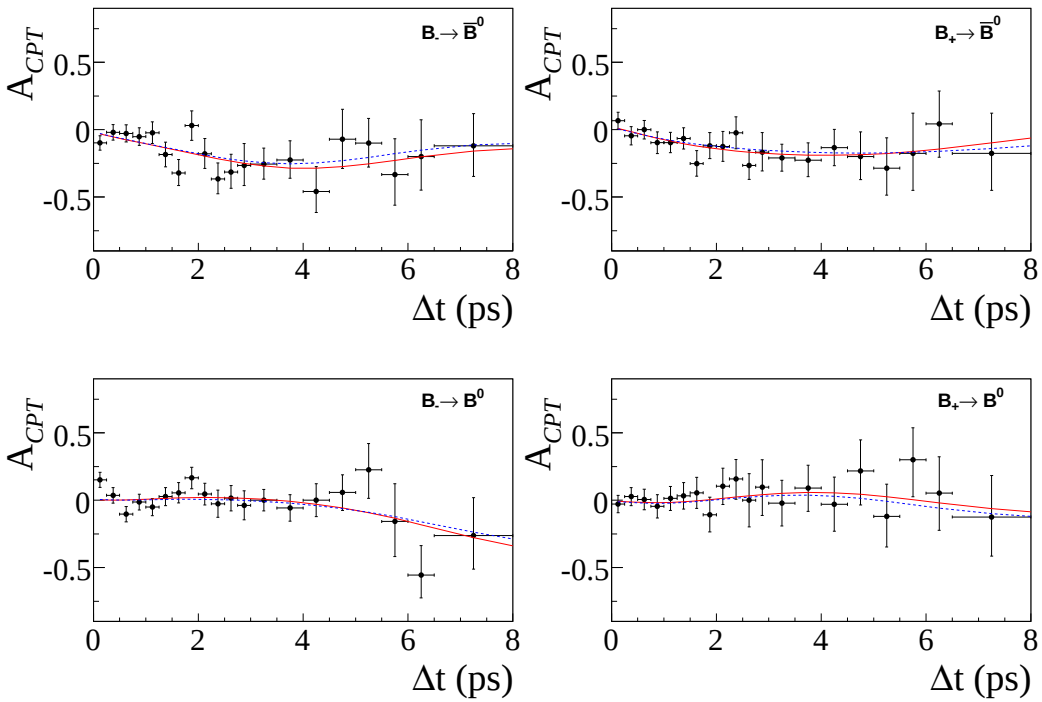

Fig. 4.22: The four independent raw *CPT*-asymmetries (lower panel) for one nominal data-sized parametrized Monte Carlo experiment (tuned to the $c\overline{c}K^0$ data) for flavor ID categories containing leptons and kaons combined, for the signal enriched region ($m_{\rm ES} > 5.27$ GeV for $c\overline{c}K_S$ modes and $|\Delta E| < 10$ MeV for the $J/\psi K_L$ mode). The legend is equivalent to the one used in Fig. 4.3.

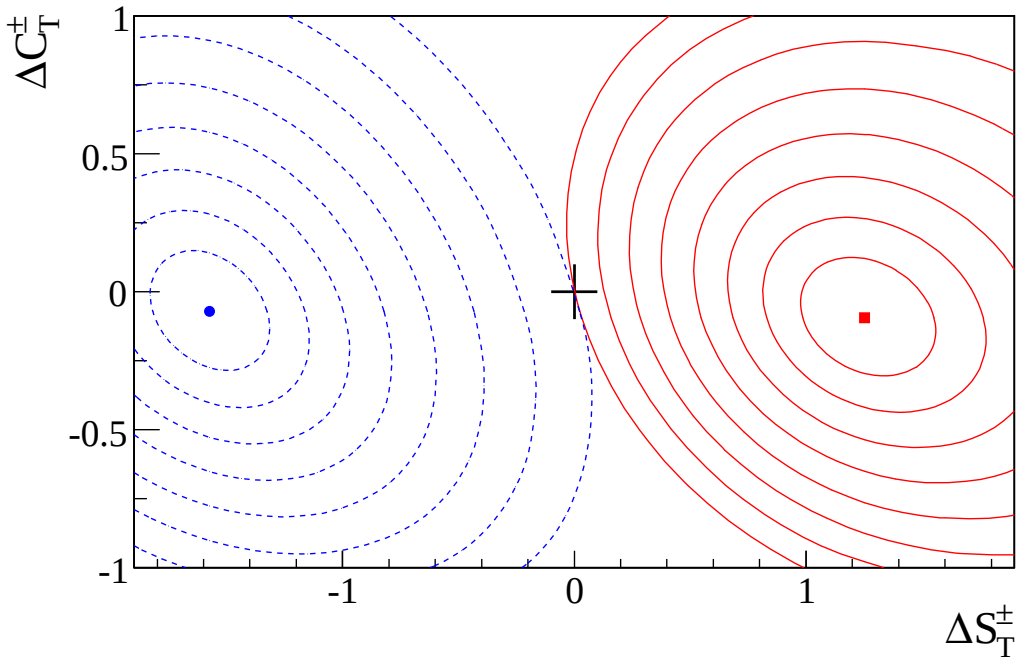

Fig. 4.23: Two-dimensional C.L. contours (up to eight standard deviations) in the $(\Delta S_T^{\pm}, \Delta C_T^{\pm})$ planes, for one nominal data-sized parametrized Monte Carlo experiment (tuned to the $c\overline{c}K^0$ data). The solid (red) and dashed (blue) contours are for the pairs of T-violating variables $(\Delta S_T^-, \Delta C_T^-)$ and $(\Delta S_T^+, \Delta C_T^+)$, respectively. These contours have been obtained using the standard likelihood ratio method, $-2\Delta ln\mathcal{L}_{\rm exp} = s^2$, with s^2 =2.30, 6.18, 11.83, 19.33, 28.74, 40.09, 53.38, 68.70, for 1-, 2-, 3-, 4-, 5-, 6-, 7-, 8-standard deviations, respectively. Thus, the C.L. in two dimensions for each pair of variables is $1-$C.L. $= 0.317, 4.6\times10^{-2}, 2.7\times10^{-3}, 6.3\times10^{-5}, 5.7\times10^{-7}$ for 1-, 2-, 3-, 4-, 5-σ. The marker at (0,0) represents the no T-invariance point, while the other markers represent the best-fit results.

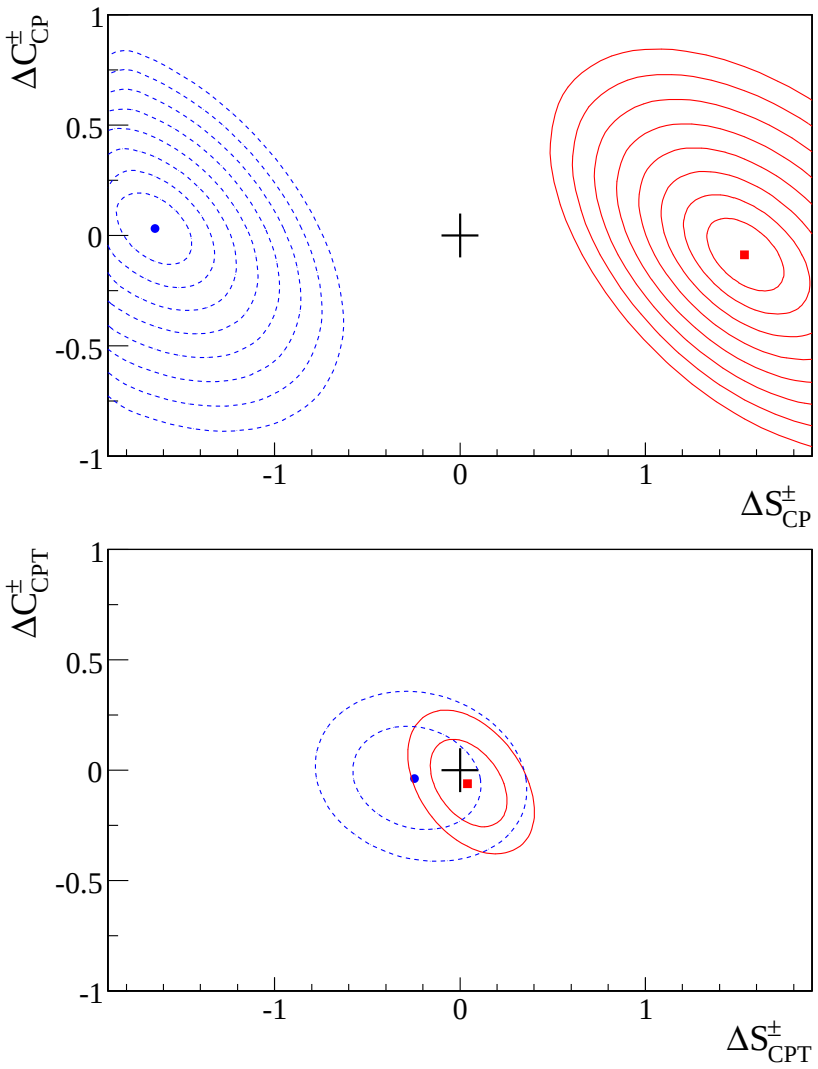

Fig. 4.24: Same as in Fig. 4.23, but for the *CP*-violating variables $(\Delta S^{\pm}_{T}, \Delta C^{\pm}_{T})$ (top) and the *CPT*-violating variables $(\Delta S^{\pm}_{CPT}, \Delta C^{\pm}_{CPT})$ (bottom). For the *CPT* case we only show the 1- and 2-σ regions. The markers at (0,0) represent the no *CP*- and no *CPT*-violating points, while the other markers represent the best-fit results.

threshold [62], instead of a Gaussian for the $m_{\rm ES}$ signal distribution, with a fixed order parameter of five and an α parameter that is different for the B_{CP} and the $B_{\rm flav}$ sample. Each CP mode is allowed to have a different α value. The differences in the physics parameters are taken as a systematic uncertainty.

4.5.2 $m_{\rm ES}$ endpoint

By default, the $m_{\rm ES}$ endpoint in the fit to the $m_{\rm ES}$ distribution is fixed to 5.291 GeV. We vary this values by ± 0.002 GeV to assign the systematic error. The largest variation in the fitted values is taken as our systematic error.

4.5.3 Statistical uncertainty in $m_{\rm ES}$ parameters

The $m_{\rm ES}$ parameters describing the per-event signal probabilities are determined in a separate pre-fit and subsequently fixed to their central values. The statistical uncertainty on these parameters is therefore not taken into account in the statistical error of our physics parameters from reference TV fit. To evaluate the associated uncertainty, we have performed a generation of 350 sets of $m_{\rm ES}$ parameters taking into account the correlation matrix from the pre-fit, and have repeated the nominal TV fit on data for each set. The RMS of the asymmetry parameters from the 350 sets is taken as systematic uncertainty.

4.5.4 Statistical uncertainty in signal misID fractions and Δt resolution parameters

The signal misID fractions and resolution function parameters are determined from the fit to the $B_{\rm flav}$ sample and then are fixed in the baseline TV fit. The statistical uncertainty on these parameters is therefore not taken into account in the statistical error of our parameters. To evaluate the associated uncertainty, we have performed a generation of 350 sets of misID and Δt resolution parameters taking into account the correlation matrix from the $B_{\rm flav}$ fit, and have repeated the nominal TV fit on data for each set. The RMS of the physics parameters from the 350 sets is taken as systematic uncertainty.

4.5.5 Signal misID

To determine the systematic error due to possibly mis-measuring the signal misID fractions of the B_{CP} sample, we use the high statistics $B_{\rm flav}$ and B_{CP}

signal Monte Carlo samples. We use about 3.5 million B_{flav} and 3.6 million B_{CP} selected events, the latter divided in 345 subsamples. We fit the B_{flav} sample for the resolution function and flavor ID parameters, and then determine our TV fit parameters on the B_{CP} samples using these values. We also determine the "true" misID parameters using the Monte Carlo truth information in the B_{CP} sample, and then fit for our TV parameters using those values. The largest between the average difference between each pair of these fits and its error is assigned as the systematic error due to incorrectly determined misID fractions using the B_{flav} sample. The correlations are assigned according to the following algorithm: if the absolute value of the average difference is twice larger than the error on the average, then we assume correlation or anticorrelation, depending on the sign of the difference; otherwise we assume no correlation.

4.5.6 Peaking background fractions

To be conservative, we vary the peaking background fractions coherently up and down (but separately for B_{flav} and B_{CP} modes) to also account for systematic uncertainties in their values. We vary the B_{flav} sample fractions by 50% and the B_{CP} modes fraction by 2σ (where σ is given in Sec. 4.2.4). The largest shift with respect to the nominal fit is assigned as systematic error.

4.5.7 The Δt resolution function

This Section discusses the systematic uncertainties related to the resolution function, in both signal and background modelings.

Different Δt resolution for misID events

The nominal TV fit assumes that the Δt resolution is the same for correctly and incorrectly flavor-identified events. However, correctly and incorrectly flavor-identified events may have different kinematics and thus different vertexing resolution. To evaluate this effect, we fit the B_{CP} Monte Carlo signal sample, split into three subsets (equivalent to about 115 times the data size, i.e, virtually infinite statistics, see Sec. 4.4.1), in two ways: (a) with a common set of Δt resolution parameters for correctly and incorrectly identified events; (b) splitting the Δt resolution parameters for correctly and incorrectly identified events. In both cases, the resolution function parameters are free parameters and the misID rates are obtained from truth (correctly identified events have $w = 0$ and incorrectly identified events have $w = 1$).

The average difference between the fitted physics parameters in the two cases is assigned as systematic error.

Signal Δt resolution function

The signal resolution function is an empirical description of the Δt residuals for which we use the sum of three Gaussian models in our nominal TV fit. To determine the sensitivity to our resolution model, we have performed a fit using two other resolution models. The first is a slight variation of the baseline model that uses separate scale factors and bias values for each of the six flavor ID categories. The second alternative model uses a "GExp" model (convolution of an exponential with a Gaussian function) instead of a single Gaussian for the description of the tail component. The systematic error assigned to this effect is the quadratic sum of the differences of the two models with respect to the standard three-Gaussian model.

Outlier component and tail scale factor

We vary the scale factor of the outlier Gaussian between 8 and 16 and the bias between -2 ps and $+2$ ps around the nominal values of 12 and 0, respectively. The scale factor of the tail is varied between 2 and 5, around the nominal 3.5. We choose the larger variation for each effect as systematic uncertainty, and calculate the quadratic sum of the three effects.

Signal Δt resolution: $c\bar{c}K^0$ vs hadronic $B_{\rm flav}$

Since we are using the $B_{\rm flav}$ sample to determine the Δt resolution function, we have to consider the possible difference between that in the $B_{\rm flav}$ sample and in the signal B_{CP} samples. We study this effect using signal Monte Carlo samples.

The true resolution functions are extracted from fits to the Δt residual for the large B_{CP} and the $B_{\rm flav}$ Monte Carlo samples. The B_{CP} sample is fitted for our set of signal parameters using both sets of fixed resolution function parameters. The flavor misID fractions are fixed to those obtained using the fit to $B_{\rm flav}$ Monte Carlo sample. No background PDFs are used in the fit and signal events are required to have $m_{\rm ES}$ greater than 5.27 GeV. The difference in the signal parameters obtained in the high statistics B_{CP} signal Monte Carlo with the two sets of resolution parameters is assigned as systematic uncertainty.

Background Δt resolution

We nominally assume that the background Δt resolution is adequately described by a double-Gaussian (core and outlier with no tail). We compute the systematic error using a triple-Gaussian resolution function for the background of the B_{CP} and $B_{\rm flav}$ samples.

4.5.8 CP content of the peaking background

In the baseline TV fit we assume the peaking background in the B_{CP} sample to have no CP content and we assign to it a PDF similar to that of the signal but without the sine term, neglecting the fact that part of this background is from $B^0\ \overline{B}^0$ decays, and neglecting direct CP violation effects. We determine a systematic uncertainty due the first assumption by including a sine term with $Im\lambda = \sin 2\beta$ and η_f (effective CP eigenvalue) for each mode given by the weighted average (using the fractions determined in Sec. 4.2.4 as weights) of the CP eigenvalues for the different contributing modes. The CP eigenvalue for charged B decays is assumed to be zero while for modes with unknown CP it has been varied between the extrema -1 and $+1$. To take into account for direct CP violation, we float $|\lambda_{\rm peaking}|$. As systematic uncertainty related to the CP content of peaking background we assume the sum in quadrature of the shift due to floating $|\lambda_{\rm peaking}|$ and the maximum shift obtained by varying η_f between the extrema -1 and $+1$.

4.5.9 CP background lifetime

As an alternative to fixing the lifetime of the CP background to that of the $B_{\rm flav}$ sample background, we determine the change in the TV physics parameters using the B^0 lifetime instead. As systematic effect we choose the difference with respect to the nominal parameters.

4.5.10 Mixing in lifetime CP background

For this contribution, we have fixed the value of Δm of the non-prompt background for all B_{CP} samples to the value obtained in the $B_{\rm flav}$ sample ($-0.33067\ \ {\rm ps}^{-1}$ instead of $0.507\ \ {\rm ps}^{-1}$).

4.5.11 MisID fractions of the $B^0\ \overline{B}^0$ peaking background

The peaking background from B^0 decays in the $B_{\rm flav}$ sample is treated as pure signal in the fit, any difference between the peaking and the signal misID fractions would affect the measurement. We determine the uncertainty in

the signal TV parameters due to a possible difference in the misID fractions of the B^0 $\overline{B}^0$ peaking background, following the recipe described in Ref. [49], Sec. 12.6. This uncertainty is studied by measuring the misID fractions for the truth matched $B_{\rm flav}$ decays, and for the background inside and outside the signal region separately. As a result of this study, conservatively one can consider a peaking background fraction of 4% and an average difference between $\omega_{\rm truth}$ and $\omega_{\rm peak}$ of 0.03. We change our signal misID parameters as extracted from the $B_{\rm flav}$ fit by 0.0012 and repeat the standard TV fit, assigning the variation in the physics parameters as systematic uncertainty. Since $|\lambda|$ depend on the misID parameter ω by a term proportional to ω^2, we assume that the shift on $|\lambda|$ is negligible for this effect.

4.5.12 Beam spot position

The Δt vertexing algorithm uses the position of the beam spot as a constraint in reconstructing the decay vertex of the flavor-identified B meson. The strongest constraint comes from the y position of the beam spot. The y position is varied to $\pm 20\,\mu$m and the error on the y position is separately increased to $20\,\mu$m as well. Since we do not have a $J/\psi K_L$ signal Monte Carlo processed with these changes, we assume

$$\begin{aligned} \mathrm{Syst}(\Delta S^+_{CP}) &= \mathrm{Syst}(\Delta S^+_{T}) = \mathrm{Syst}(\Delta S^+_{CPT}), \\ \mathrm{Syst}(\Delta S^-_{CP}) &= \mathrm{Syst}(\Delta S^-_{T}) = \mathrm{Syst}(\Delta S^-_{CPT}), \end{aligned} \tag{4.27}$$

as expected since the vertexing effects are largely independent of the CP final state.

4.5.13 Absolute z scale and boost uncertainty

The effect of the uncertainty on boost and z scale has been evaluated through scaling the measured Δt and its error by 0.6%. We have used the same approach described by Eq. (4.27).

4.5.14 SVT misalignment

We have followed the recipe from the SVT local alignment experts [63] to evaluate the systematic error from the local misalignment of the SVT wafers. The procedure is to fit our TV signal parameters in a high-statistics signal $J/\psi K_s$ Monte Carlo sample with various realistic misalignments of the SVT. Each sample has been divided in 10 subsamples. As we do not have a $J/\psi K_L$ sample with these various misalignments, we use the assumption given in Eq. (4.27). The results of these fits are compared to the result of fitting the

signal TV parameters in the same signal $J/\psi K_s$ Monte Carlo sample with the corresponding perfect SVT alignment subsample (the default condition in the Monte Carlo simulation). For each misalignment effect we build the average of the 10 subsamples and determine the change with respect to the perfect alignment scenario. We assign as systematic uncertainty the largest variation for each TV parameter.

The usual Δt quality cuts ($|\Delta t| < 20\,\text{ps}$ and $\sigma_{\Delta t} < 2.5\,\text{ps}$) are made and m_{ES} is required to be in the signal region ($> 5.27\,\text{GeV}$). A small number of events ($< 1\%$) come into or fall out of the analysis sample due to the changes in the alignment. To avoid changes in the results due to events coming into or out of the sample, we restrict the analysis to events that pass all cuts in all of the misalignment sets, including the perfect alignment. The signal misID parameters are determined from an external hadronic B_{flav} signal Monte Carlo fit and then held fixed in the TV fits.

4.5.15 External physics parameters

In the nominal TV fits we fix the B^0 lifetime and the B^0-$\overline{B}^0$ mixing frequency to the world averages [61], $\tau_{B^0} = 1.530 \pm 0.009\,\text{ps}$ and $\Delta m = 0.507 \pm 0.005\,\text{ps}^{-1}$, respectively. The systematic errors due to the uncertainties in τ_{B^0} and Δm correspond to 1 σ variations of the above values. We chose the larger variation as systematics.

4.5.16 $\Delta\Gamma$ and E parameters

In the nominal TV fits we fix $\Delta\Gamma/\Gamma = 0$. The value of $\Delta\Gamma_d/\Gamma_d$ is measured to be between -0.084 and 0.064 at 90% confidence level [24, 64] and it is predicted to be smaller than 1% in the Standard Model [61]. In our signal model the first order contribution in $\Delta\Gamma$ appears multiplying the E parameters, $E\sinh(\Delta\Gamma\Delta t/2) \approx E\Delta\Gamma\Delta t/2$, thus to evaluate this systematic effect we have performed a generation of 350 sets of $\Delta\Gamma$ and the E input parameters, using Gaussian distributions with mean 0 and a width of 2% and 5% widths, respectively. The observed RMS of the TV parameters from the 350 sets is taken as systematic uncertainty.

4.5.17 PDF asymptotic normalization

By default, the PDF is normalized with an asymptotic normalization, while Δt is restricted to the range $-20\,\text{ps} < \Delta t < 20\,\text{ps}$. We have evaluated our sensitivity to the PDF normalization by performing a TV fit using PDFs that are normalized in this finite range.

4.5.18 Uncertainty on fit bias from Monte Carlo

As shown in Sec. 4.4.1, we divide the signal Monte Carlo sample for each *CP* final state into data-sized subsamples, where the number of events in each subsample is determined according to the yield measured in the data, and then fit our *TV* signal model to check for any potential bias. The misID and resolution function parameters are obtained from the high statistics $B_{\rm flav}$ Monte Carlo sample and are kept fixed. The largest between the mean residual (fitted minus generated) and its error is assigned as systematic error. The correlations are assigned following the same algorithm as in Sec. 4.5.5.

4.5.19 Interference effects from doubly-CKM-suppressed amplitudes

The B decays that are used for flavor ID are dominated by amplitudes containing a $b \to c\bar{u}d$ transition. However, its possible that $\bar{b} \to \bar{u}c\bar{d}$ amplitudes can also contribute to the final states. For example, a flavor-identified B meson may be observed in the $D^+\pi^-$ mode and generate a K^- from the D^+. The dominant amplitude contribution is from the $\overline{B}^0$ decay ($b \to c\overline{u}d$), but a suppressed amplitude from B^0 decay ($\overline{b} \to \overline{u}c\overline{d}$) cannot be ruled out. These two amplitudes will interfere with a relative weak phase of γ and a relative strong phase δ' from final-state interactions. A rough estimate of the relative size of these amplitudes is $r' \approx |(V^*_{ub}V_{cd})/(V_{cb}V^*_{ud})| \approx 0.02$. Events where the B meson decays semileptonically are immune to this problem ($r'_{Lepton} = 0$).

The effects of the suppressed $\overline{b} \to \overline{u}c\overline{d}$ amplitude are *not* simply absorbed into the misID fractions. The *TV* time-dependent asymmetry parameters receive corrections proportional to the amplitude ratio r'. To evaluate this systematic effect we performed a scan of the hadronic parameters associated to the effect, fixing $r' = 0.04$ and varying uniformly the strong and weak phases, δ' and γ, in the interval [0,2π]. We take as systematic error the maximum deviation for each *TV* signal parameter.

4.5.20 Direct CP violation in the combinatorial background

The combinatorial background PDF for $c\bar{c}K_S$ events is described by Eq. (4.22) and is of the form $1 + \mathcal{I}m\lambda_{\rm eff} \cdot \sin\Delta m\Delta t$. To evaluate the effect of possible direct *CP* violation in the combinatorial background, we introduce a cosine term in our nominal fit.

4.5.21 D parameters and relative normalization

In the nominal *TV* fits we assume the same normalization for each $c\bar{c}K^0$ sample ($c\bar{c}K_S$ and $J/\psi K_L$) split by Δt sign, thus implies we have two inde-

pendent D parameters for the $c\bar{c}K_S$ instead of four, and analogously for the $c\bar{c}K_L$ sample. To evaluate the effect due to this normalization assumption, we made a Bayesian generation of a set of 2×2 ΔD's parameters (two ΔD parameters for the $c\bar{c}K_S$ sample and two ΔD parameters for the $J/\psi K_L$ sample) assuming a Gaussian distribution with a mean value of 0 and a width of 1%. The observed RMS of the TV parameters from the 350 sets is taken as systematic uncertainty.

4.5.22 $J/\psi K_L$ systematics

In this Section, we describe the procedure and results of the dedicated systematic error evaluation of the $J/\psi K_L$ sample.

Measured sample composition from ΔE fit

The relative amount of signal, inclusive J/ψ background and non-J/ψ background is determined from a binned likelihood fit of the ΔE spectrum, which is described in Ref. [65]. There are two statistical sources of uncertainty associated with the sample fractions from the ΔE fit that must be taken into account: the statistical error reported by the fit (data statistics) and the statistical error from the finite size of the Monte Carlo sample used to make the signal and inclusive J/ψ background templates (Monte Carlo statistics).

The uncertainty from the Monte Carlo statistics was evaluated by performing the ΔE fit 100 times where for each fit, the height of each template bin was chosen randomly from a Poisson distribution with a mean equal to the nominal bin height for the template histogram before renormalization. The average difference of the TV signal parameters from the 100 sets with respect to the nominal values is taken as the systematic uncertainty.

Branching fractions

The branching fractions (BF) for the relevant $J/\psi X$ modes were all varied by either their measured error or conservative estimates up and down. The ΔE fit for the sample composition was redesigned for each variation. For each BF variation we have chosen as systematic error the maximum of the variation up and down.

Assumed CP content of background

The CP eigenvalue for most of the components in the fit is known. The cases where it is not are:

- $B^0 \to J/\psi K^{*0}; K^{*0} \to K_L\pi^0$: We use an effective *CP* eigenvalue derived from Ref. [60], which is -0.504 ± 0.033.

- Non-itemized $J/\psi X$ background: Of the decay modes in this category, roughly 15% have known *CP* violation properties. This gives a net *CP* of $+0.036$ in the EMC and -0.003 in the IFR. If we assume that the branching fractions of the rest of the modes in the inclusive J/ψ background have an uncertainty of 50%, this gives a variation from 0.018 to 0.054 for the *CP* value of the $J/\psi X$ background in the EMC, and -0.0045 to -0.0015 for the IFR.

- Non-J/ψ background: We assume the net *CP* to be 0 and vary it by ± 0.25.

For each case we have chosen as systematic error the maximum variation.

Shape of ΔE distributions

The parameters of the different ΔE PDFs obtained from the full sample of Monte Carlo events are used in the *CP* fit. This is useful to separate signal and background events on an event-by-event basis. Unfortunately, some variations on the beam parameters that can affect the ΔE resolution and mean are not included in the Monte Carlo simulation. We need to correct for these effects in order to obtain agreement between the Monte Carlo and data samples. This can be done by studying a sample of $J/\psi K_S$ events where the K_S is reconstructed as a K_L. The advantage of using K_S's here is that their direction is well measured and can be used in the calculation of ΔE along with the B mass constraint. In turn, the ΔE resolution in this sample almost only reflects the uncertainty in the beam parameters. The ΔE distribution from Monte Carlo has to be shift by 0.5 MeV in order to be consistent with the data distribution. We also need to compensate for the beam energy smear which is underestimated. This is done by adding an additional Gaussian with a width of 1.1 MeV.

To evaluate our sensitivity to the shape of the ΔE PDFs, we performed the following variations:

- Change the additional ΔE smearing by ± 0.45 MeV with respect to the nominal 1.1 MeV.

- Change the ΔE shift by ± 0.25 MeV with respect to the nominal 0.5 MeV.

We have chosen as systematic error the maximum variation for each ΔE parameter.

Reweighting of Monte Carlo events

We do not believe that the Monte Carlo gives an accurate measure of the absolute K_L reconstruction efficiency. If the efficiency in the Monte Carlo is not correct, the composition of the inclusive J/ψ will be incorrect, since it is a mixture of backgrounds that do and do not contain K_L kaons in the final state. We estimate the K_L reconstruction efficiency in data, relative to the Monte Carlo, by comparing the fitted $J/\psi K_L$ signal yield to the expected yield based on the total branching fraction, sample luminosity, and the Monte Carlo efficiency.

To evaluate the systematic error on the data vs Monte Carlo K_L efficiency in the background, we rescale the background events from B decays with a K_L in the final state by 0.82 and 1.11 for EMC and IFR samples, respectively. The ΔE sample composition fit and the resulting itemization of the inclusive J/ψ background is redone with new templates that include this adjustment.

Non-ψ background in $J/\psi K_L$

As discussed in Sec. 6.8 of Ref. [59], we fix the $|\lambda|$ of the non-J/ψ background to 1. We fit the $|\lambda|$ of the non-J/ψ background on the J/ψ mass sideband data and find $|\lambda| = 0.986 \pm 0.029$. We evaluate the systematic error due to the difference between 1 and the value obtained from the J/ψ sideband by fixing $|\lambda|$ to this number $\pm$ its statistical error. We extract as systematic error the maximum variation of the parameters.

Systematic source		ΔS_T^+	ΔS_T^-	ΔC_T^+	ΔC_T^-	ΔS_{CP}^+	ΔS_{CP}^-	ΔC_{CP}^+	ΔC_{CP}^-
4.5.1) $m_{\rm ES}$ PDF	6)	0.011	−0.001	−0.004	−0.001	0.015	−0.007	−0.004	−0.003
4.5.2) $m_{\rm ES}$ endpoint	6)	−0.002	0.001	−0.001	−0.001	−0.003	−0.002	−0.001	0.002
4.5.3) Uncertainty in $m_{\rm ES}$ parameters	6)	0.003	0.001	0.003	0.001	0.003	0.003	0.002	0.002
4.5.4) Uncertainty in misID and Δt parameters	2)	0.019	0.021	0.012	0.012	0.014	0.015	0.009	0.009
4.5.5) Signal misID fractions	2)	0.009	0.036	0.018	0.019	0.008	0.037	0.018	0.018
4.5.6) Peaking Background Fractions	5)	0.001	−0.001	0.001	−0.002	0.004	−0.003	0.002	0.002
4.5.7.1) Δt resolution for misID events	3)	0.005	0.005	−0.002	0.003	0.005	0.004	0.000	0.003
4.5.7.2) GExp Δt resolution model	3)	0.007	−0.028	0.042	−0.051	0.049	−0.027	−0.005	−0.003
4.5.7.2) Split Δt resolution model	3)	0.002	0.005	0.002	−0.004	0.001	−0.001	−0.001	−0.003
4.5.7.3) Outlier's scale factor	3)	0.012	−0.013	−0.012	−0.018	0.007	−0.007	0.000	−0.003
4.5.7.3) Outlier's bias	3)	−0.003	−0.007	0.002	0.002	0.001	−0.004	−0.001	−0.001
4.5.7.3) Tail's scale factor	3)	0.013	−0.016	−0.019	−0.029	0.024	−0.016	0.006	−0.004
4.5.7.4) Δt resolution $c\overline{c}K$ vs $B_{\rm flav}$	3)	0.023	−0.025	0.004	−0.004	0.016	0.008	−0.009	−0.007
4.5.7.5) Background Δt resolution	3)	−0.001	−0.024	−0.002	−0.004	0.004	−0.004	0.001	−0.002
4.5.8) *CP* content of the peaking background	5)	−0.022	−0.020	−0.006	−0.009	−0.008	0.008	−0.001	−0.003
4.5.9) *CP* background lifetime	5)	−0.019	0.006	0.018	0.024	−0.009	0.009	0.000	0.001
4.5.10) Mixing in lifetime *CP* bkg	5)	0.001	−0.003	−0.006	0.001	−0.003	0.002	−0.001	0.003
4.5.11) MisID fractions of B^0 peaking background	2)	−0.004	0.004	0.000	0.000	−0.004	0.005	0.000	0.000
4.5.12) Beam spot position	1)	0.010	0.022	0.011	−0.022	0.010	0.022	0.011	−0.022
4.5.13) Z scale and boost uncertainty	1)	0.001	0.002	0.010	0.012	0.001	0.002	0.010	0.012
4.5.14) SVT misalignment	1)	−0.005	−0.027	0.013	0.013	0.008	−0.010	0.003	−0.003
4.5.15) External physics parameters	7)	−0.001	−0.005	−0.011	0.008	0.003	−0.007	−0.011	0.012
4.5.16) $\Delta\Gamma$ and E coefficients	10)	0.004	0.003	0.002	0.002	0.004	0.003	0.001	0.001
4.5.17) PDF Asymptotic normalization	11)	0.003	0.016	0.003	0.000	−0.004	0.007	0.004	−0.005
4.5.18) Uncertainty on fit bias from Monte Carlo	9)	−0.010	0.073	0.013	0.010	0.010	0.007	0.007	0.014
4.5.19) DCS interference	8)	0.018	−0.019	−0.001	0.001	0.009	−0.008	−0.006	0.006
4.5.20) Direct *CP* violation in combinatorial bkg	5)	0.001	0.000	0.004	0.004	0.002	−0.000	0.008	0.008
4.5.21) D parameters and relative normalization	11)	0.012	0.009	0.005	0.004	0.017	0.009	0.005	0.004
4.5.22.1) K_L ΔE sample composition	4)	0.024	−0.026	−0.045	−0.004	−0.000	0.000	0.000	0.000
4.5.22.2) K_L BF of K^*	4)	0.004	−0.005	−0.002	0.002	0.000	0.000	0.000	−0.000
4.5.22.2) K_L BF of K^0	4)	0.005	−0.005	−0.002	0.001	−0.000	0.000	−0.000	0.001
4.5.22.2) K_L BF of $K_L + \pi$	4)	0.003	−0.003	−0.004	0.000	−0.001	0.000	−0.000	0.001
4.5.22.2) K_L BF of χ_{c1}	4)	0.003	−0.003	0.001	0.000	−0.000	0.000	0.000	0.000
4.5.22.2) K_L BF of Other	4)	−0.013	0.019	−0.002	−0.005	−0.000	0.000	0.000	0.000
4.5.22.3) K_L *CP* content of K^* bkg	4)	0.002	−0.002	−0.000	0.000	−0.000	0.000	0.000	0.000
4.5.22.3) K_L *CP* content of $J/\psi + X$ bkg	4)	−0.002	0.003	−0.001	0.000	−0.000	0.000	0.000	0.000
4.5.22.3) K_L *CP* content of No-J/ψ bkg	4)	0.002	−0.003	−0.000	0.000	−0.001	0.001	0.000	0.000
4.5.22.4) K_L smearing ΔE shape	4)	0.016	−0.012	−0.013	−0.002	−0.001	−0.000	−0.001	0.001
4.5.22.4) K_L shift ΔE shape	4)	−0.006	0.012	−0.003	0.004	−0.001	−0.000	−0.001	0.002
4.5.22.5) K_L reweighting Monte Carlo	4)	0.000	−0.002	−0.001	0.001	−0.000	0.000	0.000	0.000
4.5.22.6) K_L mixing in lifetime *CP* bkg	4)	0.000	−0.001	−0.005	−0.006	−0.000	0.000	0.000	0.000
Total Systematics		0.064	0.112	0.080	0.077	0.068	0.061	0.034	0.041

Tab. 4.21: Detailed break-down and total systematic uncertainty on the T-, CP-, and CPT-violating parameters. The first column indicates the section where the systematic source is described, the second column refers to the entry in Table 4.23 where the given uncertainty is included. The total systematic uncertainty (last row in the tabular) is calculated adding in quadrature the individual uncertainties.

Systematic source		ΔS^{+}_{CPT}	ΔS^{-}_{CPT}	ΔC^{+}_{CPT}	ΔC^{-}_{CPT}	$S^{+}_{\ell+,K_S}$	$S^{-}_{\ell+,K_S}$	$C^{+}_{\ell+,K_S}$	$C^{-}_{\ell+,K_S}$
4.5.1) $m_{\rm ES}$ PDF	6)	0.010	−0.001	−0.005	−0.001	−0.010	0.001	0.004	0.001
4.5.2) $m_{\rm ES}$ endpoint	6)	−0.003	0.001	−0.002	−0.000	0.003	−0.001	0.001	0.000
4.5.3) Uncertainty in $m_{\rm ES}$ parameters	6)	0.003	0.001	0.002	0.001	0.002	0.001	0.002	0.001
4.5.4) Uncertainty in misID and Δt parameters	2)	0.018	0.008	0.009	0.009	0.013	0.006	0.006	0.005
4.5.5) Signal misID fractions	2)	−0.001	0.001	−0.000	−0.000	−0.004	−0.019	−0.010	−0.009
4.5.6) Peaking Background Fractions	5)	0.003	−0.001	−0.001	0.000	−0.002	0.001	−0.002	0.001
4.5.7.1) Δt resolution for misID events	3)	−0.004	−0.001	−0.004	0.001	−0.004	−0.001	0.000	−0.002
4.5.7.2) GExp Δt resolution model	3)	−0.034	0.026	0.040	−0.059	−0.042	−0.027	−0.038	0.005
4.5.7.2) Split Δt resolution model	3)	−0.001	−0.001	0.003	−0.004	0.000	0.001	−0.000	0.002
4.5.7.3) Outlier's scale factor	3)	−0.011	−0.003	−0.019	−0.011	−0.008	−0.002	−0.005	−0.004
4.5.7.3) Outlier's bias	3)	−0.013	−0.002	0.001	−0.000	−0.003	−0.002	−0.002	0.001
4.5.7.3) Tail's scale factor	3)	−0.030	0.017	0.024	−0.037	−0.017	−0.012	−0.022	−0.007
4.5.7.4) Δt resolution $c\overline{c}K$ vs $B_{\rm flav}$	3)	0.032	−0.008	−0.005	−0.014	−0.020	0.003	0.002	0.005
4.5.7.5) Background Δt resolution	3)	−0.021	−0.007	−0.001	−0.002	−0.003	0.002	−0.006	−0.005
4.5.8) *CP* content of the peaking background	5)	0.023	0.019	0.006	0.004	0.004	0.004	0.000	0.001
4.5.9) *CP* background lifetime	5)	0.002	−0.005	0.023	0.016	0.011	0.001	0.005	0.005
4.5.10) Mixing in lifetime *CP* bkg	5)	−0.007	0.000	−0.003	0.002	0.002	−0.000	0.001	−0.002
4.5.11) MisID fractions of B^0 peaking background	2)	−0.000	0.001	0.000	0.000	0.002	−0.002	−0.000	−0.000
4.5.12) Beam spot position	1)	0.010	0.022	0.011	−0.022	0.011	−0.008	−0.008	0.007
4.5.13) Z scale and boost uncertainty	1)	0.001	0.002	0.010	0.012	0.001	0.002	0.013	0.003
4.5.14) SVT misalignment	1)	0.011	−0.009	0.017	−0.003	−0.009	−0.002	−0.003	−0.004
4.5.15) External physics parameters	7)	0.004	0.001	−0.002	0.003	0.003	0.003	−0.009	−0.008
4.5.16) $\Delta\Gamma$ and E coefficients	10)	0.003	0.002	0.002	0.001	0.002	0.001	0.001	0.001
4.5.17) PDF Asymptotic normalization	11)	0.015	0.009	0.005	−0.001	0.005	−0.000	−0.002	0.003
4.5.18) Uncertainty on fit bias from Monte Carlo	9)	−0.018	0.026	0.007	0.021	0.005	−0.017	−0.006	−0.015
4.5.19) DCS interference	8)	0.026	0.010	−0.007	0.005	−0.014	−0.005	0.003	0.002
4.5.20) Direct *CP* violation in combinatorial bkg	5)	0.001	0.000	0.004	0.004	−0.001	0.000	−0.004	−0.004
4.5.21) D parameters and relative normalization	11)	0.012	0.012	0.005	0.004	0.006	0.002	0.002	0.002
4.5.22.1) K_L ΔE sample composition	4)	−0.028	0.001	−0.027	−0.013	0.000	0.000	0.000	−0.000
4.5.22.2) K_L BF of K^*	4)	−0.007	0.003	−0.001	0.001	−0.000	0.000	0.000	0.000
4.5.22.2) K_L BF of K^0	4)	−0.007	0.004	−0.001	0.000	0.000	−0.000	0.000	−0.000
4.5.22.2) K_L BF of $K_L+\pi$	4)	−0.005	0.001	−0.002	0.000	0.001	−0.000	0.000	−0.001
4.5.22.2) K_L BF of χ_{c1}	4)	−0.003	0.002	0.000	−0.000	0.001	−0.000	−0.000	0.000
4.5.22.2) K_L BF of Other	4)	0.025	−0.012	−0.002	−0.003	0.000	−0.000	−0.000	−0.000
4.5.22.3) K_L *CP* content of K^* bkg	4)	−0.002	−0.002	−0.000	0.000	0.000	−0.000	−0.000	−0.000
4.5.22.3) K_L *CP* content of $J/\psi+X$ bkg	4)	0.003	−0.002	−0.000	0.000	0.000	−0.000	−0.000	−0.000
4.5.22.3) K_L *CP* content of No-J/ψ bkg	4)	−0.002	0.002	−0.001	0.000	0.001	−0.000	−0.000	−0.000
4.5.22.4) K_L smearing ΔE shape	4)	−0.021	−0.005	0.005	0.004	0.001	0.000	0.000	−0.001
4.5.22.4) K_L shift ΔE shape	4)	0.010	−0.015	0.006	0.003	0.001	0.001	0.001	−0.001
4.5.22.5) K_L reweighting Monte Carlo	4)	−0.003	0.001	−0.001	0.000	0.000	−0.000	0.000	−0.000
4.5.22.6) K_L mixing in lifetime *CP* bkg	4)	−0.000	0.001	0.005	0.005	0.000	−0.000	−0.000	−0.000
Total Systematics		0.092	0.058	0.067	0.083	0.059	0.041	0.051	0.026

Tab. 4.22: Detailed break-down and total systematic uncertainty on the T-, CP-, and CPT-violating parameters. The first column indicates the section where the systematic source is described, the second column refers to the entry in Table 4.23 where the given uncertainty is included. The total systematic uncertainty (last row in the tabular) is calculated adding in quadrature the individual uncertainties.

Systematic source	ΔS_T^+	ΔS_T^-	ΔC_T^+	ΔC_T^-	ΔS_{CP}^+	ΔS_{CP}^-	ΔC_{CP}^+	ΔC_{CP}^-
Interaction region	0.011	0.035	0.02	0.029	0.012	0.024	0.015	0.026
Flavor misID probabilities	0.022	0.042	0.022	0.022	0.016	0.040	0.020	0.020
Δt resolution	0.030	0.050	0.048	0.062	0.057	0.033	0.012	0.011
$J/\psi K_L$ background	0.033	0.038	0.052	0.010	0.002	0.001	0.001	0.002
Background fractions and *CP* content	0.029	0.021	0.020	0.026	0.013	0.012	0.008	0.009
$m_{\rm ES}$ parametrization	0.011	0.002	0.005	0.002	0.016	0.008	0.005	0.004
Γ and Δm	0.001	0.005	0.011	0.008	0.003	0.007	0.011	0.012
CP violation for flavor ID categories	0.018	0.019	0.001	0.001	0.009	0.008	0.006	0.006
Fit bias	0.010	0.072	0.013	0.010	0.010	0.007	0.007	0.014
$\Delta\Gamma/\Gamma$	0.004	0.003	0.002	0.002	0.004	0.003	0.001	0.001
PDF normalization	0.013	0.019	0.005	0.004	0.017	0.012	0.006	0.007
Total	0.064	0.112	0.08	0.077	0.068	0.061	0.033	0.041

Systematic source	ΔS_{CPT}^+	ΔS_{CPT}^-	ΔC_{CPT}^+	ΔC_{CPT}^-	S_{ℓ^+,K_S}^+	S_{ℓ^+,K_S}^-	C_{ℓ^+,K_S}^+	C_{ℓ^+,K_S}^-
Interaction region	0.015	0.024	0.023	0.026	0.014	0.009	0.015	0.008
Flavor misID probabilities	0.018	0.008	0.009	0.009	0.013	0.020	0.012	0.010
Δt resolution	0.062	0.033	0.051	0.072	0.051	0.030	0.045	0.012
$J/\psi K_L$ background	0.046	0.021	0.029	0.015	0.002	0.001	0.001	0.001
Background fractions and *CP* content	0.024	0.020	0.024	0.016	0.012	0.004	0.007	0.007
$m_{\rm ES}$ parametrization	0.011	0.002	0.005	0.002	0.011	0.002	0.005	0.002
Γ and Δm	0.004	0.001	0.002	0.003	0.003	0.003	0.009	0.008
CP violation for flavor ID categories	0.026	0.010	0.007	0.005	0.014	0.005	0.003	0.002
Fit bias	0.018	0.026	0.007	0.021	0.005	0.017	0.006	0.015
$\Delta\Gamma/\Gamma$	0.003	0.002	0.002	0.001	0.002	0.001	0.001	0.001
PDF normalization	0.019	0.015	0.007	0.004	0.008	0.002	0.003	0.003
Total	0.092	0.058	0.067	0.083	0.059	0.041	0.051	0.026

Tab. 4.23: Breakdown of main systematic uncertainties on the T-, *CP*-, and CPT-asymmetry parameters, as obtained rearranging the entries from Tables 4.21 and 4.22. The total systematic uncertainty (last row in the tabular) is calculated adding in quadrature the individual uncertainties.

4.6 Summary and interpretation of the results

The final results for the T-, CP- and CPT-violating parameters $\Delta S_T^{\pm}$, $\Delta C_T^{\pm}$, $\Delta S_{CP}^{\pm}$, $\Delta C_{CP}^{\pm}$, $\Delta S_{CPT}^{\pm}$, $\Delta C_{CPT}^{\pm}$, $S_{\ell^+,K_S}^{\pm}$, $C_{\ell^+,K_S}^{\pm}$ including statistical and systematic uncertainties are given in Table 4.24. The complete (16×16) statistical and systematic correlation matrices are given in Tables 4.25 and 4.26, respectively (ordering of parameters in rows and columns is the same as in Table 4.24). The observation of TV in interference between decay and mixing can be summarized by the deviation from zero of the T-violating parameters

$$\begin{aligned} \Delta S_T^+ &= -1.37 \pm 0.14 \text{ (stat.)} \pm 0.06 \text{ (syst.)} , \\ \Delta S_T^- &= 1.17 \pm 0.18 \text{ (stat.)} \pm 0.11 \text{ (syst.)} . \end{aligned} \tag{4.28}$$

No evidence for TV associated to the decay (direct T violation) is found, as reflected by the consistency with zero of the parameters ΔC_T^+ and ΔC_T^-. The measurements of the remaining CP- and CPT-violating parameters are consistent with the expectation that the observed T non-invariance is compensated by the associated CP violation so that CPT remains invariant. The significance of these results, including systematic uncertainties, is discussed and evaluated below.

Parameter	Final result
ΔS_T^+	$-1.37 \pm 0.14 \pm 0.06$
ΔS_T^-	$1.17 \pm 0.18 \pm 0.11$
ΔC_T^+	$0.10 \pm 0.14 \pm 0.08$
ΔC_T^-	$0.04 \pm 0.14 \pm 0.08$
ΔS_{CP}^+	$-1.30 \pm 0.11 \pm 0.07$
ΔS_{CP}^-	$1.33 \pm 0.12 \pm 0.06$
ΔC_{CP}^+	$0.07 \pm 0.09 \pm 0.03$
ΔC_{CP}^-	$0.08 \pm 0.10 \pm 0.04$
ΔS_{CPT}^+	$0.16 \pm 0.21 \pm 0.09$
ΔS_{CPT}^-	$-0.03 \pm 0.13 \pm 0.06$
ΔC_{CPT}^+	$0.14 \pm 0.15 \pm 0.07$
ΔC_{CPT}^-	$0.03 \pm 0.12 \pm 0.08$
S_{ℓ^+,K_S}^+	$0.55 \pm 0.09 \pm 0.06$
S_{ℓ^+,K_S}^-	$-0.66 \pm 0.06 \pm 0.04$
C_{ℓ^+,K_S}^+	$0.01 \pm 0.07 \pm 0.05$
C_{ℓ^+,K_S}^-	$-0.05 \pm 0.06 \pm 0.03$

Tab. 4.24: T-, CP- and CPT-violating parameters as obtained from the TV analysis. The first error is statistical and the second is the systematic uncertainty.

$$\begin{pmatrix}
100 & & & & & & & & & & & & & & & \\
10.1 & 100 & & & & & & & & & & & & & & \\
-30.2 & 26 & 100 & & & & & & & & & & & & & \\
14 & -18.8 & 12.4 & 100 & & & & & & & & & & & & \\
48.3 & 2.19 & -8.9 & 4.4 & 100 & & & & & & & & & & & \\
-13.5 & 17.6 & -5.3 & -15.3 & -13 & 100 & & & & & & & & & & \\
-14.5 & 2.42 & 31.1 & -7.7 & -42.6 & 3.3 & 100 & & & & & & & & & \\
-2.0 & -13.3 & -9.2 & 24.2 & 2.3 & -46.6 & -31.4 & 100 & & & & & & & & \\
12.7 & 38.6 & 25.8 & 19.3 & 33.6 & -9.6 & -10.5 & -1.1 & 100 & & & & & & & \\
9.1 & 8.4 & 9.1 & 13.2 & 3.3 & 24.8 & 3.7 & -18.9 & 19.7 & 100 & & & & & & \\
15.1 & 19.6 & -17.5 & -11.3 & -9.5 & -4.7 & 30.1 & -8.9 & -7.5 & 17 & 100 & & & & & \\
6.7 & 17.9 & -13.9 & -23.9 & 5.2 & -17.3 & -8.7 & 27.3 & 22.3 & -30.5 & 14.6 & 100 & & & & \\
-57.7 & -4.9 & 3.8 & -7.2 & -84 & 23.2 & 26.2 & 3.1 & -40 & -7.3 & 4.8 & -8.5 & 100 & & & \\
-9.6 & -31.1 & -7.0 & 13.9 & -7.7 & -56 & -8.7 & 43.5 & -6.1 & -44.4 & -6.5 & 15.3 & 16.5 & 100 & & \\
6.2 & -5.4 & -39.3 & 5.2 & 24.5 & 11.8 & -79.5 & 24.1 & 4.8 & -8.03 & -37.8 & 5.7 & -12 & 18.5 & 100 & \\
-12.8 & 12.3 & 5.5 & -34.2 & -13.9 & 45 & 23.1 & -70.7 & -9.1 & 17.4 & 5.6 & -38.7 & 22.5 & -40.3 & -15.6 & 100
\end{pmatrix}$$

Tab. 4.25: Statistical correlation coefficients for the vector of measurements (in order) ΔS_T^+, ΔS_T^-, ΔC_T^+, ΔC_T^-, ΔS_{CP}^+, ΔS_{CP}^-, ΔC_{CP}^+, ΔC_{CP}^-, ΔS_{CPT}^+, ΔS_{CPT}^-, ΔC_{CPT}^+, ΔC_{CPT}^-, S_{ℓ^+,K_S}^+, S_{ℓ^+,K_S}^-, C_{ℓ^+,K_S}^+, C_{ℓ^+,K_S}^- as obtained from the reference TV fit. Only lower off-diagonal terms are written, in %.

$$
\begin{pmatrix}
100 & & & & & & & & & & & & & & & \\
-26.9 & 100 & & & & & & & & & & & & & & \\
-28.6 & 31.6 & 100 & & & & & & & & & & & & & \\
-24.3 & 32.3 & -11.2 & 100 & & & & & & & & & & & & \\
42.5 & -28.6 & 28.2 & -64.7 & 100 & & & & & & & & & & & \\
-12.8 & 44.7 & 8.9 & 47.8 & -41.9 & 100 & & & & & & & & & & \\
-6.2 & 37.8 & 10.1 & 6.85 & -11.9 & 51.7 & 100 & & & & & & & & & \\
0.9 & 30.2 & 2.8 & 44.1 & -5.5 & 6.1 & 2.6 & 100 & & & & & & & & \\
-23.9 & 22.3 & 11.7 & 37.3 & -30.6 & 31.4 & -15.2 & 0.6 & 100 & & & & & & & \\
7.2 & 14.1 & 26.9 & -54 & 36 & -10 & 12.1 & -9.5 & -18.8 & 100 & & & & & & \\
-24.3 & 0.4 & 60.8 & -41.1 & 41.9 & -18.6 & 8.3 & -16.2 & -20.7 & 42.2 & 100 & & & & & \\
-34.7 & 41.9 & -13.8 & 82.7 & -74.4 & 34.5 & -1.78 & 39.8 & 43.2 & -39.5 & -44.5 & 100 & & & & \\
-46.8 & 35 & -28.6 & 67.4 & -84.5 & 41.9 & 17.4 & 10.7 & 22.4 & -35.9 & -36 & 74.4 & 100 & & & \\
-23.8 & -27 & -47.2 & 49.8 & -62.2 & 4.49 & -27.3 & -17.5 & 36 & -65.5 & -48.8 & 54 & 59.9 & 100 & & \\
-19.7 & 18.4 & -30.6 & 70.3 & -72.3 & 30.8 & -11.1 & 5.1 & 49.5 & -51.2 & -58.3 & 79.4 & 66.9 & 71.8 & 100 & \\
-8.8 & -46.6 & 12.6 & -6.2 & -1.4 & -9.9 & -25.4 & -49.3 & 20.9 & -22.9 & 13.3 & -15.5 & -6.5 & 34.8 & 17.4 & 100
\end{pmatrix}
$$

Tab. 4.26: Systematic correlation coefficients for the vector of measurements (in order) ΔS_T^+, ΔS_T^-, ΔC_T^+, ΔC_T^-, ΔS_{CP}^+, ΔS_{CP}^-, ΔC_{CP}^+, ΔC_{CP}^-, ΔS_{CPT}^+, ΔS_{CPT}^-, ΔC_{CPT}^+, ΔC_{CPT}^-, S_{ℓ^+,K_S}^+, S_{ℓ^+,K_S}^-, C_{ℓ^+,K_S}^+, C_{ℓ^+,K_S}^- as obtained from analysis of systematic uncertainties from Sec. 4.5. Only lower off-diagonal terms are written, in %.

A first approximation to estimate the significance of the results (i.e., significance of T non-invariance) is to build two-dimensional confidence-level (C.L.) contours in the $(\Delta S_T^+, \Delta C_T^+)$ and $(\Delta S_T^-, \Delta C_T^-)$ planes, since the T asymmetry shows up if $\Delta S_T^+ \neq 0$ or $\Delta C_T^+ \neq 0$, or if $\Delta S_T^- \neq 0$ or $\Delta C_T^- \neq 0$. These two-dimensional contours for the reference TV fit including statistical uncertainties only were already shown in Sec. 4.4.3, Figs 4.16 and 4.17. Nevertheless, these contours provide independent significance in the $(\Delta S_T^+, \Delta C_T^+)$ and $(\Delta S_T^-, \Delta C_T^-)$ planes, but not a combined significance of the symmetry breaking. To quote the global significance of symmetry breaking we evaluate the change in log-likelihood between the reference TV fit and a fit with the set of eight restrictions on the physics parameters implied by the symmetry, as it was given in Table 4.2,

$$s^2_{\mathrm{No}TV} \;=\; -2\left[\ln \mathcal{L}(\mathbf{p}_{\mathrm{No}TV}) - \ln \mathcal{L}(\mathbf{p}_0)\right] \;, \tag{4.29}$$

where $\mathcal{L}$ is the experimental likelihood function minimized over all parameters, $\mathbf{p}_0$ are the parameters found with the reference TV fit, and $\mathbf{p}_{\mathrm{No}TV}$ are the parameters that minimize the NoTV configuration of the fit. The values $s^2_{\mathrm{No}CPV}$ and $s^2_{\mathrm{No}CPTV}$ are found similarly.

We obtain (statistical only)

$$\begin{aligned} s^2_{\mathrm{No}TV} &= 363.8, \\ s^2_{\mathrm{No}CPV} &= 495.0, \\ s^2_{\mathrm{No}CPTV} &= 8.3, \end{aligned}$$

In the limit of large numbers the likelihood function takes a Gaussian shape, and

$$s^2_{\mathrm{No}TV} \;=\; \Delta\chi^2_{\mathrm{No}TV} \equiv \chi^2(\mathbf{p}_{\mathrm{No}TV}) - \chi^2(\mathbf{p}_0) \;, \tag{4.30}$$

with $\nu = 8$ degrees of freedom, analogously for $s^2_{\mathrm{No}CPV}$ and $s^2_{\mathrm{No}CPTV}$. The C.L. can then be obtained by computing the probability that the value $\Delta\chi^2_{\mathrm{No}TV}$ is exceeded for a χ^2-distribution with eight degrees of freedom,

$$1 - \mathrm{C.L.} = \mathrm{Prob}(\Delta\chi^2_{\mathrm{NoTV}}, \nu = 8) = \frac{1}{\sqrt{2^\nu}\Gamma(\nu/2)} \int_{\Delta\chi^2_{\mathrm{NoTV}}}^{\infty} \mathrm{e}^{-\mathrm{t}/2}\mathrm{t}^{\nu/2-1}\mathrm{dt} \;. \tag{4.31}$$

This integral is evaluated using Mathematica.

In a non-Gaussian situation, $\Delta\chi^2_{\mathrm{No}TV}$ has to be considered as a test statistic, and we have to rely on a Monte Carlo simulation to obtain its expected distribution in order to evaluate $Prob(\Delta\chi^2_{\mathrm{No}TV}, \nu = 8)$, i.e., the probability to cover the true values of the parameters, which in general would depend on the

parameters themselves. This Monte Carlo simulation can be built as follows. First, we generate a set of N parametrized Monte Carlo experiments (as done in Sec. 4.4.6) with truth values $\mathbf{p}_0$ as obtained from the reference TV fit to the data (Table 4.15). For each sample we then determine $s'^2_{\mathrm{NoTV}} \equiv \Delta\chi'^2_{\mathrm{NoTV}}$, as done in the actual data sample. Finally, $\alpha = 1 - \mathrm{C.L.}$ is then determined by counting the number of experiments for which $\Delta\chi'^2_{\mathrm{NoTV}} < \Delta\chi^2_{\mathrm{NoTV}}$, i.e., the fraction of experiments with better $\Delta\chi^2_{\mathrm{NoTV}}$ than the actual data sample.

Since the significance of the result is expected to be large (more than 10 standard deviations), the parametrized Monte Carlo technique would require an impractical number of experiments to reach the required numerical precision (and therefore a huge amount of CPU) for a rather minor relative correction to the significance as extracted using the Gaussian approximation. On the other hand, the likelihood function has a good Gaussian behavior, as it can be observed from the two-dimensional C.L. contours shown in Figs 4.16 and 4.17 and the parametrized Monte Carlo study reported in Sec. 4.4.6. We therefore use the Gaussian method to estimate the C.L. and the number of equivalent standard deviations.

Systematic uncertainties, evaluated for all the T-, CP-, and CPT-violating parameters (Sec. 4.5), have also to be included in the evaluation of the global significance of symmetry breaking, as well as in the construction of the projected C.L. contours in the $(\Delta S_T^+, \Delta C_T^+)$ and $(\Delta S_T^-, \Delta C_T^-)$ planes.

The uncertainty of each systematic effect is evaluated for the vector $\mathbf{q}$ of T-, CP- and CPT-violating parameters (16 in total),

$$\begin{aligned}\mathbf{q} \;=\; & (\Delta S_T^+, \Delta S_T^-, \Delta C_T^+, \Delta C_T^-, \\ & \Delta S_{CP}^+, \Delta S_{CP}^-, \Delta C_{CP}^+, \Delta C_{CP}^-, \\ & \Delta S_{CPT}^+, \Delta S_{CPT}^-, \Delta C_{CPT}^+, \Delta C_{CPT}^-, \\ & S_{\ell^+,K_S}^+, S_{\ell^+,K_S}^-, C_{\ell^+,K_S}^+, C_{\ell^+,K_S}^-),\end{aligned}$$

together with their cross-correlations. The covariance matrices for each of the considered systematic effects α are added to obtain the total systematic covariance matrix, $\mathcal{S} = \sum_\alpha \mathcal{S}^\alpha$, which diagonal terms $\sqrt{\mathcal{S}_{ii}}$ and correlations $\rho_{ij} = \mathcal{S}_{ij}/\sqrt{\mathcal{S}_{ii}\mathcal{S}_{jj}}$ are reported in Tables 4.24 and 4.26, respectively. We vary parameter q_j, $j = 1, ..., 16$ within one standard deviation $\sigma_j = \sqrt{\mathcal{S}_{jj}}$ about the reference value $q_{0,j}$, $q_{j\pm} = q_{0,j} \pm \sigma_j$. As illustrated in Fig. 4.25, the error ellipse is centered at $(q_{0,j}, q_{0,i})$, the tangents to the ellipse are given by the standard deviations of the estimators σ_j, σ_i, and $\rho_{ij}\sigma_i$ gives the distance at which the ellipse becomes tangent to the vertical, at the distance $\rho_{ij}\sigma_i$ below the center line [15]. We evaluate the change in log-likelihood

$$m_{j\pm}^2 \;=\; -2\left[\ln \mathcal{L}(\mathbf{q}_{j\pm}, \mathbf{o}_j) - \ln \mathcal{L}(\mathbf{p}_0)\right] / s_{\mathrm{stat},j}^2, \qquad (4.32)$$

where $\mathcal{L}(\mathbf{q}_{j\pm}, \mathbf{o}_j)$ is the standard likelihood function with the parameter $\mathbf{q}_{j\pm}$ fixed to the $\pm\sigma_j$ variation and minimized over all the other parameters $\mathbf{o}$ (the rest of signal and background parameters). Here the $s^2_{\text{stat},j}$ is

$$s^2_{\text{stat},j} = \; -2\left[\ln \mathcal{L}(\mathbf{q}_{\text{stat},j}, \mathbf{o}_{\text{stat},j}) - \ln \mathcal{L}(\mathbf{p}_0)\right], \tag{4.33}$$

i.e., the change in log-likelihood with parameters $\mathbf{q}_{\text{stat},j}$ fixed to the 1σ statistical variation of parameter q_j minimized over all the other parameters $\mathbf{o}$. By construction should be approximately 1^2, corresponding to 68% C.L. in one dimension. Therefore, m^2_j represents the 1σ systematic C.L. relative to the statistical C.L., for $\nu = 1$. To include the systematic uncertainties in the evaluation of the combined significance we conservatively scale (divide) $s^2_{\text{No}TV}$, $s^2_{\text{No}CPV}$, and $s^2_{\text{No}CPTV}$ by $1 + \max\{m^2_j\}$. Figure 4.26 shows the distribution of all m^2_j values (32 in total, corresponding to the 16 parameters with the up and down variations), and Table 4.27 reports the association of each value to the corresponding asymmetry parameter and systematic variation up and down. The mean value of the distribution is 0.30, while the maximum value is 0.613, therefore $1 + \max\{m^2_j\} = 1.613$. As a cross-check of the procedure to include systematic uncertainties in the significance of the results, Fig. 4.26 also shows the distribution of all $s^2_{\text{stat},j}$ values. As expected this distribution is strongly peaked around one, with mean value 0.92 and a maximum value of 1.04. To improve numerical precision in the evaluation of $s^2_{\text{stat},j}$ and m^2_j we set the machine accuracy in MINUIT (EPS parameter) to 10^{-14}. Finally, we obtain including statistical and systematic uncertainties

$$\begin{aligned} s^2_{\text{No}TV} &= 225.6\,, \\ s^2_{\text{No}CPV} &= 306.9\,, \\ s^2_{\text{No}CPTV} &= 5.2\,, \end{aligned}$$

with $\nu = 8$ degrees of freedom.

The results are inconsistent with the T invariance hypothesis with $1 -$ C.L. $= 2.55 \times 10^{-44}$, including systematic uncertainties, which corresponds to a significance of T non-invariance, independent of any CP violation and CPT symmetry, equivalent to 14σ. Similarly, the results are inconsistent with the CP invariance hypothesis at $1 -$ C.L. $= 1.37 \times 10^{-61}$, which corresponds to a significance of CP violation, independent of any T reversal violation and CPT symmetry, equivalent to 17σ. The results are consistent CPT invariance hypothesis with $1 -$ C.L. $= 0.74$, equivalent to 0.3σ.

To include systematic uncertainties in the two-dimensional C.L. contours we also scale (divide) the likelihood levels by $1 + \max\{m^2_j\} = 1.613$. Figure 4.27 shows the two-dimensional C.L. contours (up to eight standard deviations) in the $(\Delta S^{\pm}_T, \Delta C^{\pm}_T)$ planes, including systematic uncertainties. It can be observed that looking at the two-dimensional projections

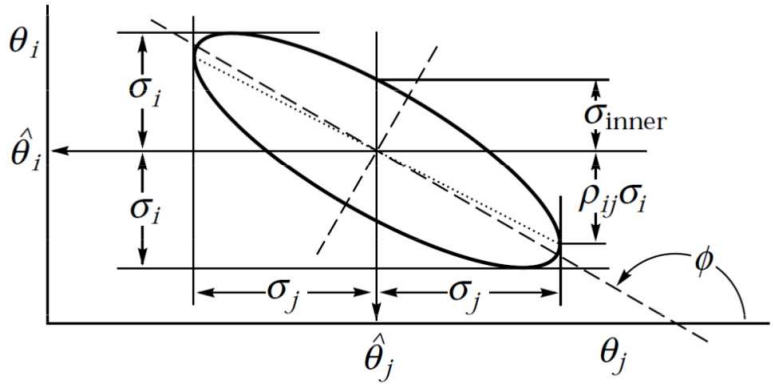

Fig. 4.25: The standard error ellipse for the parameters $\theta_j \equiv q_j$ and $\theta_i \equiv q_i$, centered at $\hat{\theta}_j \equiv q_{0,j}$, $\hat{\theta}_i \equiv q_{0,i}$, with standard deviations σ_j, σ_i, and correlation ρ_{ij} (in this example negative) [15].

$(\Delta S_T^+, \Delta C_T^+)$ and $(\Delta S_T^-, \Delta C_T^-)$ our best-fit results are inconsistent with the T-symmetry hypothesis at six standard deviations. Similar C.L. contours for the CP- and CPT-violating parameters, in the planes $(\Delta S_{CP}^{\pm}, \Delta C_{CP}^{\pm})$ and $(\Delta S_{CPT}^{\pm}, \Delta C_{CPT}^{\pm})$, respectively, are shown in Fig. 4.28. The significance of CP violation is larger than for T non-invariance, as it involves comparisons of B^0- and $\overline{B}^0$- flavor-identified subsamples, for a given Δt sign and $c\overline{c}K_S$ or $c\overline{c}K_L$ sample.

We also calculate the significance of the cross-check with the most recent CP violation analysis. For the value of s_{CP}^2, we compare our nominal TV fit with the fit described in Sec. 4.4.4, which implies fitting only one pair of S and C parameters for all the samples as in the last CPV analysis.

$$s_{CP}^2 \;=\; 10.52 \;,$$

for $\nu = 14$ degrees of freedom, including statistical and systematic uncertainties. Our analysis is compatible with our last CP violation analysis at $1 - \text{C.L.} = 0.72$, which corresponds to a significance of 0.4σ.

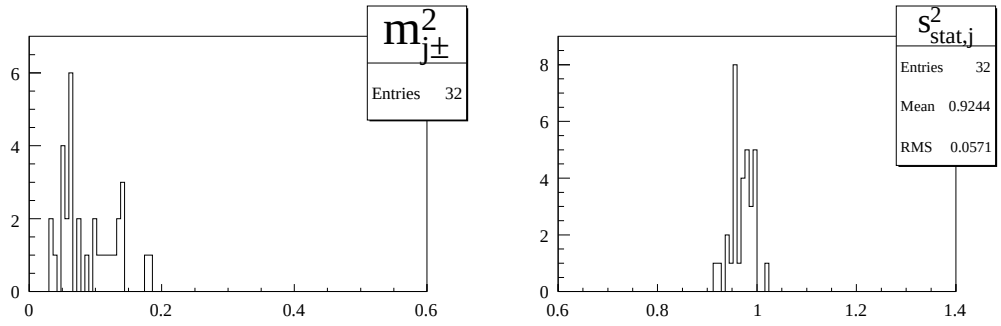

Fig. 4.26: Distributions of all $m^2_{j\pm}$ (left) and $s^2_{\mathrm{stat},j}$ (right) values (32 in total, corresponding to the 16 parameters with the up and down variations). The maximum $1 + m^2_j$ value is used to scale (divide) $s^2_{\mathrm{No}TV}$ to account for systematic uncertainties in the global significance for TV (and similarly for *CPV* and *CPTV*). The distribution of $s^2_{\mathrm{stat},j}$ is strongly peaked around one, as expected by construction of the statistical covariance matrix as reported by the reference TV fit.

Parameter name	$+\sigma_j$	$-\sigma_j$
ΔS_T^+	0.21	0.17
ΔS_T^-	0.40	0.35
ΔC_T^+	0.33	0.337
ΔC_T^-	0.30	0.25
ΔS_{CP}^+	0.40	0.37
ΔS_{CP}^-	0.25	0.22
ΔC_{CP}^+	0.12	0.11
ΔC_{CP}^-	0.17	0.14
ΔS_{CPT}^+	0.18	0.18
ΔS_{CPT}^-	0.19	0.21
ΔC_{CPT}^+	0.17	0.21
ΔC_{CPT}^-	0.44	0.46
$S^+_{\ell^+,K_S}$	0.44	0.43
$S^-_{\ell^+,K_S}$	0.48	0.46
$C^+_{\ell^+,K_S}$	0.61	0.59
$C^-_{\ell^+,K_S}$	0.21	0.20

Tab. 4.27: Values for all m^2_j (32 in total), corresponding to the 16 asymmetry parameters with the up and down systematic variations. The maximum value 0.613 is obtained for reference parameter $C^+_{\ell^+,K_S}$ and up variation.

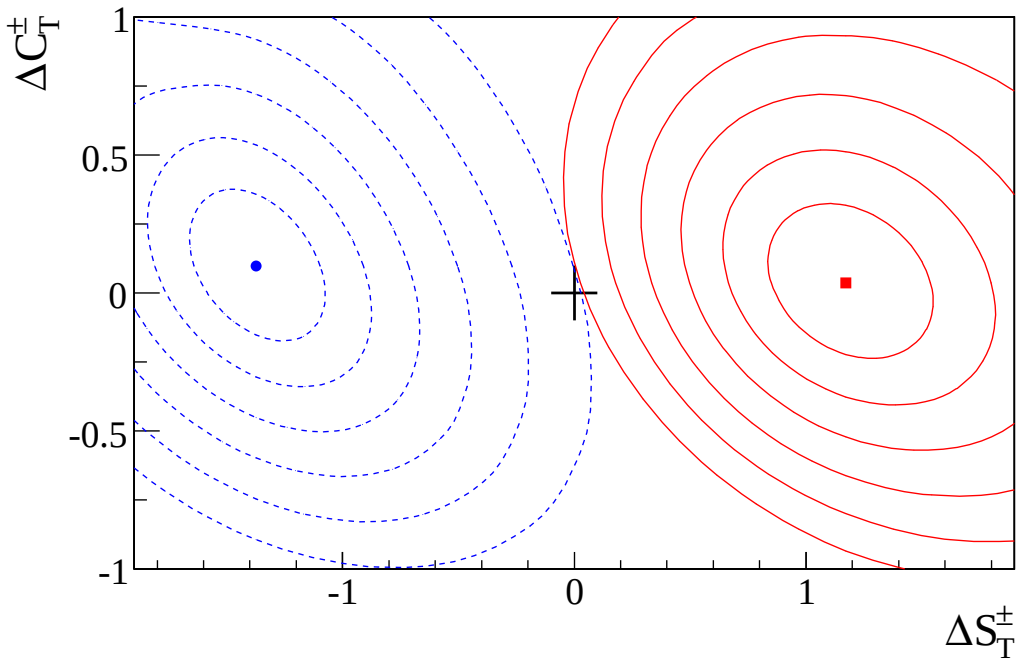

Fig. 4.27: Two-dimensional C.L. contours (up to six standard deviations) in the $(\Delta S_T^{\pm}, \Delta C_T^{\pm})$ planes, for the $c\overline{c}K^0$ data sample, including statistical and systematic uncertainties. The solid (red) and dashed (blue) contours are for the pairs of T-violating variables $(\Delta S_T^-, \Delta C_T^-)$ and $(\Delta S_T^+, \Delta C_T^+)$, respectively. These contours have been obtained using the standard likelihood ratio method, $-2\Delta ln\mathcal{L}_{\rm exp} = s^2$, with s^2 =2.30, 6.18, 11. 83, 19.33, 28.74, 40.09, 53.38, 68.70, for 1-, 2-, 3-, 4-, 5-, 6-, 7-, 8-standard deviations, respectively. Thus, the C.L. in 2 dimensions for each pair of variables is $1-$C.L. $= 0.317, 4.6\times10^{-2}, 2.7\times10^{-3}, 6.3\times10^{-5}, 5.7\times10^{-7}$ for 1-, 2-, 3-, 4-, 5-σ. The marker at (0,0) represents the no T violation point, while the other markers represent the best-fit results.

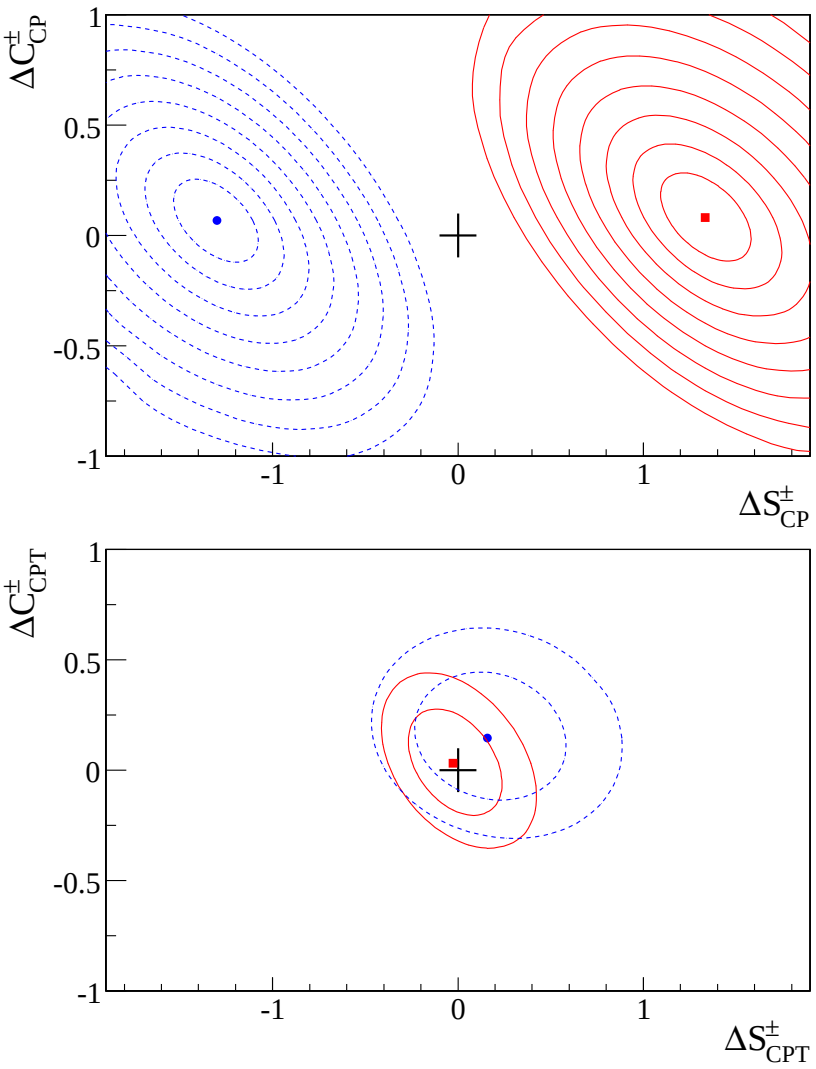

Fig. 4.28: Same as in Fig. 4.27, but for the *CP*-violating variables $(\Delta S_T^{\pm}, \Delta C_T^{\pm})$ (top) and the *CPT*-violating variables $(\Delta S_{CPT}^{\pm}, \Delta C_{CPT}^{\pm})$ (bottom). For the *CPT* case we only show the 1- and 2-σ regions. The markers at (0,0) represent the no *CP*- and no *CPT*-violating points, while the other markers represent the best-fit results.

5. DISCRETE SYMMETRIES STUDIES IN THE NEUTRAL K MESON SYSTEM

The neutral kaons are a fascinating physical system that, due to its peculiar and at the time paradoxical behavior in many respects, has lead to important discoveries, thereby triggering an enormous interest for its study. It has played a crucial role in the study of symmetries. In fact, it is the first physical system where CP violation has been observed in the $K^0 \to \pi\pi$ decay channel [12]. Relevant experimental studies continue up to date [20, 23, 66] and have been extended to entangled neutral kaon states in meson ϕ factories [67]. Moreover, neutral kaons have also been used as a probe of fundamental symmetries, such as CPT invariance [1], and deviations from the standard quantum mechanical behavior. The latter may be induced by quantum gravity fluctuations appearing as a "decoherening" environment, leading to an open system (Lindblad-type [68]) formulation [69, 70, 71, 72, 73, 74, 34].

In this Chapter, we describe a methodology, similarly as described in Ref. [2] for a B factory, to perform tests of CP, CPT and specially T in the neutral K meson system at a ϕ factory, overcoming the irreversibility problem related to T. This methodology makes use of Einstein-Podolski-Rosen (EPR) entanglement [29], and relies on the possibility of preparing the quantum mechanical individual state of the neutral K meson by the observation of particular decay channels of its orthogonal entangled partner, and studying the time evolution of the filtered state of the still living meson as illustrated in Fig. 2.1 for the B factories. We discuss the corresponding concepts needed for a direct T symmetry test in the physical context of the neutral K meson system at a ϕ factory [4]. In addition we evaluate the statistical significance of the test achievable with the KLOE-2 experiment at DAΦNE, the Frascati ϕ factory [67].

5.1 The kaon states

In order to formulate a possible T symmetry test with neutral kaons, it is necessary to precisely define the different states involved as we did in Sec. 2.2.

First, let us consider the physical states $|K_S\rangle$, $|K_L\rangle$, i.e. the states with definite masses $m_{S,L}$ and lifetimes $\tau_{S,L}$ which evolve as a function of the kaon proper time t as pure exponentials

$$\begin{aligned} |K_S(t)\rangle &= e^{-i\lambda_S t}|K_S\rangle \\ |K_L(t)\rangle &= e^{-i\lambda_L t}|K_L\rangle \ , \end{aligned} \tag{5.1}$$

with $\lambda_{S,L} = m_{S,L} - i\Gamma_{S,L}/2$, and $\Gamma_{S,L} = (\tau_{S,L})^{-1}$. They are usually expressed in terms of the flavor eigenstates $|K^0\rangle$, $|\overline{K}^0\rangle$ as:

$$\begin{aligned} |K_S\rangle &= \frac{1}{\sqrt{2\,(1+|\epsilon_S|^2)}}\left[(1+\epsilon_S)|K^0\rangle + (1-\epsilon_S)|\overline{K}^0\rangle\right] \ , \\ |K_L\rangle &= \frac{1}{\sqrt{2\,(1+|\epsilon_L|^2)}}\left[(1+\epsilon_L)|K^0\rangle - (1-\epsilon_L)|\overline{K}^0\rangle\right] \ , \end{aligned} \tag{5.2}$$

with ϵ_S and ϵ_L two small complex parameters describing the *CP* impurity in the physical states. One can equivalently define $\epsilon \equiv (\epsilon_S + \epsilon_L)/2$, and $\delta \equiv (\epsilon_S - \epsilon_L)/2$; adopting a suitable phase convention (e.g. the Wu-Yang phase convention [75]) $\epsilon \neq 0$ implies T violation, $\delta \neq 0$ implies *CPT* violation, while $\delta \neq 0$ or $\epsilon \neq 0$ implies *CP* violation, therefore the ϵ and δ parameters can easily be related to the constrains on the Hamiltonian matrix elements shown in Table 2.4.

Let us also consider the states $|K_+\rangle$, $|K_-\rangle$ defined as follows: $|K_+\rangle$ is the state filtered by the decay into $\pi\pi$ ($\pi^+\pi^+$ or $\pi^0\pi^0$), a pure *CP* even state; $|\widetilde{K}_-\rangle$ is the state orthogonal to $|K_+\rangle$, i.e. $\langle\widetilde{K}_-|K_+\rangle = 0$, which cannot decay into $\pi\pi$, $\langle\pi\pi|T|\widetilde{K}_-\rangle = 0$, and is defined as [76]:

$$|\widetilde{K}_-\rangle \equiv \widetilde{\mathrm{N}}_-\left[|K_L\rangle - \eta_{\pi\pi}|K_S\rangle\right] \ , \tag{5.3}$$

where

$$\eta_{\pi\pi} = \frac{\langle\pi\pi|T|K_L\rangle}{\langle\pi\pi|T|K_S\rangle} \ , \tag{5.4}$$

and

$$|\widetilde{\mathrm{N}}_-|^2 = \left[1 + |\eta_{\pi\pi}|^2 - 2\mathcal{R}\mathrm{e}\left(\eta_{\pi\pi}\langle \mathrm{K_L}|\mathrm{K_S}\rangle\right)\right]^{-1} \tag{5.5}$$

defines the normalization constant up to a phase factor. Therefore the state $|K_+\rangle$ can be explicitly written as the state orthogonal to $|\widetilde{K}_-\rangle$ as

$$|K_+\rangle = \mathrm{N}_+\left[|K_S\rangle + \alpha|K_L\rangle\right] \ , \tag{5.6}$$

where

$$\alpha = \frac{\eta^\star_{\pi\pi} - \langle K_L|K_S\rangle}{1 - \eta^\star_{\pi\pi}\langle K_S|K_L\rangle} \tag{5.7}$$

and

$$|\mathrm{N}_+|^2 = \left[1 + |\alpha|^2 + 2\mathcal{R}\mathrm{e}\left(\alpha\langle \mathrm{K_S}|\mathrm{K_L}\rangle\right)\right]^{-1} \ . \tag{5.8}$$

Analogously $|K_-\rangle$ is the state filtered by the decay into $3\pi^0$, a pure CP $= -1$ state; $|\widetilde{K}_+\rangle$ is the state orthogonal to $|K_-\rangle$, $\langle\widetilde{K}_+|K_-\rangle = 0$, which cannot decay into $3\pi^0$, $\langle\pi\pi|T|\widetilde{K}_-\rangle = 0$, and is defined by

$$|\widetilde{K}_+\rangle \equiv \widetilde{\mathrm{N}}_+ \left[|K_S\rangle - \left(\eta_{3\pi^0}^{-1}\right)|K_L\rangle\right] \ , \tag{5.9}$$

where

$$\left(\eta_{3\pi^0}^{-1}\right) = \frac{\langle 3\pi^0|T|K_S\rangle}{\langle 3\pi^0|T|K_L\rangle} \ , \tag{5.10}$$

and

$$|\widetilde{\mathrm{N}}_+|^2 = \left[1 + |\left(\eta_{3\pi^0}^{-1}\right)|^2 - 2\mathcal{R}\mathrm{e}\left(\left(\eta_{3\pi^0}^{-1}\right)^\star\langle \mathrm{K_L}|\mathrm{K_S}\rangle\right)\right]^{-1} \ . \tag{5.11}$$

Therefore the state $|K_-\rangle$ can be explicitly written as the state orthogonal to $|\widetilde{K}_+\rangle$ as

$$|K_-\rangle = \mathrm{N}_-\left[|K_L\rangle + \beta|K_S\rangle\right] \ , \tag{5.12}$$

where

$$\beta = \frac{\left(\eta_{3\pi^0}^{-1}\right)^\star - \langle K_S|K_L\rangle}{1 - \left(\eta_{3\pi^0}^{-1}\right)^\star\langle K_L|K_S\rangle} \tag{5.13}$$

and

$$|\mathrm{N}_-|^2 = \left[1 + |\beta|^2 + 2\mathcal{R}\mathrm{e}\left(\beta\langle \mathrm{K_L}|\mathrm{K_S}\rangle\right)\right]^{-1} \ . \tag{5.14}$$

Even though in the following we will assume that

$$\begin{aligned} |K_+\rangle &\equiv |\widetilde{K}_+\rangle \\ |K_-\rangle &\equiv |\widetilde{K}_-\rangle \ , \end{aligned} \tag{5.15}$$

here we have kept separate definitions of the states $|K_+\rangle$ and $|K_-\rangle$, which are observed through their decay, from the states $|\widetilde{K}_+\rangle$ and $|\widetilde{K}_-\rangle$, which are produced exploiting the EPR correlations in entangled kaon pairs, as we will see in the next Sec. 5.2.

The assumption given by Eq. (5.15) corresponds to impose the condition of orthogonality $\langle K_-|K_+\rangle = 0$ or $\langle\widetilde{K}_-|\widetilde{K}_+\rangle = 0$. This implies that $\beta = -\eta_{\pi\pi}$ and $\alpha = -\left(\eta_{3\pi^0}^{-1}\right)$, which in turn imply a precise relationship between the two amplitude ratios $\eta_{\pi\pi}$ and $\left(\eta_{3\pi^0}^{-1}\right)$,

$$\begin{aligned} \eta_{\pi\pi} &= \frac{\langle K_S|K_L\rangle - \left(\eta_{3\pi^0}^{-1}\right)^\star}{1 - \left(\eta_{3\pi^0}^{-1}\right)^\star\langle K_L|K_S\rangle} \\ &\simeq \langle K_S|K_L\rangle - \left(\eta_{3\pi^0}^{-1}\right)^\star \ , \end{aligned} \tag{5.16}$$

or equivalently

$$\eta_{\pi\pi} + \left(\eta_{3\pi^0}^{-1}\right)^\star \simeq \langle K_S|K_L\rangle \simeq \epsilon_L + \epsilon_S^\star \ . \tag{5.17}$$

This equation clearly indicates that we have to neglect direct *CP* violation when imposing assumption Eq. (5.15). In fact, for instance, Eq. (5.17) cannot be simultaneously satisfied for $\pi^+\pi^+$ and $\pi^0\pi^0$ decays, being $(\eta_{\pi^+\pi^-} - \eta_{\pi^0\pi^0}) = 3\epsilon'$, with ϵ' the direct *CP* violation parameter [15]. The relevance of this assumption will be discussed in Sec. 5.4, where it will be shown that direct *CP* violation can be safely neglected for our purposes.

Finally we will assume the validity of the $\Delta S = \Delta Q$ rule, so that the two flavor orthogonal eigenstates $|K^0\rangle$ and $|\overline{K}^0\rangle$ are identified by the charge of the lepton in semileptonic decays, i.e., a $|K^0\rangle$ can decay into $\pi^-\ell^+\nu$ (ℓ^+) and not into $\pi^+\ell^-\bar{\nu}$ (ℓ^-), and viceversa for a $|\overline{K}^0\rangle$.

5.2 Observables for the T symmetry test

As we did for the B factories, we are aiming for a test of T violation completely independent of and unconnected to *CP* violation through the exchange of *in* and *out* states.

As shown in [30, 32], B and ϕ factories offer the unique opportunity to show evidence for T violation (and *CP* violation) independently from the other symmetries and to measure the corresponding effects. The EPR entanglement here plays a crucial role. Let us consider the neutral kaon pair produced at a ϕ factory in a coherent quantum state with quantum numbers $J^{PC} = 1^{--}$ [77] [1]:

$$|i\rangle = \frac{1}{\sqrt{2}}\Big[|K^0(\vec{p})\rangle|\overline{K}^0(-\vec{p})\rangle - |\overline{K}^0(\vec{p})\rangle|K^0(-\vec{p})\rangle\Big] \tag{5.18}$$

$$= \frac{1}{\sqrt{2}}\Big[|K_+(\vec{p})\rangle|K_-(-\vec{p})\rangle - |K_-(\vec{p})\rangle|K_+(-\vec{p})\rangle\Big] \ . \tag{5.19}$$

It is worth noting that one can rewrite the two particle state $|i\rangle$ in terms of any pair of orthogonal states of individual neutral K mesons, e.g., K^0 and $\overline{K}^0$, or K_+ and K_- defined in Sec. 5.1. The time evolution of the initial state is simply given by $|i(t)\rangle = e^{-i(\lambda_S+\lambda_L)t}|i\rangle$, with t common proper time of the

[1] Implicitly we have assumed *CPT* at a microscopic level here as we have done for the B mesons case. According to Wald's theorem [33], if *CPT* is not a well-defined operator, due to quantum gravity, extra contamination from terms involving K^0K^0 or $\overline{K}^0\overline{K}^0$ pairs will appear in Eq. (2.1) proportional to ω [34]. We do not include this effect, or any further correction to EPR, as the data collected by the ϕ-factories and other K experiments are not sensitive [78].

two kaons; the initial EPR correlation given by $|i\rangle$ remains unaltered until one of the two kaons decays. One has also to emphasize, following what quantum mechanics dictates, that the individual state of one neutral meson in the entangled state is not defined before the decay process of its partner occurs, imposing a tag over the undecayed kaon. Thus it is possible to have a "flavor-tag", i.e. to infer the flavor (K^0 or $\overline{K}^0$) of the still alive meson by observing the specific flavor decay ($\pi^+\ell^-\bar{\nu}$ or $\pi^-\ell^+\nu$) of the other (and first decaying) meson. Similarly we may define a "CP-tag" [36] as the filter imposed by the decay of one of the entangled states to a K_+ or K_-, preparing its partner, which has not decayed yet, into the orthogonal state K_- or K_+, respectively. In this way we may proceed to a partition of the complete set of events into four categories, defined by the tag in the first decay as K_+, K_-, K^0 or $\overline{K}^0$.

Let us first consider $K^0 \to K_+$ as the reference process, by the observation of a $\pi^+\ell^-\bar{\nu}$ (ℓ^-) decay at a proper time t_1 of the opposite $\overline{K}^0$ meson[2] and a $\pi\pi$ decay at a later time $t_2 > t_1$, denoted as (ℓ^-,$\pi\pi$), and consider:

1. Its T transformed $K_+ \to K^0$ ($3\pi^0, \ell^+$), so that the asymmetry between $K^0 \to K_+$ and $K_+ \to K^0$, as a function of $\Delta t = t_2 - t_1$, is genuinely T violating.

2. Its CP transformed $\overline{K}^0 \to K_+$ (ℓ^+,$\pi\pi$), so that the asymmetry between $K^0 \to K_+$ and $\overline{K}^0 \to K_+$, as a function of $\Delta t = t_2 - t_1$, is genuinely CP violating.

3. Its CPT transformed $K_+ \to \overline{K}^0$ ($3\pi^0, \ell^-$), so that the asymmetry between $K^0 \to K_+$and $K_+ \to \overline{K}^0$, as a function of $\Delta t = t_2 - t_1$, is genuinely CPT violating.

One may check that the events used for the asymmetries 1, 2, and 3 are completely independent.

There are other three independent comparisons between T-conjugated processes, as summarized in Table 5.1. Analogously, we can apply the same methodology for similar tests of CP violation and CPT invariance. Tables 5.2 and 5.3 summarize all the possible comparisons of CP- and CPT-conjugated transitions with their corresponding decay products.

Our main goal is to demonstrate and measure the violation of time reversal invariance. Therefore we have to consider the following ratios [4] between

[2] To relax the notation we will denote $\pi^+\ell^-\bar{\nu}$ as ℓ^- and $\pi^-\ell^+\nu$ as ℓ^+.

Reference		T-conjugate	
Transition	Decay products	Transition	Decay products
$K^0 \to K_+$	$(\ell^-, \pi\pi)$	$K_+ \to K^0$	$(3\pi^0, \ell^+)$
$K^0 \to K_-$	$(\ell^-, 3\pi^0)$	$K_- \to K^0$	$(\pi\pi, \ell^+)$
$\overline{K}^0 \to K_+$	$(\ell^+, \pi\pi)$	$K_+ \to \overline{K}^0$	$(3\pi^0, \ell^-)$
$\overline{K}^0 \to K_-$	$(\ell^+, 3\pi^0)$	$K_- \to \overline{K}^0$	$(\pi\pi, \ell^-)$

Tab. 5.1: Possible comparisons between T-conjugated transitions and the associated time-ordered decay products in the experimental ϕ-factory scheme.

Reference		CP-conjugate	
Transition	Decay products	Transition	Decay products
$K^0 \to K_+$	$(\ell^-, \pi\pi)$	$\overline{K}^0 \to K_+$	$(\ell^+, \pi\pi)$
$K^0 \to K_-$	$(\ell^-, 3\pi^0)$	$\overline{K}^0 \to K_-$	$(\ell^+, 3\pi^0)$
$\overline{K}^0 \to K_+$	$(\ell^+, \pi\pi)$	$K^0 \to K_+$	$(\ell^-, \pi\pi)$
$\overline{K}^0 \to K_-$	$(\ell^+, 3\pi^0)$	$K^0 \to K_-$	$(\ell^-, 3\pi^0)$

Tab. 5.2: Possible comparisons between CP-conjugated transitions and the associated time-ordered decay products in the experimental ϕ-factory scheme.

transition probabilities:

$$\begin{aligned} R_1(\Delta t) &= P\left[K^0(0) \to K_+(\Delta t)\right] / P\left[K_+(0) \to K^0(\Delta t)\right] \ , \\ R_2(\Delta t) &= P\left[K^0(0) \to K_-(\Delta t)\right] / P\left[K_-(0) \to K^0(\Delta t)\right] \ , \\ R_3(\Delta t) &= P\left[\overline{K}^0(0) \to K_+(\Delta t)\right] / P\left[K_+(0) \to \overline{K}^0(\Delta t)\right] \ , \\ R_4(\Delta t) &= P\left[\overline{K}^0(0) \to K_-(\Delta t)\right] / P\left[K_-(0) \to \overline{K}^0(\Delta t)\right] \ . \end{aligned} \tag{5.20}$$

The measurement of any deviation from the prediction

$$R_1(\Delta t) = R_2(\Delta t) = R_3(\Delta t) = R_4(\Delta t) = 1 \ , \tag{5.21}$$

imposed by T invariance, is a signal of T violation. We can build analogous ratios for CP and CPT based on Tables 5.2 and 5.3 respectively, but as T has special interest, for the rest of the Chapter we will only focus on T.

If we express two generic orthogonal basis $\{K_X, \bar{K}_X\}$ and $\{K_Y, \bar{K}_Y\}$,

Reference		*CPT*-conjugate	
Transition	Decay products	Transition	Decay products
$K^0 \to K_+$	$(\ell^-, \pi\pi)$	$K_+ \to \overline{K}^0$	$(3\pi^0, \ell^-)$
$K^0 \to K_-$	$(\ell^-, 3\pi^0)$	$K_- \to \overline{K}^0$	$(\pi\pi, \ell^-)$
$\overline{K}^0 \to K_+$	$(\ell^+, \pi\pi)$	$K_+ \to K^0$	$(3\pi^0, \ell^+)$
$\overline{K}^0 \to K_-$	$(\ell^+, 3\pi^0)$	$K_- \to K^0$	$(\pi\pi, \ell^+)$

Tab. 5.3: Possible comparisons between *CPT*-conjugated transitions and the associated time-ordered decay products in the experimental ϕ-factory scheme.

which in our case correspond to $\{K^0, \overline{K}^0\}$ or $\{K_+, K_-\}$, as follows:

$$\begin{aligned} |K_X\rangle &= X_S|K_S\rangle + X_L|K_L\rangle \ , \\ |\bar{K}_X\rangle &= \bar{X}_S|K_S\rangle + \bar{X}_L|K_L\rangle \ , \end{aligned} \tag{5.22}$$

$$\begin{aligned} |K_Y\rangle &= Y_S|K_S\rangle + Y_L|K_L\rangle \ , \\ |\bar{K}_Y\rangle &= \bar{Y}_S|K_S\rangle + \bar{Y}_L|K_L\rangle \ . \end{aligned} \tag{5.23}$$

The inverse relations:

$$\begin{aligned} |K_S\rangle &= \frac{\bar{X}_L}{\det X}|K_X\rangle - \frac{X_L}{\det X}|\bar{K}_X\rangle \ , \\ |K_L\rangle &= -\frac{\bar{X}_S}{\det X}|K_X\rangle + \frac{X_S}{\det X}|\bar{K}_X\rangle \ , \end{aligned} \tag{5.24}$$

$$\begin{aligned} |K_S\rangle &= \frac{\bar{Y}_L}{\det Y}|K_Y\rangle - \frac{Y_L}{\det Y}|\bar{K}_Y\rangle \ , \\ |K_L\rangle &= -\frac{\bar{Y}_S}{\det Y}|K_Y\rangle + \frac{Y_S}{\det Y}|\bar{K}_Y\rangle \ , \end{aligned} \tag{5.25}$$

with

$$\begin{aligned} \det X &= X_S\bar{X}_L - X_L\bar{X}_S \ , \\ \det Y &= Y_S\bar{Y}_L - Y_L\bar{Y}_S \ . \end{aligned} \tag{5.26}$$

The generic quantum mechanical expression for the probabilities entering

in Eq. (5.20) is given by

$$\begin{aligned} P\left[K_X(0)\to K_Y(\Delta t)\right] &= \left|\langle K_Y|K_X(\Delta t)\rangle\right|^2 \\ &= \frac{1}{|\det Y|^2}\left|e^{-i\lambda_S\Delta t}X_S\bar{Y}_L - e^{-i\lambda_L\Delta t}X_L\bar{Y}_S\right|^2 \\ &= \frac{1}{|\det Y|^2}\{e^{-\Gamma_S\Delta t}|X_S\bar{Y}_L|^2 + e^{-\Gamma_L\Delta t}|X_L\bar{Y}_S|^2 \\ &\quad -2e^{-\frac{(\Gamma_S+\Gamma_L)}{2}\Delta t}\mathcal{R}e\left(e^{i\Delta m\Delta t}X_S\bar{Y}_LX_L^\star\bar{Y}_S^\star\right)\}\ , \end{aligned} \tag{5.27}$$

where

$$|\det Y|^2 = |\det X|^2 = \frac{1}{1-|\langle K_S|K_L\rangle|^2}\ . \tag{5.28}$$

Its inverse $P\left[K_Y(0)\to K_X(\Delta t)\right]$ is obtained simply with the substitution $X\leftrightarrow Y$.

If we now make the identification

$$\begin{aligned} |K_X\rangle &= |K^0\rangle\ , \\ |\bar{K}_X\rangle &= |\overline{K}^0\rangle\ , \\ |K_Y\rangle &= |K_+\rangle\ , \\ |\bar{K}_Y\rangle &= |K_-\rangle\ . \end{aligned} \tag{5.29}$$

Then we have:

$$\begin{aligned} X_S &= \frac{\sqrt{1+|\epsilon_S|^2}(1-\epsilon_L)}{\sqrt{2}(1-\epsilon_S\epsilon_L)} \simeq \frac{1-\epsilon_L}{\sqrt{2}}\ , \\ X_L &= \frac{\sqrt{1+|\epsilon_L|^2}(1-\epsilon_S)}{\sqrt{2}(1-\epsilon_S\epsilon_L)} \simeq \frac{1-\epsilon_S}{\sqrt{2}}\ , \\ \bar{X}_S &= \frac{\sqrt{1+|\epsilon_S|^2}(1+\epsilon_L)}{\sqrt{2}(1-\epsilon_S\epsilon_L)} \simeq \frac{1+\epsilon_L}{\sqrt{2}}\ , \\ \bar{X}_L &= -\frac{\sqrt{1+|\epsilon_L|^2}(1+\epsilon_S)}{\sqrt{2}(1-\epsilon_S\epsilon_L)} \simeq -\frac{1+\epsilon_S}{\sqrt{2}}\ , \\ Y_S &= N_+ \simeq 1\ , \\ Y_L &= N_+\alpha \simeq -\epsilon_S\ , \\ \bar{Y}_S &= N_-\beta \simeq -\epsilon_L\ , \\ \bar{Y}_L &= N_- \simeq 1\ , \end{aligned} \tag{5.30}$$

where in the last equalities only terms at first order in $\epsilon_{S,L}$ are retained, and the approximations $\beta\simeq-\eta_{\pi\pi}\simeq-\epsilon_L$ and $\alpha\simeq-\left(\eta_{3\pi^0}^{-1}\right)\simeq-\epsilon_S$ are applied.

With these approximations we have:

$$
\begin{aligned}
R_1(t) &= \frac{P\left[K^0(0)\to K_+(t)\right]}{P\left[K_+(0)\to K^0(t)\right]} = \frac{|\det X|^2}{|\det Y|^2}\frac{\left|X_S\bar{Y}_L e^{-i\lambda_S t} - X_L\bar{Y}_S e^{-i\lambda_L t}\right|^2}{\left|Y_S\bar{X}_L e^{-i\lambda_S t} - Y_L\bar{X}_S e^{-i\lambda_L t}\right|^2} \\
&\simeq \frac{\left|(1-\epsilon_L)e^{-i\lambda_S t} + \epsilon_L e^{-i\lambda_L t}\right|^2}{\left|-(1+\epsilon_S)e^{-i\lambda_S t} + \epsilon_S e^{-i\lambda_L t}\right|^2} \\
&\simeq \frac{e^{-\Gamma_S t}(1-2\mathcal{R}e\epsilon_L) + 2|\epsilon_L|e^{-\frac{(\Gamma_S+\Gamma_L)}{2}t}\cos\left[\Delta m t - \phi(\epsilon_L)\right]}{e^{-\Gamma_S t}(1+2\mathcal{R}e\epsilon_S) - 2|\epsilon_S|e^{-\frac{(\Gamma_S+\Gamma_L)}{2}t}\cos\left[\Delta m t - \phi(\epsilon_S)\right]}\,, \quad (5.31)
\end{aligned}
$$

$$
\begin{aligned}
R_2(t) &= \frac{P\left[K^0(0)\to K_-(t)\right]}{P\left[K_-(0)\to K^0(t)\right]} = \frac{|\det X|^2}{|\det Y|^2}\frac{\left|X_S Y_L e^{-i\lambda_S t} - X_L Y_S e^{-i\lambda_L t}\right|^2}{\left|\bar{Y}_S\bar{X}_L e^{-i\lambda_S t} - \bar{Y}_L\bar{X}_S e^{-i\lambda_L t}\right|^2} \\
&\simeq \frac{\left|-\epsilon_S e^{-i\lambda_S t} - (1-\epsilon_S)e^{-i\lambda_L t}\right|^2}{\left|\epsilon_L e^{-i\lambda_S t} - (1+\epsilon_L)e^{-i\lambda_L t}\right|^2} \\
&\simeq \frac{e^{-\Gamma_L t}(1-2\mathcal{R}e\epsilon_S) + 2|\epsilon_S|e^{-\frac{(\Gamma_S+\Gamma_L)}{2}t}\cos\left[\Delta m t + \phi(\epsilon_S)\right]}{e^{-\Gamma_L t}(1+2\mathcal{R}e\epsilon_L) - 2|\epsilon_L|e^{-\frac{(\Gamma_S+\Gamma_L)}{2}t}\cos\left[\Delta m t + \phi(\epsilon_L)\right]}\,, \quad (5.32)
\end{aligned}
$$

$$
\begin{aligned}
R_3(t) &= \frac{P\left[\overline{K}^0(0)\to K_+(t)\right]}{P\left[K_+(0)\to \overline{K}^0(t)\right]} = \frac{|\det X|^2}{|\det Y|^2}\frac{\left|\bar{X}_S\bar{Y}_L e^{-i\lambda_S t} - \bar{X}_L\bar{Y}_S e^{-i\lambda_L t}\right|^2}{\left|Y_S X_L e^{-i\lambda_S t} - Y_L X_S e^{-i\lambda_L t}\right|^2} \\
&\simeq \frac{\left|(1+\epsilon_L)e^{-i\lambda_S t} - \epsilon_L e^{-i\lambda_L t}\right|^2}{\left|(1-\epsilon_S)e^{-i\lambda_S t} + \epsilon_S e^{-i\lambda_L t}\right|^2} \\
&\simeq \frac{e^{-\Gamma_S t}(1+2\mathcal{R}e\epsilon_L) - 2|\epsilon_L|e^{-\frac{(\Gamma_S+\Gamma_L)}{2}t}\cos\left[\Delta m t - \phi(\epsilon_L)\right]}{e^{-\Gamma_S t}(1-2\mathcal{R}e\epsilon_S) + 2|\epsilon_S|e^{-\frac{(\Gamma_S+\Gamma_L)}{2}t}\cos\left[\Delta m t - \phi(\epsilon_S)\right]}\,, \quad (5.33)
\end{aligned}
$$

$$
\begin{aligned}
R_4(t) &= \frac{P\left[\overline{K}^0(0)\to K_-(t)\right]}{P\left[K_-(0)\to \overline{K}^0(t)\right]} = \frac{|\det X|^2}{|\det Y|^2}\frac{\left|\bar{X}_S Y_L e^{-i\lambda_S t} - \bar{X}_L Y_S e^{-i\lambda_L t}\right|^2}{\left|\bar{Y}_S X_L e^{-i\lambda_S t} - \bar{Y}_L X_S e^{-i\lambda_L t}\right|^2} \\
&\simeq \frac{\left|-\epsilon_S e^{-i\lambda_S t} - [-(1+\epsilon_S)]e^{-i\lambda_L t}\right|^2}{\left|-\epsilon_L e^{-i\lambda_S t} - (1-\epsilon_L)e^{-i\lambda_L t}\right|^2} \\
&\simeq \frac{e^{-\Gamma_L t}(1+2\mathcal{R}e\epsilon_S) - 2|\epsilon_S|e^{-\frac{(\Gamma_S+\Gamma_L)}{2}t}\cos\left[\Delta m t + \phi(\epsilon_S)\right]}{e^{-\Gamma_L t}(1-2\mathcal{R}e\epsilon_L) + 2|\epsilon_L|e^{-\frac{(\Gamma_S+\Gamma_L)}{2}t}\cos\left[\Delta m t + \phi(\epsilon_L)\right]}\,. \quad (5.34)
\end{aligned}
$$

This demonstrates that the ratios R_i depend on Δt, as it is also shown in Fig. 5.1.

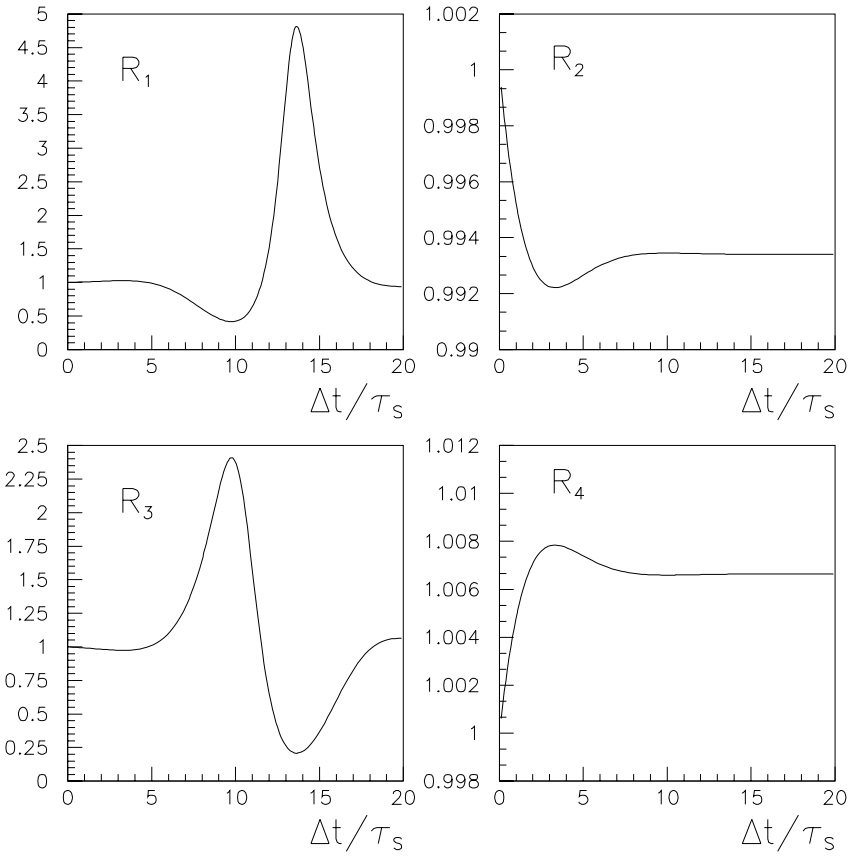

Fig. 5.1: The ratios R_i as a function of Δt; R_1 top left, R_2 top right, R_3 bottom left, and R_4 bottom right .

This result is in contrast with the Kabir T-violating asymmetry [22, 23], which is *independent of time*,

$$\begin{aligned}\frac{P\left[K^0(0)\to\overline{K}^0(\Delta t)\right]}{P\left[\overline{K}^0(0)\to K^0(\Delta t)\right]} &= \frac{\left|X_S X_L e^{-i\lambda_S\Delta t}-X_L X_S e^{-i\lambda_L\Delta t}\right|^2}{\left|\bar{X}_S\bar{X}_L e^{-i\lambda_S\Delta t}-\bar{X}_L\bar{X}_S e^{-i\lambda_L\Delta t}\right|^2}=\frac{\left|X_S X_L\right|^2}{\left|\bar{X}_S\bar{X}_L\right|^2}\\ &\simeq \frac{(1-4\mathcal{R}e\epsilon)}{(1+4\mathcal{R}e\epsilon)}\simeq 1-8\mathcal{R}e\epsilon\ . \end{aligned} \tag{5.35}$$

It is worth noting that for $\Delta t=0$ we have

$$R_1(0)=R_2(0)=R_3(0)=R_4(0)=1\ , \tag{5.36}$$

while for $\Delta t\gg\tau_S$:

$$R_2(\Delta t\gg\tau_S)\simeq\frac{1-2\mathcal{R}e\epsilon_S}{1+2\mathcal{R}e\epsilon_L}\simeq 1-4\mathcal{R}e\epsilon\ , \tag{5.37}$$

$$R_4(\Delta t\gg\tau_S)\simeq\frac{1+2\mathcal{R}e\epsilon_S}{1-2\mathcal{R}e\epsilon_L}\simeq 1+4\mathcal{R}e\epsilon\ . \tag{5.38}$$

5.3 Measurement of R_i at a ϕ factory

From the experimental point of view the observable quantity at a ϕ factory is the double differential decay rate of the state $|i\rangle$ into decay products f_1 and f_2 at proper times t_1 and t_2, respectively [77]. For the time evolution of the system it is convenient to rewrite the entangled state $|i\rangle$ as

$$|i\rangle=\frac{\mathcal{N}}{\sqrt{2}}\Big[|K_S\rangle|K_L\rangle-|K_L\rangle|K_S\rangle\Big]\ , \tag{5.39}$$

with $|\mathcal{N}|^2=|\det X|^2=[(1+|\epsilon_S|^2)(1+|\epsilon_L|^2)]/(1-\epsilon_S\epsilon_L)^2\simeq 1$ a normalization factor. The double differential decay rate is given by:

$$\begin{aligned}\Gamma(f_1,t_1;f_2,t_2)=C_{12}\{&|\eta_1|^2e^{-\Gamma_L t_1-\Gamma_S t_2}+|\eta_2|^2e^{-\Gamma_S t_1-\Gamma_L t_2}\\ -2|\eta_1||\eta_2|&e^{-\frac{(\Gamma_S+\Gamma_L)}{2}(t_1+t_2)}\cos[\Delta m(t_1-t_2)+\phi_2-\phi_1]\}\ , \end{aligned} \tag{5.40}$$

where

$$\begin{aligned}\eta_i &\equiv |\eta_i|e^{i\phi_i}=\frac{\langle f_i|T|K_L\rangle}{\langle f_i|T|K_S\rangle}\ ,\\ C_{12} &= \frac{|\mathcal{N}|^2}{2}|\langle f_1|T|K_S\rangle\langle f_2|T|K_S\rangle|^2\ . \end{aligned} \tag{5.41}$$

After integration on t_1 at fixed time difference $\Delta t = t_2 - t_1 > 0$, the decay intensity Eq. (5.40) can be rewritten in a more suitable form, putting in evidence the probabilities we are aiming for. In particular, it will be a function of the first decay product $f_1 = f_{\bar{X}}$ (which takes place at time t_1, identifies a $\bar{K}_X$ state, and tags a K_X state on the opposite side), the second decay products $f_2 = f_Y$ (which takes place at time t_2 and identifies a K_Y state):

$$\begin{aligned}\Gamma(f_{\bar{X}}, f_Y; \Delta t) &= \int_0^\infty I(f_{\bar{X}}, t_1; f_Y; t_2) dt_1 \\ &= \frac{1}{\Gamma_S + \Gamma_L} \left| \langle K_X \bar{K}_X | i \rangle \langle f_{\bar{X}} | T | \bar{K}_X \rangle \langle K_Y | K_X(\Delta t) \rangle \langle f_Y | T | K_Y \rangle \right|^2 \\ &= C(f_{\bar{X}}, f_Y) \times P\left[K_X(0) \to K_Y(\Delta t)\right] \ , \end{aligned} \tag{5.42}$$

where the coefficient $C(f_{\bar{X}}, f_Y)$, depending only on the final states $f_{\bar{X}}$ and f_Y, is given by:

$$\begin{aligned} C(f_{\bar{X}}, f_Y) &= \frac{1}{2(\Gamma_S + \Gamma_L)} \left| \langle f_{\bar{X}} | T | \bar{K}_X \rangle \langle f_Y | T | K_Y \rangle \right|^2 \\ &= \frac{\left| \langle f_{\bar{X}} | T | K_S \rangle \right|^2 \left| \langle f_Y | T | K_S \rangle \right|^2}{2(\Gamma_S + \Gamma_L)} \times \left| (\bar{X}_S + \eta_{\bar{X}} \bar{X}_L)(Y_S + \eta_Y Y_L) \right|^2 \ . \end{aligned} \tag{5.43}$$

The generic probability $P\left[K_X(0) \to K_Y(\Delta t)\right]$, containing the only time dependence, is the one given by Eq. (5.27).
From Eq. (5.43) and the condition:

$$\begin{aligned} \Gamma(f_{\bar{X}}, f_Y; \Delta t = 0) &= C(f_{\bar{X}}, f_Y) \times \left| \langle K_Y | K_X \rangle \right|^2 \\ &= C(f_Y, f_{\bar{X}}) \times \left| \langle \bar{K}_X | \bar{K}_Y \rangle \right|^2 \ , \end{aligned} \tag{5.44}$$

it can be easily shown that the coefficient $C(f_{\bar{X}}, f_Y)$ is invariant under interchange $f_Y \leftrightarrow f_{\bar{X}}$, i.e.,

$$C(f_{\bar{X}}, f_Y) = C(f_Y, f_{\bar{X}}) \ . \tag{5.45}$$

One can define the following observable ratios:

$$R_1^{\rm exp}(\Delta t) \equiv \frac{\Gamma(\ell^-, \pi\pi; \Delta t)}{\Gamma(3\pi^0, \ell^+; \Delta t)} = R_1(\Delta t) \times \frac{C(\ell^-, \pi\pi)}{C(3\pi^0, \ell^+)} \ , \tag{5.46}$$

$$R_2^{\rm exp}(\Delta t) \equiv \frac{\Gamma(\ell^-, 3\pi^0; \Delta t)}{\Gamma(\pi\pi, \ell^+; \Delta t)} = R_2(\Delta t) \times \frac{C(\ell^-, 3\pi^0)}{C(\pi\pi, \ell^+)} \ , \tag{5.47}$$

$$R_3^{\rm exp}(\Delta t) \equiv \frac{\Gamma(\ell^+,\pi\pi;\Delta t)}{\Gamma(3\pi^0,\ell^-;\Delta t)} = R_3(\Delta t) \times \frac{C(\ell^+,\pi\pi)}{C(3\pi^0,\ell^-)} \ , \tag{5.48}$$

$$R_4^{\rm exp}(\Delta t) \equiv \frac{\Gamma(\ell^+,3\pi^0;\Delta t)}{\Gamma(\pi\pi,\ell^-;\Delta t)} = R_4(\Delta t) \times \frac{C(\ell^+,3\pi^0)}{C(\pi\pi,\ell^-)} \ , \tag{5.49}$$

which are proportional to the corresponding $R_i(\Delta t)$ ratios.

It should be noted that when we perform a measurement with decay products in inverse time order (f_2, f_1) or $t_1 > t_2$, i.e. $\Delta t \to -\Delta t$, we are actually measuring the inverse of *another* ratio

$$\begin{aligned} R_2^{\rm exp}(-\Delta t) &= \frac{1}{R_3^{\rm exp}(\Delta t)} = \frac{1}{R_3(\Delta t)} \times \frac{C(3\pi^0,\ell^-)}{C(\ell^+,\pi\pi)} \ , \\ R_4^{\rm exp}(-\Delta t) &= \frac{1}{R_1^{\rm exp}(\Delta t)} = \frac{1}{R_1(\Delta t)} \times \frac{C(3\pi^0,\ell^+)}{C(\ell^-,\pi\pi)} \ . \end{aligned} \tag{5.50}$$

Due to the property (5.45), the proportionality constant between $R_{2(4)}^{\rm exp}(-\Delta t)$ and $1/R_{3(1)}(\Delta t)$ is the same as the one between $R_{2(4)}^{\rm exp}(\Delta t)$ and $R_{2(4)}(\Delta t)$. Therefore one can actually measure only two observables, $R_2^{\rm exp}(\Delta t)$ and $R_4^{\rm exp}(\Delta t)$, with $-\infty < \Delta t < +\infty$; their expected behavior is shown in Fig. 5.2.

From the point of view of a model independent and direct test of T symmetry, it would be sufficient to prove that one of the predictions in Eq. (5.21) is not satisfied, i.e., that $R_i(\Delta t) \neq 1$, for any ratio R_i. Experimentally one can adopt two different strategies to obtain this result:

1. The first one is to observe any significant dependence on Δt in the measured ratio $R_2^{\rm exp}(\Delta t)$ or $R_4^{\rm exp}(\Delta t)$; therefore one may conclude that the corresponding ratio R_i is not constant and cannot satisfy the prediction in Eq. (5.21).

2. The second strategy consists in measuring the ratio $R_2^{\rm exp}(\Delta t)$ or $R_4^{\rm exp}(\Delta t)$ in the limit $\Delta t \gg \tau_S$, where they are expected to have a constant value; given an independent evaluation of the corresponding ratio of coeffiecients $\frac{C(\ell^-,3\pi^0)}{C(\pi\pi,\ell^+)}$ or $\frac{C(\ell^+,3\pi^0)}{C(\pi\pi,\ell^-)}$ one may extract the asymptotic value $R_2(\Delta t \gg \tau_S)$ or $R_4(\Delta t \gg \tau_S)$ and verify the predicted deviation from one, Eq. (5.37) or Eq. (5.38).

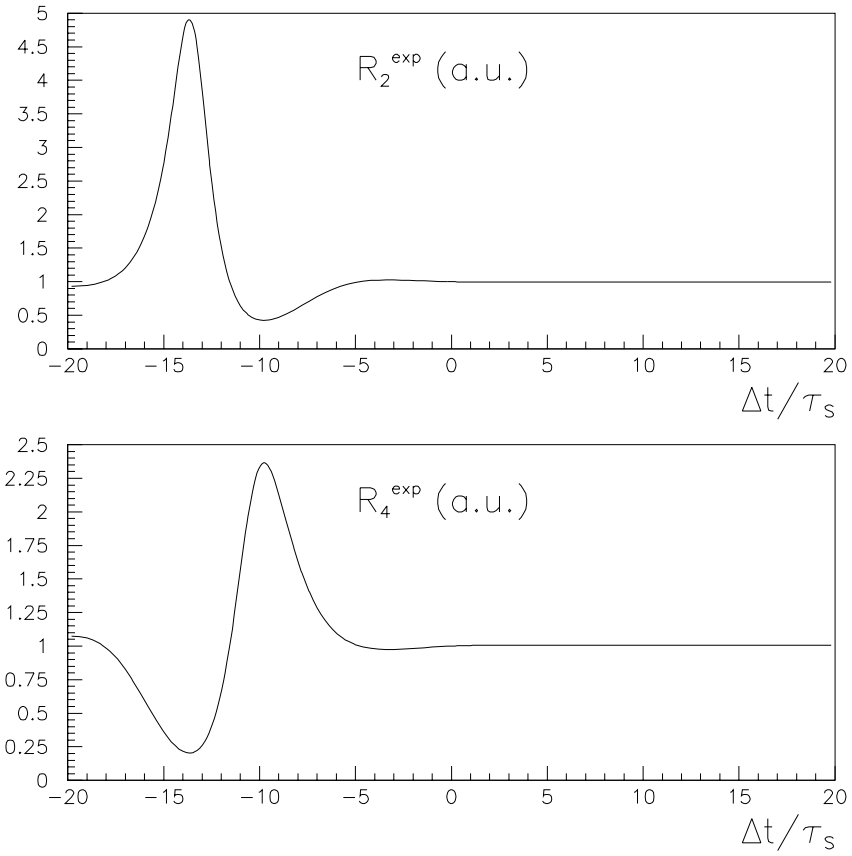

Fig. 5.2: The ratios $R_2^{\rm exp}$ and $R_4^{\rm exp}$ as a function of Δt.

For the second strategy we can consider that

$$\begin{aligned}\frac{C(\ell^-,3\pi^0)}{C(\pi\pi,\ell^+)} &= \left|\frac{\langle\ell^-|T|\overline{K}^0\rangle\langle 3\pi^0|T|K_-\rangle}{\langle\ell^+|T|K^0\rangle\langle\pi\pi|T|K_+\rangle}\right|^2 \\ &= \left|\frac{\langle 3\pi^0|T|K_-\rangle}{\langle\pi\pi|T|K_+\rangle}\right|^2 , \end{aligned} \tag{5.51}$$

$$\begin{aligned}\frac{C(\ell^+,3\pi^0)}{C(\pi\pi,\ell^-)} &= \left|\frac{\langle\ell^+|T|K^0\rangle\langle 3\pi^0|T|K_-\rangle}{\langle\ell^-|T|\overline{K}^0\rangle\langle\pi\pi|T|K_+\rangle}\right|^2 \\ &= \left|\frac{\langle 3\pi^0|T|K_-\rangle}{\langle\pi\pi|T|K_+\rangle}\right|^2 , \end{aligned} \tag{5.52}$$

neglecting possible *CPT* violation effects in semileptonic decays.

Neglecting second order terms, one has

$$\begin{aligned}\mathrm{BR}\,(K_S\to\pi\pi)\,\Gamma_S &= |\langle\pi\pi|T|K_S\rangle|^2 = \left|\frac{\langle\pi\pi|T|K_+\rangle}{\mathrm{N}_+(1-\alpha\beta)}\right|^2 \\ &\simeq |\langle\pi\pi|T|K_+\rangle|^2 , \end{aligned} \tag{5.53}$$

$$\begin{aligned}\mathrm{BR}\left(K_L\to 3\pi^0\right)\Gamma_L &= \left|\langle 3\pi^0|T|K_L\rangle\right|^2 = \left|\frac{\langle 3\pi^0|T|K_-\rangle}{\mathrm{N}_-(1-\alpha\beta)}\right|^2 \\ &\simeq \left|\langle 3\pi^0|T|K_-\rangle\right|^2 . \end{aligned} \tag{5.54}$$

Using the above relations, Eqs (5.53) and (5.54), one has

$$\frac{C(\ell^-,3\pi^0)}{C(\pi\pi,\ell^+)} \simeq \frac{C(\ell^+,3\pi^0)}{C(\pi\pi,\ell^-)} \simeq \frac{\mathrm{BR}\,(K_L\to 3\pi^0)}{\mathrm{BR}\,(K_S\to\pi\pi)}\frac{\Gamma_L}{\Gamma_S} . \tag{5.55}$$

Therefore in the case of the second strategy, one can evaluate the ratio of coefficients in terms of measurable branching ratios, and convert with the correct normalization the measured ratios $R_2^{\rm exp}$ and $R_4^{\rm exp}$ into the corresponding values for R_2 and R_4, making possible a direct comparison of these values with the prediction given by Eq. (5.21) obtained in the case of T symmetry invariance.

One can define the statistical sensitivity of an experiment

$$Q_i(\Delta t) \equiv \frac{|1-R_i(\Delta t)|}{\sigma\left(R_i(\Delta t)\right)} , \tag{5.56}$$

as the ratio between the expected deviation of R_i from prediction (5.21), as given by the measured value of ϵ, and the statistical uncertainty on R_i, in a bin width of 1 τ_S centered at the value Δt, as shown in Figs 5.3 and 5.4 [3] .

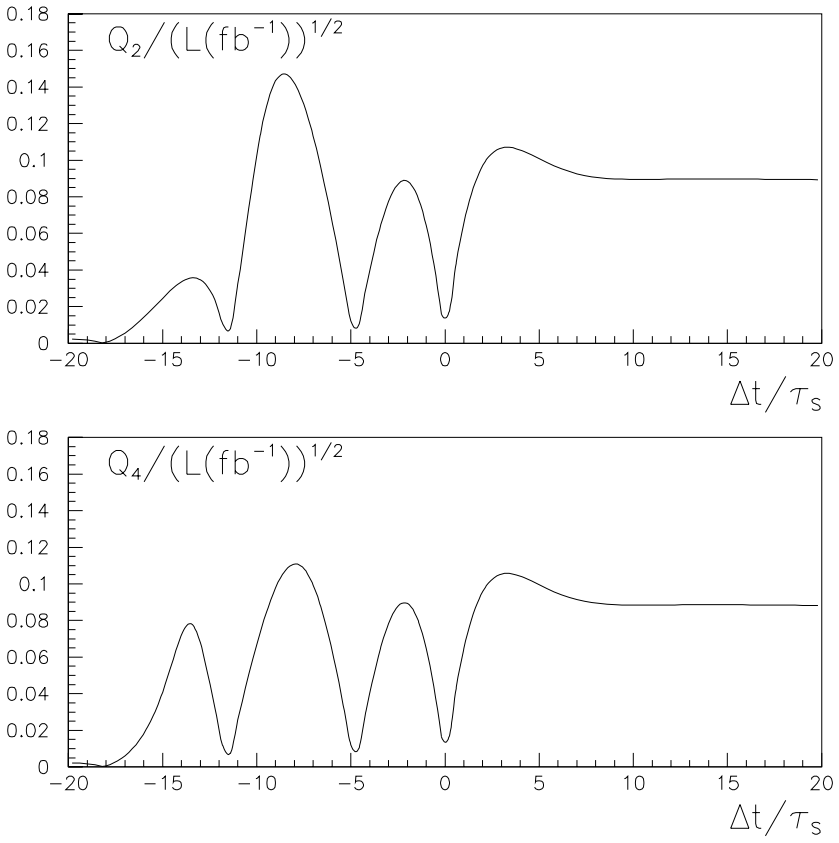

Fig. 5.3: The statistical sensitivity $Q_2(\Delta t)$ (top) and $Q_4(\Delta t)$ (bottom) as a function of Δt and normalized to the square root of the integrated luminosity $\sqrt{\mathcal{L}(\mathrm{fb}^{-1})}$.

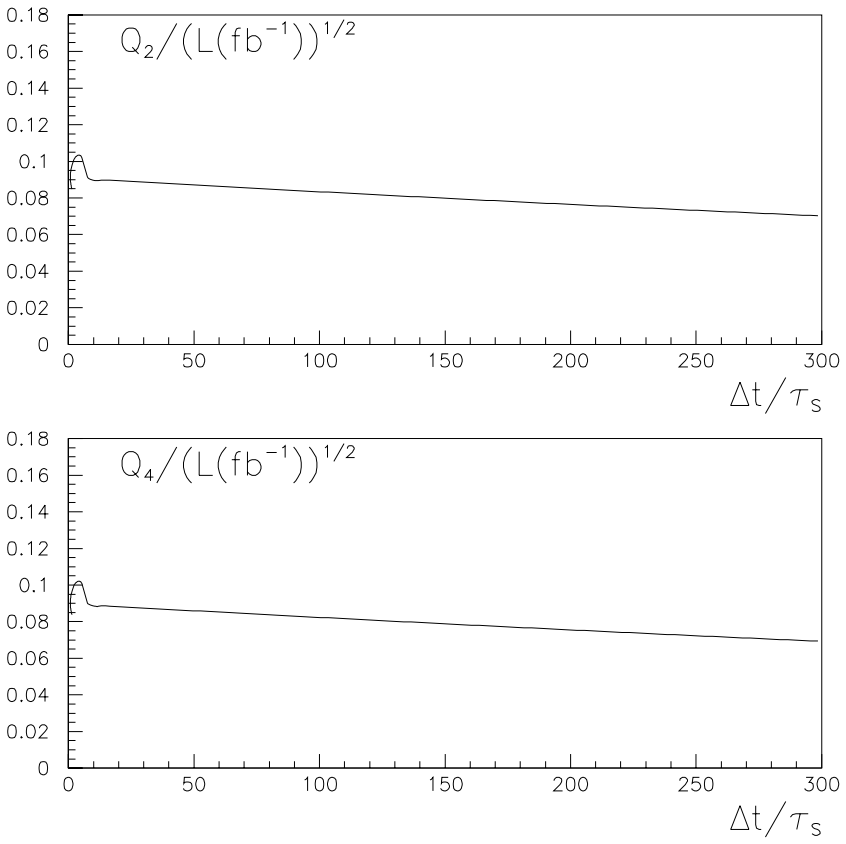

Fig. 5.4: Same as in Fig. 5.3 but in the range $0 < \Delta t < 300\ \tau_S$.

It is worth noting that the sensitivity of the test in the region $\Delta t < 0$ is limited by the large statistical uncertainties on R_i (due to a fast exponential decrease of the events in this region) despite the expected large deviations of R_i from unity. On the other hand, in the statistically most populated region at $\Delta t > 0$, the sensitivity is not large because small deviations of R_i from unity are expected here (see Eqs (5.37) and (5.38)).

In the case of the KLOE-2 experiment at DAΦNE, where an integrated luminosity $\mathcal{L}$ of $\mathcal{O}(10\ \text{fb}^{-1})$ is expected [67], the $\Gamma(f_1, f_2; \Delta t)$ distributions have been evaluated with a simple Monte Carlo simulation, making the approximation of a Gaussian Δt experimental resolution with $\sigma = 1\ \tau_S$, and a full detection efficiency, as shown in Fig. 5.5. It can be noticed that the $\Gamma(\ell^{\pm}, 3\pi^0; \Delta t)$ distributions have very few or no events for $\Delta t \lesssim -5\ \tau_S$. While a complete feasibility study is beyond the scope of the present paper, it appears that the first strategy described above is difficult to be implemented at KLOE-2 due to the lack of enough statistics, whereas the second strategy is much more viable. In fact, considering a large Δt interval in the statistically most populated region, $0 \leq \Delta t \leq 300\ \tau_S$, a much larger global sensitivity of $Q \simeq 4.4, 6.2$, and 8.8 is obtained for $\mathcal{L} = 5$, 10, and 20 fb^{-1}, respectively [4].

It has been shown that, by exploiting the EPR entanglement of neutral kaon pairs produced at a ϕ-factory, it is possible to perform a direct test of the time reversal symmetry in the neutral kaon system, independently from *CP* violation and *CPT* invariance constraints, and therefore overcoming some conceptual difficulties affecting previous tests. The proposed test [4] is highly model-independent, relying only on the validity of quantum mechanical prescriptions and EPR correlations. From the experimental point of view, the test would require to measure the ratios of intensities given by Eq. (5.40) with a suitable choice of decay products in definite time ordering. The absolute normalization of the measured ratios requires the knowledge of measurable kaon branching ratios and lifetimes and would not suffer from other uncertainties. The KLOE-2 experiment at the DAΦNE ϕ-factory could make a significant T symmetry test with an integrated luminosity of $\mathcal{O}(10\ \text{fb}^{-1})$.

5.4 Orthogonality constrains

The orthogonality assumption in Eq. (5.15) and the condition Eq. (5.17) constrain the $\eta_{\pi\pi}$ and $\left(\eta_{3\pi^0}^{-1}\right)$ parameters. Concerning the $\eta_{\pi\pi}$ parameter

[3] The plots in Figs 5.3 and 5.4 have been evaluated assuming a large number of events and Poisson fluctuations in each Δt bin of the measured $\Gamma(f_1, f_2; \Delta t)$ distributions, and negligible uncertainties due to the knowledge of the ratio of coefficients Eq. (5.55) (needed for the second strategy).

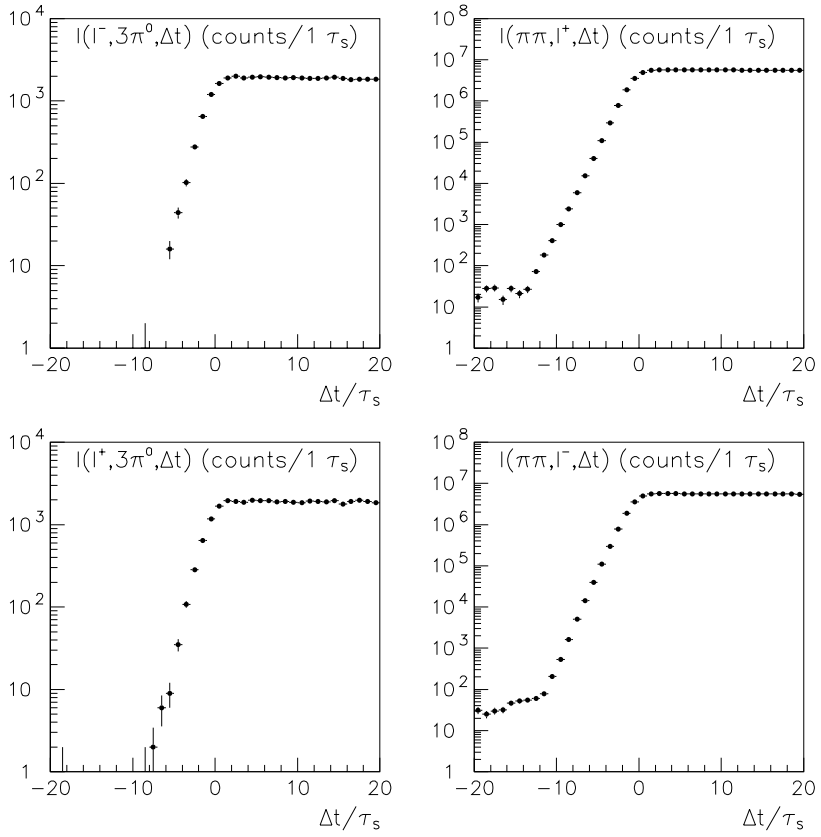

Fig. 5.5: The $\Gamma(\ell^-, 3\pi^0; \Delta t)$ (top left), $\Gamma(\pi\pi, \ell^+; \Delta t)$ (top right), $\Gamma(\ell^+, 3\pi^0; \Delta t)$ (bottom left), and $\Gamma(\pi\pi, \ell^-; \Delta t)$ (bottom right) distributions as a function of Δt evaluated with a simple Monte Carlo simulation, making the approximation of a Gaussian Δt experimental resolution with $\sigma = 1\ \tau_S$, a full detection efficiency, and assuming $\mathcal{L} = 10\ \text{fb}^{-1}$.

one could safely neglect any contribution from direct *CP* violation, because (ϵ'/ϵ) is experimentally known to be $\mathcal{O}(10^{-3})$ [15]. One can also safely neglect possible contributions from direct *CPT* violation in the $\pi\pi$ decay. Therefore for the purposes of the present test, one can assume $\eta_{\pi\pi} \simeq \epsilon_L$ (e.g. adopting the Wu-Yang phase convention).

Even though it would be reasonable to expect also for the $\left(\eta_{3\pi^0}^{-1}\right)$ parameter a negligible contribution from direct *CP* and *CPT* violations [79, 80], $\left(\eta_{3\pi^0}^{-1}\right) \simeq \epsilon_S$, unfortunately the experimental knowledge on this parameter is much less precise than for $\eta_{\pi\pi}$, resulting at present in an upper limit $\left(\eta_{3\pi^0}^{-1}\right) < 9 \times 10^{-3}$ at 90% C.L. [81]. However, assuming a contribution from direct *CP* violation much larger than in the case of $\pi\pi$, e.g., allowing for a $\pm 10\%$ variation in the absolute value of $\left(\eta_{3\pi^0}^{-1}\right)$, or a $\pm 10^\circ$ variation of its phase with respect to the expected value $\left(\eta_{3\pi^0}^{-1}\right) \simeq \epsilon_S \simeq \epsilon$, does not spoil the significance of the T symmetry test in the Δt region statistically relevant for the KLOE-2 experiment at DAΦNE, i.e. $\Delta t \gtrsim -5\tau_S$, as shown in Figs 5.6 and 5.7, where $|\langle 3\pi^0|T|K_L\rangle|^2$ has been kept fixed to its measured value [15] while varying $\left(\eta_{3\pi^0}^{-1}\right)$. Thus one can conclude that direct *CP* violation can be safely neglected.

Apart from these considerations, it is also possible to experimentally perform a direct test of the assumption in Eq. (5.15) by measuring the ratio of processes $K^0 \to K_+$ vs. $\widetilde{K}_+ \to \overline{K}^0$. In fact, taking into account the difference between the tagged state $\widetilde{K}_+$ and the decaying state K_+, using Eq. (5.27) one can easily evaluate the ratio

$$\frac{P[K^0(0) \to K_+(\Delta t)]}{P[\widetilde{K}_+(0) \to \overline{K}^0(\Delta t)]} \simeq \frac{\left| e^{-i\lambda_S \Delta t}\left(\frac{1-\epsilon_L}{\sqrt{2}}\right) + e^{-i\lambda_L \Delta t}(\eta_{\pi\pi})\left(\frac{1-\epsilon_S}{\sqrt{2}}\right)\right|^2}{\left| e^{-i\lambda_S \Delta t}\left(\frac{1-\epsilon_S}{\sqrt{2}}\right) + e^{-i\lambda_L \Delta t}(\eta_{3\pi^0}^{-1})\left(\frac{1-\epsilon_L}{\sqrt{2}}\right)\right|^2}, \tag{5.57}$$

which is constrained to be one if the condition $\eta_{\pi\pi} = (\eta_{3\pi^0}^{-1})$ holds, with the assumption of *CPT* invariance ($\epsilon_S = \epsilon_L = \epsilon$). Thus measuring this ratio with enough precision, one can evaluate whether the direct *CP* violation contribution to the $3\pi^0$ decay is negligible or not. Analogous considerations apply to other ratios like:

- $P[\overline{K}^0(0) \to K_+(\Delta t)]/P[\widetilde{K}_+(0) \to K^0(\Delta t)]$,
- $P[K^0(0) \to K_-(\Delta t)]/P[\widetilde{K}_-(0) \to \overline{K}^0(\Delta t)]$,
- $P[\overline{K}^0(0) \to K_-(\Delta t)]/P[\widetilde{K}_-(0) \to K^0(\Delta t)]$.

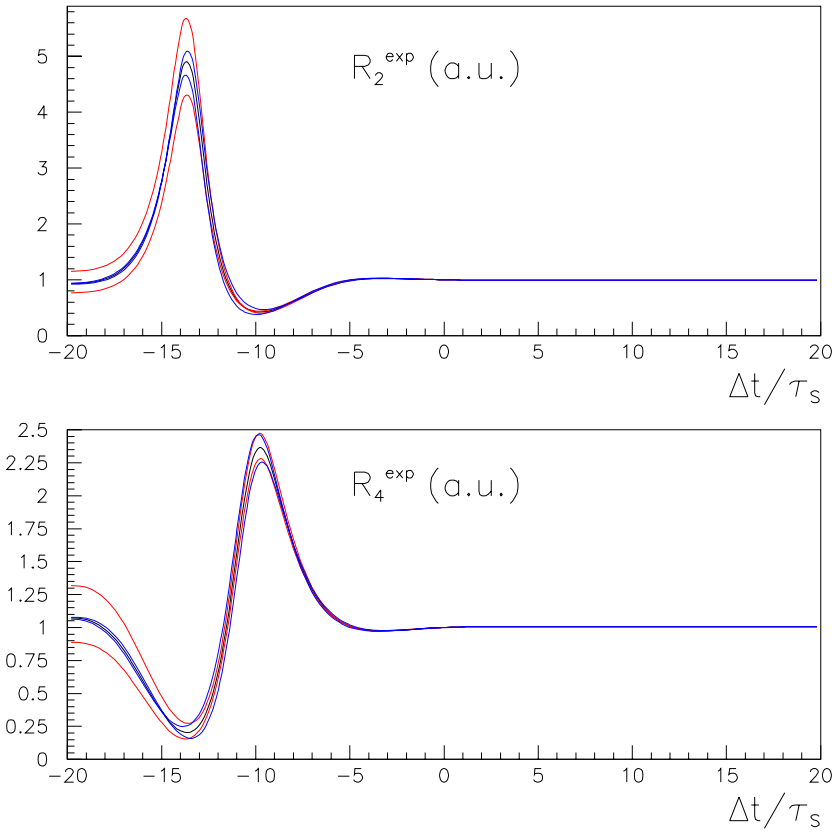

Fig. 5.6: The expected ratios $R_2^{\rm exp}(\Delta t)$ (top) and $R_4^{\rm exp}(\Delta t)$ (bottom) as a function of Δt (black line); red lines correspond to $\pm 10\%$ variation in the absolute value of $\left(\eta_{3\pi^0}^{-1}\right)$, while blue lines correspond to a $\pm 10^\circ$ variation of its phase (with respect to the expected value, i.e. $\left(\eta_{3\pi^0}^{-1}\right) \simeq \epsilon_S \simeq \epsilon$). The value of $\left|\langle 3\pi^0|T|K_L\rangle\right|^2$ has been kept fixed while varying $\left(\eta_{3\pi^0}^{-1}\right)$.

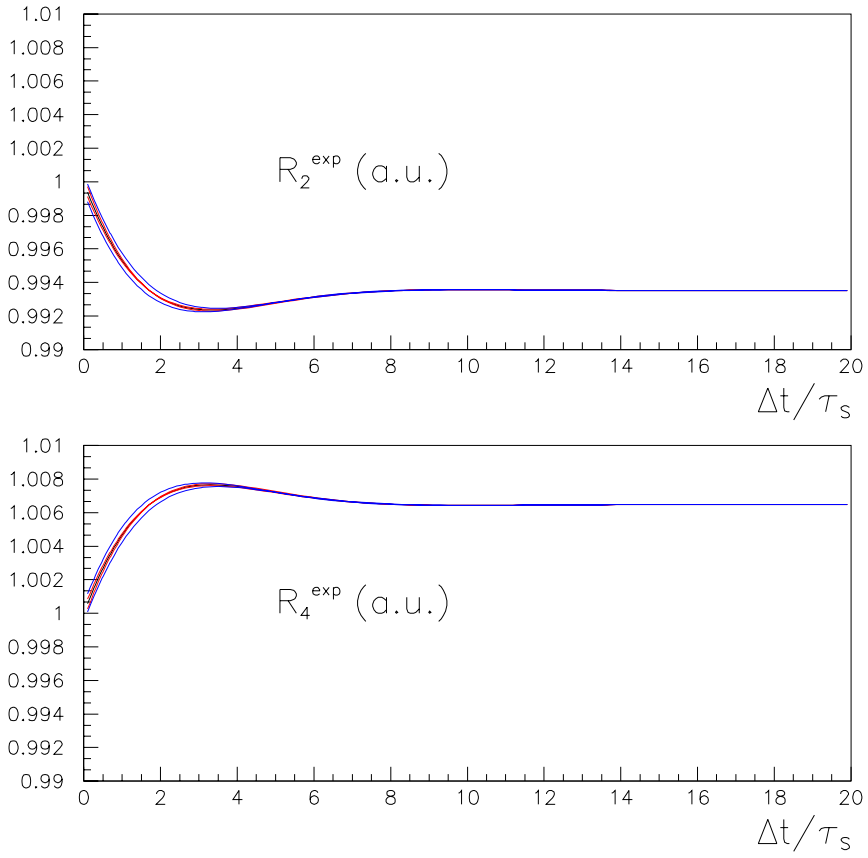

Fig. 5.7: A zoom of the plots shown in Fig. 5.6 in the region $0 \leq \Delta t \leq 20\tau_S$, which is statistically relevant for the KLOE-2 experiment at DAΦNE.

6. REPRESENTATION OF THE DECAYING NEUTRAL KAON AS AN OPEN SYSTEM

The neutral kaon is one of the most intriguing systems in Nature, it has both *CP* violation in the mass matrix and a non-vanishing lifetime difference in the width matrix. This leads to an effective Hamiltonian which is not a normal operator, with incompatible (non-commuting) masses and widths. In the Weisskopf-Wigner Approach (WWA) [39, 41], by diagonalizing the entire Hamiltonian, the unphysical non-orthogonal "stationary" states $K_{L,S}$ are obtained. These states have complex eigenvalues whose real (imaginary) part does not coincide with the eigenvalues of the mass (width) matrix. To avoid the usage of these states, we describe the system as an open Lindblad-type quantum mechanical system. This approach, in terms of density matrices for initial and final states, provides a consistent probabilistic description, avoiding the mentioned problems because the width matrix becomes a composite operator not included in the Hamiltonian. We consider the dominant-decay channel to two pions, so that one of the kaon states with definite lifetime becomes stable. As it is shown, this new approach [5] provides results for the time dependent decay rates in agreement with those provided by the WWA.

6.1 Subtleties of Weiskopff-Wigner approach for the K^0-$\overline{K}^0$ system

The standard description of the neutral-kaon system follows the Weisskopf-Wigner Approach for unstable particles using the non-Hermitian Hamiltonian

$$\mathcal{H} = \mathcal{M} - i\,\frac{\Gamma}{2}\ . \tag{6.1}$$

However, the simultaneous presence of *CP* violation in the mass matrix $\mathcal{M}$ and a difference of lifetimes in the antihermitian matrix $i\Gamma/2$ leads to a quantum incompatibility between $\mathcal{M}$ and Γ, $\big[\mathcal{M},\Gamma\big] \neq 0$ (see discussion below), i.e., one cannot define states of definite mass and lifetime simultaneously, because $\mathcal{H}$ is not a normal operator. In this situation, the eigenstates K_L and K_S, obtained by a non-unitary diagonalization of $\mathcal{H}$, lack physical meaning

and their non-orthogonality prevents a consistent probabilistic description of this and any other system with a Hamiltonian which is not a normal operator [1]. Consequently, we cannot answer which is the probability to observe a K_L or a K_S at a given time. This is the central point of our discussion for neutral kaons in this Chapter, in contrast to the B_d meson case, in which the non-hermitian $\mathcal{H}$ is a normal operator with a very good approximation.

The lack of a proper probabilistic interpretation of the neutral Kaon system has been addressed previously [82, 83] by distinguishing the ket and bra Hilbert spaces, so that the non-orthogonality of the K_L, K_S states is avoided with the use of these states and their duals. In our treatment, we do not make use of those unphysical states by considering not only the dynamics of pure initial states but also the inclusion of the final decay products, which will lead to a time evolution to mixed states.

6.2 Non-orthogonality constrains

As it has been mentioned $\langle K_L|K_S\rangle \neq 0$ would vanish only if $[\mathcal{M}, \Gamma] = 0$. In this Section we are going to discuss the orthogonality equation based on the matrix elements of $\mathcal{H}$, and how just implementing unitarity we can constrain the $\langle K_L|K_S\rangle$ value.

We have shown in Eq. (2.23)

$$|\langle K_L|K_S\rangle|^2 = \frac{2|\mathcal{H}_{12}|^2 + 2|\mathcal{H}_{21}|^2 - |\Delta\omega|^2(1-|\delta|^2)}{2|\mathcal{H}_{12}|^2 + 2|\mathcal{H}_{21}|^2 + |\Delta\omega|^2(1+|\delta|^2)} \ , \tag{6.2}$$

where $\mathcal{H}_{12}$ and $\mathcal{H}_{21}$ are the non-diagonal elements of the Hamiltonian, $\Delta\omega$ is the difference between the two complex eigenvalues of the Hamiltonian, and $\delta = (\mathcal{H}_{22} - \mathcal{H}_{11})/\Delta\omega$ (proportional to the difference of the Hamiltonian-diagonal elements). It can be seen that the $\langle K_L|K_S\rangle$ becomes 0 if $Im\delta$ and $|\mathcal{H}_{12}| - |\mathcal{H}_{21}| = 0$.

Once it is known that the product is not null and it cannot be neglected, we can constrain its value using unitarity. To derive the expressions needed, we use that [7]

$$\langle K_S|\frac{1}{2}\Gamma + iM|K_L\rangle = (\frac{1}{2}\Gamma_L + im_L)\langle K_S|K_L\rangle \ , \tag{6.3}$$

$$\langle K_L|\frac{1}{2}\Gamma + iM|K_S\rangle = (\frac{1}{2}\Gamma_S + im_S)\langle K_L|K_S\rangle \ . \tag{6.4}$$

[1] We mention here that the issue of the physical meaning of $K_{L,S}$ has also been addressed within a S-matrix formalism, instead of a time-dependent approach, with controversial conclusions [84, 85].

Complex conjugating Eq. (6.3) and adding it to Eq. (6.4) yields

$$\langle K_L|\Gamma|K_S\rangle = \Big[\frac{1}{2}(\Gamma_S+\Gamma_L)+i(m_S-m_L)\Big]\langle K_L|K_S\rangle \ . \tag{6.5}$$

Taking Eq. (2.15) we obtain

$$\langle K_L|\Gamma|K_S\rangle = 2\pi\sum_f \delta(m_0-m_f)\langle K_L|\mathcal{H}_W|f\rangle\langle f|\mathcal{H}_W|K_S\rangle \ , \tag{6.6}$$

and using the Schwartz inequality

$$|\langle K_L|\Gamma|K_S\rangle|^2 \leq \sum_f \Gamma_{HH}\Gamma_{LL} \ , \tag{6.7}$$

we finally obtain the Bell-Steinberger inequality [86]

$$|\langle K_S|K_L\rangle| \leq \sqrt{\frac{\sum_f 4\Gamma_{HH}\Gamma_{LL}}{(\Gamma_S+\Gamma_L)^2+4(m_S-m_L)^2}} \ . \tag{6.8}$$

This relation can be rewritten as

$$\begin{aligned} |\langle K_L|K_S\rangle|^2 \ &\leq \frac{4\Gamma_S\Gamma_L}{\Gamma^2+4(\Delta m_K)^2}\Big[\sum_f \sqrt{BR(K_S\to f)BR(K_L\to f)}\Big]^2 \\ &\leq \frac{4\Gamma_S\Gamma_L}{\Gamma^2+4(\Delta m_K)^2} \ , \end{aligned} \tag{6.9}$$

where we have defined $\Delta m_K = (m_S - m_L)$. Using that $\Gamma_L \ll \Gamma_S \approx 2\Delta m_K$, we can obtain a conservative bound:

$$|\langle K_L|K_S\rangle| \leq \sqrt{\frac{2\Gamma_L}{\Gamma_S}} \approx 0.06 \ . \tag{6.10}$$

6.3 Open system formalism

In [87, 88] a suggestion has been made to view a decaying quantum system as an open system interacting with an appropriate "*environment*" obtained by enlarging the original Hilbert space by states representing the decay products. The time evolution of such a system can be described by an effective hermitian Hamiltonian, essentially $\mathcal{M}$ above, and an additional dissipative term of Lindblad form (*dissipator*) [68]. As shown in [88], the non-Hermitian part of the Hamiltonian in the WWA, associated with the particle decay width operator Γ, can be incorporated into the dissipator of the enlarged space via a specific Lindblad operator $\mathcal{B}$. That work, however, was only

applied to the trivial case of the decay of a single particle and it did not address this method to the interesting case of the neutral kaon system with its problem of the incompatibility of $\mathcal{M}$ and Γ. This will be the focus of attention of the present Chapter.

To understand in simple terms the logic behind this open-quantum-system formalism for decaying systems, we first concentrate our attention on the evolution equation for the initial density matrix, $\rho = |\Psi\rangle\langle\Psi|$, restricted to the $|K^0\rangle$ $|\bar{K}^0\rangle$ system:

$$\dot{\rho} = -i\mathcal{H}\,\rho + i\rho\mathcal{H}^\dagger = -i\Big[\mathcal{M},\rho\Big] - \frac{1}{2}\Big\{\rho,\Gamma\Big\}\ , \tag{6.11}$$

where $\dot{\rho}$ denotes time derivative. This equation can be *formally* obtained from the Schrödinger equation for the state vector $|\Psi\rangle$ with the *non-Hermitian* Hamiltonian $\mathcal{H}$. In Eq. (6.11), Γ is viewed as a single quantum mechanical operator. The anti-Hermitian part of $\mathcal{H}$ leads to the anticommutator term in the right-hand side of this evolution equation. As a consequence, the description of the system in terms of pure states, for which $\mathrm{Tr}\rho^2 = \mathrm{Tr}\rho$, breaks down at time $t > 0$. This can be readily shown by calculating the rate of the Von-Neumann entropy $\mathcal{S} = -\mathrm{Tr}\big(\rho\ln\rho\big)$ using the evolution Eq. (6.11), where only the anticommutator part contributes.

As a consequence of the restriction to the initial Hilbert space ignoring the decay products, one has $\mathrm{Tr}\dot{\rho}(t) \neq 0$. To restore Unitarity [86] we include the final states when taking the trace $\mathrm{Tr}\rho$ through a mapping from the initial Hilbert space to the final one (decay products): $H_i \to H_f$. This mapping is implemented [88] by the transition operator $\mathcal{B}$, which is related to Γ via:

$$\mathcal{B}^\dagger\mathcal{B} = \Gamma = \sum_{j=1}^{\dim H_i} \gamma_j |\varphi_j\rangle\langle\varphi_j|\ ,\ \text{with}\ \gamma_j \geq 0\ , \tag{6.12}$$

where $\{\varphi_j\}$ is an orthonormal basis in H_i. If $\{f_k\}$ denotes an orthonormal basis in H_f, then one may write

$$\mathcal{B} = \sum_{k=1}^{d_f}\sum_{j=1}^{d_i} b_{kj}\,|f_k\rangle\langle\varphi_j|\ , \tag{6.13}$$

where $d_f = \dim H_f$, and $d_i = \dim H_i$. The width operator Γ is thus a positive definite self-adjoint operator with non-negative eigenvalues. The latter can include possible zero eigenvalues, corresponding to stable states. This is to be contrasted with the corresponding expression given in [88] and will have important consequences for the neutral kaon system.

The operator $\mathcal{B}$ can be considered as a sort of "*environment*" operator from the point of view of the initial state Hilbert space, and the evolution Eq. (6.11) can be replaced now by an appropriate Lindblad evolution [68], with ρ spanning the combined initial (H_i) and final (H_f) Hilbert spaces, $H_{tot} \equiv H_i \bigoplus H_f$. The Lindblad evolution can be understood as follows: in view of Eq. (6.12), the simple commutator structure of Eq. (6.11) in the conventional WWA [73] will now be replaced by an appropriate *quantum* ordering of the constituent operators $\mathcal{B}, \mathcal{B}^\dagger$ and ρ in such a way that the time evolution has the following properties [68]: (i) preserves the complete positivity of the density matrix operators at any time, i.e., the fact that their eigenvalues are positive or zero, so that the concept of probabilities associated with the eigenvalues of these operators makes sense, (ii) ensures the conservation of the total probability through $\mathrm{Tr}\rho = 1$, including the final states (decay products) and (iii) implies increase of the entropy (of quantum-mixed states).

Our density matrix ρ in the total Hilbert space $H_{tot} \equiv H_i \bigoplus H_f$ is:

$$\rho = \begin{pmatrix} \rho_{ii'} & \rho_{if} \\ \rho_{fi} & \rho_{ff'} \end{pmatrix} , \tag{6.14}$$

where Hermiticity of ρ is fulfilled in blocks and the subindices ii' (ff') run over the initial (final) states. We have for the dimension of the relevant Hilbert spaces:

$$\dim H_i < \infty , \quad \text{and} \quad \dim H_f \geq r = \dim H_i - n_0 , \tag{6.15}$$

with n_0 the degeneracy of the eigenvalue zero of the width operator. The evolution equations for the density matrix ρ in the H_{tot} Hilbert space are then described by the Lindblad form [68]:

$$\dot{\rho} = -i\big[\mathcal{H}, \rho\big] - \frac{1}{2}\big(B^\dagger B\rho + \rho B^\dagger B - 2B\rho B^\dagger\big) , \tag{6.16}$$

with

$$\mathcal{H} = \mathcal{H}^\dagger = \begin{pmatrix} \mathcal{M} & 0 \\ 0 & 0 \end{pmatrix}, \quad B = \begin{pmatrix} 0 & 0 \\ \mathcal{B} & 0 \end{pmatrix}, \tag{6.17}$$

in total Hilbert space. The new formulation of the time evolution on the enlarged space has a Hermitian Hamiltonian and is probability conserving. The complete positivity, that is guaranteed by construction in the Lindblad formalism [68], ensures that this feature characterizes the decaying quantum system, exactly as it happens in systems with Hermitian Hamiltonians.

6.4 Kaon system as an open Lindblad system

We would like to discuss here the application of this Lindblad open-system formulation of particle decay to physically realistic systems, such as neutral kaons, which are known to exhibit *CP* violation and non-zero width difference $\Delta\Gamma \neq 0$. Contrary to WWA and the dynamics given by Eq. (6.11), the open-system formalism is applicable in terms of the transition operator B Eq. (6.17), irrespective of the commutativity of the composite Γ operator with $\mathcal{M}$. In this respect, the Lindblad dynamics Eq. (6.16) for the decay is particularly interesting for neutral kaons. Other neutral mesons, such as B_d-$\overline{B}_d$ systems, are characterized by very small width differences between the physical eigenstates, practically $\Delta\Gamma \simeq 0$, for which the non-Hermitian Hamiltonian is a normal operator and the WWA solution by diagonalization of the entire Hamiltonian $\mathcal{H}$ is satisfactory.

For this discussion, we focus our attention from now on to two-state unstable systems. We can write Eq. (6.16) as :

$$\begin{pmatrix} \dot{\rho}_{ii'} & \dot{\rho}_{if} \\ \dot{\rho}_{fi} & \dot{\rho}_{ff'} \end{pmatrix} = \begin{pmatrix} -i\big[\mathcal{M}, \rho_{ii'}\big] - \frac{1}{2}\big\{\Gamma, \rho_{ii'}\big\} & -i\mathcal{M}\rho_{if} - \frac{1}{2}\Gamma\rho_{if} \\ i\rho_{fi}\mathcal{M} - \frac{1}{2}\rho_{fi}\Gamma & \mathcal{B}\rho_{ii'}\mathcal{B}^{\dagger} \end{pmatrix}. \tag{6.18}$$

One notes the following: (i) the new dynamical behavior of the final state coupled to the initial one, with effects which cannot be described in general by Γ only and the explicit form of the Lindblad operator $\mathcal{B}$, is needed; (ii) the formally identical structure of the equation for the time evolution of the initial-state density matrix, which is uncoupled to the final states, to that of Eq. (6.11), as a result of the anticommutator $\{\Gamma, \rho_{ii'}\}$; however, in this description, the last term is originated by an "external" agent and it is not included in the Hamiltonian of the two body system itself, therefore this term is responsible of the evolution from pure to mixed states in the sense of $\mathrm{Tr}\rho(t)^2 \neq \mathrm{Tr}\rho(t)$ at a time $t > 0$; (iii) the uncoupled dynamical behavior of $\rho_{if}(t)$, so that it is consistent to take $\rho_{if}(t) = 0$, if there is no initial ($t = 0$) mixed component between initial and final states; this implies that the description of the time evolution and decay is expressed in terms of initial and final density matrices only. Due to the separate treatment of commutator and anticommutator terms in the initial submatrix of Eq. (6.18), the non-commutativity of $\mathcal{M}$ and Γ is not an issue, avoiding $|K_L\rangle$ and $|K_S\rangle$ states to be used explicitly in the time evolution of the system.

We should recall once more that in the Lindblad approach, total probability conservation for the density matrix, including the decay products, is

guaranteed by construction, i.e., $\mathrm{Tr}\rho_{ii} + \mathrm{Tr}\rho_{ff} = 1$ for any t, so that Unitarity [86] is implied by the simple relation:

$$\frac{dTr[\rho_{ii}(t)]}{dt} = -\frac{dTr[\rho_{ff}(t)]}{dt} \ . \tag{6.19}$$

This relation can be verified explicitly for the solutions we obtain here for the case of the neutral kaon system.

For the neutral $K^0 - \overline{K}^0$ system we incorporate properly *CP* violation and the dynamics of its dominant decay to two-pion final states. We use the $|K_{1,2}\rangle$ basis for the kaon states defined as:

$$|K_1\rangle = \frac{1}{\sqrt{2}}\big(|K^0\rangle - |\overline{K}^0\rangle\big) \ , \quad |K_2\rangle = \frac{1}{\sqrt{2}}\big(|K^0\rangle + |\overline{K}^0\rangle\big), \tag{6.20}$$

which, as we show below, is a convenient choice in which the width operator is diagonal.

The existence of a *dominant* decay channel in the neutral kaon system, $\pi\pi$ in isospin $I = 0$ as dictated by the $\Delta I = 1/2$ rule, implies via Eq. (6.15), that $n_0 = 1$, which is correct, given that there is only one zero eigenvalue in the spectrum of Γ. Ignoring *CPT* Violation and *CP* violation in the decay, the choice of a real $\mathcal{B}$ leads to the result that the $K_{1,2}$ states are the ones with definite lifetimes, so that the width operator in the $|K_{1,2}\rangle$ basis is given by the following 2×2 diagonal matrix with eigenvalues 0 and Γ_S:

$$\Gamma_{\mathrm{WWA}} = \begin{pmatrix} \Gamma - Re(\Gamma_{12}) & 0 \\ 0 & \Gamma + Re(\Gamma_{12}) \end{pmatrix} = \gamma \begin{pmatrix} 0 & 0 \\ 0 & 1 \end{pmatrix} \ . \tag{6.21}$$

In this case the Lindblad operator Eq. (6.16), related to Γ via Eq. (6.12), is given by the following row matrix:

$$\mathcal{B} \ = \ \sqrt{\gamma}(0 \ , \ 1) \ . \tag{6.22}$$

In the $|K_{1,2}\rangle$ basis Eq. (6.20), the mass $\mathcal{M}$ matrix, which will play the rôle of the Hermitian Hamiltonian, is written as [73]:

$$\mathcal{M} = \begin{pmatrix} M - Re(M_{12}) & -iIm(M_{12}) \\ iIm(M_{12}) & M + Re(M_{12}) \end{pmatrix} \ , \tag{6.23}$$

ignoring again possible *CPT*-Violating effects. The *CP* violation parameter ϵ is introduced as:

$$\epsilon = |\epsilon| \, e^{-i\phi} = \frac{Im(M_{12})}{\frac{\gamma}{2} + i\Delta m} \ , \quad \tan\phi = \frac{2\Delta m}{\gamma} \ , \tag{6.24}$$

where $\Delta m = 2|M_{12}|$ is the difference between the mass eigenvalues ($m_{1,2} = M \mp |M_{12}|$) of the kaon mass eigenstates. And γ is the difference between the width eigenvalues of K_1 and K_2.

The mass eigenstates are found to differ from the $K_{1,2}$ states by terms of order of the CP violation parameter ϵ:

$$\begin{aligned} |\mathcal{M}_1\rangle &= \mathcal{N}_+ \left(i,\ \frac{Im(M_{12})}{Re(M_{12}) + |M_{12}|}\right) &= i|K_1\rangle + \frac{|\epsilon|}{\sin\phi}|K_2\rangle + O(|\epsilon|^2) \\ |\mathcal{M}_2\rangle &= \mathcal{N}_- \left(i\frac{Re(M_{12}) - |M_{12}|}{Im(M_{12})},\ 1\right) &= -i\frac{|\epsilon|}{\sin\phi}|K_1\rangle + |K_2\rangle + O(|\epsilon|^2)\ , \end{aligned} \tag{6.25}$$

where

$$\mathcal{N}_+ = \frac{Re(M_{12}) + |M_{12}|}{\left(2(|M_{12}|^2 + Re(M_{12})|M_{12}|)\right)^{1/2}} \tag{6.26}$$

and

$$\mathcal{N}_- = \frac{|Im(M_{12})|}{\left(2(|M_{12}|^2 - Re(M_{12})|M_{12}|)\right)^{1/2}} \tag{6.27}$$

are normalization factors.

As this transformation between life time and mass eigenstates connects two orthogonal bases, it is unitary, as shown clearly in Eq. (6.25). The existence of this unitary transformation is a consequence of the incompatibility of M and Γ matrices, which is described by the invariant determinant of the commutator:

$$\mathrm{Det}\Big(\big[\mathcal{M}\ ,\ \Gamma\ \big]\Big) = \left(2Re(\epsilon)\left[(\Delta m)^2 + \frac{\Delta\gamma^2}{4}\right]\right)^2\ . \tag{6.28}$$

Notice that the mass-width commutator in Eq. (6.28) vanishes when $Re(\epsilon) = 0$, i.e., when the width difference $\gamma = 0$ or in the absence of CP violation in the mixing (which implies $ImM_{12} = 0$).

In spite of this incompatibility, the WWA treatment of the problem follows the path of diagonalizing the entire Hamiltonian $\mathcal{H}$ which is not a normal operator. In this latter case, the eigenvalues are complex with real and imaginary parts differing from the mass and width eigenvalues by terms of order $|\epsilon|^2$. The corresponding eigenvectors are the well-known K_S, K_L states, which are not orthogonal as a consequence of Eq. (6.28),

$$\langle K_L|K_S\rangle = 2Re(\epsilon)\ . \tag{6.29}$$

To solve the evolution equations given by Eq. (6.18) we shall use a perturbation method [73], by which we expand the density matrix elements at any

time t in powers of the absolute value of the small CP-violation parameter $|\epsilon|$ in Eq. (6.24):

$$\rho_{IJ}(t) = \sum_{n=0}^{\infty} \rho_{IJ}^{(n)}(t)\,|\epsilon|^n \ , \quad n \in \mathbb{N} \ , \tag{6.30}$$

where the indices I, J span the full Hilbert space of states $\{i, f\}$, including the decay product (final) state.

In our analysis we shall restrict ourselves to second order in $|\epsilon|$, which matches the currently expected experimental sensitivity. From Eq. (6.18), first one solves the evolution equation for the initial states $\rho_{ii'}(t)$, $i, i' = \{1, 2\}$, in the $|K_1\rangle\ |K_2\rangle$ basis, to order $|\epsilon|^2$, and then obtain $\dot{\rho}_{ff}(t)$, associated with the $f = \big(\pi, \pi\big)$ decay channel, through

$$\dot{\rho}_{ff}(t) = \gamma\,\rho_{22}(t) \ . \tag{6.31}$$

Notice that with our simplified choice Eq. (6.22) of the Lindblad operator $\mathcal{B}$ for a single decay channel, the rate to this final state is proportional to the probability of having the state $|K_2\rangle$ at time t.

The result for the different $\rho_{IJ}(t)$ expressed in terms of the initial conditions for $\rho_{ii'}(0)$, reads:

$$\begin{aligned}
\rho_{11}(t) \;=\;& -2|\epsilon||\rho_{12}(0)|\Big[\cos(\phi-\phi_{12}) - e^{-\frac{\gamma}{2}t}\cos(\Delta m t+\phi-\phi_{12})\Big] \\
& +|\epsilon|^2\Big[\rho_{22}(0)e^{-\gamma t} \\
& -2e^{-\frac{\gamma}{2}\ t}\Big(\rho_{11}(0)\cos(\Delta m t+2\phi)+\rho_{22}(0)\cos(\Delta m t)\Big) \\
& +\rho_{11}(0)\Big(2\cos(2\phi)-\gamma t\Big)+\rho_{22}(0)\Big] \ ,
\end{aligned} \tag{6.32}$$

$$\begin{aligned}
\rho_{22}(t) \;=\;& \rho_{22}(0)e^{-\gamma t} \\
& -2|\epsilon||\rho_{12}(0)|\Big[e^{-\gamma t}\cos(\phi+\phi_{12}) - e^{-\frac{\gamma}{2}t}\cos(\Delta m t-\phi-\phi_{12})\Big] \\
& +|\epsilon|^2\Big[\rho_{11}(0)+e^{-\gamma t}\Big(\rho_{11}(0)+\rho_{22}(0)\big(2\cos(2\phi)+\gamma t\big)\Big) \\
& -2e^{-\frac{\gamma}{2}t}\Big(\rho_{11}(0)\cos(\Delta m t)+\rho_{22}(0)\cos(\Delta m t-2\phi)\Big)\Big] \ ,
\end{aligned} \tag{6.33}$$

$$\begin{aligned}\rho_{12}(t) &= \rho_{12}(0)e^{-(\frac{\gamma}{2}+i\Delta m)t} \\ &+|\epsilon|\Big[\rho_{11}(0)e^{-i\phi}\Big(1-e^{-(\frac{\gamma}{2}+i\Delta m)t}\Big)+\rho_{22}(0)e^{i\phi}\Big(e^{-\gamma t}-e^{-(\frac{\gamma}{2}+i\Delta m)t}\Big)\Big] \\ &+|\epsilon|^2|\rho_{12}(0)|\Big[-2\cos(\phi-\phi_{12})e^{-i\phi} \\ &+2\Big(e^{-(\frac{\gamma}{2}+i\Delta m)t}-e^{-\gamma t}\Big)\cos(\phi+\phi_{12})e^{i\phi} \\ &+2e^{-(\frac{\gamma}{2}+i\Delta m)t}\cos(\phi-\phi_{12})e^{-i\phi}-i\gamma t\ e^{-(\frac{\gamma}{2}+i\Delta m)t}e^{i\phi_{12}}\tan(\phi) \\ &+2ie^{-\frac{\gamma}{2}\ t}e^{-i\phi_{12}}\sin(\Delta m t)\Big]\ ,\end{aligned} \tag{6.34}$$

$$\begin{aligned}\rho_{ff}(t) &= \rho_{22}(0)(1-e^{-\gamma t}) \\ &+2|\epsilon||\rho_{12}(0)|\Big[e^{-\gamma t}\cos(\phi+\phi_{12}) \\ &-2e^{-\gamma/2t}\cos(\phi)\cos(\Delta m t-\phi_{12})+\cos(\phi-\phi_{12})\Big] \\ &+|\epsilon|^2\Big[-e^{-\gamma t}\Big(\rho_{11}(0)+\rho_{22}(0)\big(\cos^2(\phi)(3-\tan^2(\phi))+\gamma t\big)\Big) \\ &+4e^{-\frac{\gamma}{2}\ t}\Big(\rho_{11}(0)\cos(\phi)\cos(\Delta m t+\phi)+\rho_{22}(0)\cos(\phi)\cos(\Delta m t-\phi)\Big) \\ &-\rho_{11}(0)\big(\cos^2(\phi)(3-\tan^2(\phi))-t\gamma\big)-\rho_{22}(0)\Big]\ ,\end{aligned} \tag{6.35}$$

with $\phi_{12}=\mathrm{Arg}\rho_{12}(0)$.

6.5 Observables

We can use this result in order to calculate various observables of the kaon system, in the above approximation of non-decaying K_1 state, and compare them with the corresponding ones within the WWA formalism. We can build useful observables preparing initially pure K^0, $\overline{K}^0$, K_1, and K_2 states, which they will decay to $\pi\pi$ or semileptonically ($\pi l\nu$). For our purposes here we shall concentrate on three specific observables. The Kabir asymmetry, ($P(K^0\to\overline{K}^0)$ versus $P(\overline{K}^0\to K^0)$) and the decay rates $R(K^0\to\pi\pi)$ and $R(\overline{K}^0\to\pi\pi)$.

To perform this calculation we need the initially pure K^0 and $\overline{K}^0$ states, prepared experimentally, in the $|K_{1,2}\rangle$ basis. These are described at $t=0$ in the total Hilbert space H_{tot} by the density matrices:

$$\rho_{K^0}=\frac{1}{2}\begin{pmatrix}1&1&0\\1&1&0\\0&0&0\end{pmatrix}\ ,\quad \rho_{\overline{K}^0}=\frac{1}{2}\begin{pmatrix}1&-1&0\\-1&1&0\\0&0&0\end{pmatrix}\ . \tag{6.36}$$

As we observe, preparing a K^0 or a $\overline{K}^0$ they only differ in the non-diagonal elements. Let us name the nondiagonal element $a = \pm 1$ for K^0 and $\overline{K}^0$, respectively. So a general probability of any K initial state given by an initial density matrix ρ, to K^0 or $\overline{K}^0$ is

$$Tr\left[\begin{pmatrix} \rho_{11}(t) & \rho_{12}(t) & \rho_{1f}(t) \\ \rho_{21}(t) & \rho_{22}(t) & \rho_{2f}(t) \\ \rho_{f1}(t) & \rho_{f2}(t) & \rho_{ff}(t) \end{pmatrix} \begin{pmatrix} 1 & a & 0 \\ a & 1 & 0 \\ 0 & 0 & 0 \end{pmatrix}\right] = \rho_{11}(t) + \rho_{22}(t) + 2aRe(\rho_{12}(t)) \ . \tag{6.37}$$

If we prepare a K^0 or a $\overline{K}^0$ it is easy to deduce from Eqs (6.32), (6.33), (6.34), and (6.35), that the only contributing term to the Kabir asymmetry is the order $|\epsilon|$ term. This term in our formalism appears through the mismatch of the $\mathcal{M}$ and the Γ matrices, Eq. (6.25).

$$A_{\rm Kabir} = -4|\epsilon| \cos\phi + o(|\epsilon|^3) \ . \tag{6.38}$$

To study the rates, we will construct separately the sum of rates, sensitive to even powers of $|\epsilon|$, and their difference (or *CP*-violating asymmetry), sensitive to odd powers of $|\epsilon|$.

To order $|\epsilon|^2$ we obtain:

$$\begin{aligned}
&\Delta R \equiv R(K^0 \to \pi\pi) - R(\overline{K}^0 \to \pi\pi) \\
&= -2|\epsilon|\, \gamma e^{-t\gamma}\big(\cos\phi - e^{\frac{\gamma}{2}t}\cos(\Delta m t - \phi)\big) \ , \\
&\\
&\Sigma R \equiv R(\overline{K}^0 \to \pi\pi) + R(K^0 \to \pi\pi) \\
&= \gamma\, e^{-t\gamma}\Big[1 + |\epsilon|^2\big(1 + e^{t\gamma} + t\gamma + 2\cos(2\phi) - 4e^{\frac{\gamma}{2}t}\cos(\Delta m t - \phi)\cos\phi\big)\Big] \\
&= \gamma\,\Big[e^{-t\gamma}\Big(1 + |\epsilon|^2\big(-1 + t\gamma + 4\cos^2\phi\big)\Big) \\
&+ |\epsilon|^2 - 4|\epsilon|^2 e^{-\frac{\gamma}{2}t}\cos(\Delta m t - \phi)\cos\phi\Big] \\
&= \gamma(1 - |\epsilon|^2)\Big(e^{-t\gamma(1-|\epsilon|^2)}\big(1 + |\epsilon|^2 4\cos^2\phi\big)\Big) \\
&+ \gamma|\epsilon|^2 - 4\gamma|\epsilon|^2 e^{-\frac{\gamma}{2}t}\cos(\Delta m t - \phi)\cos\phi \ .
\end{aligned} \tag{6.39}$$

In our approach, where Δm and γ are viewed as physical parameters, the time evolution for this transition comes from the mismatch between the basis consisting of states $|K_{1,2}\rangle$ with definite life times and the basis of stationary states $|\mathcal{M}_{1,2}\rangle$ with definite mass, as implied by the unitary matrix, Eq. (6.25). This mismatch is a consequence of their incompatibility, condensed in the

non-vanishing commutator of Eq. (6.28). For a comparison of the result with WWA, ΣR is rewritten as in the last line of Eq. (6.39). To order $|\epsilon|^2$, one notes the appearance of "*effective widths*" with values $\Gamma_S = \gamma(1 - |\epsilon|^2)$ and $\Gamma_L = \gamma|\epsilon|^2$. These are precisely the imaginary parts of the complex eigenvalues of the total Hamiltonian in WWA. The difference between the widths and the "*effective widths*" has therefore to be taken into account in order to reproduce the same result in both approaches.

Such corrections between the masses and the real part of the complex eigenvalues of the total Hamiltonian are not seen to order $|\epsilon|^2$, because, as becomes evident from the expressions for ΔR and ΣR in Eq. (6.39), the appearance of Δm occurs at least at order $|\epsilon|$. Moreover, the expression of the *CP* violating parameter ϵ in Eq. (6.24) differs from the one given by WWA, through the different values for Δm and $\Delta\Gamma$ between the two approaches. These differences induce a relative $|\epsilon|^2$ correction to the complex parameter ϵ itself.

For those readers concerned by a possible competition of the effects of order $|\epsilon|^2$ with those coming from direct *CP* violation of order ϵ' we point out that what we call "$\big(\pi\pi\big)$" in this work denotes the combination of rates $\frac{1}{3}\big[2(\pi^+\,\pi^-) + (\pi^0\,\pi^0)\big]$, in which the contributions linear in ϵ' cancel out.

To conclude, we have presented a description of the decaying neutral kaon system as an open Lindblad system involving evolution of pure to mixed states. It satisfies all the physical requirements of a probabilistic quantum mechanical interpretation and guarantees unitarity, provided that the width operator in the dynamics of the initial states is a composite operator expressed in terms of the transition operator $\mathcal{B}$ between initial and final Hilbert spaces. Even if the states $K_{L,S}$ are not physical states filtered by observables, because there is no measurement associated with the Γ_S and Γ_L effective values, we have demonstrated the equivalence of the observables rates between our approach and the Weisskopf-Wigner Approach to order $|\epsilon|^2$. It remains to be seen whether a more complete treatment of the Lindblad operator $\mathcal{B}$ going beyond the row matrix for a single decay channel, which leads to the factorized dynamics for the rate in Eq. (6.31), would still give this equivalence between the two approaches. We would like to stress once more that the important feature of the Lindblad approach to the neutral kaon system is the avoidance of using the non-orthogonal $|K_L\rangle$, $|K_S\rangle$ states as a "*stationary*" basis. We have thus proven that a consistent probabilistic description for the neutral kaon system exists.

7. RESUMEN

El estudio de las simetrías es fundamental para la Física. Una ley de conservación en Física corresponde a la invariancia de un sistema bajo una operación de simetría asociada a un observable, es más, el conocimiento de las simetrías de un sistema físico determina su comportamiento. Por ello es importante conocer la naturaleza de las transformaciones de simetría y cómo actúan sobre los sistemas físicos.

En esta tesis estudiamos las simetrías de CP, CPT y T en sistemas de mesones neutros entrelazados. El entrelazamiento cuántico en los sistemas de mesones B y K neutros se consigue a través de la desintegración de las resonancias $\Upsilon(4S)$ y ϕ, respectivamente. Uno de los principales objetivos de esta tesis es obtener la primera observación de la ruptura de la simetría bajo inversión temporal T en cualquier sistema a través del intercambio de estados iniciales y finales en transiciones que sólo pueden ser conectadas mediante una transformación bajo T. La ruptura de CP ha sido encontrada en los sistemas de mesones neutros K [12] y B [21, 26], y los resultados experimentales son consistentes con el mecanismo de la matriz de mezcla de las tres familias de quarks del Modelo Estándar (ME), conocido como mecanismo de Cabibbo-Kobayashi-Maskawa (CKM) [13]. Invariancia local Lorentz y hermiticidad implican invariancia CPT [1], que está en acuerdo con todas las observaciones experimentales [14]. Por consiguiente, se espera que las interacciones débiles que no son invariantes bajo CP tampoco lo sean bajo T.

La mayor ruptura de CP en la naturaleza ha sido observada entre la tasa de desintegración de $B^0 \to J/\psi K_S$ (CP impar) o el estado final $J/\psi K_L$ (CP par) y sus tasas conjugadas CP para la desintegración del $\overline{B}^0$ al mismo autoestado de CP (estado final). Fenómeno se origina por la interferencia entre las amplitudes de desintegración con o sin mezcla [26, 27]. Por tanto, el mayor efecto esperado de violación de T debe ser encontrado en estos canales.

Usando estos estados finales y desarrollando el método descrito en la Ref. [2] basado en las ideas propuestas en la Ref. [30], presentamos la primera observación directa de ruptura de T en el sistema de mesones B, a partir del intercambio de estados iniciales y finales en transiciones únicamente conectadas por la simetría T. Usamos para ello una muestra de datos con una luminosidad integrada de 426 fb^{-1} sobre la resonancia $\Upsilon(4S)$, que corre-

sponde a 468×10^6 parejas de sucesos $B\overline{B}$, y otra de 45 fb^{-1} registrada a 40 MeV en centro de masas (c.m.) por debajo de la $\Upsilon(4S)$. Estos datos fueron tomados por el detector *BABAR* [42] en el colisionador e^+e^- asimétrico en energía PEP-II de SLAC.

Tras la desintegración de la $\Upsilon(4S)$, el par de mesones B producidos se encuentra en un estado entrelazado asimétrico, tal y como se requiere por conservación de momento angular para un sistema en onda P. Este estado es descrito generalmente en función de los estados de sabor, B^0 y $\overline{B}^0$, pero puede expresarse en términos de cualquier combinación de B^0 y $\overline{B}^0$, por ejemplo, los estados B_+ y B_- introducidos en la Ref. [2]. Estos estados son los definidos como los mesones neutros B filtrados por su desintegración a estados de *CP* definida $J/\psi K_L$ (*CP* par) y $c\overline{c}K_S$, con $K_S \to \pi\pi$ (*CP* impar), respectivamente. Los estados B_+ y B_- son ortogonales entre sí cuando sólo una fase débil está presente en la amplitud de desintegración del B, tal y como sucede en las desintegraciones de B a los estados finales $J/\psi K^0$ [28], y la ruptura de *CP* en kaones neutros es despreciada.

El análisis experimental [3] utiliza algoritmos de reconstrucción, criterios de selección, técnicas de calibrado y muestras de mesones B idénticos a los utilizados en la medida más reciente de ruptura de *CP* en desintegraciones $B \to c\overline{c}K^{(*)0}$ realizada por el experimento *BABAR* [37], excluyendo los estados finales $\eta_c K_S$ y $J/\psi K^{*0}(\to K_S\pi^0)$. La identificación del sabor ("flavor tagging") se combina por primera vez con el "*CP* tagging" [30], requisito para la construcción de los procesos transformados T. Mientras que la descripción de la composición de las muestras y los fondos son los mismos que los descritos en la Ref. [37], la señal es tratada de forma diferente para obtener los parámetros de ruptura de T. Esto se refleja en las diferencias entre los parámetros de ruptura de T y *CP*. El procedimiento para determinar los parámetros de T y su significancia es innovador [2].

Seleccionamos sucesos en los que un mesón B es reconstruido en un estado B_+ o B_-, y el sabor del otro B es identificado ("flavor ID"). Denotamos genéricamente los estados finales que identifican el sabor del B como $\ell^- X$ para $\overline{B}^0$ y $\ell^+ X$ para B^0. La notación (f_1, f_2) se usa para indicar el sabor o el contenido de *CP* del estado final reconstruido en t_1 y t_2, donde $t_2 > t_1$, o sea, $B_1 \to f_1$ es la primera desintegración del suceso y $B_2 \to f_2$ la segunda. Para su posterior uso en la Ec. (7.1), definimos $\Delta\tau = t_2 - t_1 > 0$. Una vez el estado B_1 es filtrado a tiempo t_1, el B acompañante B_2 es preparado (etiquetado o"tagged") por entrelazamiento al estado ortogonal a B_1. La notación $B_2(t_1) \to B_2(t_2)$ describe la transición del B cuya desintegración se produce a t_2, habiendo preparado su estado inicialmente a t_1. Por ejemplo, un suceso reconstruido mediante los estados finales ordenados temporalmente $(\ell^+ X, J/\psi K_S)$ identifica la tran-

sición $\overline{B}^0 \to B_-$ para el B que se desintegra después. Comparamos esta tasa con la T conjugada $B_- \to \overline{B}^0$ (intercambiando estados iniciales y finales) reconstruyendo los estados finales $(J/\psi K_L, \ell^- X)$. Cualquier diferencia entre estas dos tasas es una evidencia de ruptura de la simetría T. Hay otras tres comparaciones independientes de T que pueden efectuarse entre las transiciones $B_+ \to B^0$ $(J/\psi K_S, \ell^+ X)$, $\overline{B}^0 \to B_+$ $(\ell^+ X, J/\psi K_L)$, y $B_- \to B^0$ $(J/\psi K_L, \ell^+ X)$ y sus T conjugadas, $B^0 \to B_+$ $(\ell^- X, J/\psi K_L)$, $B_+ \to \overline{B}^0$ $(J/\psi K_S, \ell^- X)$, y $B^0 \to B_-$ $(\ell^- X, J/\psi K_S)$, respectivamente. Similarmente, existen cuatro comparaciones diferentes que pueden llevarse a cabo para testear CP (CPT), por ejemplo, entre $\overline{B}^0 \to B_-$ y su transformada CP (CPT) $B^0 \to B_-$ ($B_- \to B^0$) [2].

Tomando $\Delta\Gamma = 0$, las ocho transiciones tienen una tasa de desintegración genérica dada por:

$$g^{\pm}_{\alpha,\beta}(\Delta\tau) \propto e^{-\Gamma\Delta\tau}\big\{1 + S^{\pm}_{\alpha,\beta}\sin(\Delta m\Delta\tau) + C^{\pm}_{\alpha,\beta}\cos(\Delta m\Delta\tau)\big\}, \qquad (7.1)$$

donde los índices $\alpha = \ell^+, \ell^-$ y $\beta = K_S, K_L$ representan los estados finales $\ell^+ X, \ell^- X$ y $c\overline{c}K_S, J/\psi K_L$, respectivamente. El símbolo + o − indica si la desintegración a un estado de sabor ha ocurrido antes o después de la desintegración a un estado de CP. Γ es la anchura de desintegración promedio y Δm es la diferencia de masas entre los autoestados de masas de los dos mesones neutros B. Finalmente, $C^{\pm}_{\alpha,\beta}$ y $S^{\pm}_{\alpha,\beta}$ son coeficientes independientes del modelo. El término del seno, cuyo valor esperado es grande en el contexto del ME, aparece como resultado de la interferencia entre la amplitud de desintegración a $J/\psi K^0$ con o sin oscilación B^0-$\overline{B}^0$, mientras que el término del coseno aparece por la interferencia entre las amplitudes de desintegración con diferentes fases fuertes o débiles, y se espera despreciable [28]. De los 2×8 coeficientes de señal, construimos seis pares de parámetros independientes para testear las simetrías $(\Delta S^{\pm}_T, \Delta C^{\pm}_T)$, $(\Delta S^{\pm}_{CP}, \Delta C^{\pm}_{CP})$, y $(\Delta S^{\pm}_{CPT}, \Delta C^{\pm}_{CPT})$, tal y como se muestra en la Tabla 7.1. La ventaja de los parámetros para la simetría T es que su ruptura se manifiesta directamente por una desviación de cero en $\Delta S^{\pm}_T$ o $\Delta C^{\pm}_T$, o cualquier diferencia entre $\Delta S^{\pm}_{CP}$ y $\Delta S^{\pm}_{CPT}$, o entre $\Delta C^{\pm}_{CP}$ y $\Delta C^{\pm}_{CPT}$ (análogamente para la ruptura de CP y CPT).

Además de reconstruir el estado B_- a partir $J/\psi K_S$ utilizamos $\psi(2S)K_S$ y $\chi_{c1}K_S$ (denotados genéricamente como $c\overline{c}K_S$), con $J/\psi, \psi(2S) \to e^+e^-, \mu^+\mu^-$, $\psi(2S) \to J/\psi\pi^+\pi^-$, $\chi_{c1} \to J/\psi\gamma$ y $K_S \to \pi^+\pi^-, \pi^0\pi^0$ (este último únicamente para $J/\psi K_S$). Los estados B_+ se identifican por la desintegración a $J/\psi K_L$. Los candidatos a $J/\psi K_L$ se caracterizan por la diferencia ΔE entre la energía reconstruida del B y la energía del haz en el c.m. de la colisión e^+e^-, $E^*_{\rm beam}$. Por otro lado, para los modos $c\overline{c}K_S$ usamos la masa invariante $m_{\rm ES} = \sqrt{(E^*_{\rm beam})^2 - (p^*_B)^2}$, donde p^*_B es el momento del B calculado en el c.m. de producción.

El "flavor ID" o identificación del sabor del otro mesón B en el suceso, el no asociado con la reconstrucción B_+ o B_-, se realiza teniendo en cuenta la carga de los leptones, kaones, piones emitidos por el mesón D^*, y partículas cargadas de alto momento. Las entradas para el "flavor ID" se combinan mediante una red neuronal (NN), entrenada mediante datos Monte Carlo. La salida de la NN se divide en seis categorías de sabor excluyentes con probabilidad w en sentido creciente del error en la identificación del sabor del mesón B ("misID"). Los sucesos para los que la salida de la NN indica un poder muy bajo de discriminación se excluyen en este análisis. Determinamos la diferencia del tiempo con signo $\Delta t = t_{CP} - t_{\rm flavor}$ entre las desintegraciones de los dos mesones B midiendo la separación de los vértices de desintegración a lo largo del eje de colisión. Los sucesos son aceptados si $|\Delta t|$ y su error estimado, $\sigma_{\Delta t}$, son menores que 20 ps y 2.5 ps, respectivamente. El rendimiento del "flavor ID" y los algoritmos de reconstrucción de Δt se evalúan usando grandes muestras donde se determina el sabor de ambos mesones B (muestra de $B_{\rm flav}$) mediante la desintegración a los estados finales $D^{(*)-}[\pi^+, \rho(770)^+, a_1(1260)^+]$ y $J/\psi K^{*0}(\to K^+\pi^-)$. La función de resolución de Δt es la misma que en la Ref. [37] excepto por el hecho que todos los sesgos y anchuras de las gausianas se modelizan proporcionales a $\sigma_{\Delta t}$.

La composición de nuestras muestras se determina mediante ajustes a las distribuciones de $m_{\rm ES}$ y ΔE, usando configuraciones parametrizadas y distribuciones extraídas de simulaciones Monte Carlo y regiones de ruido de fondo de los datos (bandas laterales), para describir las componentes de señal y fondo.

Realizamos un ajuste de máxima verosimilitud no binado para obtener las distribuciones Δt para los sucesos $c\overline{c}K_S$ y $J/\psi K_L$ con sabor identificado, divididos por categoría de sabor. La función de densidad de probabilidad (PDF) es [2]

$$\begin{aligned} G_{\alpha,\beta}(\Delta t) \;\propto\; & g^+_{\alpha,\beta}(\Delta t_{\rm true}) H(\Delta t_{\rm true}) \otimes \mathcal{R}(\delta t;\sigma_{\Delta t}) + \\ & g^-_{\alpha,\beta}(-\Delta t_{\rm true}) H(-\Delta t_{\rm true}) \otimes \mathcal{R}(\delta t;\sigma_{\Delta t}), \end{aligned} \tag{7.2}$$

donde $\Delta t_{\rm true}$ es la diferencia con signo del tiempo entre las dos desintegraciones de los mesones B en el límite de reconstrucción perfecta, H es la función escalón de Heaviside, $\mathcal{R}(\delta t;\sigma_{\Delta t})$ con $\delta t = \Delta t - \Delta t_{\rm true}$ es la función de resolución, y $g^\pm_{\alpha,\beta}$ viene dada por la Ec. (7.1). Nótese que $\Delta t_{\rm true}$ es equivalente a $\Delta\tau$ ($-\Delta\tau$) cuando sucede realmente un flavor (CP) tag. A causa de la convolución con la función de resolución, la distribución para $\Delta t > 0$ contiene fundamentalmente sucesos "flavor-tagged", con una reducida contribución de sucesos "CP-tagged" a Δt pequeño, y a la inversa para $\Delta t < 0$. Errores en el "flavor ID" mezclan sucesos con asignación correcta e incorrecta de sabor, y diluyen las asimetrías de T en un factor aproximadamente

$(1-2w)$. Los efectos debidos a fondos se tienen en cuenta añadiendo términos a la Ec. (7.2) [37]. A los sucesos se les asignan probabilidades de ser señal o fondo basándonos en las distribuciones de $m_{\rm ES}$ o ΔE, para los sucesos $c\overline{c}K_S$ o $J/\psi K_L$ respectivamente.

Se ajustan un total de 27 parámetros se dejan libres en el ajuste: los 16 coeficientes de señal recogidos en la Tabla 7.1, y 11 parámetros que describen posibles violaciones de *CP* y *T* en los fondos. El resto de parámetros de señal y fondo se fijan a los obtenidos en las muestras de $B_{\rm flav}$, bandas de los candidatos J/ψ para $J/\psi K_L$, los promedios para Γ y Δm [15], o simulación Monte Carlo [37]. Los valores obtenidos para los parámetros de la asimetría se recogen en la Tabla 7.1. Hay otros 2×3 pares de parámetros para *T*, *CP* y *CPT*, pero no son independientes y pueden ser obtenidos a partir de los mostrados en la Tabla 7.1.

Usando muestras de Monte Carlo de alta estadística, determinamos que los parámetros obtenidos no están sesgados y tienen errores gausianos. Dividiendo los datos por categorías de sabor o período de toma de datos, los resultados son consistentes. Ajustando un solo par de coeficientes (S,C), invirtiendo el signo de S bajo el intercambio de $\Delta t \leftrightarrow -\Delta t$, de $B_+ \leftrightarrow B_-$ o de $B^0 \leftrightarrow \overline{B}^0$ y el signo de C bajo el intercambio de $B^0 \leftrightarrow \overline{B}^0$, obtenemos resultados idénticos a los obtenidos en la Ref. [37]. Realizando el análisis con desintegraciones de B a $c\overline{c}K^{\pm}$ y $J/\psi K^{*\pm}$ en lugar de $c\overline{c}K_S$ y $J/\psi K_L$, respectivamente, encontramos que todos los parámetros de las asimetrías son consistentes con cero.

Para evaluar los errores sistemáticos de los parámetros, seguimos el mismo procedimiento que en la Ref. [37], con algunos cambios. Consideramos los errores estadísticos en las probabilidades de "flavor misID", función de resolución Δt, y los parámetros de $m_{\rm ES}$. También hemos tenido en cuenta las diferencias entre las probabilidades de "misID", y la función de resolución entre la muestra de $B_{\rm flav}$ y estados finales de *CP*, incertidumbres debidas a conjeturas en la función de resolución para las componentes de señal y fondo, composición de señal y fondo, las PDFs para $m_{\rm ES}$ y ΔE y las fracciones de desintegración de los fondos y sus propiedades de *CP*. También asignamos un error sistemático correspondiente a cualquier desviación de los datos ajustados en Monte Carlo respecto a sus valores generados, tomando como error el mayor valor entre la diferencia y su error estadístico. Otras fuentes de error son las incertidumbres en el conocimiento de Γ, Δm y otros parámetros fijados, la región de interacción, el alineamiento del detector, efectos debidos a $\Delta\Gamma \neq 0$ en la dependencia temporal y en la normalización de la PDF. El tratamiento de $c\overline{c}K_S$ y $J/\psi K_L$ como estados ortogonales y despreciar la ruptura de *CP* para categorías de sabor sin leptones, tiene un efecto mucho menor que la incertidumbre estadística. Los errores sistemáticos totales se

Tab. 7.1: Valores medidos para los parámetros de las asimetrías de T, CP y CPT, definidos por las diferencias de $S^{\pm}_{\alpha,\beta}$ y $C^{\pm}_{\alpha,\beta}$ con sus transformados bajo las simetrías. Los valores de los coeficientes de referencia son dados al final de la tabla. El primer error es el estadístico, el segundo el sistemático. Los índices ℓ^-, ℓ^+, K_S, y K_L se utilizan para identificar los estados finales de reconstrucción de los mesones B como $\overline{B}^0$, B^0, B_-, y B_+, respectivamente.

Parámetro	Resultado
$\Delta S^+_T = S^-_{\ell^-,K_L} - S^+_{\ell^+,K_S}$	$-1.37 \pm 0.14 \pm 0.06$
$\Delta S^-_T = S^+_{\ell^-,K_L} - S^-_{\ell^+,K_S}$	$1.17 \pm 0.18 \pm 0.11$
$\Delta C^+_T = C^-_{\ell^-,K_L} - C^+_{\ell^+,K_S}$	$0.10 \pm 0.14 \pm 0.08$
$\Delta C^-_T = C^+_{\ell^-,K_L} - C^-_{\ell^+,K_S}$	$0.04 \pm 0.14 \pm 0.08$
$\Delta S^+_{CP} = S^+_{\ell^-,K_S} - S^+_{\ell^+,K_S}$	$-1.30 \pm 0.11 \pm 0.07$
$\Delta S^-_{CP} = S^-_{\ell^-,K_S} - S^-_{\ell^+,K_S}$	$1.33 \pm 0.12 \pm 0.06$
$\Delta C^+_{CP} = C^+_{\ell^-,K_S} - C^+_{\ell^+,K_S}$	$0.07 \pm 0.09 \pm 0.03$
$\Delta C^-_{CP} = C^-_{\ell^-,K_S} - C^-_{\ell^+,K_S}$	$0.08 \pm 0.10 \pm 0.04$
$\Delta S^+_{CPT} = S^-_{\ell^+,K_L} - S^+_{\ell^+,K_S}$	$0.16 \pm 0.21 \pm 0.09$
$\Delta S^-_{CPT} = S^+_{\ell^+,K_L} - S^-_{\ell^+,K_S}$	$-0.03 \pm 0.13 \pm 0.06$
$\Delta C^+_{CPT} = C^-_{\ell^+,K_L} - C^+_{\ell^+,K_S}$	$0.14 \pm 0.15 \pm 0.07$
$\Delta C^-_{CPT} = C^+_{\ell^+,K_L} - C^-_{\ell^+,K_S}$	$0.03 \pm 0.12 \pm 0.08$
$S^+_{\ell^+,K_S}$	$0.55 \pm 0.09 \pm 0.06$
$S^-_{\ell^+,K_S}$	$-0.66 \pm 0.06 \pm 0.04$
$C^+_{\ell^+,K_S}$	$0.01 \pm 0.07 \pm 0.05$
$C^-_{\ell^+,K_S}$	$-0.05 \pm 0.06 \pm 0.03$

recogen en la Tabla 7.1.

La significancia de la ruptura de T se evalúa estudiando el cambio de la función de verosimilitud respecto a su valor máximo ($-2\Delta \ln \mathcal{L}$). Para incluir los efectos sistemáticos en la significancia, reducimos $-2\Delta \ln \mathcal{L}$ en un factor $1 + \max\{m_i^2\} = 1.61$. Definimos $m_i^2 = -2(\ln \mathcal{L}_i - \ln \mathcal{L})/s^2$, donde $\ln \mathcal{L}$ es el máximo de la verosimilitud, $\ln \mathcal{L}_i$ es la función de verosimilitud fijando el parámetro i a su variación sistemática y maximizando respecto al resto de parámetros, y $s^2 \approx 1$ es el cambio en $2 \ln \mathcal{L}$ con un nivel de

confianza (C.L.) del 68% para un grado de libertad (d.o.f). La Fig. 7.1 muestra los contornos de C.L. calculados midiendo la variación de $-2\Delta \ln \mathcal{L}$ en dos dimensiones para los parámetros de T $(\Delta S_T^+, \Delta C_T^+)$ y $(\Delta S_T^-, \Delta C_T^-)$. Análogamente se calculan los contornos de C.L. para CP y CPT mostrados en la Fig. 4.28. La diferencia entre el valor de $2 \ln \mathcal{L}$ entre el ajuste con o sin violación de T es 226 para ocho d.o.f., incluyendo errores sistemáticos. Si asumimos errores gausianos, esto corresponde a una significancia equivalente a unas 14 desviaciones estándar (σ), lo que constituye observación directa de la ruptura de T. La significancia de la ruptura de CP y CPT se determina de forma análoga, obteniendo 307 y 5 respectivamente, equivalente a 17σ y 0.3σ, consistente con ruptura de CP e invariancia CPT.

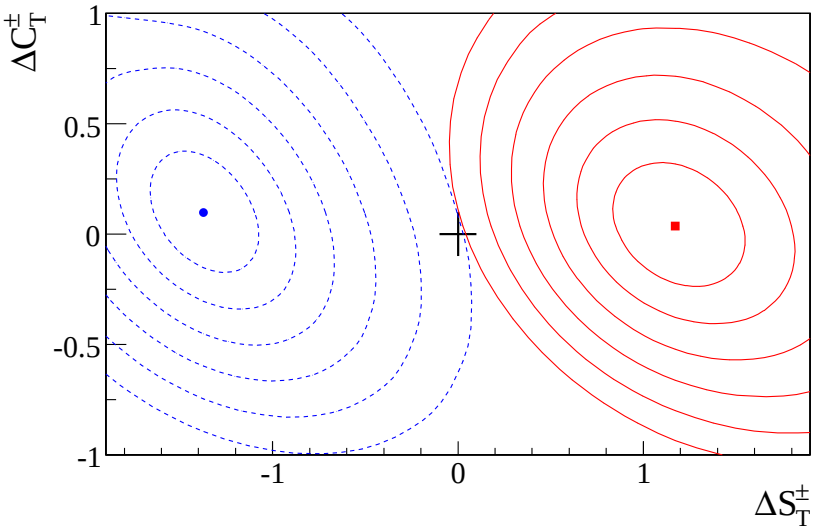

Fig. 7.1: Los valores centrales (punto azul y cuadrado rojo) y los contornos de C.L. en dos dimensiones para $1 - \text{C.L.} = 0.317,\ 4.55 \times 10^{-2},\ 2.70 \times 10^{-3},\ 6.33 \times 10^{-5},\ 5.73 \times 10^{-7}$, y 1.97×10^{-9}, calculados mediante el cambio en $-2\Delta \ln \mathcal{L}$ comparado con el máximo $(-2\Delta \ln \mathcal{L} = 2.3, 6.2, 11.8, 19.3, 28.7, 40.1)$, para los pares de los parámetros de T $(\Delta S_T^+, \Delta C_T^+)$ (curvas azules discontinuas) y $(\Delta S_T^-, \Delta C_T^-)$ (curvas rojas continuas). Los errores sistemáticos están incluídos. El punto de invariancia T se muestra con el signo $+$.

Como resumen de la primera parte de la tesis, hemos medido los parámetros de ruptura de T en la evolución temporal del sistema de mesones neutros B, comparando las probabilidades de transición para $\overline{B}^0 \to B_-$, $B_+ \to B^0$, $\overline{B}^0 \to B_+$, y $B_- \to B^0$, y sus transformadas por T. Hemos determinado los principales parámetros de violación de T $\Delta S_T^+ = -1.37 \pm 0.14$ (stat.) $\pm$

0.06 (syst.) y $\Delta S_T^- = 1.17 \pm 0.18$ (stat.) $\pm$ 0.11 (syst.), y observado por primera vez directamente la ruptura de T, en el sistema de mesones B, con una significancia de 14σ. Nuestros resultados son consistentes con las medidas actuales de ruptura CP si asumimos invariancia CPT. Estos resultados constituyen la primera observación de ruptura de T en cualquier sistema a través del intercambio de estados iniciales y finales para transiciones que sólo pueden ser conectadas mediante T.

Las factorías de mesones B no son las únicas instalaciones capaces de producir mesones entrelazados. Las factorías de mesones ϕ nos permiten también utilizar la propiedad cuántica del entrelazamiento para los kaones y con ello construir tests para estudiar las simetrías de CP, CPT y especialmente T.

La evolución temporal del sistema de kaones neutros es fascinante, y nos ha llevado a obtener descubrimientos importantes, jugando un rol crucial en el estudio de las simetrías. De hecho, es el sistema físico donde se encontró por primera vez la ruptura de CP para el canal de desintegración a dos piones $K^0 \to \pi\pi$ [12]. Hasta la fecha se sigue estudiando este sistema [20, 23, 66] y se han construido experimentos para explotar la producción entrelazada de mesones en las llamadas factorías de ϕ [67]. Es más, los kaones neutros también han sido utilizados como sondas para testear las simetrías fundamentales, como invariancia CPT [1] y desviaciones del comportamiento esperado en el ME. En cuanto a esto último, se puede introducir mediante una fluctuación debida a gravedad cuántica apareciendo como un medio decoherente, lo que nos lleva a usar una formulación de sistema abierto (tipo Lindblad [68]) [69, 70, 71, 72, 73, 74, 34].

Describimos una metodología para realizar tests de CP, CPT y especialmente T para el sistema de mesones neutros K en una factoría de mesones ϕ, evitando así el problema de la irreversibilidad que surge en T. Esta metodología, tal y como se ha mencionado anteriormente, hace uso de las propiedades de entrelazamiento [29], y se basa en la posibilidad de preparar un estado cuántico de un kaón usando la observación de la desintegración de su compañero ortogonal, permitiendo así estudiar la evolución temporal del kaón filtrado, que aún no se ha desintegrado.

En primer lugar estudiamos la posibilidad de extender el análisis al sistema de kaones, para ello necesitamos estados análogos a B_+ y B_- en el sistema de kaones. Esos estados los llamaremos K_+ y K_-. K_+ es el estado filtrado por su desintegración a $\pi\pi$ ($\pi^+\pi^-$ o $\pi^0\pi^0$), un estado puro de CP par. Mientras que el K_- es el estado filtrado por su desintegración a $3\pi^0$, un estado puro de CP impar. Tal y como se hizo con los mesones B, requerimos $\langle K_+|K_-\rangle = 0$, que se satisface si y sólo si hay una única fase débil en la desintegración del kaón, es decir, despreciamos la violación directa entre $\pi^+\pi^-$ y $\pi^0\pi^0$. Otra conjetura importante para este análisis es la validez de la

regla $\Delta S = \Delta Q$, por la que los estados de sabor $|K^0\rangle$ y $|\overline{K}^0\rangle$ pueden ser identificados por la carga del leptón en desintegraciones de tipo semileptónico, es decir, un $|K^0\rangle$ se puede desintegrar a $\pi^-\ell^+\nu$ (ℓ^+) y no a $\pi^+\ell^-\bar{\nu}$ (ℓ^-), y viceversa para un $|\overline{K}^0\rangle$.

Consideremos el par de kaones coherentes producidos en una factoría ϕ con los siguientes números cuánticos $J^{PC} = 1^{--}$ [77]:

$$|i\rangle = \frac{1}{\sqrt{2}}\Big[|K^0(\vec{p})\rangle|\overline{K}^0(-\vec{p})\rangle - |\overline{K}^0(\vec{p})\rangle|K^0(-\vec{p})\rangle\Big] \tag{7.3}$$

$$= \frac{1}{\sqrt{2}}\Big[|K_+(\vec{p})\rangle|K_-(-\vec{p})\rangle - |K_-(\vec{p})\rangle|K_+(-\vec{p})\rangle\Big] \ . \tag{7.4}$$

Remarcamos el hecho de que uno puede escribir este estado inicial $|i\rangle$ en función de cualquier par de estados ortogonales, por ejemplo, K^0 y $\overline{K}^0$, o K_+ y K_-. Tal y como dicta la mecánica cuántica, el estado de uno de los mesones no está definido para un sistema entrelazado antes de que se produzca la desintegración de uno de ellos, de modo que dicha desintegración impone un filtro al mesón que todavía no se ha desintegrado. Por consiguiente es posible definir una etiqueta de sabor ("flavor tag"), es decir, inferir el sabor (K^0 o $\overline{K}^0$) del mesón que todavía vive como el sabor ortogonal al otro mesón que se ha desintegrado ($\pi^+\ell^-\bar{\nu}$ o $\pi^-\ell^+\nu$). De manera similar podemos definir un "CP-tag" [36] como el filtro impuesto por la desintegración de uno de los kaones al estado K_+ o K_-, preparando su compañero, que todavía no se ha desintegrado, en el estado ortogonal K_- o K_+, respectivamente. Siguiendo este método podemos proceder a la partición del set completo de sucesos en cuatro categorías, definidas por la etiqueta ("tag") obtenida por la primera desintegración a K_+, K_-, K^0 o $\overline{K}^0$.

Consideremos $K^0 \to K_+$ como proceso de referencia, obtenido por la observación de la desintegración $\pi^+\ell^-\bar{\nu}$[1] (ℓ^-) a tiempo t_1 de un mesón $\overline{K}^0$ y la desintegración a $\pi\pi$ posteriormente a un tiempo $t_2 > t_1$, denotado por (ℓ^-,$\pi\pi$), y consideramos:

1. Su T transformado $K_+ \to K^0$ ($3\pi^0, \ell^+$), de forma que la diferencia entre $K^0 \to K_+$ y $K_+ \to K^0$, como función de $\Delta t = t_2 - t_1$, es una señal de ruptura de T.

2. Su CP transformado $\overline{K}^0 \to K_+$ (ℓ^+,$\pi\pi$), por lo que la diferencia entre $K^0 \to K_+$ y $\overline{K}^0 \to K_+$, en función de $\Delta t = t_2 - t_1$, sería una evidencia de ruptura de CP.

[1] Para aligerar la notación denotaremos $\pi^+\ell^-\bar{\nu}$ como ℓ^- y $\pi^-\ell^+\nu$ como ℓ^+.

3. Su CPT transformado $K_+ \to \overline{K}^0$ $(3\pi^0, \ell^-)$, por lo que la diferencia entre $K^0 \to K_+$ y $K_+ \to \overline{K}^0$, como función de $\Delta t = t_2 - t_1$, sería una evidencia de ruptura de CPT.

Se puede verificar fácilmente que los sucesos utilizados para las asimetrías 1, 2 y 3 son independientes. Hay otras tres comparaciones independientes para procesos conjugados T. Análogamente, podemos utilizar esta misma metodología para elaborar tests similares para CP y CPT.

Para testear la ruptura de T, estudiamos los siguientes cocientes [4] de probabilidades:

$$\begin{aligned} R_1(\Delta t) &= P\left[K^0(0) \to K_+(\Delta t)\right] / P\left[K_+(0) \to K^0(\Delta t)\right] \ , \\ R_2(\Delta t) &= P\left[K^0(0) \to K_-(\Delta t)\right] / P\left[K_-(0) \to K^0(\Delta t)\right] \ , \\ R_3(\Delta t) &= P\left[\overline{K}^0(0) \to K_+(\Delta t)\right] / P\left[K_+(0) \to \overline{K}^0(\Delta t)\right] \ , \\ R_4(\Delta t) &= P\left[\overline{K}^0(0) \to K_-(\Delta t)\right] / P\left[K_-(0) \to \overline{K}^0(\Delta t)\right] \ . \end{aligned} \tag{7.5}$$

Cualquier desviación de la predicción

$$R_1(\Delta t) = R_2(\Delta t) = R_3(\Delta t) = R_4(\Delta t) = 1 \ , \tag{7.6}$$

impuesta por la invariancia de T, es una señal de ruptura de T.

Desde un punto de vista experimental la cantidad observable en una factoría ϕ es la tasa doble de desintegración del estado inicial $|i\rangle$ a dos productos de desintegración f_1 y f_2 a tiempos t_1 y t_2, respectivamente [77]. Por consiguiente, podemos redefinir nuestros cocientes teniendo nuestra medida experimental:

$$R_1^{\rm exp}(\Delta t) \equiv \frac{\Gamma(\ell^-, \pi\pi; \Delta t)}{\Gamma(3\pi^0, \ell^+; \Delta t)} = R_1(\Delta t) \times \frac{C(\ell^-, \pi\pi)}{C(3\pi^0, \ell^+)} \tag{7.7}$$

$$R_2^{\rm exp}(\Delta t) \equiv \frac{\Gamma(\ell^-, 3\pi^0; \Delta t)}{\Gamma(\pi\pi, \ell^+; \Delta t)} = R_2(\Delta t) \times \frac{C(\ell^-, 3\pi^0)}{C(\pi\pi, \ell^+)} \tag{7.8}$$

$$R_3^{\rm exp}(\Delta t) \equiv \frac{\Gamma(\ell^+, \pi\pi; \Delta t)}{\Gamma(3\pi^0, \ell^-; \Delta t)} = R_3(\Delta t) \times \frac{C(\ell^+, \pi\pi)}{C(3\pi^0, \ell^-)} \tag{7.9}$$

$$R_4^{\rm exp}(\Delta t) \equiv \frac{\Gamma(\ell^+, 3\pi^0; \Delta t)}{\Gamma(\pi\pi, \ell^-; \Delta t)} = R_4(\Delta t) \times \frac{C(\ell^+, 3\pi^0)}{C(\pi\pi, \ell^-)} \ , \tag{7.10}$$

donde el coeficiente $C(f_{\bar{X}}, f_Y)$, depende únicamente de los estados finales $f_{\bar{X}}$ y f_Y, y viene dado por:

$$\begin{aligned} C(f_{\bar{X}}, f_Y) &= \frac{1}{2(\Gamma_S+\Gamma_L)} \left|\langle f_{\bar{X}}|T|\bar{K}_X\rangle\langle f_Y|T|K_Y\rangle\right|^2 \\ &= \frac{\left|\langle f_{\bar{X}}|T|K_S\rangle\right|^2 \left|\langle f_Y|T|K_S\rangle\right|^2}{2(\Gamma_S+\Gamma_L)} \times \left|(\bar{X}_S+\eta_{\bar{X}}\bar{X}_L)(Y_S+\eta_Y Y_L)\right|^2 \ . \end{aligned} \tag{7.11}$$

Notemos que si invertimos el orden de los productos de desintegración (f_2, f_1) o $t_1 > t_2$, es decir, $\Delta t \to -\Delta t$, estaríamos determinando el inverso de *otro* cociente:

$$\begin{aligned} R_2^{\rm exp}(-\Delta t) &= \frac{1}{R_3^{\rm exp}(\Delta t)} = \frac{1}{R_3(\Delta t)} \times \frac{C(3\pi^0, \ell^-)}{C(\ell^+, \pi\pi)} \ , \\ R_4^{\rm exp}(-\Delta t) &= \frac{1}{R_1^{\rm exp}(\Delta t)} = \frac{1}{R_1(\Delta t)} \times \frac{C(3\pi^0, \ell^+)}{C(\ell^-, \pi\pi)} \ . \end{aligned} \tag{7.12}$$

Debido a la propiedad $C(f_{\bar{X}}, f_Y) = C(f_Y, f_{\bar{X}})$, la proporcionalidad constante entre $R_{2(4)}^{\rm exp}(-\Delta t)$ y $1/R_{3(1)}(\Delta t)$ es la misma que entre $R_{2(4)}^{\rm exp}(\Delta t)$ y $R_{2(4)}(\Delta t)$. Por todo esto se pueden medir únicamente dos observables, $R_2^{\rm exp}(\Delta t)$ y $R_4^{\rm exp}(\Delta t)$, con $-\infty < \Delta t < +\infty$. ; su valor esperado se muestra en la Fig. 7.2.

Desde el punto de vista de una evidencia independiente de modelo de la simetría de T, sería suficiente con probar que una de las predicciones de la Ec. (7.6) no se satisface, es decir, que $R_i(\Delta t) \neq 1$, para cualquier cociente R_i. Experimentalmente, medimos el cociente $R_2^{\rm exp}(\Delta t)$ o $R_4^{\rm exp}(\Delta t)$ en el límite $\Delta t \gg \tau_S$, donde se espera que los cocientes tengan un valor constante. Dando una evaluación independiente de los coeficientes de los cocientes $\frac{C(\ell^-,3\pi^0)}{C(\pi\pi,\ell^+)}$ o $\frac{C(\ell^+,3\pi^0)}{C(\pi\pi,\ell^-)}$ se puede extraer el comportamiento asintótico $R_2(\Delta t \gg \tau_S)$ o $R_4(\Delta t \gg \tau_S)$ y verificar la desviación de 1.

Para evaluar la sensibilidad estadística del experimento definimos

$$Q_i(\Delta t) \equiv \frac{|1 - R_i(\Delta t)|}{\sigma\left(R_i(\Delta t)\right)} \ , \tag{7.13}$$

como el cociente entre la desviación de R_i de su predicción por la Ec. (7.6), y el error estadístico en R_i.

El experimento KLOE-2 en DAΦNE, con una luminosidad integrada $\mathcal{L}$ esperada de $\mathcal{O}(10\ \text{fb}^{-1})$ [67], hemos elaborado simulaciones Monte Carlo para las tasas de desintegración $\Gamma(f_1, f_2; \Delta t)$, haciendo la aproximación de resolución temporal gausiana en Δt con $\sigma = 1\ \tau_S$, y una eficiencia de detección

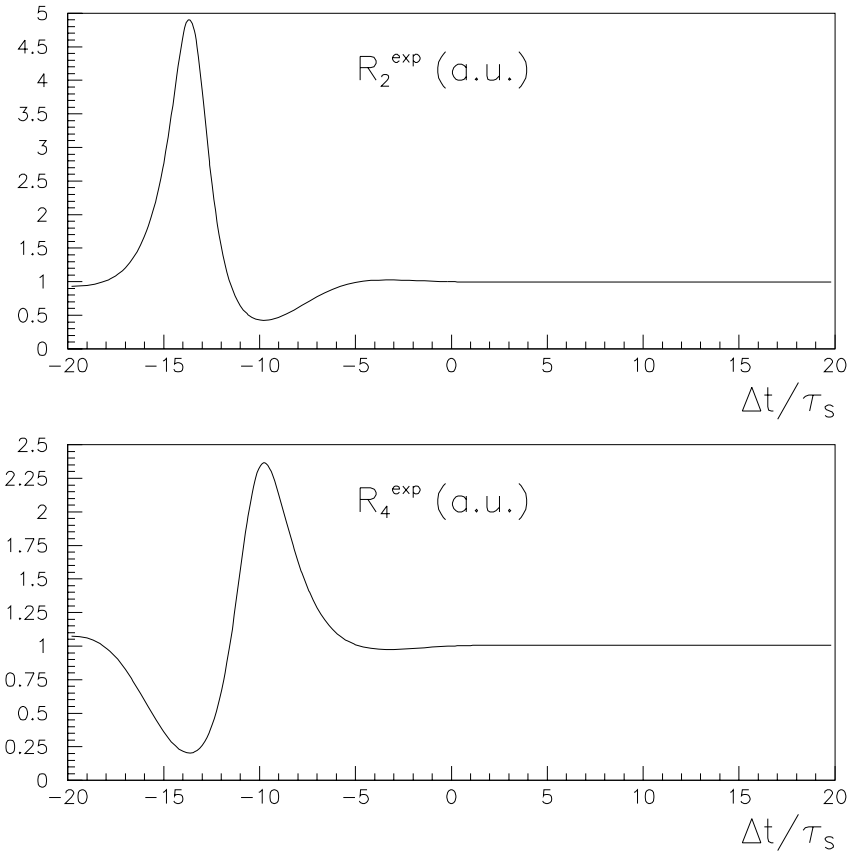

Fig. 7.2: Los cocientes $R_2^{\rm exp}$ y $R_4^{\rm exp}$ en función de Δt.

global. Para Δt grandes en la región de mayor estadística, por ejemplo, $0 \leq \Delta t \leq 300\ \tau_S$, se puede obtener una sensibilidad global $Q \simeq 4.4, 6.2$, y 8.8 para $\mathcal{L} = 5$, 10, y 20 fb^{-1}, respectivamente [4].

Como resument de la segunda parte de la tesis, hemos mostrado que usando el entralazamiento EPR en el sistema de mesones neutros, es posible en una factoría ϕ realizar un test directo de la simetría de T, independiente de CP y CPT, evitando los problemas de tests anteriores. El test propuesto [4] es independiente de modelo, y utiliza únicamente los principios de la mecánica cuántica y entrelazamiento EPR. Desde un punto de vista experimental, el test requiere medir los cocientes de las tasas de desintegración de la Ec. (7.12) con la elección adecuada de productos de desintegración y ordenación temporal. La normalización absoluta de los cocientes medidos requiere un conocimiento de la medida de las anchuras de desintegración y las vidas medias, no dependiendo de nada más. El experimento KLOE-2 en DAΦNE podrá hacer un test de T con una luminosidad integrada de $\mathcal{O}(10\ \text{fb}^{-1})$.

La evolución temporal de los kaones, que contiene ruptura de CP en la matriz de masas y una diferencia de vidas medias que no desaparece, viene descrita por un Hamiltoniano efectivo que no es un operador normal, ya que la matriz de masas no conmuta con la de anchuras. En el formalismo de Weisskopf-Wigner, diagonalizando el Hamiltoniano completo, se obtienen los estados estacionarios $K_{L,S}$ que no son ortogonales. Estos estados tienen autovalores cuyas partes reales (imaginaria) no coinciden con los autovalores de la matriz de masa (anchuras). Para evitar el uso de estos estados, describimos los kaones neutros como un sistema mecánico cuántico abierto de tipo Lindblad. Las ecuaciones de evolución para la matriz densidad ρ en el espacio completo de Hilbert $\mathcal{H}$, que incluye los estados finales, son:

$$\dot{\rho} = -i\big[\mathcal{H}, \rho\big] - \frac{1}{2}\big(B^\dagger B\rho + \rho B^\dagger B - 2B\rho B^\dagger\big)\ , \tag{7.14}$$

con

$$\mathcal{H} = \mathcal{H}^\dagger = \begin{pmatrix} \mathcal{M} & 0 \\ 0 & 0 \end{pmatrix}, \quad B = \begin{pmatrix} 0 & 0 \\ \mathcal{B} & 0 \end{pmatrix}, \tag{7.15}$$

donde $\mathcal{M}$ es la matriz de masas Hermítica y $\mathcal{B}$ es el operador de transición, que implementa el "mapeo" del espacio de Hilbert inicial al final (productos de desintegración). $\mathcal{B}$ está relacionado con el operador de anchuras Γ a través de $\mathcal{B}\mathcal{B}^\dagger = \Gamma$. Este método, en función de la matriz densidad para los estados iniciales y finales, provee una descripción probabilística consistente, evitando los problemas usuales, ya que la matriz de anchuras se convierte en un operador compuesto no incluido en el Hamilatoniano garantizando la unitariedad al incorporar los estados finales.

Aplicamos este formalismo al caso en el que la desintegración a dos piones es el canal de desintegración principal, por lo que uno de los estados del sistema de kaones es estable. Este nuevo método genera resultados para la evolución temporal de las tasas de desintegración equivalentes a los obtenidas con WWA hasta orden $|\epsilon|^2$, el parámetro de ruptura de CP usado como parámetro de desarrollo en la expansión perturbativa. Incluso si los estados $K_{L,S}$ no son físicos y no pueden ser filtrados por observables, porque no hay ninguna medida asociada con los valores efectivos de Γ_S y Γ_L, hemos demostrado la equivalencia de las tasas de desintegración entre nuestro método y la aproximación de Weisskopf-Wigner. Falta por ver si un tratamiento más completo del operador de Lindblad $\mathcal{B}$, teniendo más de un canal de desintegración, no altera la equivalencia entre ambos métodos. Nos gustaría recalcar una vez más que el método de Lindblad aplicado al sistema de kaones evita el uso de los estados no ortogonales $|K_L\rangle$, $|K_S\rangle$ como base "*estacionaria*". Con ello hemos obtenido una descripción probabilística consistente para el sistema de kaones.

En resumen, hemos desarrollado métodos para estudiar simetrías discretas en las factorías de mesones B y ϕ. Hemos medido los parámetros de ruptura de T en la evolución temporal de los mesones neutros B, $\Delta S_T^+ = -1.37 \pm 0.14\ (\text{stat.}) \pm 0.06\ (\text{syst.})$ y $\Delta S_T^- = 1.17 \pm 0.18\ (\text{stat.}) \pm 0.11\ (\text{syst.})$. Estos valores diferentes de cero representan la primera observación directa de la ruptura de T a través del intercambio de estados iniciales y finales en transiciones que sólo pueden ser conectadas a través de T. Para los kaones hemos hecho un estudio similar, mostrando que el experimento KLOE-2 en DAΦNE, la factoría de ϕ, puede hacer un test importante para T con una luminosidad integrada de $\mathcal{O}(10\ \text{fb}^{-1})$. Finalmente, hemos estudiado la evolución temporal del sistema de kaones neutros, descrito por un Hamiltoniano efectivo que no es un operador normal, es decir, la matriz de masas y la de anchuras no conmutan. Para ello hemos introducido un formalismo basado en el uso de los operadores Lindblad evitando el uso de los estados estacionarios $K_{L,S}$ que no son ortogonales. Este nuevo método da lugar a tasas de desintegración compatibles con las obtenidas con WWA hasta orden $|\epsilon|^2$, generando así una descripción probabilista consistente para el sistema de kaones neutros.

8. SUMMARY

The study of symmetries is fundamental in Physics. A conservation law in Physics corresponds to the invariance of the system under a definite symmetry operation which is associated to an observable, whose knowledge determines the behavior of the system. Thus it is relevant to understand the nature of symmetry transformations and the way they act on physical systems.

In this thesis we study CP, CPT, and T symmetries in entangled neutral meson systems. The quantum entanglement in the neutral B and neutral K meson systems is achieved through the decay of the $\Upsilon(4S)$ and the ϕ, respectively. One of the main aims of this work is to obtain the first observation of T violation in any system through the exchange of initial and final states in transitions that can only be connected through a T-symmetry transformation. As it is well established, CP is violated in neutral K [12] and neutral B meson decays [21, 26], and the experimental observations are consistent with the standard model (SM) mechanism of the three-family Cabibbo-Kobayashi-Maskawa (CKM) quark-mixing matrix being the dominant source of CP violation [13]. Local Lorentz invariant quantum field theories imply CPT invariance [1], in accordance with all experimental evidence [14]. Hence, it is expected that the CP-violating weak interaction also violates T.

The largest CP-violating asymmetry in Nature has been found between the rate for $B^0 \to J/\psi K_S$ (CP-odd final state), or $J/\psi K_L$ (CP-even final state), and the CP-conjugate rate for $\overline{B}^0$ to decay to the same CP-eigenstate, which is originated in the interference between the time-dependent decay amplitudes with and without mixing [26, 27]. Therefore the largest T-violating effect is expected to be found here.

Using these final states and implementing the method described in Ref. [2] based on the concepts proposed in Ref. [30], we report the first direct observation of T violation in the B meson system, through the exchange of initial and final states in transitions that can only be connected by a T-symmetry transformation. We use a data sample of 426 fb^{-1} of integrated luminosity at the $\Upsilon(4S)$ resonance, corresponding to 468×10^6 $B\overline{B}$ pairs, and 45 fb^{-1} at a center-of-mass (c.m.) energy 40 MeV below the $\Upsilon(4S)$, recorded by

the *BABAR* detector [42] at the PEP-II asymmetric-energy e^+e^- collider at SLAC.

In the decay of the $\Upsilon(4S)$, the two B mesons are in an entangled, antisymmetric state, as required by angular momentum conservation for a P-wave particle system. This two-body state is usually written in terms of flavor eigenstates, B^0 and $\overline{B}^0$, but can be expressed in terms of any linear combinations of B^0 and $\overline{B}^0$, e.g., the B_+ and B_- states introduced in Ref. [2]. They are defined as the neutral B states filtered by the decay to the *CP*-eigenstates $J/\psi K_L$ (*CP*-even) and $c\overline{c}K_S$, with $K_S \to \pi\pi$ (*CP*-odd), respectively. The B_+ and B_- states are orthogonal to each other when there is only one weak phase involved in the B decay amplitude, as it occurs in B decays to $J/\psi K^0$ final states [28], and *CP* violation in neutral kaons is neglected.

The experimental analysis [3] exploits identical reconstruction algorithms, selection criteria, calibration techniques, and B meson samples to the most recent time-dependent *CP* asymmetry measurement in $B \to c\overline{c}K^{(*)0}$ decays performed by the *BABAR* experiment [37], with the exception of $\eta_c K_S$ and $J/\psi K^{*0}(\to K_S\pi^0)$ final states. The "flavor tagging" is combined here, for the first time, with the "*CP* tagging" [30], as required for the construction of T-transformed processes. Whereas the descriptions of the sample composition and time-dependent backgrounds are the same as described in Ref. [37], the signal giving access to the T-violating parameters needs a different data treatment. This echoes the fundamental differences between observables for T and *CP* symmetry breaking. The procedure to determine the T-violating parameters and their significance is thus novel [2].

We select events in which one B candidate is reconstructed in a B_+ or B_- state, and the flavor of the other B is identified, referred to as flavor identification (ID). We generically denote reconstructed final states that identify the flavor of the B as $\ell^- X$ for $\overline{B}^0$ and $\ell^+ X$ for B^0. The notation (f_1, f_2) is used to indicate the flavor or *CP* final states that are reconstructed at corresponding times t_1 and t_2, where $t_2 > t_1$, i.e., $B_1 \to f_1$ is the first decay in the event and $B_2 \to f_2$ is the second decay. For later use in Eq. (8.1), we define $\Delta\tau = t_2 - t_1 > 0$. Once the B_1 state is filtered at time t_1, the living partner B_2 is prepared ("tagged") by entanglement as its orthogonal state. The notation $B_2(t_1) \to B_2(t_2)$ describes the transition of the B which decays at t_2, having tagged its state at t_1. For example, an event reconstructed in the time-ordered final states $(\ell^+ X, J/\psi K_S)$ identifies the transition $\overline{B}^0 \to B_-$ for the second B to decay. We compare the rate for this transition to its T-reversed $B_- \to \overline{B}^0$ (exchange of initial and final states) by reconstructing the final states $(J/\psi K_L, \ell^- X)$. Any difference in these two rates is evidence for T-symmetry violation. There are three other independent comparisons that can be made between $B_+ \to B^0$ $(J/\psi K_S, \ell^+ X)$, $\overline{B}^0 \to B_+$ $(\ell^+ X, J/\psi K_L)$,

and $B_- \to B^0$ ($J/\psi K_L, \ell^+ X$) transitions and their T-conjugates, $B^0 \to B_+$ ($\ell^- X, J/\psi K_L$), $B_+ \to \overline{B}^0$ ($J/\psi K_S, \ell^- X$), and $B^0 \to B_-$ ($\ell^- X, J/\psi K_S$), respectively. Similarly, four different CP (CPT) comparisons can be made, e.g., between the $\overline{B}^0 \to B_-$ transition and its CP (CPT)-transformed $B^0 \to B_-$ ($B_- \to B^0$) [2].

Taking $\Delta\Gamma = 0$, the eight transitions have a general, time-dependent decay rate

$$g^{\pm}_{\alpha,\beta}(\Delta\tau) \propto e^{-\Gamma\Delta\tau}\big\{1 + S^{\pm}_{\alpha,\beta}\sin(\Delta m\Delta\tau) + C^{\pm}_{\alpha,\beta}\cos(\Delta m\Delta\tau)\big\}, \qquad (8.1)$$

where indices $\alpha = \ell^+, \ell^-$ and $\beta = K_S, K_L$ stand for $\ell^+ X, \ell^- X$ and $c\overline{c}K_S, J/\psi K_L$ final states, respectively, and the symbol $+$ or $-$ indicates whether the decay to the flavor final state α occurs before or after the decay to the CP final state β. Here, Γ is the average decay width, Δm is the mass difference between the neutral B mass eigenstates, and $C^{\pm}_{\alpha,\beta}$ and $S^{\pm}_{\alpha,\beta}$ are model independent coefficients. The sine term, expected to be large in the SM, results from the interference between direct decay of the neutral B to the $J/\psi K^0$ final state and decay after B^0-$\overline{B}^0$ oscillation, while the cosine term arises from the interference between decay amplitudes with different weak and strong phases, and is expected to be negligible [28]. From the 2×8 signal coefficients, we construct six pairs of independent asymmetry parameters ($\Delta S^{\pm}_T, \Delta C^{\pm}_T$), ($\Delta S^{\pm}_{CP}, \Delta C^{\pm}_{CP}$), and ($\Delta S^{\pm}_{CPT}, \Delta C^{\pm}_{CPT}$), as shown in Table 8.1. The T-asymmetry parameters have the advantage that T-symmetry breaking would directly manifest itself through any nonzero value of $\Delta S^{\pm}_T$ or $\Delta C^{\pm}_T$, or any difference between $\Delta S^{\pm}_{CP}$ and $\Delta S^{\pm}_{CPT}$, or between $\Delta C^{\pm}_{CP}$ and $\Delta C^{\pm}_{CPT}$ (analogously for CP- or CPT-symmetry breaking).

In addition to $J/\psi K_S$, B_- states are reconstructed through the $\psi(2S)K_S$ and $\chi_{c1}K_S$ final states (denoted generically as $c\overline{c}K_S$), with $J/\psi, \psi(2S) \to e^+e^-, \mu^+\mu^-$, $\psi(2S) \to J/\psi\pi^+\pi^-$, $\chi_{c1} \to J/\psi\gamma$, and $K_S \to \pi^+\pi^-, \pi^0\pi^0$ (the latter only for $J/\psi K_S$). B_+ states are identified through $J/\psi K_L$. The $J/\psi K_L$ candidates are characterized by the difference ΔE between the reconstructed energy of the B and the beam energy in the e^+e^- c.m. frame, $E^*_{\rm beam}$, while for the $c\overline{c}K_S$ modes we use the beam-energy substituted invariant mass $m_{\rm ES} = \sqrt{(E^*_{\rm beam})^2 - (p^*_B)^2}$, where p^*_B is the B momentum in the c.m. frame.

The flavor ID of the other neutral B meson in the event, not associated with the reconstructed B_+ or B_-, is made on the basis of the charges of prompt leptons, kaons, pions from D^* mesons, and high-momentum charged particles. These flavor ID inputs are combined using a neural network (NN), trained with Monte Carlo simulated data. The output of the NN is then divided into six hierarchical, mutually exclusive flavor categories of increasing misidentification (misID) probability w. Events for which the NN output

indicates very low discriminating power are excluded from further analysis. We determine the signed difference of proper time $\Delta t = t_{CP} - t_{\rm flavor}$ between the two B decays from the measured separation of the decay vertices along the collision axis. Events are accepted if the reconstructed $|\Delta t|$ and its estimated uncertainty, $\sigma_{\Delta t}$, are lower than 20 ps and 2.5 ps, respectively. The performances of the flavor ID and Δt reconstruction algorithms are evaluated by using a large sample of flavor-specific neutral B decays to $D^{(*)-}[\pi^+, \rho(770)^+, a_1(1260)^+]$ and $J/\psi K^{*0}(\to K^+\pi^-)$ final states (referred to as $B_{\rm flav}$ sample). The Δt resolution function is the same as in Ref. [37] except that all Gaussian offsets and widths are modeled to be proportional to $\sigma_{\Delta t}$.

The composition of the final sample is determined through fits to the $m_{\rm ES}$ and ΔE distributions, using parametric forms and distributions extracted from Monte Carlo simulation and dilepton mass sidebands in data to describe the signal and background components.

We perform a simultaneous, unbinned maximum likelihood fit to the Δt distributions for flavor identified $c\overline{c}K_S$ and $J/\psi K_L$ events, split by flavor category. The signal probability density function (PDF) is [2]

$$\begin{aligned} G_{\alpha,\beta}(\Delta t) \;\propto\; & g^+_{\alpha,\beta}(\Delta t_{\rm true}) H(\Delta t_{\rm true}) \otimes \mathcal{R}(\delta t;\sigma_{\Delta t}) + \\ & g^-_{\alpha,\beta}(-\Delta t_{\rm true}) H(-\Delta t_{\rm true}) \otimes \mathcal{R}(\delta t;\sigma_{\Delta t}), \end{aligned} \tag{8.2}$$

where $\Delta t_{\rm true}$ is the signed difference of proper time between the two B decays in the limit of perfect Δt reconstruction, H is the Heaviside step function, $\mathcal{R}(\delta t;\sigma_{\Delta t})$ with $\delta t = \Delta t - \Delta t_{\rm true}$ is the resolution function, and $g^\pm_{\alpha,\beta}$ are given by Eq. (8.1). Note that $\Delta t_{\rm true}$ is equivalent to $\Delta\tau$ ($-\Delta\tau$) when a true flavor (CP) tag occurs. Because of the convolution with the resolution function, the distribution for $\Delta t > 0$ contains predominantly true flavor-tagged events, with a small contribution from true CP-tagged events at low Δt, and conversely for $\Delta t < 0$. Mistakes in the flavor ID algorithm mix correct and incorrect flavor assignments, and dilute the T-violating asymmetries by a factor of approximately $(1 - 2w)$. Backgrounds are accounted for by adding terms to Eq. (8.2) [37]. Events are assigned signal and background probabilities based on the $m_{\rm ES}$ or ΔE distributions, for $c\overline{c}K_S$ or $J/\psi K_L$ events, respectively.

A total of 27 parameters are varied in the likelihood fit: 16 signal coefficients summarized in Table 8.1, and 11 parameters describing possible CP and T violation in the background. All remaining signal and background parameters are fixed to values taken from the $B_{\rm flav}$ sample, J/ψ-candidate sidebands in $J/\psi K_L$, world averages for Γ and Δm [15], or Monte Carlo simulation [37]. The measured values for the asymmetry parameters are reported

in Table 8.1. There is another two times three pairs of T-, CP-, and CPT-asymmetry parameters, but they are not independent and can be derived from Table 8.1.

Tab. 8.1: Measured values of the T-, CP-, and CPT-asymmetry parameters, defined as the differences in $S^{\pm}_{\alpha,\beta}$ and $C^{\pm}_{\alpha,\beta}$ between symmetry-transformed transitions. The values of reference coefficients are also given at the bottom. The first uncertainty is statistical and the second systematic. The indices ℓ^-, ℓ^+, K_S, and K_L stand for reconstructed final states that identify the B meson as $\overline{B}^0$, B^0, B_-, and B_+, respectively.

Parameter	Result
$\Delta S^+_T = S^-_{\ell^-,K_L} - S^+_{\ell^+,K_S}$	$-1.37 \pm 0.14 \pm 0.06$
$\Delta S^-_T = S^+_{\ell^-,K_L} - S^-_{\ell^+,K_S}$	$1.17 \pm 0.18 \pm 0.11$
$\Delta C^+_T = C^-_{\ell^-,K_L} - C^+_{\ell^+,K_S}$	$0.10 \pm 0.14 \pm 0.08$
$\Delta C^-_T = C^+_{\ell^-,K_L} - C^-_{\ell^+,K_S}$	$0.04 \pm 0.14 \pm 0.08$
$\Delta S^+_{CP} = S^+_{\ell^-,K_S} - S^+_{\ell^+,K_S}$	$-1.30 \pm 0.11 \pm 0.07$
$\Delta S^-_{CP} = S^-_{\ell^-,K_S} - S^-_{\ell^+,K_S}$	$1.33 \pm 0.12 \pm 0.06$
$\Delta C^+_{CP} = C^+_{\ell^-,K_S} - C^+_{\ell^+,K_S}$	$0.07 \pm 0.09 \pm 0.03$
$\Delta C^-_{CP} = C^-_{\ell^-,K_S} - C^-_{\ell^+,K_S}$	$0.08 \pm 0.10 \pm 0.04$
$\Delta S^+_{CPT} = S^-_{\ell^+,K_L} - S^+_{\ell^+,K_S}$	$0.16 \pm 0.21 \pm 0.09$
$\Delta S^-_{CPT} = S^+_{\ell^+,K_L} - S^-_{\ell^+,K_S}$	$-0.03 \pm 0.13 \pm 0.06$
$\Delta C^+_{CPT} = C^-_{\ell^+,K_L} - C^+_{\ell^+,K_S}$	$0.14 \pm 0.15 \pm 0.07$
$\Delta C^-_{CPT} = C^+_{\ell^+,K_L} - C^-_{\ell^+,K_S}$	$0.03 \pm 0.12 \pm 0.08$
$S^+_{\ell^+,K_S}$	$0.55 \pm 0.09 \pm 0.06$
$S^-_{\ell^+,K_S}$	$-0.66 \pm 0.06 \pm 0.04$
$C^+_{\ell^+,K_S}$	$0.01 \pm 0.07 \pm 0.05$
$C^-_{\ell^+,K_S}$	$-0.05 \pm 0.06 \pm 0.03$

Using large samples of Monte Carlo simulated data, we determine that the asymmetry parameters are unbiased and have Gaussian errors. Splitting the data by flavor category or data-taking period give consistent results. Fitting a single pair of (S, C) coefficients, reversing the sign of S under $\Delta t \leftrightarrow -\Delta t$, or $B_+ \leftrightarrow B_-$ or $B^0 \leftrightarrow \overline{B}^0$ exchanges, and the sign of C under $B^0 \leftrightarrow \overline{B}^0$ exchange, we obtain identical results to those obtained in Ref. [37].

Performing the analysis with B decays to $c\bar{c}K^{\pm}$ and $J/\psi K^{*\pm}$ final states instead of the signal $c\bar{c}K_S$ and $J/\psi K_L$, respectively, we find that all the asymmetry parameters are consistent with zero.

In evaluating systematic uncertainties in the asymmetry parameters, we follow the same procedure as in Ref. [37], with small changes. We considered the statistical uncertainties on the flavor misID probabilities, Δt resolution function, and $m_{\rm ES}$ parameters. Differences in the misID probabilities and Δt resolution function between $B_{\rm flav}$ and *CP* final states, uncertainties due to assumptions in the resolution for signal and background components, compositions of the signal and backgrounds, the $m_{\rm ES}$ and ΔE PDFs, and the branching fractions for the backgrounds and their *CP* properties, have also been accounted for. We also assign a systematic uncertainty corresponding to any deviation of the fit for Monte Carlo simulated asymmetry parameters from their generated Monte Carlo values, taking the largest between the deviation and its statistical uncertainty. Other sources of uncertainty such as our limited knowledge of Γ, Δm, and other fixed parameters, the interaction region, the detector alignment, and effects due to a nonzero $\Delta\Gamma$ value in the time dependence and the normalization of the PDF, are also considered. Treating $c\bar{c}K_S$ and $J/\psi K_L$ as orthogonal states and neglecting *CP* violation for flavor categories without leptons, has an impact well below the statistical uncertainty. The total systematic uncertainties are shown in Table 8.1.

The significance of the T-violation signal is evaluated based on the change in log-likelihood with respect to the maximum ($-2\Delta\ln\mathcal{L}$). We reduce $-2\Delta\ln\mathcal{L}$ by a factor $1+\max\{m_i^2\}=1.61$ to account for systematic errors in the evaluation of the significance. Here, $m_i^2=-2(\ln\mathcal{L}_i-\ln\mathcal{L})/s^2$, where $\ln\mathcal{L}$ is the maximum log-likelihood, $\ln\mathcal{L}_i$ is the log-likelihood with asymmetry parameter i fixed to its total systematic variation and maximized over all other parameters, and $s^2\approx 1$ is the change in $2\ln\mathcal{L}$ at 68% confidence level (C.L.) for one degree of freedom (d.o.f). Figure 8.1 shows C.L. contours calculated from the change $-2\Delta\ln\mathcal{L}$ in two dimensions for the T-asymmetry parameters $(\Delta S_T^+, \Delta C_T^+)$ and $(\Delta S_T^-, \Delta C_T^-)$, analogous C.L. contours for *CP* and *CPT* are reported in Fig. 4.28. The difference in the value of $2\ln\mathcal{L}$ at the best fit solution with and without T violation is 226 with eight d.o.f., including systematic uncertainties. Assuming Gaussian errors, this corresponds to a significance equivalent to 14.0 standard deviations (σ), and thus constitutes direct observation of T violation. The significance of *CP* and *CPT* violation is determined analogously, obtaining 307 and 5, respectively, equivalent to 17σ and 0.3σ, consistent with *CP* violation and *CPT* invariance.

As summary of the first part of this thesis, we have measured T-violating parameters in the time evolution of neutral B mesons, by comparing the probabilities of $\overline{B}^0\to B_-$, $B_+\to B^0$, $\overline{B}^0\to B_+$, and $B_-\to B^0$ transitions, to

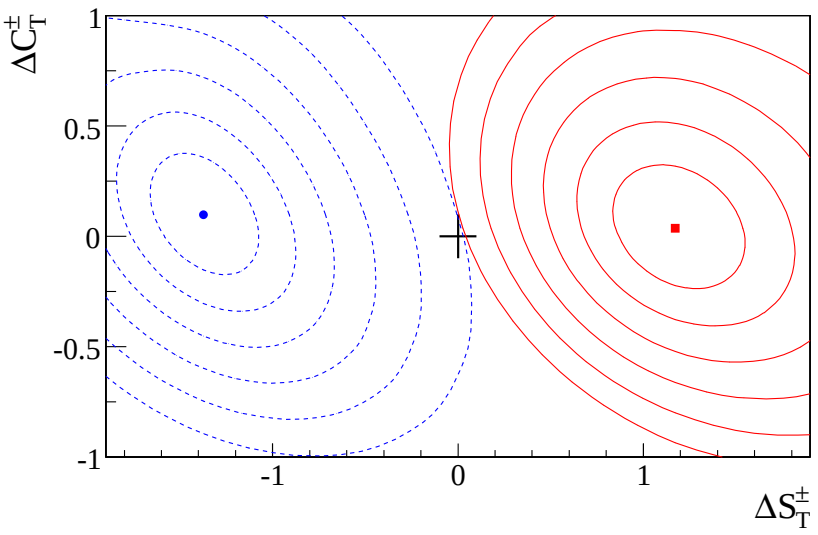

Fig. 8.1: The central values (blue point and red square) and two-dimensional C.L. contours for $1 - \text{C.L.} = 0.317,\ 4.55 \times 10^{-2},\ 2.70 \times 10^{-3},\ 6.33 \times 10^{-5},\ 5.73 \times 10^{-7}$, and 1.97×10^{-9}, calculated from the change in the value of $-2\Delta \ln \mathcal{L}$ compared with its value at maximum ($-2\Delta \ln \mathcal{L} = 2.3, 6.2, 11.8, 19.3, 28.7, 40.1$), for the pairs of T-asymmetry parameters $(\Delta S_T^+, \Delta C_T^+)$ (blue dashed curves) and $(\Delta S_T^-, \Delta C_T^-)$ (red solid curves). Systematic uncertainties are included. The T-invariance point is shown as a + sign.

their T conjugate. We have determined for the main T-violating parameters $\Delta S_T^+ = -1.37 \pm 0.14$ (stat.) ± 0.06 (syst.) and $\Delta S_T^- = 1.17 \pm 0.18$ (stat.) $\pm$ 0.11 (syst.), and have observed directly for the first time a departure from T invariance in the B meson system, with a significance equivalent to 14σ. Our results are consistent with current CP-violating measurements obtained invoking CPT invariance. They constitute the first observation of T violation in any system through the exchange of initial and final states in transitions that can only be connected by a T-symmetry transformation.

The B factories is not the only facility producing entangled mesons. The ϕ factories allow us also to exploit this intriguing quantum property for the neutral kaons to build comparisons to test CP, CPT, and specially T symmetries.

The neutral kaons are a fascinating physical system that, due to its peculiar and at the time paradoxical behavior in many respects, has lead to important discoveries, thereby triggering an enormous interest for its study. It has played a crucial role in the study of symmetries. In fact, it has been

the first physical system where CP violation has been observed in the two-pion $K^0 \to \pi\pi$ decay channel [12]. Relevant experimental studies continue up to date [20, 23, 66] and have been extended to entangled neutral kaon states in meson ϕ factories [67]. Moreover, neutral kaons have also been used as a probe of fundamental symmetries, such as CPT invariance [1], and deviations from the standard quantum mechanical behavior. The latter may be induced by quantum gravity fluctuations appearing as a "decoherening" environment, leading to an open system (Lindblad-type [68]) formulation [69, 70, 71, 72, 73, 74, 34].

We describe a methodology to perform tests of CP, CPT and specially T in the neutral K meson system at a ϕ factory, overcoming the irreversibility problem related T. This methodology, as explained before, makes use of entanglement properties [29], and relies on the possibility of preparing the quantum mechanical individual state of the neutral K meson by the observation of particular decay channels of its orthogonal entangled partner, and studying the time evolution of the filtered state of the still living meson.

As a first step to study the possibility to extend the analysis to the kaon system, we need to describe the analogous states to B_+ and B_- in the kaon system. Those states are denoted by K_+ and K_-. K_+ is the state filtered by the decay into $\pi\pi$ ($\pi^+\pi^-$ or $\pi^0\pi^0$), a pure CP-even state. While K_- is the state filtered by the decay into $3\pi^0$, a pure CP-odd state. As in the case of the B mesons, we required $\langle K_+|K_-\rangle = 0$, which is fulfilled if there is only one weak phase involved in the K decay amplitude, i.e., we neglect direct CP violation in the decay to $\pi^+\pi^-$ and $\pi^0\pi^0$. Another important assumption for this analysis is the validity of the $\Delta S = \Delta Q$ rule, so that the two flavor orthogonal eigenstates $|K^0\rangle$ and $|\overline{K}^0\rangle$ are identified by the charge of the lepton in semileptonic decays, i.e., a $|K^0\rangle$ can decay into $\pi^-\ell^+\nu$ (ℓ^+) and not into $\pi^+\ell^-\bar{\nu}$ (ℓ^-), and vice-versa for a $|\overline{K}^0\rangle$.

Let us consider the neutral kaon pair produced at a ϕ factory in a coherent quantum state with quantum numbers $J^{PC} = 1^{--}$ [77]:

$$|i\rangle = \frac{1}{\sqrt{2}}\Big[|K^0(\vec{p})\rangle|\overline{K}^0(-\vec{p})\rangle - |\overline{K}^0(\vec{p})\rangle|K^0(-\vec{p})\rangle\Big] \tag{8.3}$$

$$= \frac{1}{\sqrt{2}}\Big[|K_+(\vec{p})\rangle|K_-(-\vec{p})\rangle - |K_-(\vec{p})\rangle|K_+(-\vec{p})\rangle\Big] \ . \tag{8.4}$$

It is worth noting that one can rewrite the two particle state $|i\rangle$ in terms of any pair of orthogonal states of individual neutral K mesons, e.g., K^0 and $\overline{K}^0$, or K_+ and K_-. Following what quantum mechanics dictates, that the individual state of one neutral meson in the entangled state is not defined before the decay process of its partner occurs, imposing a tag over the undecayed kaon.

Thus it is possible to have a "flavor-tag", i.e., to infer the flavor (K^0 or $\overline{K}^0$) of the still alive meson by observing the specific flavor decay ($\pi^+\ell^-\bar{\nu}$ or $\pi^-\ell^+\nu$) of the other (and first decaying) meson. Similarly we may define a "CP-tag" [36] as the filter imposed by the decay of one of the entangled states to a K_+ or K_-, preparing its partner, which has not decayed yet, into the orthogonal state K_- or K_+, respectively. In this way we may proceed to a partition of the complete set of events into four categories, defined by the tag in the first decay as K_+, K_-, K^0 or $\overline{K}^0$.

Let us first consider $K^0 \to K_+$ as the reference process, by the observation of a $\pi^+\ell^-\bar{\nu}$ (ℓ^-) decay at a proper time t_1 of the opposite $\overline{K}^0$ meson[1] and a $\pi\pi$ decay at a later time $t_2 > t_1$, denoted as (ℓ^-,$\pi\pi$), and consider:

1. Its T transformed $K_+ \to K^0$ ($3\pi^0, \ell^+$), so that the difference between $K^0 \to K_+$ and $K_+ \to K^0$, as a function of $\Delta t = t_2 - t_1$, is T violating.

2. Its CP transformed $\overline{K}^0 \to K_+$ (ℓ^+,$\pi\pi$), so that the difference between $K^0 \to K_+$ and $\overline{K}^0 \to K_+$, as a function of $\Delta t = t_2 - t_1$, is CP violating.

3. Its CPT transformed $K_+ \to \overline{K}^0$ ($3\pi^0, \ell^-$), so that the difference between $K^0 \to K_+$and $K_+ \to \overline{K}^0$, as a function of $\Delta t = t_2 - t_1$, is CPT violating.

One may check, that the events used for the asymmetries 1, 2, and 3 are completely independent. There are other three independent comparisons between T-conjugated processes. Analogously, we can apply the same methodology for similar tests of CP violation and CPT invariance.

To test T violation, we study the following ratios [4] of probabilities:

$$\begin{aligned}
R_1(\Delta t) &= P\left[K^0(0) \to K_+(\Delta t)\right] / P\left[K_+(0) \to K^0(\Delta t)\right] \ , \\
R_2(\Delta t) &= P\left[K^0(0) \to K_-(\Delta t)\right] / P\left[K_-(0) \to K^0(\Delta t)\right] \ , \\
R_3(\Delta t) &= P\left[\overline{K}^0(0) \to K_+(\Delta t)\right] / P\left[K_+(0) \to \overline{K}^0(\Delta t)\right] \ , \\
R_4(\Delta t) &= P\left[\overline{K}^0(0) \to K_-(\Delta t)\right] / P\left[K_-(0) \to \overline{K}^0(\Delta t)\right] \ . \qquad (8.5)
\end{aligned}$$

The measurement of any deviation from the prediction

$$R_1(\Delta t) = R_2(\Delta t) = R_3(\Delta t) = R_4(\Delta t) = 1 \ , \qquad (8.6)$$

imposed by T invariance is a signal of T violation.

From the experimental point of view the observable quantity at a ϕ factory is the double differential decay rate of the state $|i\rangle$ into decay products f_1

[1] To relax the notation we will denote $\pi^+\ell^-\bar{\nu}$ as ℓ^- and $\pi^-\ell^+\nu$ as ℓ^+.

and f_2 at proper times t_1 and t_2, respectively [77]. Therefore we can redefine our ratios taking into account the experimental measurement:

$$R_1^{\rm exp}(\Delta t) \equiv \frac{\Gamma(\ell^-,\pi\pi;\Delta t)}{\Gamma(3\pi^0,\ell^+;\Delta t)} = R_1(\Delta t) \times \frac{C(\ell^-,\pi\pi)}{C(3\pi^0,\ell^+)} \tag{8.7}$$

$$R_2^{\rm exp}(\Delta t) \equiv \frac{\Gamma(\ell^-,3\pi^0;\Delta t)}{\Gamma(\pi\pi,\ell^+;\Delta t)} = R_2(\Delta t) \times \frac{C(\ell^-,3\pi^0)}{C(\pi\pi,\ell^+)} \tag{8.8}$$

$$R_3^{\rm exp}(\Delta t) \equiv \frac{\Gamma(\ell^+,\pi\pi;\Delta t)}{\Gamma(3\pi^0,\ell^-;\Delta t)} = R_3(\Delta t) \times \frac{C(\ell^+,\pi\pi)}{C(3\pi^0,\ell^-)} \tag{8.9}$$

$$R_4^{\rm exp}(\Delta t) \equiv \frac{\Gamma(\ell^+,3\pi^0;\Delta t)}{\Gamma(\pi\pi,\ell^-;\Delta t)} = R_4(\Delta t) \times \frac{C(\ell^+,3\pi^0)}{C(\pi\pi,\ell^-)}\ , \tag{8.10}$$

where the coefficient $C(f_{\bar X}, f_Y)$, depending only on the final states $f_{\bar X}$ and f_Y, is given by:

$$\begin{aligned} C(f_{\bar X}, f_Y) &= \frac{1}{2(\Gamma_S+\Gamma_L)} \left|\langle f_{\bar X}|T|\bar K_X\rangle\langle f_Y|T|K_Y\rangle\right|^2 \\ &= \frac{\left|\langle f_{\bar X}|T|K_S\rangle\right|^2 \left|\langle f_Y|T|K_S\rangle\right|^2}{2(\Gamma_S+\Gamma_L)} \times \left|(\bar X_S+\eta_{\bar X}\bar X_L)(Y_S+\eta_Y Y_L)\right|^2\ . \end{aligned} \tag{8.11}$$

It should be noted that when we perform a measurement with decay products in inverse time order (f_2, f_1) or $t_1 > t_2$, i.e. $\Delta t \to -\Delta t$, we are actually measuring the inverse of *another* ratio, i.e.:

$$\begin{aligned} R_2^{\rm exp}(-\Delta t) &= \frac{1}{R_3^{\rm exp}(\Delta t)} = \frac{1}{R_3(\Delta t)} \times \frac{C(3\pi^0,\ell^-)}{C(\ell^+,\pi\pi)} \\ R_4^{\rm exp}(-\Delta t) &= \frac{1}{R_1^{\rm exp}(\Delta t)} = \frac{1}{R_1(\Delta t)} \times \frac{C(3\pi^0,\ell^+)}{C(\ell^-,\pi\pi)}\ . \end{aligned} \tag{8.12}$$

Due to the property $C(f_{\bar X}, f_Y) = C(f_Y, f_{\bar X})$, the proportionality constant between $R_{2(4)}^{\rm exp}(-\Delta t)$ and $1/R_{3(1)}(\Delta t)$ is the same as the one between $R_{2(4)}^{\rm exp}(\Delta t)$ and $R_{2(4)}(\Delta t)$. Therefore one can actually measure only two observables, $R_2^{\rm exp}(\Delta t)$ and $R_4^{\rm exp}(\Delta t)$, with $-\infty < \Delta t < +\infty$. ; their expected behavior is shown in Fig. 8.2.

From the point of view of a model independent and direct test of T symmetry, it would be sufficient to prove that one of the predictions in Eq. (8.6)

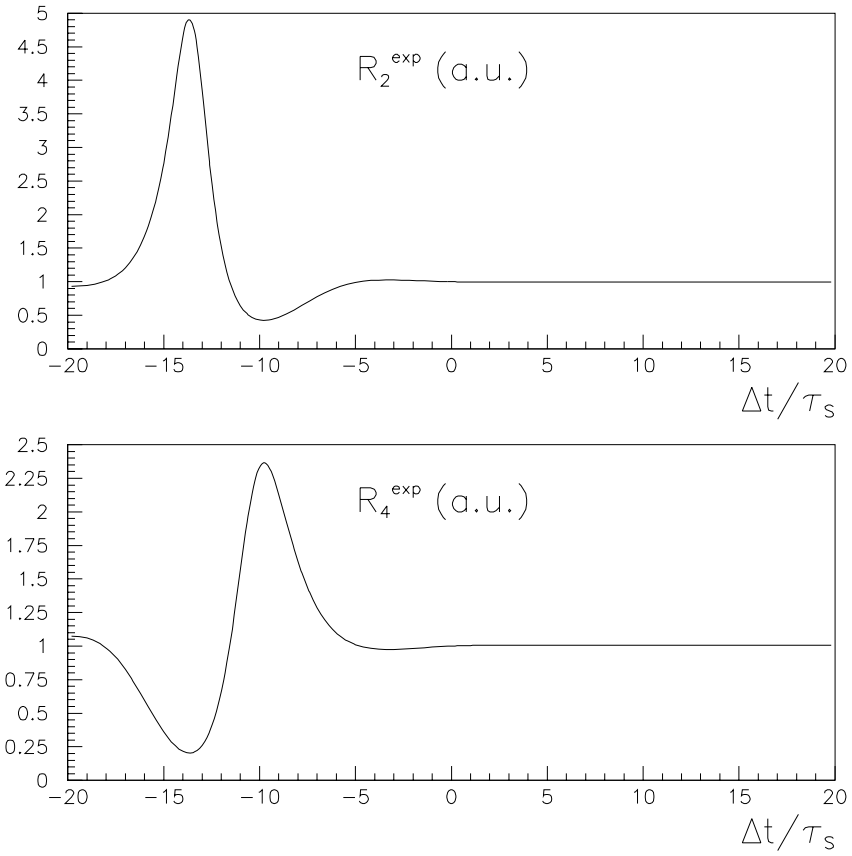

Fig. 8.2: The ratios $R_2^{\rm exp}$ and $R_4^{\rm exp}$ as a function of Δt.

is not satisfied, i.e. that $R_i(\Delta t) \neq 1$, for any ratio R_i. Experimentally, we measure the ratio $R_2^{\rm exp}(\Delta t)$ or $R_4^{\rm exp}(\Delta t)$ in the limit $\Delta t \gg \tau_S$, where they are expected to have a constant value. Given an independent evaluation of the corresponding ratio of coefficients $\frac{C(\ell^-,3\pi^0)}{C(\pi\pi,\ell^+)}$ or $\frac{C(\ell^+,3\pi^0)}{C(\pi\pi,\ell^-)}$ one may extract the asymptotic value $R_2(\Delta t \gg \tau_S)$ or $R_4(\Delta t \gg \tau_S)$ and verify the predicted deviation from one.

To evaluate the statistical sensitivity of an experiment we define

$$Q_i(\Delta t) \equiv \frac{|1 - R_i(\Delta t)|}{\sigma\left(R_i(\Delta t)\right)} \ , \tag{8.13}$$

as the ratio between the expected deviation of R_i from prediction Eq. (8.6), as given by the measured value of ϵ, and the statistical uncertainty on R_i, in a bin width of 1 τ_S centered at the value Δt.

In the case of the KLOE-2 experiment at DAΦNE, where an integrated luminosity $\mathcal{L}$ of $\mathcal{O}(10\ \text{fb}^{-1})$ is expected [67], the time-dependent decay rate distributions $\Gamma(f_1, f_2; \Delta t)$ have been evaluated with a simple Monte Carlo simulation, making the approximation of a Gaussian Δt experimental resolution with $\sigma = 1\ \tau_S$, and a full detection efficiency. Considering a large Δt interval in the statistically most populated region, e.g. $0 \leq \Delta t \leq 300\ \tau_S$, an approximate global sensitivity of $Q \simeq 4.4, 6.2$, and 8.8 is obtained for $\mathcal{L} = 5$, 10, and 20 fb^{-1}, respectively [4].

As summary of the second part of the thesis, we have shown that, by exploiting the EPR entanglement of neutral kaon pairs produced at a ϕ factory, it is possible to perform a direct test of the time reversal symmetry in the neutral kaon system, independently from *CP* violation and *CPT* invariance constraints, and therefore overcoming some conceptual difficulties affecting previous tests. The proposed test [4] is highly model-independent, relying only on the validity of quantum mechanical prescriptions and EPR correlations. From the experimental point of view, the test would require to measure the ratios of decay rates of intensities Eq. (8.12) with a suitable choice of decay products in definite time ordering. The absolute normalization of the measured ratios requires the knowledge of measurable kaon branching ratios and lifetimes and would not suffer from other uncertainties. The KLOE-2 experiment at the DAΦNE ϕ factory could make a significant T symmetry test with an integrated luminosity of $\mathcal{O}(10\ \text{fb}^{-1})$.

The time evolution of the neutral kaon system, which has both *CP* violation in the mass matrix and a non-vanishing lifetime difference in the width matrix, is delineated by an effective Hamiltonian which is not a normal operator, with incompatible (non-commuting) masses and widths. In the Weisskopf-Wigner Approach (WWA), by diagonalizing the entire Hamiltonian, the unphysical non-orthogonal "stationary" states $K_{L,S}$ are obtained.

These states have complex eigenvalues whose real (imaginary) part does not coincide with the eigenvalues of the mass (width) matrix. To avoid the usage of these states, we describe the system as an open Lindblad-type quantum mechanical system due to kaon decays. The evolution equations for the density matrix ρ in the total Hilbert space $\mathcal{H}$, including the final states, are

$$\dot{\rho} = -i\big[\mathcal{H}, \rho\big] - \frac{1}{2}\big(B^\dagger B\rho + \rho B^\dagger B - 2B\rho B^\dagger\big) \ , \tag{8.14}$$

with

$$\mathcal{H} = \mathcal{H}^\dagger = \begin{pmatrix} \mathcal{M} & 0 \\ 0 & 0 \end{pmatrix}, \quad B = \begin{pmatrix} 0 & 0 \\ \mathcal{B} & 0 \end{pmatrix}, \tag{8.15}$$

where $\mathcal{M}$ is the Hermitian mass matrix and $\mathcal{B}$ is the transition operator, which implements the mapping from the initial Hilbert space to the final one (decay products). $\mathcal{B}$ is related to the width operator Γ via $\mathcal{B}\mathcal{B}^\dagger = \Gamma$. This approach, in terms of density matrices for initial and final states, provides a consistent probabilistic description, avoiding the standard problems because the width matrix becomes a composite operator not included in the Hamiltonian and guarantying unitarity as the final states are included.

We apply this formalism to the case when the two-pions system is the dominant-decay channel, so that one of the kaon states with definite lifetime becomes stable. This new approach provides results for the time dependent decay rates in agreement with those of the WWA to order $|\epsilon|^2$, the *CP* violation parameter used as perturbative-expansion parameter. Even if the states $K_{L,S}$ are not physical states filtered by observables, because there is no measurement associated with the Γ_S and Γ_L effective values, we have demonstrated the equivalence of the observables rates between our approach and the Weisskopf-Wigner Approach. It remains to be seen whether a more complete treatment of the Lindblad operator $\mathcal{B}$ going beyond a single decay channel would still give this equivalence between the two approaches. We would like to stress once more that the important feature of the Lindblad approach to the neutral kaon system is the avoidance of using the non-orthogonal $|K_L\rangle$, $|K_S\rangle$ states as a "*stationary*" basis. We have thus proven that a consistent probabilistic description for the neutral kaon system exists.

In summary, we have developed methods exploiting entanglement to study discrete symmetries at B and ϕ factories. We have measured T-violating parameters in the time evolution of neutral B mesons, yielding $\Delta S_T^+ = -1.37 \pm 0.14\,(\text{stat.}) \pm 0.06\,(\text{syst.})$ and $\Delta S_T^- = 1.17 \pm 0.18\,(\text{stat.}) \pm 0.11\,(\text{syst.})$. These nonzero results represent the first direct observation of T violation through the exchange of initial and final states in transitions that can only be connected by a T-symmetry transformation. For the K mesons a similar study has been done, illustrating that the KLOE-2 experiment at the

DAΦNE ϕ factory could make a significant T symmetry test with an integrated luminosity of $\mathcal{O}(10\ \text{fb}^{-1})$. Finally we have studied the time evolution of the neutral kaon system, delineated by an effective Hamiltonian which is not a normal operator, with incompatible (non-commuting) masses and widths. We have introduced a new formalism based on Lindblad operators avoiding the use of the unphysical non-orthogonal "stationary" states $K_{L,S}$. This new approach provides results for the time dependent decay rates in agreement with those of the WWA to order $|\epsilon|^2$, in a consistent probabilistic description for the neutral kaon system.

BIBLIOGRAPHY

[1] G. Luders, Annals Phys. **2**, 1 (1957); W. Pauli in Niels Bohr and the Development of Physics (Pergamon Press, New York, 1955) p. 30.

[2] J. Bernabéu, F. Martínez-Vidal, P. Villanueva-Pérez, JHEP **1208**, 064 (2012).

[3] J. P. Lees *et al.*, *BABAR* Coll., Phys. Rev. Lett. **109**, 211801 (2012).

[4] J. Bernabéu, A. Di Domenico, P. Villanueva-Pérez Nucl. Phys. B **868**, 102 (2013).

[5] J. Bernabéu, N. E. Mavromatos and P. Villanueva-Pérez, arXiv:1208.3572 [hep-ph] (Submitted to PLB).

[6] G. C. Branco, L. Lavoura, and J. P. Silva, "*CP* violation", Oxford Science Publications, (1999).

[7] I. I. Bigi and A. I. Sanda, "*CP* violation", Cambridge Monographies, (2000).

[8] H.R. Quinn, J. Phys. Conf. Ser. **171**, 011001 (2009).

[9] T. D. Lee and C. N. Yang, Phys. Rev. [104], 254 (1956).

[10] C. S. Wu *et al.*, Phys. Rev. [105], 1413 (1957); F. S. Crawford *et al.*, Phys. Rev. [108], 1102 (1957); F. Eisler *et al.*, Phys. Rev. [108], 1353 (1957); L. B. Leipuner and R. K. Adir, Phys. Rev. [109], 1358 (1958).

[11] L. D. Landau Nucl. Phys. **3**, 127 (1957).

[12] J.H. Christenson, J. W. Cronin, V. L. Fitch and R. Turlay, Phys. Rev. Lett. **13**, 138 (1964).

[13] N. Cabibbo, Phys. Rev. Lett. **10**, 531 (1963); M. Kobayashi and T. Maskawa, Prog. Theor. Phys. **49**, 652 (1973).

[14] See "*CPT* invariance tests in neutral kaon decay" and "Tests of conservations laws" reviews in [15].

[15] K. Nakamura *et al.*, Particle Data Group, J. Phys. **G37**, 075021 (2010).

[16] L. Wolfenstein, Int. J. Mod. Phys. E**8**, 501 (1999).

[17] J. J. Hudson *et al.*, Nature **473**, 493 (2011).

[18] W. C. Griffith *et al.*, Phys. Rev. Lett. **102**, 101601 (2009).

[19] L. M. Sehgal and M. Wanninger. Phys. Rev. D **46**, 1035 (1992).

[20] A. Alavi-Harati *et al.*, Phys. Rev. Lett. **84**, 408 (2000).

[21] B. Aubert *et al.*, *BABAR* Coll., Phys. Rev. Lett. **93**, 131801 (2004).

[22] P. K. Kabir, Phys. Rev. D **2**, 540 (1970).

[23] A. Angelopoulus *et al.*, CPLEAR Coll., Phys. Lett. B **444**, 43 (1998); A. Angelopoulos *et al.*, CPLEAR Coll., Eur. Phys. C **22**, 55 (2001).

[24] B. Aubert *et al.*, *BABAR* Coll., Phys. Rev. Lett. **96**, 251802 (2006), Phys. Rev. Lett. **92**, 181801 (2004).

[25] M. Ciuchini, E. Franco, V. Lubicz, F. Mescia, and C. Tarantino, JHEP **308**, 031 (2003); S. Laplace, Z. Ligeti, Y. Nir, and G. Perez, Phys. Rev. D **65**, 094040 (2002); M. Beneke, G. Buchalla, A. Lenz, and U. Nierste, Phys. Lett. B **576**, 173 (2003).

[26] B. Aubert *et al.*, *BABAR* Coll., Phys. Rev. Lett. **87**, 091801 (2001); K. Abe *et al.*, Belle Coll., Phys. Rev. Lett. **87**, 091802 (2001). Y. Chao *et al.*, Belle Coll., Phys. Rev. Lett. **93**, 191802 (2004).

[27] M. Antonelli *et al.*, Phys. Rept. **494**, 197 (2010).

[28] See for example "*CP* violation in meson decays" review in [15].

[29] A. Einstein, B. Podolski and N. Rosen, Phys. Rev. **47**, 777 (1935).

[30] M.C. Bañuls and J. Bernabéu, Phys. Lett. B **464**, 117 (1999); Nucl. Phys. B **590**, 19 (2000).

[31] T. Nakada, J. Phys. Conf. Ser. **171**, 011001 (2009).

[32] J. Bernabéu, J. Phys. Conf. Ser. **335**, 012011 (2011).

[33] R. Wald, Phys. Rev. D **21**, 2742 (1980).

[34] J. Bernabéu, N. E. Mavromatos and J. Papavassiliou, Phys. Rev. Lett. **92**, 131601 (2004)

[35] A. Go *et al.*, Belle Coll., Phys. Rev. Lett. **99** 131802 (2007).

[36] M.C. Bañuls, J. Bernabéu, JHEP **032**, 9906 (1999).

[37] B. Aubert *et al.*, *BABAR* Coll., Phys. Rev. D **79**, 072009 (2009); I. Adachi *et al.*, Belle Coll., arXiv:1201.4643 [hep-ex].

[38] T. D. Lee and C. N. Yang, Phys. Rev. **98**, 1501 (1955).

[39] T. D. Lee, R. Oehme and C. N. Yang, Phys. Rev. **106**, 340 (1957).

[40] R. G. Sachs, Ann. Phys. [**22**], 239 (1963) .

[41] V.F. Weisskopf and E.P. Wigner, Z. Phys. **65**, 18 (1930).

[42] B. Aubert *et al.*, *BABAR* Coll., Nucl.Instrum. Meth. **A479**:1-116 (2002).

[43] `http://www.slac.stanford.edu/BFROOT/www/Physics/Analysis/AWG/Luminosity/lumiScriptHelp.html`

[44] *BABAR* Analysis Document #729.

[45] *BABAR* Analysis Document #730.

[46] *BABAR* Analysis Document #1025.

[47] B. Aubert *et al.*, *BABAR* Coll., Phys. Rev. D **66**, 032003 (2002).

[48] H. Albrecht *et al.*, ARGUS Coll., Phys. Lett. B **241**, 278 (1990).

[49] *BABAR* Analysis Document #929.

[50] *BABAR* Analysis Document #1996.

[51] *BABAR* Analysis Document #1993.

[52] C. Callender, Thermodynamic Asymmetry in Time, The Stanford Encyclopedia of Philosophy, E. N. Zalta ed. (2008).

[53] Y. K . Semertzidis, Symposium on Prospects in the Physics of Discrete Symmetries (Discrete 2010). J. Phys. Conf. Ser. 335, 012012 (2011).

[54] R. D. Peccei and H. R. Quinn, Phys. Rev. Lett. **38**, 1440 (1977); Phys. Rev. D **16**, 1791 (1977).

[55] M.C. Bañuls, J. Bernabéu Nucl. Phys. B Proc. Suppl. **87**, 315 (2000).

[56] `http://www.slac.stanford.edu/BFROOT/www/Physics/Analysis/AWG/TDBC/Tutorials/S2bFitting.html`

[57] `http://www.slac.stanford.edu/BFROOT/www/Physics/CP/beta/RooFitCPTdoc/`

[58] *BABAR* Analysis Document #125.

[59] *BABAR* Analysis Document #1447.

[60] *BABAR* Analysis Document #1404.

[61] W.-M. Yao *et al.*, Particle Data Group, J. Phys. **G33**, 1 (2006).

[62] T. Skwarnicki, A study of the radiative CASCADE transitions between the Upsilon-Prime and Upsilon resonances, Ph.D Thesis, DESY F31-86-02(1986), Appendix E.

[63] `http://www.slac.stanford.edu/BFROOT/www/Detector/SVT/LocalAlignment/systematics-14/.`

[64] T. Higuchi *et al.*, Belle Coll., Phys. Rev. D **85**, 071105(R) (2012).

[65] *BABAR* Analysis Document #358 (2002).

[66] G. Anzivino, J. Phys. Conf. Ser. **335**, 012015 (2011) and references therein. See also: J. R. Batley *et al.*, NA48 Coll., Phys. Lett. B **544**, 97 (2002).

[67] G. Amelino-Camelia *et al.*, Eur. Phys. J. C **68**, 619 (2010).

[68] G. Lindblad, Commun. Math. Phys. **48**, 119 (1976).

[69] M. S. Marinov, Yad. Fiz. **19**, 350 (1974).

[70] J. R. Ellis, J. S. Hagelin, D. V. Nanopoulos and M. Srednicki, Nucl. Phys. B **241**, 381 (1984).

[71] J. R. Ellis, N. E. Mavromatos and D. V. Nanopoulos, Phys. Lett. B **293**, 142 (1992); Int. J. Mod. Phys. **A11**, 1489 (1996).

[72] A. D. Dolgov, Sov. J. Nucl. Phys. **33**, 700 (1981) [Yad. Fiz. **33**, 1309 (1981)]; G. Sigl and G. Raffelt, Nucl. Phys. B **406**, 423 (1993).

[73] J. R. Ellis, J. L. Lopez, N. E. Mavromatos and D. V. Nanopoulos, Phys. Rev. D **53**, 3846 (1996).

[74] P. Huet and M. E. Peskin, Nucl. Phys. B **434**, 3 (1995).

[75] T. T. Wu, C. N. Yang, Phys. Rev. Lett. **13**, 380 (1964).

[76] H. J. Lipkin, Phys. Lett. B **219**, 474 (1989).

[77] A. Domenico *et al.* , Handbook on Neutral Kaon Interferometry at a ϕ-factory, Frascati Phys. Ser. **43** (2007).

[78] Bertlmann *et al.* , CPLEAR Coll., Phys. Rev. D **60**, 114032 (1999); R. Adler*et al.* , CPLEAR Coll., Phys. Lett. B **364**, 239 (1999); A. Di Domenico *et al.* KLOE Coll., Found. Phys. **40** (2010) 852.

[79] L. Maiani, N. Paver Maiani, *CP violation in $K \to 3\pi$ decays*, and G. D'Ambrosio, G. Isidori, A. Pugliese, *CP and CPT measurements at DAΦNE*, in The second DAPHNE physics handbook, ed. L. Maiani, G. Pancheri, N. Paver, Vol. 1, p.51-62 and 63-95, INFN-LNF, Frascati, 1995.

[80] L. F. Li and L. Wolfenstein, Phys. Rev. D **21**, 178 (1980).

[81] M. Silarski, KLOE-2 Coll. arXiv:1111.4149v3 [hep-ex], F. Ambrosino et al., KLOE Coll., Phys. Lett. B **619**, 61 (2005).

[82] L. Alvarez-Gaume, C. Kounnas, S. Lola and P. Pavlopoulos, Phys. Lett. B **458**, 347 (1999).

[83] J. P. Silva, Phys. Rev. D **62**, 116008 (2000).

[84] L. Stodolsky, Phys. Rev. D **1**, 2683 (1970).

[85] A. Pilaftsis, Nucl. Phys. B **504**, 61 (1997) [hep-ph/9702393].

[86] J. S. Bell and J. Steinberger, in Proc. *Oxford Intl. Conf. on Elementray Particles*, Rutherford Lab., Chilton UK, p. 195 (1965). e pdf

[87] P. Caban, J. Rembielinski, K. A. Smolinski and Z. Walczak, Phys. Rev. A **72**, 032106 (2005).

[88] R. A. Bertlmann, W. Grimus and B. C. Hiesmayr, Phys. Rev. A **73**, 054101 (2006).